

RATIONAL DESIGN AND SYNTHESIS OF BIODEGRADABLE POLYURETHANE
BASED BIOMATERIALS

by

CANCAN XU

Presented to the Faculty of the Graduate School of
The University of Texas at Arlington in Partial Fulfillment
of the Requirements
for the Degree of

DOCTOR OF PHILOSOPHY

THE UNIVERSITY OF TEXAS AT ARLINGTON

December 2018

Copyright © by Cancan Xu 2018

All Rights Reserved

Acknowledgements

I would like to express my deepest appreciation to my supervising professor, Dr. Yi Hong, who guides me with his profound knowledge and sharp insights and inspires me to keep going by his research passion and dedication to his career. I cannot find words to thank him for all the instructions and help in the past 5 years and in future. Without his guidance and support this dissertation would not have been possible.

I am sincerely grateful to my dissertation committee, Dr. Liping Tang, Dr. Baohong Yuan, Dr. Zui Pan, Dr. Jun Liao, and Dr. Yi Hong, for their great insight and help for me outlining and writing the dissertation. Also, I would like to acknowledge Dr. Liping Tang and Yihui Huang for their great assistance with all of my *in vivo* studies. Moreover, I would like to acknowledge Dr. Zui Pan and Xian Liu for their assistance with some of my biological experiments. I also sincerely thank Dr. Jun Liao for his patient guidance of my research and study and Dr. Xiaodan Shi for her assistance with my biomechanical testing. In addition, I would like to thank Dr. Alejandro Bugarin from Chemistry and Biochemistry department in the University of Texas at Arlington for his kind help with some of my chemical synthesis.

Many thanks to my colleagues, Dr. Jinglei Wu, Danh Truong, Yihui Huang, Dr. Zi Wei, and Aneetta E Kuriakose, for their support, contributions, and encouragements during the past years. In addition, thanks to Dr. Baohong Yuan, Dr. Kytai T. Nguyen, Dr. Guohao Dai, Dr. Mario I. Romero-Ortega, Shuai Yu, Dr. Nikhil Pandey, Taylor B. Dorsey, and Sanjay Anand for working together on so many exciting projects.

A special gratitude goes to all research grants for partial support of my research work listed below: Research Enhancement Program (Y.H.) of the University of Texas at Arlington, Beginning Grant-in-Aid 14BGIA20510066 (Y.H.) from the American Heart Association, Faculty Career Development (CAREER) award #1554835 (Y.H.) from the National Science Foundation, and R21HD090680 (Y.H.) from the National Institutes of Health.

And finally, last but not the least, I am so grateful to my parents for their support and love. They always keep me going. Also, I would like to thank my friends for sharing my sorrows and happiness in the past years.

Abstract

RATIONAL DESIGN AND SYNTHESIS OF BIODEGRADABLE POLYURETHANE
BASED BIOMATERIALS

Cancan Xu, PhD

The University of Texas at Arlington, 2018

Supervising Professor: Yi Hong

Biodegradable polyurethanes have been applied in biomedical field since 1960s. In recent years, biodegradable polyurethanes have been widely investigated for tissue repair and regeneration because of their good mechanical properties, elasticity, biodegradability, biocompatibility and processability. Compared with some commonly used biodegradable polymers, such as poly(glycolide) (PGA), poly(lactide) (PLA), poly(ϵ -caprolactone) (PCL) and polyhydroxyalkanoates (PHA), the favorable aspects of biodegradable polyurethane are its mechanical, physicochemical and biological properties can be tailored by varying the three blocks in polyurethane backbone, diisocyanate, diol and chain extender. In this thesis, we focus on the development of different functional biodegradable polyurethanes to study their structure-property relationships and satisfy different requirements in cardiac tissue repair and regeneration.

We firstly designed a series of degradation-controllable polyurethanes containing various amounts of disulfide bonds in the backbones (PU-SS), which

made the polyurethane selectively sensitive to antioxidants. Glutathione (GSH) is a natural antioxidant existing in intracellular and extracellular fluids as well as in extracellular matrices (ECM). The *in vivo* degradation of the PU-SS can be initiated by the GSH existing in the cardiac ECM and accelerated via intramuscular injection of GSH to induce the fast degradation of the implant on demand. The PU-SS polymer can be processed into films and electrospun fibrous scaffolds. Synthesized materials exhibited robust mechanical properties and high elasticity. Accelerated degradation of the materials was observed in the presence of GSH, and the rate of such degradation depends on the amount of disulfide present in the polymer backbone. The polymers and their degradation products exhibited no apparent cell toxicity while the electrospun scaffolds supported fibroblast growth *in vitro*. The *in vivo* subcutaneous implantation model showed that the polymers prompt minimal inflammatory responses, and as anticipated, the polymer with the higher disulfide bond amount had faster degradation *in vivo*.

Secondly, we developed series of electroactive biodegradable elastomeric polyurethanes as potential cardiac patch because electromechanical coupling of myocytes is crucial for their synchronous response to electrical pacing signals and conductive material can improve the ability of cardiac patch to contract effectively as a unit. First of all, a biodegradable conductive polyurethane (CPU) was synthesized from polycaprolactone diol (PCL), hexadiisocyanate (HDI), and aniline trimer and subsequently doped with (1S)-(+)-10-camphorsulfonic acid (CSA). The electrical conductivity of the CPU films, as enhanced with increasing amounts of CSA, ranged $4.2 \pm 0.5 \times 10^{-8}$ to $7.3 \pm 1.5 \times 10^{-5}$ S/cm in a wet state. The initial moduli of CPU films

increased from 7 ± 1 MPa to 35 ± 11 MPa with increased CSA amount. The doped CPU film could maintain 87% of initial conductivity after 150 hours charge under physiological environment. After 7 days of enzymatic degradation, the conductivity of all CSA-doped CPU films had decreased to that of the undoped CPU film. Furthermore, most CPU films showed high cell viability except for the group with highest CSA amount. Hence, we found the addition of dopant, CSA, can increase the polymer stiffness and deteriorated its electrical stability and biocompatibility due to the dopant leaching-out. To address this issue, we improved our design by introducing the dopant molecule into the polyurethane backbone via covalent bonding to form a biodegradable, dopant-free conductive polyurethane (DCPU) without adding extra dopant, which possessed improved mechanical properties, electrical conductivity and conductive stability, compared with the CPU polymer. Specifically, a biodegradable PCL, conductive aniline trimer, and dopant dimethylolpropionic acid (DMPA) were linked into DCPU polymer chain through HDI. The electrical conductivities of DCPU s increased with increasing DMPA amounts, ranging from $4.4 \pm 0.4 \times 10^{-7}$ to $4.7 \pm 0.8 \times 10^{-3}$ S/cm in wet state, which were higher than those of CPU polymers doped with different amounts of CSA. The initial moduli of CPU films ranged from 3.0 ± 0.6 MPa to 5.2 ± 1.1 MPa with decreasing DMPA content, which were lower than those of CPU films. The DCPU film showed excellent electrical stability (264% of initial conductivity after 150h charge) under a physiological condition. Furthermore, mouse 3T3 fibroblasts proliferated on these films exhibiting good cytocompatibility. DCPU can also be processed into a porous scaffold using salt leaching. *In vivo* mouse subcutaneous model exhibited good tissue compatibility with

extensive cell infiltration over 4 weeks of the DCPU scaffold compared to PCL porous scaffold.

Subsequently, because tissue engineered cardiac patch is also required to have mechanical and bioactive properties mimicking the native myocardium, we firstly developed a family of biodegradable elastomeric polyurethanes (PU) with low initial moduli to mechanically mimic the native myocardium. Specifically, random copolymers poly(δ -valerolactone-co- ϵ -caprolactone) (PVCL) and hydrophilic poly(ethylene glycol) (PEG) were combined into a triblock copolymer, PVCL-PEG-PVCL, and was used as a soft segment in the polyurethane backbone. The triblock copolymers were varied in chemical components, molecular weights, and hydrophilicities. The mechanical properties of polyurethanes in dry and wet states can be tuned by altering the molecular weights and hydrophilicities of the soft segments. Increasing the length of either PVCL or PEG in the soft segments reduced initial moduli of the polyurethane films and scaffolds in dry and wet states. The polymer films are found to have good cell compatibility and to support fibroblast growth in vitro. Selected polyurethanes were then processed into anisotropic porous scaffolds by a thermally induced phase-separation technique and their mechanical properties can be tailored by altering the soft segment molecular weight in the polyurethane backbone, and subsequently by varying the polymer concentration parameters during the scaffold fabrication process. The uniaxial mechanical properties, suture retention strength, ball-burst strength and biaxial mechanical properties of the polyurethane anisotropic porous scaffolds were optimized to mechanically match the native myocardium. The optimal PU-PEG_{1K}-PVCL_{6K}-10% scaffold had ball burst strength

(20.7 ± 1.5 N) comparable to that of native porcine myocardium (20.4 ± 6.0 N) and showed anisotropic mechanical behavior close to the biaxial behavior of the native porcine myocardium. Furthermore, the optimized synthetic polyurethane scaffold was combined with myocardium-derived hydrogel to form a biohybrid scaffold to improve its bioactivity. The biohybrid scaffold had morphologies similar to the decellularized porcine myocardial scaffold. The mechanical testing results showed the combination of the myocardium-derived hydrogel with the synthetic polyurethane scaffold did not affect the optimal mechanical properties of the synthetic scaffold. *In vivo* rat subcutaneous implantation of the biohybrid scaffold showed minimal immune response and exhibited higher cell penetration than the synthetic polyurethane scaffold, indicating its good tissue compatibility and high bioactivity.

Based on the above three aims, our future study will focus on exploring the biological function of these developed polyurethanes for cardiovascular application. For example, C2C12 cells have been cultured on the DCPU films and the abilities of this electroactive polymer to support cell proliferation, promote myogenic differentiation and maturation, and induce cell-to-cell interactions are studied at present. Also, in our future work, combining those desired functions into one polymer, which is degradation-controllable, electroactive biodegradable polyurethane with mechanical properties and bioactivities comparable to native myocardium, will be a promising method to create ideal cardiac patch.

In summary, this work demonstrates the design and synthesis of functionalized biodegradable polyurethanes for cardiac repair and regeneration from three different aspects: degradation controllability, electroactivity, and mechanical match with native

myocardium. These functionalized polyurethane-based scaffolds are not just physical templates for cell growth and tissue formation, but can also provide various signals (e.g., electrical and mechanical signals) to cells, thus can regulate cell proliferation and tissue regeneration. These exciting functionalized polyurethanes may find great opportunities not only for cardiac tissue regeneration, but also for other soft tissue repair and regeneration, such as skeletal muscle, nerve and skin.

Table of Contents

Acknowledgements	iii
Abstract	v
List of Illustrations.....	xvii
CHAPTER 1	1
INTRODUCTION.....	1
1.1 Introduction of biodegradable polyurethanes	1
1.2 Biodegradable polyurethane synthesis	2
1.3 Conventional biodegradable polyurethane synthesis	8
1.4 Functional biodegradable polyurethane design.....	12
1.4.1 Conductive polyurethane	12
1.4.2 Shape memory polyurethane	14
1.4.3 Waterborne polyurethane	16
1.4.4 Amino-acid-based polyurethane	16
1.4.5 Antibacterial polyurethane	18
1.4.6 Nonthrombogenic polyurethane	19
1.4.7 Others	20
1.5 Polyurethane scaffolds for tissue engineering applications.....	21
1.5.1 Polyurethane scaffolds for cardiovascular applications.....	21
1.5.2 Polyurethane scaffolds for musculoskeletal applications	24
1.5.3 Polyurethane scaffolds for neural applications.....	26
1.5.4 Polyurethane scaffolds for wound healing	27
1.6 Research goal and specific aims.....	29
CHAPTER 2	33
TRIGGERABLE DEGRADATION OF POLYURETHANES FOR TISSUE	
ENGINEERING APPLICATIONS	33
2.1 Introduction	33
2.2 Experimental section.....	35
2.2.1 Materials	35

2.2.2	Synthesis of polyurethane containing disulfides (PU-SS)	35
2.2.3	Fabrication of polymer films and electrospun fibrous scaffolds	36
2.2.4	Polymer characterization	37
2.2.5	Scaffold characterization	38
2.2.6	<i>In vitro</i> degradation	39
2.2.7	Cell toxicity of degradation products	39
2.2.8	<i>In vitro</i> cellular growth on the films	40
2.2.9	<i>In vitro</i> cellular growth on the fibrous scaffolds	41
2.2.10	Mouse subcutaneous implantation	41
2.2.11	Statistical analysis	42
2.3	Results	42
2.3.1	Polymer characterization	42
2.3.2	<i>In vitro</i> degradation of polymer films	46
2.3.3	Cytotoxicity of PU-SS degradation products	48
2.3.4	<i>In vitro</i> cellular growth on the films	50
2.3.5	Scaffold characterization	50
2.3.6	<i>In vitro</i> degradation of the scaffolds	52
2.3.7	<i>In vivo</i> cellular growth on the scaffolds	55
2.3.8	<i>In vivo</i> mouse subcutaneous implantation	56
2.4	Discussion	57
2.5	Conclusion	63
CHAPTER 3		64
DEVELOPMENT OF ELECTROACTIVE, BIODEGRADABLE POLYURETHANE		
ELASTOMERS		64
3.1		64
SYNTHESIS AND CHARACTERIZATION OF CONDUCTIVE, BIODEGRADABLE,		
ELASTOMERIC POLYURETHANES FOR BIOMEDICAL APPLICATIONS		64
3.1.1	Introduction	64
3.1.2	Experimental section	66
3.1.2.1	Materials	66

3.1.2.2	Synthesis of oxidized aniline trimer	66
3.1.2.3	Synthesis of CPU	67
3.1.2.4	Fabrication of CSA-doped CPU films	68
3.1.2.5	CPU film characterization	69
3.1.2.6	Electrical conductivity and electrochemical measurements	70
3.1.2.7	Mechanical testing	70
3.1.2.8	<i>In vitro</i> hydrolytic and enzymatic degradation	71
3.1.2.9	Electrical stability	72
3.1.2.10	<i>In vitro</i> cellular growth on the CPU films	72
3.1.2.11	Statistical analysis.....	73
3.1.3	Results	73
3.1.3.1	CPU characterization	73
3.1.3.2	Electrical and electrochemical properties.....	77
3.1.3.3	Mechanical properties.....	77
3.1.3.4	<i>In vitro</i> degradation	79
3.1.3.5	Electrical stability	80
3.1.3.6	<i>In vitro</i> cellular growth on the CPU films	81
3.1.4	Discussion.....	83
3.1.5	Conclusion	88
3.2	89
DEVELOPMENT OF DOPANT-FREE CONDUCTIVE BIOELASTOMERS.....		89
3.2.1	Introduction	89
3.2.2	Experimental section.....	91
3.2.2.1	Materials	91
3.2.2.2	Synthesis of oxidized aniline trimer with two amine end groups	91
3.2.2.3	Synthesis of DCPU	92
3.2.2.4	Fabrication of DCPU films.....	93
3.2.2.5	Polymer characterization	93
3.2.2.6	Electrical conductivity and electrochemical measurements	94
3.2.2.7	Mechanical testing	95
3.2.2.8	Polymer degradation.....	96
3.2.2.9	Electrical stability of DCPU films	96

3.2.2.10 Cytotoxicity of DCPU degradation products	97
3.2.2.11 <i>In vitro</i> biocompatibility of polymer films.....	97
3.2.2.12 Porous scaffold fabrication and characterization.....	98
3.2.2.13 Mouse subcutaneous implantation model.....	99
3.2.2.14 Statistical analysis.....	99
3.2.3 Results and discussion	100
3.2.3.1 Characterization of the DCPU.....	100
3.2.3.2 Electrical and electrochemical properties of DCPU.....	104
3.2.3.3 Mechanical properties of DCPU films	106
3.2.3.4 <i>In vitro</i> degradation of DCPU films.....	108
3.2.3.5 Electrical stability of DCPU	110
3.2.3.6 Cytotoxicity and cytocompatibility of DCPUs	113
3.2.3.7 Fabrication and characterization of porous DCPU scaffold.....	115
3.2.3.8 <i>In vivo</i> mouse subcutaneous implantation	116
3.2.4 Conclusion	117
CHAPTER 4	119
4.1	119
SYNTHESIS AND CHATACTERIZATION OF LOW-INITIAL-MODULUS	
BIODEGRADABLE POLYURETHANE ELASTOMERS	
4.1.1 Introduction	119
4.1.2 Experimental section.....	121
4.1.2.1 Materials	121
4.1.2.2. Synthesis of PVCL copolymer diols and PVCL-PEG-PVCL triblock copolymer diols.....	122
4.1.2.3 Synthesis of polyurethanes.....	123
4.1.2.4 Polymer characterization	123
4.1.2.5 Uniaxial mechanical properties	124
4.1.2.6 <i>In vitro</i> degradation	125
4.1.2.7 <i>In vitro</i> cytocompatibility of polyurethane films.....	125
4.1.2.8 Porous scaffold fabrication.....	126
4.1.2.9 Scaffold characterization.....	126

4.1.2.10 Mouse subcutaneous implantation.....	127
4.1.2.11 Statistical analysis.....	127
4.1.3 Results	127
4.1.3.1 Synthesis and characterization of PVCL and PVCL-EPG-PVCL diols..	127
4.1.3.2 Synthesis and characterization of polyurethanes.....	129
4.1.3.4 <i>In vitro</i> degradation of polyurethane films	135
4.1.3.5 <i>In vitro</i> cytocompatibility of polyurethane films.....	137
4.1.3.6 Porous scaffold characterization.....	139
4.1.3.7 Mouse subcutaneous implantation of scaffolds	142
4.1.4 Discussion.....	144
4.1.5 Conclusion	149
4.2	150
OPTIMIZING ANISOTROPIC POLYURETHANE SCAFFOLDS TO MECHANICALLY	
MATCH WITH THE NATIVE MYOCARDIUM.....	
4.2.1 Introduction	150
4.2.2 Experimental section.....	153
4.2.2.1 Materials	153
4.2.2.2 PU-PEG-PVCL polymer synthesis and anisotropic scaffold fabrication	153
4.2.2.3 Scaffold characterization.....	154
4.2.2.4 Scaffold uniaxial mechanical properties.....	155
4.2.2.5 Biomechanical measurement.....	155
4.2.2.6 Biohybrid scaffold fabrication and characterization	155
4.2.2.7 Rat subcutaneous implantation.....	158
4.2.2.8 Statistical analysis.....	159
4.2.3 Results	159
4.2.3.1 Anisotropic scaffold characterization.....	159
4.2.3.2 Anisotropic scaffold mechanical properties.....	161
4.2.3.3 Anisotropic scaffold mechanical properties.....	166
4.2.3.4 Biohybrid scaffold characterization	172
4.2.3.5 Rat subcutaneous implantation.....	175
4.2.4 Discussion.....	176

4.2.5 Conclusion	181
CHAPTER 5	182
CONCLUSION AND FUTURE WORK	182
5.1 Conclusions	182
5.2 Future work	187
5.2.1 Further characterization of reduction-sensitive polyurethane.....	187
5.2.2 Further characterization and improvement of electroactive polyurethane	188
5.2.3 Further optimization of polyurethane cardiac patch	189
5.2.4 Combination of all the functionalized polyurethanes.....	189
Appendix A.....	191
Related Publications.....	191
Appendix B.....	196
Abbreviations.....	196
References.....	200
Biographical Information.....	242

List of Illustrations

Table 1. 1	Polymer film characterization.....	6
Table 1. 2	Polymer film characterization.....	7
Table 1. 3	Polymer film characterization.....	8
Figure 1. 1	Biodegradable polyurethanes: chemistry, functionalization and potential tissue engineering applications.....	4
Table 2. 1	Polymer film characterizatio.....	44
Table 2. 2	Scaffold characterization.	52
Figure 2.1	Schematic synthesis of biodegradable polyurethane containing disulfide bonds (PU-SS)	36
Figure 2. 2	FT-IR spectra of PU-SS polymers.	43
Figure 2. 3	DSC heating curves of PU-SS polymers.	44
Figure 2. 4	Stress-strain curves of PU-SS films.....	45
Figure 2. 5	Cyclic stretch of PU-SS films at 30% and 300% deformation.....	46
Figure 2. 6	Polymer film degradation. (A) Mass remaining of PU-SS films in PBS and 10 mM GSH at 37 °C. (B) Inherent viscosity, (C) Tensile strength and (D) initial modulus changes of polymer films with degradation in GSH. * represented significant different groups (p<0.05).	48

Figure 2. 7 Cytotoxicity of polymer degradation products and cell growth on polymer films. (A) Metabolic index of 3T3 fibroblasts cultured with medium mixed with PU-SS degradation products at 0.1 mg/mL. DMEM culture medium was a control. (B) Metabolic index of 3T3 fibroblast seeded on PU-SS films (TCPS as a control) at days 1, 3 and 5. * represented significant different groups ($p < 0.05$)49

Figure 2. 8 Polymer cytotoxicity and cytocompatibility. (A) Cytotoxicity of degradation products of PU-SS polymers. Live/dead stained 3T3 fibroblasts with cell culture medium (control) and culture medium mixed with PU-1SS degradation products. Other groups showed the similar results. Live: SYTO 10 green fluorescent nucleic acid stain; Dead: ethidium homodimer-1(EthD-1) nucleic acid stain. (B) Cytocompatibility of PU-SS films. Live /dead stained 3T3 fibroblasts on the surface of PU-1SS films at days 1, 3 and 5. TCPS was a control.....49

Figure 2. 9 Electrospun fibrous morphology of PU-SS scaffolds. (A) PU-BDO, (B) PU-0.5SS, (C) PU-1SS, (D) PU-1.5SS, and (E) PU-1.8SS.....51

Figure 2. 10 Cyclic stretch of PU-SS fibrous scaffolds at 30% deformation.52

Figure 2. 11 Scaffold degradation. (A) Mass remaining of fibrous scaffolds in GSH and PBS at 37°C. (B) Scaffold controllable degradation. Scaffolds were immersed in PBS for 14 d and then in 10 mM GSH for another 14 d. (C) PU-BDO, (D) PU-0.5SS, (E) PU-1SS, (F) PU-1.5SS and (G) PU-1.8SS scaffold morphology after 14 d immersion in 10 mM GSH solution. * represented significant different groups ($p < 0.05$).54

Figure 2. 12 Cell growth on scaffolds. (A) Metabolic index to show the 3T3 fibroblast viability on the scaffold (TCPS as a control). SEM micrographs of 3T3 fibroblasts on the surface of PU-1SS scaffold at (B) 1 d, (C) 3 d, and (D) 5 d. * represented significant different groups ($p < 0.05$).55

Figure 2. 13 Histological evaluation of explanted scaffolds in a mouse subcutaneous model. (A) H&E staining were carried out on the scaffolds implanted in mice for 1 and 2 months. Red arrows indicate location of inflammatory cells at the tissue:implant interfaces. (B) Explanted scaffold thicknesses were measured after 1 and 2 month implantation. * : $p < 0.05$, PU-1.8SS compared with other groups at 1 month and 2 month.....57

Table 3. 1. 1	Polymer film characterization.....	69
Figure 3. 1. 1	Synthesis of a biodegradable conductive polyurethane (CPU).	68
Figure 3. 1. 2	ATR-FTIR spectra of a) CPU, b) CPU0.5, c) CPU1, and d) CPU1.5.....	74
Figure 3. 1. 3	SEM images of CPU films at two levels of magnification, (A-D) at 2000x, (E-H) at 5000x.....	75
Figure 3. 1. 4	XRD spectra of a) CPU and b) CPU1.5.	76
Figure 3. 1. 5	(A) UV-vis spectra of a) undoped CPU and b) CPU1.5 in DMF. (B) Cyclic voltammogram of CPU1.5 polymer on Pt electrode in 1.0 M H ₂ SO ₄ using Ag/AgCl as reference at a scan rate of 50 mV/s.....	76
Figure 3. 1. 6	(A) Stress-strain curves of a) CPU, b) CPU0.5, c) CPU1, and d) CPU1.5 films. (B) Cyclic stretching curves of CPU films at 30% deformation.	78
Figure 3. 1. 7	CPU film degradation. (A) Mass remaining of CPU films in PBS solution at 37 °C. (B) Mass remaining of CPU films in 100 U/mL lipase/PBS solution at 37 °C. (C) Changes in electrical conductivities of CPU films during degradation in lipase/PBS solution for 14 days.* represented significant different groups ($p < 0.05$).....	80
Figure 3. 1. 8	Electrical stability. Relationship between electrical current and incubation time of CPU1.5 film in cell culture medium charged with a fixed voltage.	81
Figure 3. 1. 9	Cytocompatibility of CPU films. (A) Metabolic index of mouse 3T3 fibroblasts seeded on polymer films (TCPS as a control) at days 1, 3 and 5. +, #: $p < 0.05$, CPU1.5 compared with other groups at days 3 and 5, respectively. (B) SEM	

images of mouse 3T3 fibroblasts cultured on the polymer films at day 5.	82
Table 3. 2. 1 Polymer film characterization.....	103
Figure 3. 2. 1 Dopant-free conductive polyurethane elastomer (DCPU) synthesis. (A) Synthetic scheme of DCPU. (B) Biodegradable DCPU film and its high elasticity presented by bending, knotting, stretching and recoiling.....	102
Figure 3. 2. 2 FTIR spectra of DCPU.....	103
Figure 3. 2. 3 Electroactivity of DCPU. (A) UV-vis spectra PU-trimer, DCPU-0.3/1 and PU-COOH in DMF. (B) Cyclic voltammogram of DCPU-0.3/1 polymer on Pt electrode in 1.0 M H ₂ SO ₄ using Ag/AgCl as reference with scan rate of 50 mV s ⁻¹	104
Figure 3. 2. 4 Mechanical properties of DCPU films. (A) Stress-strain curves of DCPU films. (B) Dependence of electrical conductivity of DCPU-0.3/1 on applied strains varied from 30% to 100%. (C) Cyclic stretching of PU-trimer, DCPU-0.1/1, DCPU-0.2/1 and DCPU-0.3/1 at 30% and 300% deformations.	108
Figure 3. 2. 5 DCPU film degradation. (A) Mass remaining for DCPU in PBS at 37 °C. (B) Mass remaining for DCPU in 100 U mL ⁻¹ lipase in PBS solution at 37 °C. The changes of (C) tensile strengths, (D) initial moduli and (E) breaking strains of DCPU films with enzymatic degradation at 37 °C. * represented significant different groups (<i>p</i> <0.05).	110
Figure 3. 2. 6 Electrical stability of DCPU. (A) Changes in electrical conductivities of DCPU films in lipase/PBS solution within 14 d. (B) Relationship between electrical current and incubation time in the electrical stability test of DCPU-0.3/1 film in cell culture medium. Camphor doped PU-trimer film was used as a control.....	112

Figure 3. 2. 7 In vitro DCPU cytotoxicity and cytocompatibility. (A) Metabolic index of mouse 3T3 fibroblasts cultured with DMEM medium mixed with DCPU degradation products at concentrations of 1, 0.1, 0.01 and 0.001 mg mL⁻¹. (B) Optical microscopy images of mouse 3T3 fibroblasts cultured with DMEM medium mixed with DCPU-0.3/1 degradation products at concentrations of 0.1, 0.01 and 0.001 mg mL⁻¹. DMEM medium was used as the control. (C) Metabolic index of mouse 3T3 fibroblasts seeded on polyurethane films (TCPS as a control) at days 1, 3 and 5. (D) Scanning electron micrographs of mouse 3T3 fibroblasts cultured on the DCPU-0.3/1 (500 × and 1000× magnification), PU-trimer, DCPU-0.1/1, DCPU-0.2/1 and PU-COOH films at day 5.* represented significant different groups ($p < 0.05$).
 114

Figure 3. 2. 8 Porous DCPU scaffold. (A) Digital image and (B) SEM image of porous DCPU-0.3/1 scaffold fabricated by salt leaching..... 116

Figure 3. 2. 9 In vivo biocompatibility of DCPU porous scaffolds in a mouse subcutaneous model. H&E (A, C, E and G) and DAPI (B, D, F and H) staining of the tissue surrounding PCL (A-D) and DCPU-0.3/1 (E-H) porous scaffolds which were implanted for 2 weeks (A, B, E and F) and 4 weeks (C, D, G and H). PCL scaffolds were used as a positive control.....117

Table 4. 1. 1 Block length of polyurethane soft segment.....129

Table 4. 1. 2 Polymer film characterization.....132

Table 4. 1. 3 Scaffold characterization.....141

Figure 4. 1. 1 Synthetic scheme of (A) PVCL or PVCL-PEG-PVCL copolymer diols and (B) polyurethanes.122

Figure 4. 1. 2 ¹H-NMR spectra of (A) PVCL and (B) PVCL-PEG-PVCL copolymer diols.....128

Figure 4. 1. 3 FTIR spectra of polyurethane.....131

Figure 4. 1. 4	Typical stress-strain curves of polyurethane films in (A) dry and (B) wet states.	134
Figure 4. 1. 5	Cyclic stretching of polyurethane films in dry state with (A-E) 30% and (F-I) 300% strains and in wet state with (a-e) 30% and (f-i) 300% strains. The PU-PEG _{2K} -PVCL _{6K} film is too weak to obtain cyclic stretching curves at 300% deformation in both dry and wet states.....	135
Figure 4. 1. 6	Mass remaining for polyurethane films in (A) PBS and (B) 100 units/mL lipase/PBS at 37 °C.....	136
Figure 4. 1. 7	Cell compatibility of polyurethane films. (A) Metabolic index of 3T3 fibroblasts cultured on polyurethane films. Tissue cultured polystyrene (TCPS) was a positive control. (+) $p < 0.0003$, PU-PEG _{1K} -PVCL _{1K} compared to other groups at day 1. (++) and (&) $p < 0.0001$, PU-PEG _{1K} -VCL _{1K} compared with other groups at day 3 and day 5, respectively. (# and ##) $p < 0.05$, PU-PEG _{2K} -PVCL _{6K} compared with other groups at days 3 and 5, respectively. (B) Electron micrographs of the PU-PEG-PVCL films seeded with 3T3 fibroblasts at 5 days.....	138
Figure 4. 1. 8	Porous scaffold characterization. (A-C) Electron micrographs of (A) PU-PVCL _{6K} , (B) PU-PEG _{1K} -PVCL _{6K} and (C) PU-PEG _{2K} -PVCL _{6K} porous scaffolds. (D, E) Typical stress-strain curves of PU-PVCL _{6K} , PU-PEG _{1K} -PVCL _{6K} and PU-PEG _{2K} -PVCL _{6K} porous scaffolds in (D) dry and (E) wet states... ..	140
Figure 4. 1. 9	Cyclic stretching curves of PU-PVCL _{6K} , PU-PEG _{1K} -PVCL _{6K} and PU-PEG _{2K} -PVCL _{6K} porous scaffolds at 30% deformation in (A-C) dry and (D-F) wet states.....	142
Figure 4. 1. 10	Histological analysis of tissue responses to subcutaneous implanted scaffolds made of PU-PVCL _{6K} , PU-PEG _{1K} -VCL _{6K} , or PU-PEG _{2K} -VCL _{6K} . (A) Representative images of H/E stains of implants and surrounding tissue at 2 weeks reveal mild inflammatory cell accumulation at the implant-tissue interface (200x magnification). Significant cell infiltration was also found inside all scaffolds. (B) Cell number per area on the implants was quantified and statistically analyzed with Student's t-test (mean \pm SD, * $p < 0.05$).	143

Table 4. 2. 1 Anisotropic porous scaffold characterization in dry state.....	161
Table 4. 2. 2 Anisotropic porous scaffold characterization in wet state.....	164
Table 4. 2. 3 PU-PEG _{1K} -VCL _{6K} anisotropic porous scaffold characterization in dry state.....	169
Table 4. 2. 4 PU-PEG _{1K} -VCL _{6K} anisotropic porous scaffold characterization in wet state.....	169
Table 4. 2. 5 Mechanical properties of PU-PEG _{1K} -VCL _{6K} -5%, 8% and 10% scaffold with or without ECM in wet state.....	174
Figure 4. 2. 1 Anisotropic polyurethane porous scaffold fabrication by thermally induced phase separation (TIPS).154
Figure 4. 2. 2 Electron micrographs of anisotropic porous scaffolds prepared from 5% polymer concentrations at -80 °C quenching temperature. (A-B) PU-PVCL _{6K} (5%) in transversal (A) and longitudinal (B) directions. (C-D) PU-PEG _{1K} -VCL _{6K} (5%) in transversal (C) and longitudinal (D) directions. (E-F) PU-PEG _{2K} -VCL _{6K} (5%) in in transversal (E) and longitudinal (F) directions.	160
Figure 4. 2. 3 Stress-strain curve of anisotropic porous scaffolds in (A) longitudinal direction and (B) transversal direction at dry state; (C) longitudinal direction and (D) transversal direction at wet state.....	163
Figure 4. 2. 4 Cyclic stretch of anisotropic porous scaffolds at 30% deformation. (A), (B), (C) in dry state in longitudinal direction; (D) and (E) in dry state in transversal direction; (F), (G), (H) in wet state in longitudinal direction; (I) and (J) in wet state in transversal direction.	165
Figure 4. 2. 5 Electron micrographs of PU-PEG _{1K} -PVCL _{6K} anisotropic porous scaffolds prepared from 5%, 8% and 10% polymer concentrations at -80 °C quenching temperature. (A-B) PU-PVCL _{6K} -5% in transversal (A) and longitudinal (B) directions. (C-D) PU-PEG _{1K} -VCL _{6K} -8% in transversal (C) and longitudinal (D)	

directions. (E-F) PU-PEG_{2K}-VCL_{6K}-10% in transversal (E) and longitudinal (F) directions.168

Figure 4. 2. 6 Stress-strain curve of PU-PEG_{1K}-VCL_{6K} anisotropic porous scaffolds in (A) longitudinal direction and (B) transversal direction at dry state; (C) longitudinal direction and (D) transversal direction at wet state.170

Figure 4. 2. 7 Ball-burst test results for all anisotropic porous scaffolds. Native left ventricle (LV) was used as the control group. * represents statistically different from the native LV group.....171

Figure 4. 2. 8 Biaxial testing of PU-PEG_{1K}-PVCL_{6K}-10% in cross-fiber direction (CD) and fiber-preferred direction (LD).....171

Figure 4. 2. 9 Biohybrid scaffolds fabricated by combining PU-PEG_{1K}-VCL_{6K} anisotropic scaffolds (5%,8% and 10% w/v) with myocardium-derived hydrogel. (A), (D) and (G) Digital images of PU-PEG_{1K}-VCL_{6K}-5%, PU-PEG_{1K}-VCL_{6K}-8% and PU-PEG_{1K}-VCL_{6K}-10%.(B), (E), and (H) electron micrographs of PU-PEG_{1K}-VCL_{6K}-5%, PU-PEG_{1K}-VCL_{6K}-8% and PU-PEG_{1K}-VCL_{6K}-10% biobybrid scaffolds in transversal direction. (C), (F), and (I) electron micrographs of PU-PEG_{1K}-VCL_{6K}-5%, PU-PEG_{1K}-VCL_{6K}-8% and PU-PEG_{1K}-VCL_{6K}-10% biobybrid scaffolds in longitudinal direction
.....173

Figure 4. 2. 10 In vivo tissue compatibility of biohybrid scaffolds (PU-PEG_{1K}-VCL_{6K}-10% combined with myocardium-derived hydrogel) in a rat subcutaneous model. (A) H&E staining of the implanted scaffolds and surrounding tissues after 2 and 4 weeks of implantation; (B) Cell number in inner, middle, and outer area on the implants was quantified176

CHAPTER 1

INTRODUCTION

1.1 Introduction of biodegradable polyurethanes

Tissue engineering is an interdisciplinary field dedicated to replace or regenerate the biological functions of human tissues or organs, relying on the combination of biomaterial scaffolds, cells and bioactive molecules.[1] *In vivo* tissue engineering uses biomaterial scaffold to recruit endogenous cells for tissue repair under physiological environment, while, the *in vitro* tissue engineering constructs tissue-like implant based on biomaterial scaffolds under simulated physiological environment *in vitro*. In both of the two tissue engineering processes, biodegradable scaffolds play a critical role. An ideal tissue engineered scaffold should: (i) be biocompatible to effectively support cell adhesion, migration and proliferation and elicit a negligible immune reaction; (ii) be biodegradable at a comparable rate to that of new tissue growth at the implanted site and its degradation products should be non-toxic; (iii) have mechanical properties consistent with the native tissue and effectively transmit forces from the environment to the growing tissue over a long period of time; and (iv) have interconnected pore structure and high porosity to allow cell penetration and nutrients and oxygen transportation.[2, 3] Various biomaterials have been developed as tissue engineered scaffolds, including ceramics, natural macromolecules and synthetic polymers. Among the three groups of biomaterials,

synthetic polymers have gained much attention because of their biodegradability, good flexibility and mechanical properties.[2]

Polyurethanes are a very important class of synthetic polymers with many biomedical applications. The earliest biomedical application of polyurethanes can date to 1960s. Biomer® served as a biostable material, was the first polyurethane product for cardiovascular applications because of its durability, good mechanical properties and biocompatibility.[4] Since 1990s, to satisfy the needs for tissue engineering, biodegradable polyurethanes have drawn great interests by incorporating hydrolyzable segments into the polymer backbones.[5, 6] Compared with some commonly used biodegradable polymers, such as poly(glycolide) (PGA),[7] poly(lactide) (PLA),[8] poly(ϵ -caprolactone) (PCL)[9] and polyhydroxyalkanoates (PHA),[10] the favorable aspects of polyurethane is that its mechanical, biological and physical properties and its biodegradability can be tailored by selection of different segments based on its segmented-block structure. Further, polyurethanes can be easily processed into scaffolds by a variety of techniques,[11] rendering their great potentials as tissue-engineering scaffolds. In chapter 1, we provide a brief introduction to the synthesis of biodegradable polyurethanes, current functional biodegradable polyurethanes and their potential applications in tissue engineering (**Figure 1.1**).

1.2 Biodegradable polyurethane synthesis

Polyurethanes are synthesized through the reaction between isocyanate group and hydroxyl or amine group to generate urea or urethane groups. This reaction can

obtain both thermoplastic and thermoset polyurethanes, in which the thermoset polyurethanes are crosslinked polymer, difficult to degrade and mainly applied in industry, whereas the thermoplastic polyurethanes are linear, segmented and have been widely used in biomedical field.[12] The synthesis of thermoplastic polyurethanes involves three compounds: a diisocyanate, a diol and a dihydroxy or diamine chain extender.[12] These three compounds react to form linear, segmented copolymers consisting of hard and soft segments due to microphase separation.[13] The diisocyanate and chain extender comprise the hard segment, whereas the long linear chain of diol comprises the soft segment. The hard segments function as the physical cross-links and determine the high glass-transition temperature (T_g), high melting temperature (T_m), modulus and strength of polyurethanes.[11, 14] The soft segments determine the low T_g , low T_m , and elasticity of polyurethanes.[14, 15] Besides, to realize the degradability of the segmented polyurethanes, diols containing hydrolyzable bonds are usually hired as the soft segments in polyurethane backbones.[16] Therefore, varying the soft and hard segments in polyurethane backbone can tailor its thermal and mechanical properties and degradation profile for a specific tissue engineering application.

Thermoplastic polyurethanes can be synthesized via one- or two-step methods. In one-step method, all reactants including diisocyanate, diol, chain extender and catalyst are mixed together and reacted at once, which is hard to control the architecture of polyurethane.[12] Currently, the synthesis of polyurethane is usually via two-step method, in which diol and diisocyanate are reacted first, followed by the

addition of chain extender in the second step. The two-step method allows better control over polyurethane structure and properties.[17]



Figure 1.1 Biodegradable polyurethanes: chemistry, functionalization and potential tissue engineering applications.

Diisocyanates react with diamines or dihydroxys via a nucleophilic addition. The diisocyanates used to synthesize biodegradable polyurethanes are listed in **Table 1.1**. The first generation of polyurethanes are typically synthesized from aromatic diisocyanate, 4,4'-methylenebis(phenylisocyanate) (MDI) and toluene diisocyanate (TDI).[18, 19] However, their toxic and carcinogenic degradation

products, aromatic diamines greatly limit their application in biomedical field.[19, 20] Hence, the second generation of biodegradable polyurethanes are generally based on aliphatic (e.g., 1,4-butane diisocyanate (BDI), 1,6-hexamethylene diisocyanate (HDI) and lysine-based diisocyanate (LDI)) or cyclophatic diisocyanates (e.g., isophorone diisocyanate (IPDI) and 4,4'-methylene bis(cyclohexyl isocyanate) (HMDI)).

Diols used in biodegradable polyurethane synthesis have two hydroxyl end groups and polyether, polyester, polycarbonate, polydimethylsiloxane, or polybutadiene backbone, although most are polyether or polyester diols. The commonly used diols in formulating biodegradable polyurethanes are summarized in **Table 1.2**. Most polyether diols (e.g., poly(ethylene oxide) (PEO) and poly(propylene oxide) (PPO)) and polyester diols (e.g., PCL, poly(D,L-lactide) (PDLLA), poly(glycolide)) are prepared by ring-opening polymerization.[11, 12, 21] In these diols, PCL diol is arguably the most widely investigated diol in biodegradable polyurethane synthesis because of its good biocompatibility and low T_g (-60 °C) which can result in high flexibility.[22]

Conventional chain extender, such as 1,4-butanediol (BDO), ethylene glycol (EG), ethylenediamine (ED) and 1,4-butanediamine (BDA), are listed in **Table 1.3**. BDA is most often used as chain extender in biodegradable polyurethane preparation since it is a naturally occurring compound, also known as putrescine.[15, 23] One of the important functions of chain extender is to promote highly ordered hard segments in polyurethane backbone.[19] Hence, chain extenders are usually short-chain compact with symmetrical structure to favor better ordering of hard segments.

Table 1.1 Diisocyanates used to synthesize biodegradable polyurethanes

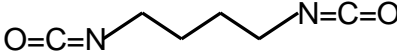
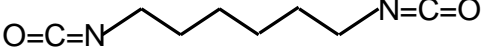
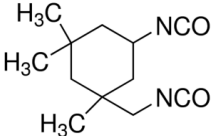
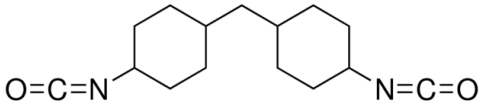
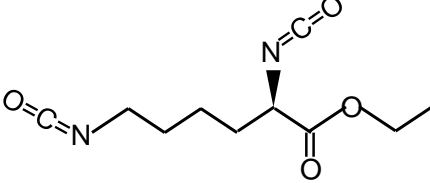
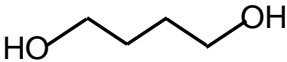
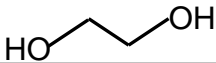
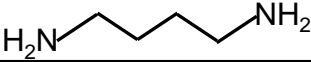
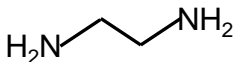
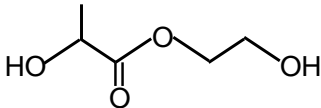
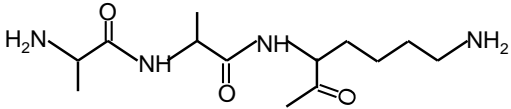

Chemical name	Structure
1,4-butane diisocyanate (BDI)	
1,6-hexamethylene diisocyanate (HDI)	
isophorone diisocyanate (IPDI)	
4,4'-methylene bis(cyclohexyl isocyanate) (HMDI)	
Lysine ethyl ester diisocyanate (LDI)	

Table 1.2 Diols used to synthesize biodegradable polyurethanes

Chemical name	Structure
Poly(ethylene oxide) (PEO)/Poly(ethylene glycol) (PEG)	
Poly(propylene oxide) (PPO)	
Poly(D,L-lactide) (PDLLA)	
Poly(ε-caprolactone) (PCL)	
Poly(glycolide)	
poly(1,6-hexamethylene carbonate) (PHC)	
poly(trimethylene carbonate) (PTMC)	
poly(δ-valerolactone-co-ε-caprolactone) (PVCL)	
Poly(ε-caprolactone-co-ethylene glycol-co-ε-caprolactone) (PCL-PEG-PCL)	

Table 1.3 Chain extenders used to synthesize biodegradable polyurethanes

Chemical name	Structure
1,4-Butanediol (BDO)	
Ethylene glycol (EG)	
1,4-Butanediamine (BDA)	
Ethylenediamine (ED)	
Lactic acid-co-ethylene glycol	
Ala-Ala-Lys	
Aniline trimer	

1.3 Conventional biodegradable polyurethane synthesis

Conventional biodegradable polyurethanes are synthesized from commonly-used diisocyanates (e.g., HDI, BDI, LDI, IPDI and HMDI), diols (e.g., PCL,

poly(ethylene glycol) (PEG), and PDLLA), and chain extenders (e.g., BDO, BDA and EG). Their thermal, mechanical and biological properties and biodegradability are determined by these three blocks.

For biodegradable polyurethanes based on aliphatic diisocyanates, BDI and HDI are the most widely used two diisocyanates because of their relatively non-toxic degradation products, 1,4-butanediamine and 1,6-hexanediamine.[14, 24, 25] Besides, their symmetric chemical structures lead to better ordered hard segments through hydrogen bonds, thus resulting in higher strength and elasticity.[12] De Groot et al prepared biodegradable polyurethanes based on HDI and BDI with polycaprolactone diol (MW=2000) as soft segment and 1,4-butanediamine as chain extender.[23] HDI based polyurethane showed higher tensile strength and breaking strain, however larger permanent deformation than BDI based polyurethane, all due to less ordered hard segments. Cycloaliphatic diisocyanates, such as IPDI and HMDI, also have been used in biodegradable polyurethane synthesis, although to a lesser extent than the aliphatic diisocyanates.[26, 27] The cyclo-hexane rings in cycloaliphatic diisocyanates limit the flexibility of polymer chains, thus result in stiffer polyurethanes compared to those based on aliphatic diisocyanates. Furthermore, amino acid-derived diisocyanates (e.g., LDI) have been widely used in biodegradable polyurethane synthesis because of their non-toxic degradation amino acid products and higher hydrolytic degradation rate due to the hydrolyzable ester bonds in hard segments.[28-31]

Copolymer diols with two or more blocks have been utilized as soft segments in polyurethane backbone to further control the physical and chemical

properties and degradation behavior of polyurethanes, such as poly(δ -valerolactone-co- ϵ -caprolactone) (PVCL), PCL-PEG-PCL, PEO-PPO-PEO, poly(trimethylene carbonate)-poly(ethylene oxide)-poly(propylene oxide)-poly(ethylene oxide)-poly(trimethylene carbonate) (PTMC-PEO-PPO-PEO-PTMC).[25, 32-35] Some of these copolymer diols are listed in **Table 2**. The physical, chemical properties and degradation rate of polyurethanes are tunable by varying the block length and hydrophilicity of the copolymer diols. For example, PVCL copolymer diol reached the minimal crystallinity when the feeding ratio of VL to CL was 50/50, consequently resulting in that the polyurethane based on this copolymer diol had lower initial modulus and tensile strength, but higher elasticity than that based on pure semi-crystalline PCL diol.[25] In addition, increasing the block length of PVCL copolymer diol from 2000 to 6000 significantly decreased the initial modulus and tensile strength of the polyurethane, which is consistent with the rubber thermodynamic theory. The theory indicates the initial modulus of elastomers increases with the decreasing average molecular weight between the physical cross-link points.[36] Because of the lack of specific knowledge about the optimal period over which the implanted scaffold should be present, the degradation rate of tissue engineered scaffold should be tunable to meet different requirements.[37] To fabricate polyurethane scaffold with slower degradation rate, polycarbonate diols are introduced in soft segments.[25, 35, 37] For example, poly(1,6-hexamethylene carbonate) (PHC) was incorporated into the PCL soft segment (PHC-co-PCL) to greatly reduce the hydrolytic degradation rate of the polyurethanes.[37] To reach faster degradation rate, hydrophilic moieties (e.g., PEG) can be introduced into soft segment in polyurethane backbone.[32] For

example, the incorporation of PEG into PCL soft segment (PCL-PEG-PCL) significantly increased the polyurethane hydrolytic degradation rate.[32] It is worth noting that the incorporation of PEG may not be able to accelerate the enzymatic degradation of polyurethane in lipase/PBS solution, although it can greatly accelerate the hydrolytic degradation of polyurethane.[38] Lipase has been used to accelerate the degradation of polymers containing ester, amide, carbonate, urea, and urethane groups.[25, 39, 40] One reason to explain the phenomenon is ether group is less susceptible to lipase than ester group.[41, 42] The other reason is introducing PEG segment into polyurethane backbone led to an increase of polymer surface hydrophilicity, which would reduce the protein adsorption, thus compromise the polymer enzymatic degradation.[42, 43]

Chain extenders with hydrolyzable bonds (e.g., ester and phosphate ester) can also accelerate the hard segment degradation.[44, 45] For example, a degradable ester chain extender based on lactic acid and ethylene glycol was introduced into a polyurethane backbone, which contributed to the accelerated hydrolytic degradation of the polyurethane *in vitro*.[44] Moreover, amino acid based chain extenders have been utilized to improve the enzyme mediated degradation and biocompatibility of polyurethanes.[19, 46] Some of the hydrolyzable chain extenders, amino acid based chain extenders, and some special chain extenders used in functional polyurethanes which will be discussed in the following sections are also listed in **Table 3**.

1.4 Functional biodegradable polyurethane design

Besides those intrinsic advantages of biodegradable polyurethane discussed above, functional designed polyurethane will be endowed with a specific function to meet the relevant requirements in tissue repair and regeneration. For example, conductive polyurethane scaffold can enhance the cell-to-cell interactions by delivering electrical signals. Shape memory polyurethane scaffold can be implanted via minimally invasive surgery and adapt to defects after stimulus activation. Waterborne polyurethane is non-toxic and environmentally friendly. The amino-acid-based polyurethanes possess good biocompatibility, biodegradability, and some specific biological functionality (e.g., enzyme liability and enhanced cell adhesion). Antibacterial polyurethane wound dressing can prevent bacterial infection to achieve better and faster wound healing. And nonthrombogenic polyurethane has enhanced blood compatibility, thus is promising for cardiovascular applications.

1.4.1 Conductive polyurethane

Conductive biomaterials, including conductive composites and polymers, have gained great interest as smart tissue engineered scaffolds because of their impressive performance in regulating cell behaviors (e.g., adhesion, migration, proliferation and differentiation) and promoting tissue repair and regeneration (e.g., myocardium, nerve, muscle, skin and bone).[47-51] Conductive composites consist of biodegradable polymers (e.g. polylactide, polycaprolactone and polyurethane) and organic conductive polymers (e.g. polyaniline, polypyrrole and poly(3,4-ethylenedioxythiophene (PEDOT)) or inorganic additives (e.g. metals, carbon

nanotube, graphene), in which the biodegradable polymers provides mechanical behavior, and the additives provide electric conductivity.[48, 52-54] Biodegradable polyurethanes in particular have great potential to be involved in conductive composites because of their tunable mechanical properties, good elasticity, biodegradability, good biocompatibility and ease of processing into scaffolds for tissue engineering application.[25, 37] Therefore, polyurethanes blended with conductive materials have been widely investigated.[55-58] For example, a biodegradable conductive nanofibrous scaffold based on polyurethane and carbon black was prepared by electrospinning, in which the polyurethane was synthesized from PCL diol, polydimethylsiloxane (PDMS) diol, and HDI.[57] The conductivity of the nanofibrous scaffold increased nearly 6 orders of magnitude with the carbon black amount increasing from 0% to 40% in the composites. PC12 cells cultured on the nanofibrous scaffold exhibited improved cell proliferation and inter-cellular communication and interaction. In another example, a patterned polyurethane substrate was coated with gold or titanium by electron beam evaporation deposition.[58] C2C12 cells were cultured on the substrates for 7 days. The conductive substrates were shown promote myogenic differentiation and maturation, as indicated by the upregulation of myogenic regulatory factors *Myf5*, *MyoD* and myogenin (*MyoG*).

However, those conductive materials dispersed in or coated on polyurethane matrices without covalent bonding, which may lead to poor controllability in mechanics and conductivity due to the immiscibility of two materials. Besides, after the degradation of polyurethane, the residual conductive materials may cause chronic

inflammation and infection and even implant failure. It is hypothesized that covalently conjugating conductive oligomers (e.g., aniline oligomers) into the polyurethane backbone to achieve a conductive polymer with desirable degradable, electrical and mechanical properties may address the above concern. The segmented-block structure of polyurethane with three tunable blocks, diisocyanate, diols and chain extender, can just provide the possibility to realize the hypothesis. A electroactive biodegradable polyurethane was synthesized from poly(glycerol sebacate), aniline pentamer and HDI, doped by camphorsulfonic acid (CSA) and then processed into film by solvent casting.[59] The conductivities of the polymer films with different amounts of aniline pentamer in polyurethane backbone ranged from 1.4×10^{-6} to 8.5×10^{-5} S/cm, which were relative low but sufficient to conduct electrical signals *in vivo*. [60] RSC96 Schwann neural cells were cultured on the conductive polyurethane films and the abilities of these conductive films to enhance myelin gene expression and sustained neurotrophin secretion were successfully demonstrated. Furthermore, the neurotrophin medium suspension produced from RSC96 cells-laden conductive polyurethane films could induce the neurite growth and elongation of PC12 cells.

1.4.2 Shape memory polyurethane

Shape memory polymers (SMPs) are a group of smart, adaptive materials with the ability to recover their shapes via exposure to a stimulus, such as temperature,[61-63] magnetic field,[64, 65] light,[66, 67] and ultrasound,[68, 69] et al. Their great potentials have been explored in the past decade on various biomedical applications, such as self-tightening sutures,[62] cardiovascular stents,[63, 70]

dialysis needle adapters,[71] and thrombectomy device for clot removal,[72] Besides, SMPs have also been of great interest as tissue engineered scaffolds because of their ability to allow minimally invasive surgery implantation as well as to adapt themselves to the native physiological environment to regulate cell behavior.[57] Polyurethane-based SMP have been widely developed for tissue engineering application because of their good biocompatibility, elasticity and tailorable transition temperatures (T_g and T_m).[73] Most reported tissue engineered scaffolds based on shape memory polyurethane are triggered by thermal stimulus, in which their shape recovery temperature is near or slightly higher than body temperature.[74-76] For example, a polyurethane SMP foam based on PCL, hydroxyapatite, castor oil and HDI was fabricated to induce bone regeneration.[74] The SMP foam was implanted into a rabbit femoral defect with a compact shape to realize minimally invasive delivery. Subsequently, the compacted SMP foam self-matched the bone defect after thermal stimulation (40 °C saline). Fast bone ingrowth and neovascularization were observed at 12 weeks post-surgery. The polyurethane shape recovery temperature which is mainly determined by T_g or T_m is mostly tuned by changing the component and the block length of soft segments, and the soft-to-hard segment ratio in polyurethane backbone.[77-79] For example, in a PCL based polyurethane, by changing the PCL block length from 2000 to 10000, the lowest shape recovery temperature which is more practical than T_m increased from 23.5 to 48.2 °C.[77]

1.4.3 Waterborne polyurethane

Waterborne polyurethanes (WBPU) have attracted increasing attention in biomedical field because compared with conventional polyurethane, their green and water-based synthetic process can avoid the possible toxicity from residual organic solvents, thus being more biocompatible.[80-82] The most commonly used biodegradable WBPU for tissue engineering application is anionic polyurethane which contains anionic hydrophilic segment with carboxyl group in the backbone via self-emulsion method, such as 2,2-bis(hydroxymethyl)propionic acid (DMPA) and lysine.[80, 81, 83, 84] Jiang et al. have synthesized series of WBPU from PCL and PEG as soft segments, IPDI, and L-lysine with carboxyl groups as chain extender.[85, 86] The obtained WBPU had good mechanical properties, biocompatibility, biodegradability and can be processed into porous scaffold by freeze-drying, thus, were promising for soft tissue engineering. Tsai et al. prepared a WBPU based on PCL, polyethylene butylenen adipate diol, IPDI, DMPA and ethylenediamine, which was then processed into porous scaffold by freeze-drying or particulate leaching method.[80] The obtained WBPU had good mechanical properties and cell compatibility, and its porous scaffold can induce the chondrogenic differentiation of human bone marrow-derived mesenchymal stem cells (MSCs) as early as 7 days after induction.

1.4.4 Amino-acid-based polyurethane

Synthetic polypeptides have been explored for various biomedical applications because of their unique physical, chemical and biological properties.[87] However,

their unfavorable physico-mechanical properties has led to the development of amino-acid-based polymers.[88] Amino-acid-based polyurethanes can be classified into two main categories: polyurethanes surface-modified by peptide and polyurethanes containing amino acids in backbone or as pedant. Many groups have reported grafting RGD peptide, the most common peptide responsible for cell attachment to the extracellular matrix (ECM), onto the polyurethane surface to improve cell adhesion.[89-91] For example, RGD peptide was firstly conjugated to a PEO-MDI-PEO copolymer via sulfonyl chloride activation routes, and then grafted onto the polyurethane surface non-covalently by physical blending.[89] The obtained RGD peptide grafted polyurethane could significantly promote the attachment of the human umbilical vein endothelial cells (HUVECs), and subsequently affected the cell growth positively, suggesting its potential for cardiovascular tissue engineering.

Covalently conjugating amino acids into the hard segments in polyurethane backbone as diisocyanate (LDI) or chain extenders can endow the polyurethane with improved biocompatibility and biodegradability, and some specific biological functionality such as enzyme liability or enhanced cell attachment.[19, 46, 92-94] A YIGSR peptide was introduced into a polyurethane backbone as chain extender to enhance the endothelialization of the polyurethane as small diameter vascular graft.[92] L-tyrosine based and lysine based chain extenders have been conjugated into the polyurethane backbone to promote the polymer biocompatibility and biodegradability.[19, 93, 94] An AAK peptide which can be specifically cleaved by elastase was utilized as chain extender for polyurethane preparation to improve the polymer enzymatic degradation.[46] Besides, Hong et al. grafted the RGD peptide

onto a polyurethane backbone as a pedant via amide bonds to improve the endothelial cell adhesion.[95]

1.4.5 Antibacterial polyurethane

Bacterial infection impedes wound healing significantly and results in disfiguration or even life threat.[96] Antibacterial wound dressing can inhibit the bacterial growth within the wound and on the dressing itself. Polyurethane is promising as wound dressing because of its good barrier properties and oxygen permeability.[97] Various antibacterial agents have been reported to improve the antibacterial efficiency of polyurethane wound dressing, such as silver,[98, 99] quaternary ammonium salts,[100] curcumin,[101] and antibiotics.[102] Those antibacterial agents can either be physically blended with polyurethane or covalently anchored to the polyurethane wound dressing. For example, antibacterial polyurethane nanofibers containing argentum (Ag) nanoparticles were fabricated by electrospinning.[98] The obtained polyurethane/Ag fabrics showed excellent antimicrobial effect against *Staphylococcus aureus* and *methicillin resistant Staphylococcus aureus*. In another example, an electrospun polyurethane scaffold containing mupirocin (Mu), a commonly used antibiotic in wound care, had good antibacterial activity against *Staphylococcus aureus*. [102] However, the released antibacterial agents may kill or weaken cells exposed in the wounded area and with the leaching-out of those agents, bacteria become resistant against those diluted antibacterial agents.[103, 104] Hence, to avoid these concerns, covalently incorporating antibacterial agents to polyurethane wound dressing has been

developed.[105, 106] An epoxy-terminated polyurethane prepolymer (EPU) based on castor oil which has antibacterial property as soft segment was synthesized and mixed with glycidyltriethylammonium chloride (GTEAC), a reactive bactericidal agent, to form polyurethane membrane through cocuring of EPU and GTEAC with putrescine.[105] The obtained polyurethane membrane with 50% GTEAC showed effective antibacterial activity with acceptable cell compatibility. In another approach, chitooligosaccharide (COS), a low molecular weight chitosan with antibacterial activity, was grafted onto the polyurethane surface based on the self-polymerization of dopamine.[106] The antibacterial activity of the polyurethane membrane against *Escherichia coli* and *Staphylococcus aureus* can be significantly increased by incorporation of COS onto polymer surface.

1.4.6 Nonthrombogenic polyurethane

Biodegradable polyurethanes have been investigated for device applications with extended blood contact, because of their good mechanical properties, biocompatibility and processability. To enhance their nonthrombogenicity, nonthrombogenic moieties have been physically or chemically combined with biodegradable polyurethanes, such as phosphorylcholine (PC),[107-109] sulfobetaine,[110, 111] sulfate,[112, 113] and PEG.[92, 114] A biodegradable polyurethane and a PC copolymer, poly(2-methacryloyloxyethyl phosphorylcholine-co-methacryloyloxyethyl butylurethane) (PMBU) were blended and electrospun into fibrous scaffold.[107] The platelet deposition on the polyurethane/PMBU blended scaffold decreased significantly with increasing PMBU amount. Besides physically

blending, polyurethane surface modification by nonthrombogenic moieties have also been studied.[109, 111] Sulfobetaine was immobilized on the polyurethane surface to enhance its blood compatibility.[111] In another approach, those nonthrombogenic moieties can be covalently incorporated into the polyurethane backbone or onto polymer chain as pedants. For example, biodegradable polyurethanes with PC or sulfate pedant groups were designed and synthesized based on the incorporated DMPA segments with carboxyl groups in the polyurethane backbone.[108, 112] Those PC or sulfate modified polyurethanes had good thromboresistance *in vitro*. To further amplify the capacity of grafted nonthrombogenic moieties, incorporating those moieties into polyurethane backbone is an effective way. PEG diols and sulfobetaine diols were introduced into polyurethane backbone to achieve nonthrombogenic polymers for cardiovascular applications.[92, 110]

1.4.7 Others

Besides the polyurethanes mentioned above, there are some other functional polyurethanes developed for tissue engineering application. For example, the degradation controllable polyurethanes with tunable degradation rate to match that of new tissue growth. A series of poly(thioketal)urethane (PTK-UR) scaffolds were synthesized that can degrade specifically by cell-generated reactive oxygen species (ROS).[115] The obtained ROS-degradable PTK-UR scaffold showed cell-mediated controllable degradation rate matching that of tissue in-growth in a rat subcutaneous implantation model, suggesting their potential for guiding new tissue formation.

1.5 Polyurethane scaffolds for tissue engineering applications

Tissue engineering scaffolds have been fabricated from biodegradable polyurethanes by applying various techniques, such as particle leaching,[116, 117] thermally-induced phase separation (TIPS),[118] freeze-drying,[84, 119] and electrospinning[120-122]. The polyurethane tissue engineered scaffolds applied in cardiovascular, musculoskeletal and neural regeneration are discussed in the following sections.

1.5.1 Polyurethane scaffolds for cardiovascular applications

Biodegradable polyurethanes are attractive materials for cardiovascular regeneration because of their good biocompatibility, strong mechanical properties and high elasticity similar to those of cardiovascular tissues.[123, 124] In recent years, polyurethane scaffolds mechanically matching native cardiovascular tissues have aroused great attentions because mechanical mismatch between implanted scaffold and native tissue would trigger foreign body reactions and/or even implant failure.[125, 126] A bilayer polyurethane scaffold was fabricated as small diameter vascular graft with a highly porous inner layer by TIPS technique to allow cell penetration, and a fibrous reinforcing outer layer by electrospinning to provide mechanical support.[127] Both layers were made of polyurethane synthesized from PCL diol, BDI and putrescine. The obtained bilayer polyurethane scaffold possessed mechanical properties (compliance = $4.6 \pm 0.5 \times 10^{-4}$ mmHg⁻¹, β stiffness at around 20, elastic modulus = 1.4 ± 0.4 MPa comparable to those of healthy human coronary arteries (compliance = $14.1 \pm 5.9 \times 10^{-4}$ mmHg⁻¹, β stiffness = 16.9 ± 7.1 , elastic modulus =

1.4 ± 0.7 MPa).[128] Besides, the scaffolds were able to maintain a high level of muscle-derived stem cells prior to prospective implantation in an animal model.

To improve the bioactivity of polyurethane scaffolds, natural materials, such as collagen, elastin/elastin-like peptide (ELP) and fibrin have been combined with polyurethane to form a synthetic/natural material composite for cardiovascular repair and regeneration.[120, 129-131] A polycarbonate-urethane was synthesized from PHC, HDI and BDO, and then electrospun into fibrous scaffold.[129] ELP-4 was subsequently grafted on the fibrous scaffold surface to enhance the smooth muscle cell adhesion. In another approach, collagen type I particles and elastin were blended with polyurethane solution respectively and electrospun into aligned scaffolds.[120] The obtained aligned collagen/polyurethane and elastin/polyurethane scaffolds favored the growth of smooth muscle cells.

Conductive polyurethanes have also been developed as cardiac patch because native cardiac muscle is an electroactive tissue and can transfer electrical signals and allow the heart to beat.[132] Conductive materials may support the electrical signal transferring process and improve the cardiac patch contractibility. Baheiraei et al. synthesized a series of electroactive polyurethanes based on PCL, PEG, IPDI and aniline pentamer, which were then processed into porous scaffolds by particulate leaching method.[133, 134] The obtained scaffold had conductivity at $10^{-5} \pm 0.09$ S/cm, and can support neonatal cardiomyocytes adhesion and growth. Besides, more expression of the cardiac genes involved in muscle contraction and relaxation and cytoskeleton alignment was observed on the electroactive polyurethane scaffold than those on PCL and tissue culture plate.

There are some other functional designs in polyurethane based scaffolds in order to satisfy specific application requirements for cardiovascular tissue engineering. For example, for small diameter vascular grafts, anti-thrombogenesis, intimal hyperplasia inhibition and rapid and adequate endothelialization on graft lumen are required. Many approaches have been utilized to reduce thrombogenicity and improve intimal hyperplasia inhibition of biodegradable polyurethanes for small diameter vascular grafts, such as surface/compositional modification with nonthrombogenic moieties,[107-109] nitric oxide (NO) release,[135-137] drug release[138, 139] and endothelialization.[140, 141] Polyurethanes modified with nonthrombogenic moieties such as PC, sulfate, PEG and sulfobetaine have been discussed above and are candidate materials for small diameter vascular grafts. Besides, NO producing polyurethane was able to reduce platelet adhesion, inhibit smooth muscle cell growth and stimulate endothelial cell growth.[135] Our group mixed dipyridamole (DPA), a clinically used antithrombogenic drug, together with a biodegradable polyurethane and then electrospun into fibrous scaffold.[138] The DPA loaded polyurethane scaffold reduced human platelet deposition, inhibited proliferation of human aortic smooth muscle cell and improved endothelial cell proliferation. To improve endothelialization, heparin and vascular endothelial growth factor (VEGF) were immobilized on polyurethane electrospun fibrous scaffold via self-polymerization and deposition of DPA.[140] The result showed the surface heparinization significantly inhibited platelet deposition and VEGF immobilization significantly increased endothelialization.

1.5.2 Polyurethane scaffolds for musculoskeletal applications

Polyurethane scaffolds have been investigated for their applications in skeletal muscle tissue engineering. There are several cues important in designing skeletal muscle tissue engineered scaffolds. First, scaffold stiffness plays an important role in skeletal muscle regeneration. Generally, polyurethane scaffolds with modulus similar to healthy muscle tissue (~12 kPa) are optimal for skeletal muscle cell growth and differentiation.[142-144] However, Andriani et al. hypothesized since skeletal muscles also attach to bones via tendons *in vivo*, biomaterials with moduli in the range of those of tendons and bones (hundreds of MPa to several GPa) can also be used as human muscle cell culture substrates.[145] The synthesized polyurethane acrylate with tendon-like surface moduli in the higher 150 MPa to 2.4 GPa range can support long-term *in vitro* culture of human myoblasts (proliferation, differentiation and sustenance beyond 35 days). Besides, as discussed above, polyurethane scaffolds with electroactivity can also promote myoblast adhesion, proliferation and differentiation.[59, 146, 147] In addition, scaffold micro/nano-scale topography is also a major influence on skeletal muscle cell culture because the skeletal muscle structure is highly organized and consists of long parallel bundles of multinucleated myotubes that are formed by differentiation and fusion of myoblast satellite cells.[148] Riboldi et al. fabricated a highly oriented fibrous polyurethane scaffold by electrospinning which enabled skeletal myogenesis *in vitro* by aiding in myoblast adhesion, myotube alignment, and noncoplanar arrangement of cells.[149] In another approach, Shen et al. manufactured micropatterned polyurethane films with microchannels by ultra violet (UV) micro-embossing.[150] It turned out the

dimensions of both channel and wall would significantly affect the skeletal muscle cell elongation.

Biodegradable polyurethane scaffolds have also been investigated for their potential to treat irreparable meniscus defects clinically.[151-153] Dhollander et al. studied a treatment of painful, irreparable partial meniscal defects using biodegradable polyurethane scaffold implant with a minimum 5-year follow-up.[151] The polyurethane meniscal implant can improve knee joint function and reduce pain. However, the chondroprotective ability of the implant was questioned and a relatively high implantation failure rate (~40%) was noticed during the follow-up period. Good functional outcome of biodegradable polyurethane meniscal scaffolds was also confirmed by Schüttler et al. and Monllau et al. with a 4-year and 5-year follow-up, respectively.[152, 153] In Monllau's study, polyurethane scaffold resorption was observed and the implanted scaffold didn't show normal meniscus tissue although the incomplete in-growth of new meniscus-like tissue was observed at the last follow-up.[153]

Biodegradable polyurethane scaffolds also have shown great potential in bone regeneration because of their strong elasticity, the ability to support calcium phosphate crystal formation (calcification) *in vivo*, and good processability.[154] It is reported that the scaffold hydrophilicity can significantly affect the calcification.[155] A poly[(R)-3-hydroxybutyrate] (PHB)-based polyurethane with improved hydrophilicity by incorporating hydrophilic PEG segment into soft segments possessed enhanced mineralization capability.[156] Similar results were published by Gogolewski et al., in which the newly-formed bone in the polyurethane scaffold with higher hydrophilicity

had more bone mineral than the bone formed in the scaffolds with less hydrophilicity.[157] Another way to promote calcification is incorporation of carbon nanotubes to scaffolds due to their ability to induce nucleation of hydroxyapatite.[158] A polyurethane foam with surface deposition of carbon nanotubes can accelerate the precipitation of calcium phosphate.[159]

In order to enhance the bioactivity of polyurethane scaffold for bone regeneration, various bioactive materials have been introduced, such as native ECM proteins,[160] bioactive ceramics,[161, 162] and growth factors.[163] For example, a polyurethane/hydroxyapatite scaffold was fabricated by electrospinning and showed the ability to enhance the viability of osteoblasts and human embryonic mesenchymal progenitor cells, calcification, and collagen deposition.[161] In another approach, a polyurethane scaffold encapsulating recombinant human bone morphogenetic protein-2 (rhBMP-2), an osteoinductive growth factor, was fabricated.[163] The obtained rhBMP-2 encapsulated polyurethane scaffold was then implanted into a rat femoral plug defect, which supported bone ingrowth only after 2 weeks of implantation. Besides, more new bone formation in polyurethane scaffold incorporating rhBMP-2 powder were observed than that in scaffold incorporating rhBMP-2 encapsulated in poly(L-lactide-co-glycolic acid) (PLGA) microspheres at 4 weeks.

1.5.3 Polyurethane scaffolds for neural applications

Conductive polyurethane scaffolds have gained great attentions for neural tissue engineering, because neurons are electrically active cells that their electrical

activity originates from the depolarization of plasma membrane and the scaffold conductivity may support this process.[164] An aligned polyurethane nanofibers were fabricated by electrospinning and then decorated with gold nanoparticles.[165] Rat pheochromocytoma (PC-12) cells were then seeded on the polyurethane nanofibers. It was found that the incorporation of gold nanoparticles enhanced the PC-12 attachment and proliferation. Besides, with nerve growth factor (NGF) and electrical stimulations, more neurite outgrowth and elongation were observed. In another example, a conductive composite based on polyurethane, poly(3,4-ethylenedioxythiophene) (PEDOT) doped with poly(4-styrenesulfonate) (PSS), and liquid crystal graphene oxide (LCGO) was prepared.[166] The obtained conductive composite can support human neural stem cell (NSC) growth and differentiation to neurons and supporting neuroglia. Besides, electrical stimulation can enhance the NSC differentiation on the conductive composite.

1.5.4 Polyurethane scaffolds for wound healing

Biodegradable polyurethanes are promising candidates for wound healing due to their good barrier properties and oxygen permeability.[97] However, the antibacterial activity and hydrophilicity of polyurethanes still need improvements to prevent bacterial infection and enhance cell affinity, respectively.[167] To enhance the antibacterial activity, various antibacterial agents (e.g., silver, quaternary ammonium salts, curcumin, and antibiotics) have been combined with polyurethanes as discussed above. For example, a porous polyurethane scaffold incorporating hydrophobic vancomycin free base, a tricyclic glycopeptide antibiotic, was fabricated

and can significantly reduce infection in a rat femoral segmental defect model.[168] To improve the hydrophilicity of antibacterial polyurethanes, hydrophilic moieties can be incorporated into polyurethanes, such as dextran,[169] cellulose acetate (CA),[167] and COS.[106] Polyurethane, water-soluble dextran, and antibiotic ciprofloxacin HCl (CipHCl) were mixed and electrospun into fibrous scaffold.[169] The composite scaffold presented good bacterial activity against both of Gram-positive and Gram-negative bacteria, and favorable cell-material interaction. Similar results were observed in the development of an antibacterial electrospun scaffolds based on polyurethane, highly hydrophilic CA and antibacterial protein zein.[167]

Besides antibacterial agents and hydrophilic moieties, antioxidant moieties have also been incorporated into polyurethanes to protect tissue from oxidative stress during wound healing process. Oxidative stress is caused by overproduction of ROS, a hallmark of inflammation and the pathogenesis of various diseases, and thus leads to tissue damage, infection and chronic wound healing.[170, 171] An antioxidant moiety, ascorbic acid was introduced into polyurethane backbone as chain extender and the obtained antioxidant polyurethane can scavenge free radicals and protect cardiomyocytes from oxidative stress induced cell death , indicating its potential for treatment of various diseases related to oxidative stress, such as chronic wound healing and myocardial infarction.[172] Besides, conductive polyurethanes have also been investigated for wound healing since conductive polymers can scavenge free radicals.[173] An antioxidant polyurethane/siloxane dressing was fabricated based on castor oil as antibacterial segment and aniline trimer as conductive segment.[174] The obtained polyurethane/siloxane dressing membrane showed good antimicrobial

activity, antioxidant efficiency and supported fibroblasts growth. In a rat model of skin wound healing, the electroactive, antibacterial and antioxidant dressing can promote wound contraction and collagen deposition, and encourage vascularization in the wounded area.

1.6 Research goal and specific aims

As discussed in **1.5.1**, biodegradable polyurethane scaffolds mechanically matching with native artery have been studied.[127] However, it is rarely reported that polyurethane based cardiac patch mechanically mimics the native myocardium. Besides, to our knowledge, no report is found to combine a myocardium-derived hydrogel with synthetic polyurethane scaffolds to form bioactive cardiac patch. Hence, we seek to develop a myocardium mimic from biodegradable polyurethane porous scaffold and myocardium-derived hydrogel as a cardiac patch, which has both mechanical match with native myocardium and high bioactivity. Moreover, as mentioned in **1.5.1**, conductive polyurethane scaffolds can promote cardiomyocytes attachment, proliferation and cell-to-cell interaction.[133, 134] Thus, we also designed series of novel electroactive polyurethanes for myocardial tissue engineering. In addition, controllable degradation is one of the most important characteristics of an ideal tissue engineered scaffold. Therefore, in this thesis, we designed a variety of novel functionalized polyurethanes for cardiac tissue repair and regeneration from three aspects: degradation controllability, electroactivity, and mechanical match with native myocardium. These three aspects are divided into three chapters for discussion, which are listed below.

In chapter 2, to realize degradation controllability, reduction-sensitive biodegradable polyurethanes with disulfide bonds in the polymer backbone (PU-SS) were synthesized. Because a reducing agent, glutathione (GSH), naturally exists in human body, we hypothesized the degradation of the reduction-sensitive polyurethane scaffold can be triggered in the presence of the GSH *in vivo* after implantation. Besides, intramuscular injection of GSH can also be used as a safe on-demand trigger to induce fast degradation of the implant *in vivo*. [175, 176] The chemical structure, mechanical and degradation properties of the synthesized PU-SS polymer films were examined. The toxicity of degradation products and the cellular compatibility of the films were also evaluated. The polymers were further processed into fibrous scaffolds by electrospinning. The mechanical properties and cytocompatibility of these scaffolds were characterized. The *in vivo* tissue compatibility of the scaffolds was also investigated using mouse subcutaneous implantation model.

In chapter 3, we firstly designed a biodegradable conductive polyurethane (CPU) by covalently conjugating conductive oligomer, aniline trimer, into the polyurethane backbone and then doped with (1S)-(+)-10-camphorsulfonic acid (CSA). The CPU films were fabricated by solvent evaporation and their mechanical, electrical, and biodegradable properties were characterized. Electrical stability of the films was assessed with degradation and in cell culture medium with long-time charging, respectively. Cytocompatibility evaluation of the CPU film was conducted using mouse 3T3 fibroblasts. However, the addition of CSA dopant increased the polymer stiffness and deteriorated the electrical stability and biocompatibility of the CPU due

to the dopant leaching-out. To address this issue, we improved our design by introducing the dopant molecule into the polyurethane backbone via covalent bonding to form a biodegradable, dopant-free conductive polyurethane (DCPU) without adding extra dopant, whose mechanical properties, electrical conductivity and conductive stability were characterized and compared with the CPU polymer. Furthermore, the DCPU was processed into porous scaffolds using salt-leaching, and then implanted into a mouse subcutaneous model for *in vivo* biocompatibility evaluation.

In chapter 4, we firstly sought to develop low-initial-modulus biodegradable polyurethane elastomer because the native heart tissue exhibits low initial modulus at 0.02-0.5 MPa. To achieve a biodegradable low initial modulus elastomer, we firstly synthesized a triblock copolymer (PVCL-PEG-PVCL) based on random copolymers poly(δ -valerolactone-co- ϵ -caprolactone) (PVCL) and hydrophilic poly(ethylene glycol) (PEG), and then synthesized a biodegradable elastomeric polyurethanes (PU-PEG-PVCL) using a soft segment PVCL-PEG-PVCL ,a hard segment hexamethylene diisocyanate (HDI) and a chain extender putrescine. The chemical structure, thermal properties, *in vitro* degradation, and cell compatibility of polyurethane films were investigated. Mechanical properties were tested in dry and wet states. The selected polyurethanes were processed into anisotropic porous scaffolds by thermally induced phase separation (TIPS) technique, and their mechanical properties (e.g. uniaxial mechanics, ball burst, suture retention, and biaxial mechanics) were optimized to mechanically match the native myocardium by altering the soft segment molecular weight in the polyurethane backbone, and subsequently by varying the polymer concentration parameters during the scaffold fabrication process. To further improve

the bioactivity of the PU-PEG-PVCL anisotropic scaffolds, myocardium-derived hydrogel was prepared and combined with the PU-PEG-PVCL scaffolds to form biohybrid scaffold. Morphologies of the biohybrid scaffolds were observed. Their mechanical properties were characterized to compare with the synthetic PU-PEG-PVCL anisotropic scaffolds. A Lewis rat subcutaneous model was used to evaluate the *in vivo* bioactivity of the biohybrid scaffold.

Finally, we make conclusions based on the three chapters and then summarize our future studies in functionalized biodegradable polyurethane development. We will further exploit the biological function of those developed biodegradable polyurethanes in regulating cell growth and inducing new tissue formation.

CHAPTER 2
TRIGGERABLE DEGRADATION OF POLYURETHANES FOR TISSUE
ENGINEERING APPLICATIONS

2.1 Introduction

Personalized medicine has gained increasing attention in the field of tissue engineering.[177] To facilitate tissue repair and regeneration, it is critical that the scaffolds be customized to meet needs of an individual patient. For example, children, who exhibit high regenerative ability, will benefit from faster degrading scaffolds that allow for rapid tissue development. On the other hand, a scaffold that degrades more slowly may suit those patients who exhibit low regenerative ability, such as older adults and people with poor health. As another example, at the early stage of tissue regeneration, tissue scaffold with slow degradation rate is needed to provide sufficient mechanical support while permitting cell infiltration and growth. Fast and complete scaffold degradation is required to minimize foreign body reactions at the later stage of the tissue regeneration. Unfortunately, this pattern of material degradation behavior cannot be reproduced using the existing polymers in which degradation rate can only be controlled passively via hydrolysis or enzymatic processes. The goal of this work is to fabricate a new group of polymers in which the polymer degradation can be initiated and facilitated with the presence of a biological trigger.

Several strategies have been implemented in the development of polymers with the active-induced degradation property. A common method is to conjugate functional labile groups into the polymer backbone wherein the polymer can be

degraded in the presence of physical or chemical cues, such as light, ultrasound, redox, and enzyme.[178-185] Most of these materials are hydrogel or peptide based.[186-188] For example, peptide-conjugated polymers have been shown to permit collagenase-mediated degradation.[189] However, collagenase and many other enzymes cannot be administered into the patients to trigger degradation on demand without damaging healthy tissues. To overcome these drawbacks, our goal was to fabricate a new material whose degradation can be induced on demand via nonenzymatic processes.

To achieve this goal, we developed a new group of degradable polymers in which degradation can be induced via redox reactions involving thiols and disulfides. For this process, we fabricated a family of biodegradable polyurethane elastomers containing disulfide bonds (SS) that would trigger material degradation in the presence of a biological antioxidant and reducing agent—glutathione (GSH). GSH is the most abundant non-protein thiol compound found in living organisms, including mammalian cells. GSH has been shown to have many beneficial effects on health, including antioxidant and immune-boosting properties.[190, 191] It has been documented that large quantities of GSH can be administered via oral (up to 3 grams/day), intravenous (up to 2.4 grams/day), intramuscular (up to 0.6 grams/day) and aerosol (up to 1.2 grams/day) routes with no sign of side effect.[175, 192-196] These advantageous properties make this degradation strategy suitable for tissue-engineering applications. As a result, studies have examined the chemical structure as well as mechanical and degradation properties of synthesized polymer films. The toxicity of degradation products and the cellular compatibility of the films were also

evaluated. The polymers were further processed into fibrous scaffolds by electrospinning. The mechanical properties and cytocompatibility of these scaffolds were characterized. The *in vivo* tissue compatibility of the scaffolds was also investigated using a mouse subcutaneous implantation model.

2.2 Experimental section

2.2.1 Materials

PCL (average number molecular weight=2000, Sigma) and BDO (Sigma) were dried in a vacuum oven at 60°C to remove residual water before synthesis. HDI (Sigma) was purified by distillation before use. Hydroxyethyl disulfide (HDS, Sigma), stannous octoate ($\text{Sn}(\text{Oct})_2$, Sigma), anhydrous dimethyl sulfoxide (DMSO, Sigma), 1,1,1,3,3,3-hexafluoroisopropanol (HFIP, Oakwood Product), GSH (Sigma) and sodium hydroxide (NaOH, Sigma) were used as received.

2.2.2 Synthesis of polyurethane containing disulfides (PU-SS)

The polyurethanes containing disulfide bonds in the backbone were synthesized from PCL and HDI with a chain extender HDS using a two-step process according to a previous report (Figure 2.1).[197] First, PCL was dissolved in DMSO at 70°C in a 3-neck flask under N_2 protection with stirring. HDI was then added to the solution, followed by 1 droplet of catalyst $\text{Sn}(\text{Oct})_2$ (0.5%). After 3 h reaction, drops of HDS/DMSO solution were added into the prepolymer solution. The final polymer solution concentration was approximately 4% (w/v). Afterwards, the reaction was kept at 70°C for 5 d. The polymer was precipitated in an excess volume of cool deionized

water, rinsed 3 times, and then dried in a vacuum oven at 60°C for 2 d. The molar ratios of PCL/HDI/HDS were set as 1.5:2:0.5, 1:2:1, 0.5:2:1.5 and 0.2:2:1.8, which were referred to as PU-0.5SS, PU-1SS, PU-1.5SS and PU-1.8SS, respectively. Polyurethane with a chain extender BDO (PU-BDO) was used as a control. The PCL: HDI: BDO was fixed at 1:2:1. The yields of all products were above 90%.

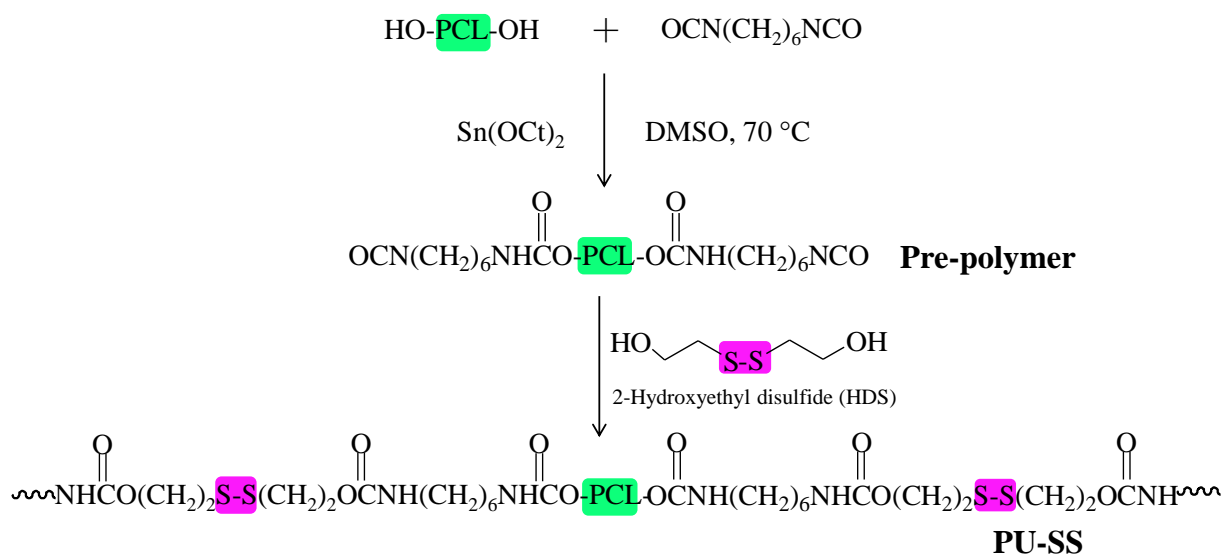


Figure 2.1 Schematic synthesis of biodegradable polyurethane containing disulfide bonds (PU-SS).

2.2.3 Fabrication of polymer films and electrospun fibrous scaffolds

For PU-SS film preparation, the polymers were firstly dissolved in HFIP with a concentration of 2% (w/v). All films were solvent casted into a Teflon dish. After HFIP completely evaporated, the films were dried in vacuum oven at 60 °C for 2 d to remove the residual solvent.

For electrospun fibrous scaffold fabrication, a 10% (w/v) polymer solution in HFIP was used for each group. The polymer solution was electrospun under the following conditions: 1) the positive voltage to the steel tip (1.2 mm inner diameter)

connected with the polymer solution-loaded syringe was 15 kV, 2) the negative voltage to the collector steel disc was -10 kV, 3) the distance between the tip and the collector was 19 cm, 4) the solution infuse rate was 1 mL/h, and 5) the electrospinning time was fixed at 2 h. The electrospun fibrous scaffolds were removed from the disc and dried in a vacuum oven at room temperature overnight for further use.

2.2.4 Polymer characterization

The Fourier transform infrared spectrometer (FTIR, Nicolet 6700, Thermo Electron Corporation) was used to verify polymer chemical structure. Glass transition temperature (T_g) and melting temperature (T_m) were determined using a differential scanning calorimeter (DSC, Shimadzu T60) from -100 to 200°C at a heating rate of 10 °C/min with nitrogen flow. For water absorption, the films ($n=3$ per polymer) were weighted (W_0) and then incubated in a phosphate buffer solution (PBS, Sigma) at 37°C. After 24 h, the films were weighted (W_1) after removing surface water using filter paper. The water absorption ratio was calculated as $(W_1 - W_0) / W_0 \times 100\%$.

For uniaxial tensile mechanical properties, the strips (2 width \times 20 length mm, $n = 6$) were cut from the polymer films, and their mechanical properties were measured on a MTS Tytron 250 MicroForce Testing Workstation with a 500 N load cell and a cross-head rate of 10 mm/min according to ASTM D638-03.[198] The sample was measured at dry state and at room temperature. The instant strain recovery ($n = 4$) was measured under the same conditions as described above. The sample was stretched to 10% strain, held for 1 min, and then released. The procedure was

repeated 3 times. The original length (L_0) and the length after stretching (L_1) were measured using a caliper. The instant strain recovery was calculated as $(1 - (L_1 - L_0)/L_0) \times 100\%$.

For cyclic stretch, the strips (2×20 mm, n=3) were stretched to 30% and 300% strains, respectively, and released back to 0% strain, which was repeated 10 times at a rate of 10 mm/min.[25]

The inherent viscosity (IV) associated with molecular weight was measured using an Ubbelohde viscometer, since polyurethanes tend to stick to GPC columns because of the strong hydrogen bonding.[199] Each polymer solution (0.1g/dl) was prepared using HFIP and filtered by a 1.2 μm glassfiber filter. Each sample was tested at 25°C and the IV was calculated as $\ln(t_p/t_s)/C_p$, where t_p is the time for the polymer solution flowing through the capillary, t_s is the time for the solvent HFIP, and C_p represents the polymer concentration.

2.2.5 Scaffold characterization

The morphology of electrospun fibrous scaffolds was observed using a scanning electronic microscope (SEM, HITACHI S-3000N). The fiber diameter was measured using ImageJ (National Institutes of Health, US). The mechanical properties of the fibrous scaffolds at dry state were measured using the same protocol as for the polymer film at room temperature.

2.2.6 *In vitro* degradation

The hydrolytic and reductive degradation of polymer films and scaffolds were measured in PBS and GSH/PBS solutions, respectively. For hydrolysis, the weighed sample (W_0) was immersed in 10 mL PBS at 37 °C. For reductive degradation, the weighed sample (W_0) was placed in 10 mL GSH/PBS solution (10 mM) at 37°C. For controlled degradation, the samples (W_0) were first immersed in PBS at 37°C for 2 wk, and then immersed into 10 mM GSH/PBS solution at 37°C for another 2 wk. At a predetermined time point, the sample was rinsed 3 times with deionized water, dried in a freeze-dryer for 3 d, and then weighed (W_1). The mass remaining was calculated as $W_1/W_0 \times 100\%$. Three samples were used for each polymer at each time point. The IVs were measured for the remained polymer films after degradation in GSH solution for 7 d and 14 d using a viscometer as described above. The mechanical properties of the films after GSH treatment (n=3) were measured as described above. The scaffold morphologies after degradation were observed under an SEM.

2.2.7 Cell toxicity of degradation products

The toxicity of the polymers' degradation products was measured as described earlier.[32] The PU-SS film (50 mg) was immersed in 10 mL 1 M NaOH solution at 37°C for 1 wk to achieve complete degradation. The degradation solution was neutralized using 10 M HCl solution to pH = 7.4 and then sterilized by 0.22 μ m membrane filter prior to cell culture study. Mouse 3T3 fibroblast (ATCC, Manassas, VA) were seeded on 96-well cell culture plates with a density of 2×10^3 cells per well in culture medium of Dulbecco's modified eagle's medium (DMEM), which was

supplemented with 10% fetal bovine serum, 100 U/mL penicillin, and 100 µg/mL streptomycin (Sigma). After incubation for 1 d, the neutralized degradation solution (final concentration of 0.1 mg/mL) or DMEM medium (control) was added to each well. The cellular metabolic activity (n = 4) was measured using a mitochondrial activity assay (MTT, Sigma) at days 1, 3, and 5.[200] For the 5-day cell toxicity group, a media change was carried out at day 3 with media containing the same type of degradation products (0.1 mg/mL). In brief, 20 µL of MTT solution (5 mg/mL in PBS solution) was added into each well. After 4h incubation, the medium was removed completely, and then 200µL DMSO was added to each well to dissolve formed formazan crystals. The metabolic index was recorded as absorbance intensity at 490 nm on a microplate reader. A live and dead staining (Live: SYTO 10 green fluorescent nucleic acid stain; Dead: ethidium homodimer-1 nucleic acid stain, Life Technologies, Inc.) kit was used to observe cellular morphology.

2.2.8 *In vitro* cellular growth on the films

The polymer disks (6 mm diameter) were punched from the films using standard biopsy punches (6 mm, Miltex), sterilized in 70 % ethanol for 30 min, and then rinsed 3 times using PBS prior to the study. The sterilized disks were immersed in the cell medium overnight and then placed into the wells of 96-well cell culture plate. The mouse 3T3 fibroblasts were seeded on the sample surface with a density of 2×10^3 per well in 96 well plates. The cell medium (DMEM supplemented with 10% fetal bovine serum, 100 U/mL penicillin, and 100 µg/mL streptomycin) were exchanged every 3 d. The MTT assay (n = 5) was used to evaluate the cellular

viability at days 1, 3, and 5 as described above. Each day, MTT results were verified using a live/dead kit to visualize the fibroblast cells on the films, and the images were taken on a fluorescence microscope. Tissue culture polystyrene (TCPS) was a control.

2.2.9 *In vitro* cellular growth on the fibrous scaffolds

The 6 mm diameter scaffold disks were placed in 96-well plates, and the 3T3 fibroblasts (2×10^3 cells per well) were seeded on the scaffold surface. The cell medium (DMEM supplemented with 10% fetal bovine serum, 10% fetal bovine serum, 100 U/mL penicillin, and 100 μ g/mL streptomycin) were replenished every 3 d. The MTT assay was used to evaluate the cell growth on the scaffold at days 1, 3, and 5 ($n = 5$ for each group). The morphology of 3T3 fibroblasts cultured on the scaffolds was observed using SEM. TCPS was used as a control.

2.2.10 Mouse subcutaneous implantation

The animal use protocols were reviewed and approved by the Institutional Animal Care and Use Committee of the University of Texas at Arlington. Female Balb/C mice (20–25 grams, from Taconic Farms, Germantown, NY) were used in this investigation. Selected scaffolds (6 mm diameter disks with 300 μ m thickness) were implanted in the dorsal subcutaneous region of the mice. After being implanted for 1 to 2 months, the implants and surrounding tissues were isolated for histological analyses. All tissue samples were frozen as sections into an 8- μ m thick segment using a Leica Cryostat (CM1850, Leica Microsystem, Wetzlar, Germany) and then

stained with hematoxylin-eosin (H&E). Based on the H&E staining, ImageJ was utilized to analyze the thickness of implants at different time points. The material *in vivo* degradation rate was then calculated by dividing the thickness of 2 month implants with the thickness of 1 month implant to reflect the percentages of thickness reduction per month.

2.2.11 Statistical analysis

All results are shown by mean \pm standard deviation. All data (different time points and groups) except for degradation were analyzed by one-way ANOVA, followed by a post hoc Tukey-Kramer test. Repeated measures ANOVA was used for polymer and scaffold degradation using Statistics Analysis System (SAS). Significant difference was considered at $p < 0.05$.

2.3 Results

2.3.1 Polymer characterization

The chemical structure of PU-SS polymers was verified by FTIR spectra (Figure 2.2). The symmetric and asymmetric stretching vibrations of $-\text{CH}_2-$ were shown at 2940 cm^{-1} and 2860 cm^{-1} , respectively. The peak at 1720 cm^{-1} corresponded to C=O stretching. The peak at $1240\text{-}1260\text{ cm}^{-1}$ belongs to the C-O-C stretching. The existence of urethane groups was verified by peaks at 3320 cm^{-1} (N-H stretching) and 1540 cm^{-1} (N-H bending). The S-S bonds were observed at 1000 cm^{-1} (C-S bending) and 540 cm^{-1} (S-S dihedral bending). The intensities of the two peaks increased with increased HDS addition.

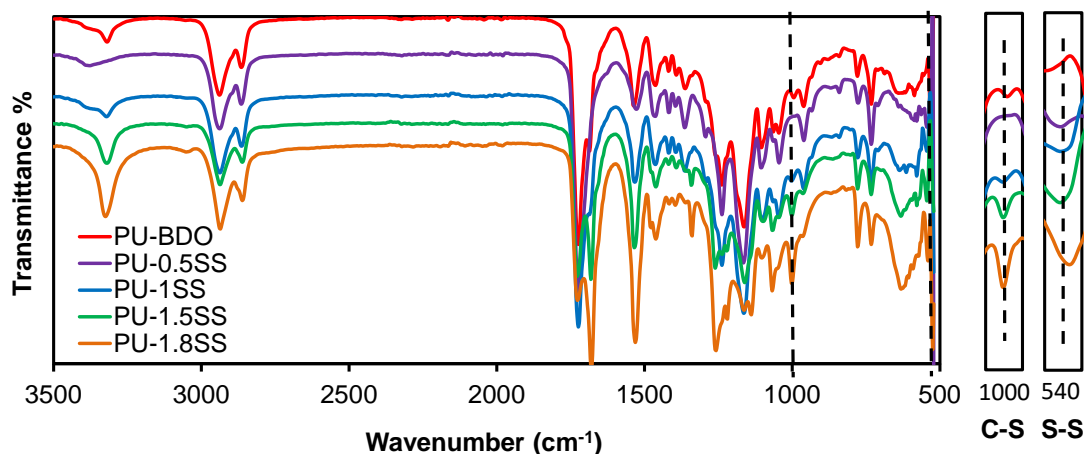


Figure 2.2 FT-IR spectra of PU-SS polymers.

All polymers had low glass transition temperatures (T_g s) below -55°C , which belonged to the soft segment of PCL in the polyurethane (Table 2.1 and Figure 2.3). The T_g increased by reducing the soft segment PCL amount. Single melting temperature was seen for PU-BDO, PU-0.5SS, and PU-1SS, while double melting temperatures (T_m s) were observed for PU-1.5SS and PU-1.8SS. The low T_m s resulted from the semicrystalline PCL soft segment (from 36 to 16°C).^[37] The high T_m s may be attributed to the HDS hard segment (PU-1.5SS: 110°C , and PU-1.8SS: 126°C). Water absorption of PU-SS films enhanced with increasing HDS content (Table 1). PU-1.8SS has the highest water absorption ($76\pm 10\%$).

Table 2.1 Polymer film characterization*

Samples	T _g (°C)	T _{m1} (°C)	T _{m2} (°C)	Peak stress (MPa)	Breaking strain (%)	Initial modulus (MPa)	Inherent viscosity (dL/g)	Water absorption (%)	Instant recovery (%)
PU-BDO	-58	26	-	12.3±0.8	729±126 ^a	15±2 ^a	1.72	43±5 ^a	99±1
PU-0.5SS	-60	36	-	12.2±1.4	1021±274 ^a	4±1 ^b	2.43	32±16 ^a	100±1
PU-1SS	-59	35	-	11.9±0.5	1098±231 ^a	8±1 ^c	2.32	40±7 ^a	99±1
PU-1.5SS	-59	16	110	12.0±0.6	821±116 ^a	26±4 ^d	1.72	67 ±4 ^b	99±1
PU-1.8SS	-57	-	126	11.5±1.4	337±45 ^b	44±3 ^e	1.63	76±10 ^b	98±1

*a, b, c, d, e represent significantly different groups for each characteristic.

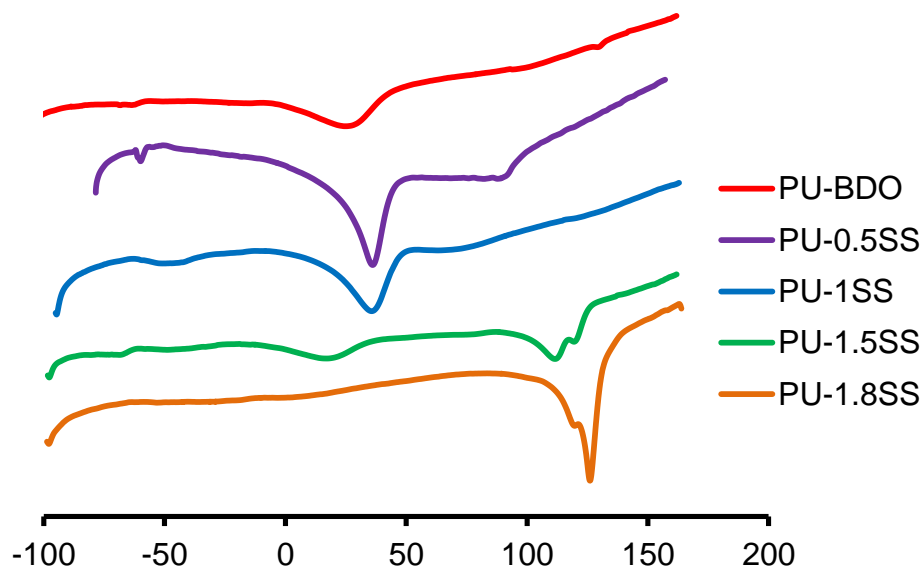


Figure 2.3 DSC heating curves of PU-SS polymers.

Mechanical properties for polymer films are summarized in Table 1, and typical stress-strain curves of PU-SS polymers are shown in Figure 2.4. The tensile strengths and the breaking strains of the polymers ranged from 11.5 ± 1.4 to 12.3 ± 0.8 MPa and from 337 ± 45 to $1098 \pm 231\%$, respectively. The tensile strengths and breaking strains of all polymers had insignificant difference. The initial moduli of PU-SS increased with increasing HDS contents ($p < 0.05$). The PU-1.8SS had the highest initial modulus (44 ± 3 MPa), while the PU-0.5SS had the lowest initial modulus (4 ± 1 MPa). The initial modulus of PU-BDO was 15 ± 2 MPa. The instant recoveries for all polymers had no significant difference ($p > 0.05$).

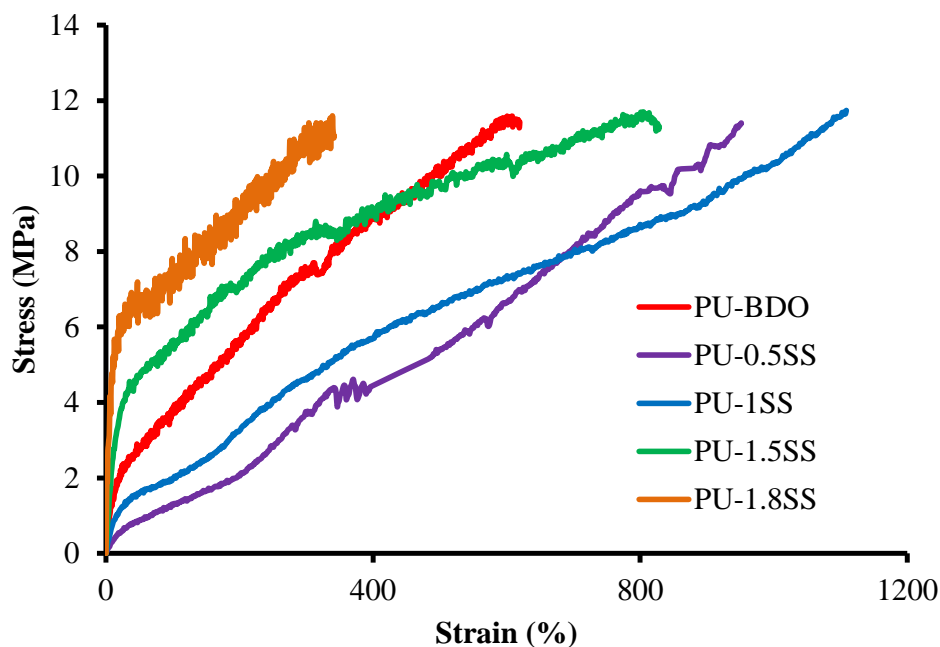


Figure 2.4 Stress-strain curves of PU-SS films.

For the resilience of the PU-SS films, the cyclic stretching was performed at a maximum strain of 30% or 300% (Figure 3). All PU-SS polymers and PU-BDO had large hysteresis loops in the first cycle that was not observed in the following nine

cycles. With a maximum strain of 30%, all samples showed small irreversible deformations at ~5% (Figure 2.5A-D), except for the PU-1.8SS (~18%) (Figure 2.5E). With a maximum strain of 300%, the irreversible deformations became appreciable for polymer samples (~200%) (Figure 2.5F-I). The cyclic stretching test was not done on the PU-1.8SS film due to the fact that its breaking strain ($337\pm 45\%$) is close to 300%.

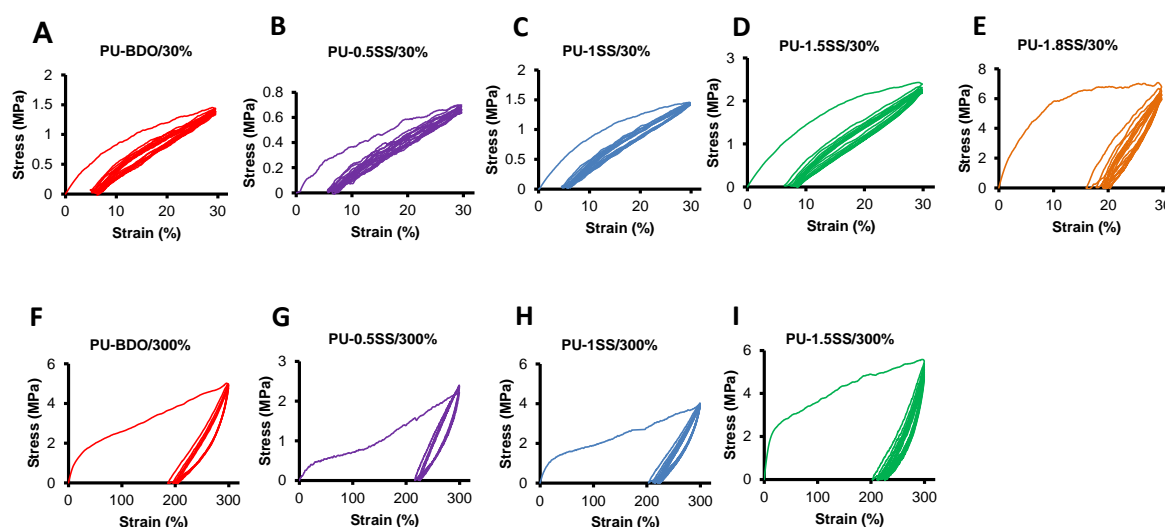


Figure 2.5 Cyclic stretch of PU-SS films at 30% and 300% deformation.

2.3.2 *In vitro* degradation of polymer films

The hydrolytic and reductive degradations of the PU-SS films were measured in PBS and GSH solution, respectively (Figure 2.6A). The degradation rate increased with increasing HDS content in the polymer. For hydrolysis at day 28, the mass remaining of the polymers ranged from $92.8\pm 0.5\%$ to $97.6\pm 0.3\%$. The degradation rates of PU-1.5SS and PU-1.8SS were significantly higher than those of PU-BDO, PU-0.5SS, and PU-1SS. For reductive degradation, PU-BDO had the lowest

degradation rate ($97.2\pm 0.9\%$ mass remaining at day 28), while PU-1.8SS had the highest degradation rate ($55.3\pm 5.5\%$ mass remaining at day 28) ($p < 0.05$). The degradation rates of PU-BDO in PBS and GSH solution had no significant difference ($p > 0.05$). The degradation rates of PU containing disulfide bonds in GSH solution were statistically higher than those in PBS ($p > 0.05$).

The IV changes of the polymer films degraded in GSH solution for 28 days are shown in Figure 2.6B. The IVs decreased with the incubation time for all polymers. The PU-BDO had the lowest IV reduction ($19.2\pm 2.9\%$ at day 28), and the PU-1.8SS had the highest IV reduction ($94.4\pm 2.1\%$ at day 28) ($p < 0.05$). PU-1.5SS had a higher IV reduction than PU-1SS and PU-0.5SS ($p < 0.05$).

The mechanical property changes of the PU-SS films degraded in GSH solution were determined at day 7 (Figure 2.6C-D), because PU-1.8SS and PU-1.5SS films became brittle at days 14 and 28 in GSH solution and were hard to handle. The tensile strengths of polymer films decreased with increased incubation time. The PU-BDO film had the lowest decrease ($17.1\pm 4.1\%$ at day 7), and the PU-1.8SS film had the highest decrease ($57.1\pm 3.2\%$ at day 7).

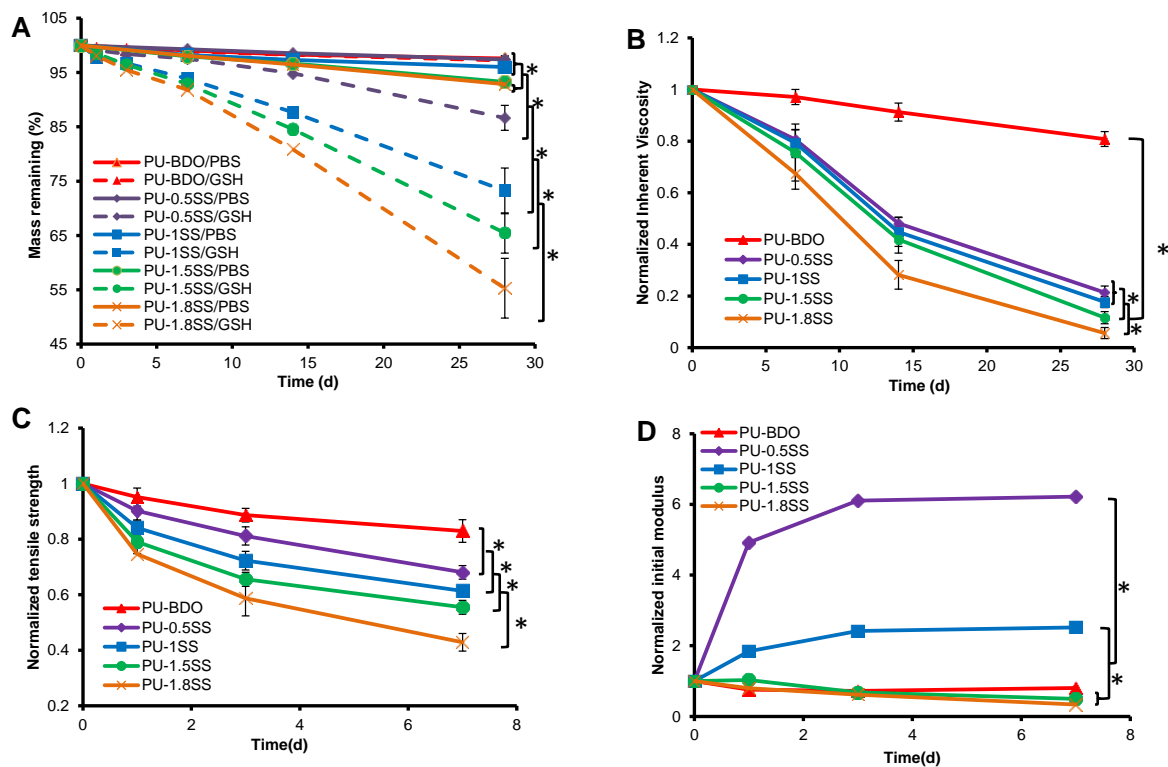


Figure 2.6 Polymer film degradation. (A) Mass remaining of PU-SS films in PBS and 10 mM GSH at 37 °C. (B) Inherent viscosity, (C) Tensile strength and (D) initial modulus changes of polymer films with degradation in GSH. * represented significant different groups ($p < 0.05$).

2.3.3 Cytotoxicity of PU-SS degradation products

The mouse 3T3 fibroblasts were utilized to evaluate the cell toxicity of the degradation products of the polyurethanes (Figure 2.7A). The cell viabilities in cell culture mediums containing degradation products showed no statistical difference from that of the medium controls ($p > 0.05$). The cell numbers increased from day 1 to day 3 for cell culture medium and culture mediums containing degradation products

($p < 0.05$). In live/dead stained images (Figure 2.8A), the increase of live cell (green) numbers from day 1 to day 3 was observed without any dead cells (red) as shown in the live/dead cell stained images (Figure 2.8B). These results support that the presence of degradation products have little or no influence on cell growth.

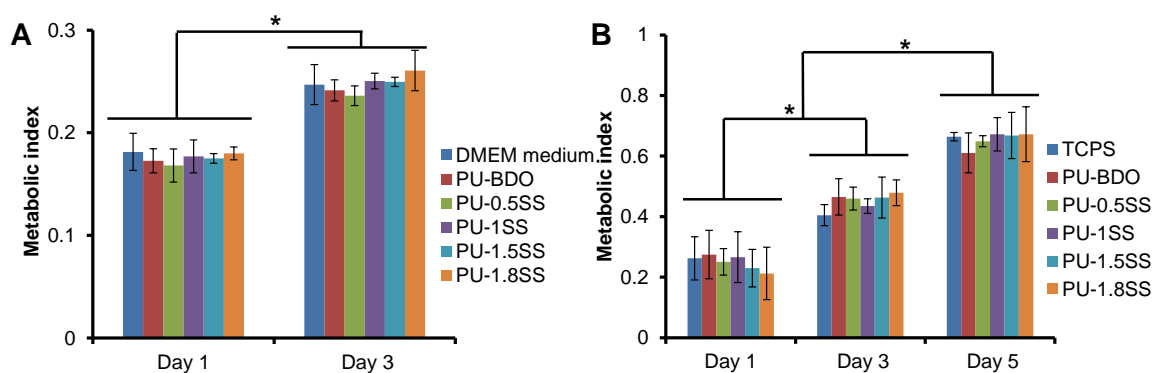


Figure 2.7 Cytotoxicity of polymer degradation products and cell growth on polymer films. (A) Metabolic index of 3T3 fibroblasts cultured with medium mixed with PU-SS degradation products at 0.1 mg/mL. DMEM culture medium was a control. (B) Metabolic index of 3T3 fibroblast seeded on PU-SS films (TCPS as a control) at days 1, 3 and 5. * represented significant different groups ($p < 0.05$).

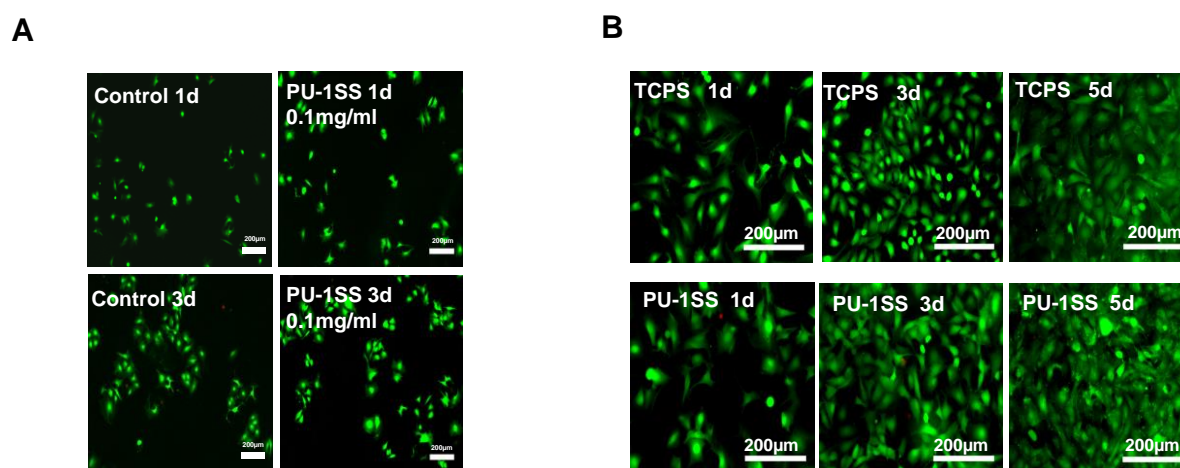


Figure 2.8 Polymer cytotoxicity and cytocompatibility. (A) Cytotoxicity of

degradation products of PU-SS polymers. Live/dead stained 3T3 fibroblasts with cell culture medium (control) and culture medium mixed with PU-1SS degradation products. Other groups showed the similar results. Live: SYTO 10 green fluorescent nucleic acid stain; Dead: ethidium homodimer-1(EthD-1) nucleic acid stain. (B) Cytocompatibility of PU-SS films. Live /dead stained 3T3 fibroblasts on the surface of PU-1SS films at days 1, 3 and 5. TCPS was a control.

2.3.4 *In vitro* cellular growth on the films

The 3T3 fibroblasts were seeded on the PU-SS films to assess their *in vitro* cell compatibility (Figure 2.7B). The numbers of adherent cells on the polymer films and TCPS increased from day 1 to day 5 ($p < 0.05$). However, there was no significant difference between the polymer films and the control TCPS during 5 days in culture. As anticipated, live/dead stained images show that there are no dead cells found on both PU-1SS films and TCPS (Figure 2.8B). In addition, with increasing incubation time, adherent cells spread to form cell sheets on PU-1SS forms as well as on TCPS.

2.3.5 Scaffold characterization

The SEM images of electrospun fibrous scaffolds showed continuous fibers without beads and drops (Figure 2.9). The fiber diameters of BDO, PU-0.5SS, PU-1SS, PU-1.5SS, and PU-1.8SS scaffolds were 1043 ± 190 nm, 1070 ± 182 nm, 503 ± 258 nm, 1156 ± 414 nm, and 456 ± 21 nm, respectively (Table 2.2). The peak stresses of the scaffolds ranged from 1.9 ± 0.3 MPa to 2.8 ± 0.7 MPa without significant differences ($p > 0.05$) (Table 2.2). Raising HDS contents increased the

initial moduli of the scaffolds in the following order: PU-BDO \approx PU-0.5SS \approx PU-1SS < PU-1.5SS < PU-1.8SS. The strains of PU-1.5SS and PU-1.8SS scaffolds were lower than those of PU-BDO, PU-0.5SS, and PU-1SS scaffolds ($p < 0.05$) (Table 2.2).

The cyclic stretches of scaffolds, at a maximum strain of 30%, are shown in Figure 2.10. Most of the PU-SS scaffolds showed a larger hysteresis loop in the first cycle than in the additional 9 cycles. Most of the samples showed a very small irreversible deformation ($\sim 5\%$) (Figure 2.10A-C), while the irreversible deformation at $\sim 10\%$ exists for PU-1.5SS and PU-1.8SS (Figure 2.10D,E).

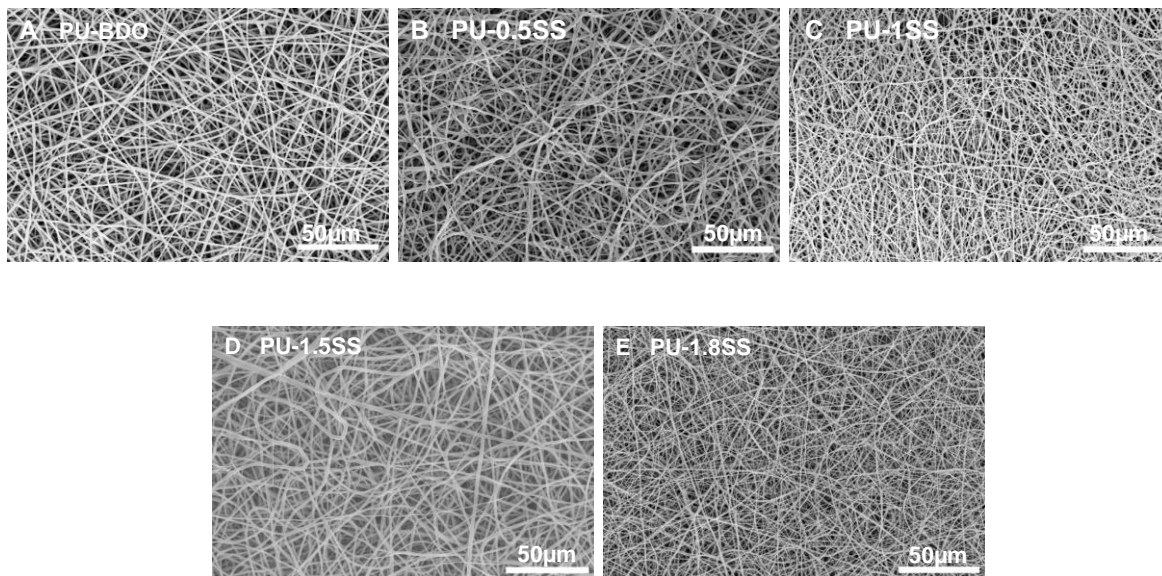


Figure 2.9 Electrospun fibrous morphology of PU-SS scaffolds. (A) PU-BDO, (B) PU-0.5SS, (C) PU-1SS, (D) PU-1.5SS, and (E) PU-1.8SS.

Table 2.2 Scaffold characterization*

Samples	Fiber diameter (nm)	Peak stress (MPa)	Initial modulus (MPa)	Breaking strain (%)
PU-BDO	1043±190 ^a	2.6±0.6	1.5±0.3 ^a	411±50 ^a
PU-0.5SS	1070±182 ^a	2.6±0.8	1.5±0.4 ^a	531±168 ^a
PU-1SS	503±258 ^b	2.8±0.7	2.0±0.2 ^a	552±191 ^a
PU-1.5SS	1156±414 ^a	2.0±0.2	3.4±0.5 ^b	282±35 ^b
PU-1.8SS	456±214 ^b	1.9±0.3	7.8±1.1 ^c	255±61 ^b

*a, b, c represent significantly different groups for each characteristic.

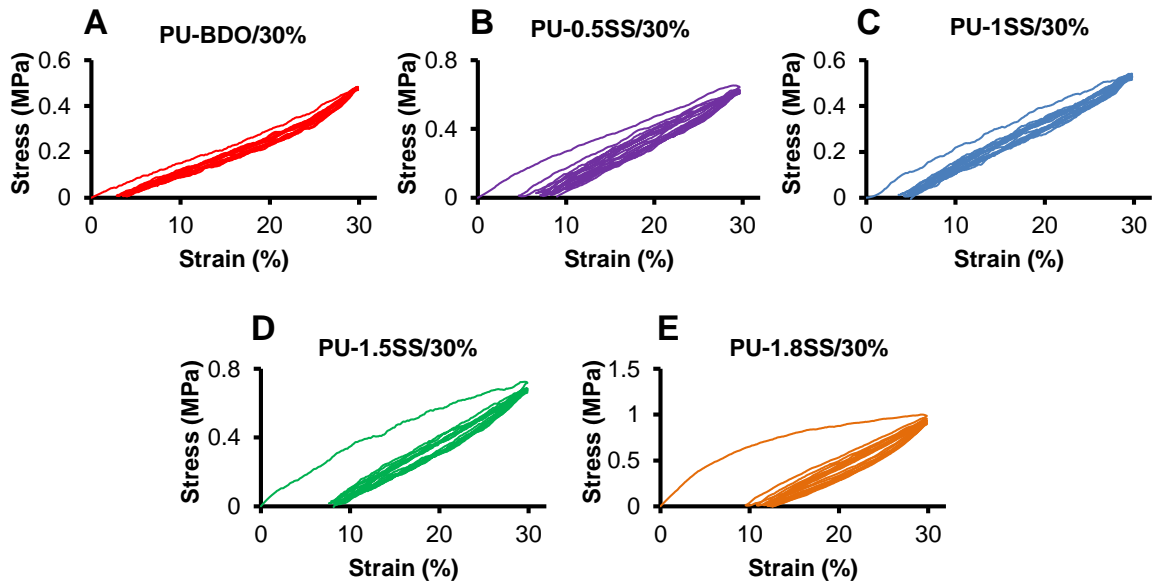


Figure 2.10 Cyclic stretch of PU-SS fibrous scaffolds at 30% deformation.

2.3.6 *In vitro* degradation of the scaffolds

The hydrolytic and reductive degradations of the PU-SS scaffolds were measured in PBS and GSH solution, respectively (Figure 2.11A). The degradation

rate increased with increasing the amount of HDS in polyurethanes. For hydrolytic degradation, the mass remaining of the polymers ranged from 92.7 ± 1.1 to $97.2\pm 0.4\%$ within 2 wk. The degradation rates of PU-BDO and PU-0.5SS were significantly lower than those of PU-1SS, PU-1.5SS, and PU-1.8SS. In GSH solution, all polymers containing HDS showed markedly faster degradation than in PBS solution. There was no significant difference between PU-BDO degradation rates in PBS and GSH solutions ($p>0.05$). At day 14, PU-BDO showed the lowest degradation rate ($95.9\pm 0.2\%$ mass remaining), while PU-1.8SS showed the highest degradation rate ($42.0\pm 8.3\%$ mass remaining) ($p<0.05$). Additionally, the degradation rates of PU-SS scaffolds were greater than those of corresponded PU-SS films within 14 d in both PBS and GSH solution.

The controlled degradation of scaffolds was conducted first in PBS solution for 2 wk and then in GSH solution for another 2 wk (Figure 2.11B). Within the first 2 wk, scaffold mass remaining in PBS ranged from $92.6\pm 0.6\%$ to $98.0\pm 0.3\%$. However, after the scaffolds were transferred to the 10mM GSH solution, the scaffold degradation rates increased markedly when compared to their degradation rates in PBS. The degradation rate increased with increasing the amount of HDS in polymers, which is consistent with the mass remaining results of scaffolds. At day 28, the PU-BDO had the lowest degradation rate ($95.5\pm 0.2\%$ mass remaining), while the PU-1.8SS had the highest degradation rate ($43.6\pm 9.0\%$ mass remaining) ($p<0.05$).

SEM images were used to further study the degradation behavior of scaffolds in GSH at week 2 (Figure 2.11C-G). The morphology of PU-BDO electrospun fibers barely changed (Figure 2.11C). The fibers of PU-0.5SS and PU-1SS scaffolds

exhibited swollen and some fibers broke, but they still maintained fibrous morphology (Figure 2.11D,E). The PU-1.5SS and PU-1.8SS scaffolds completely lost the fibrous morphology (Figure 2.11F,G).

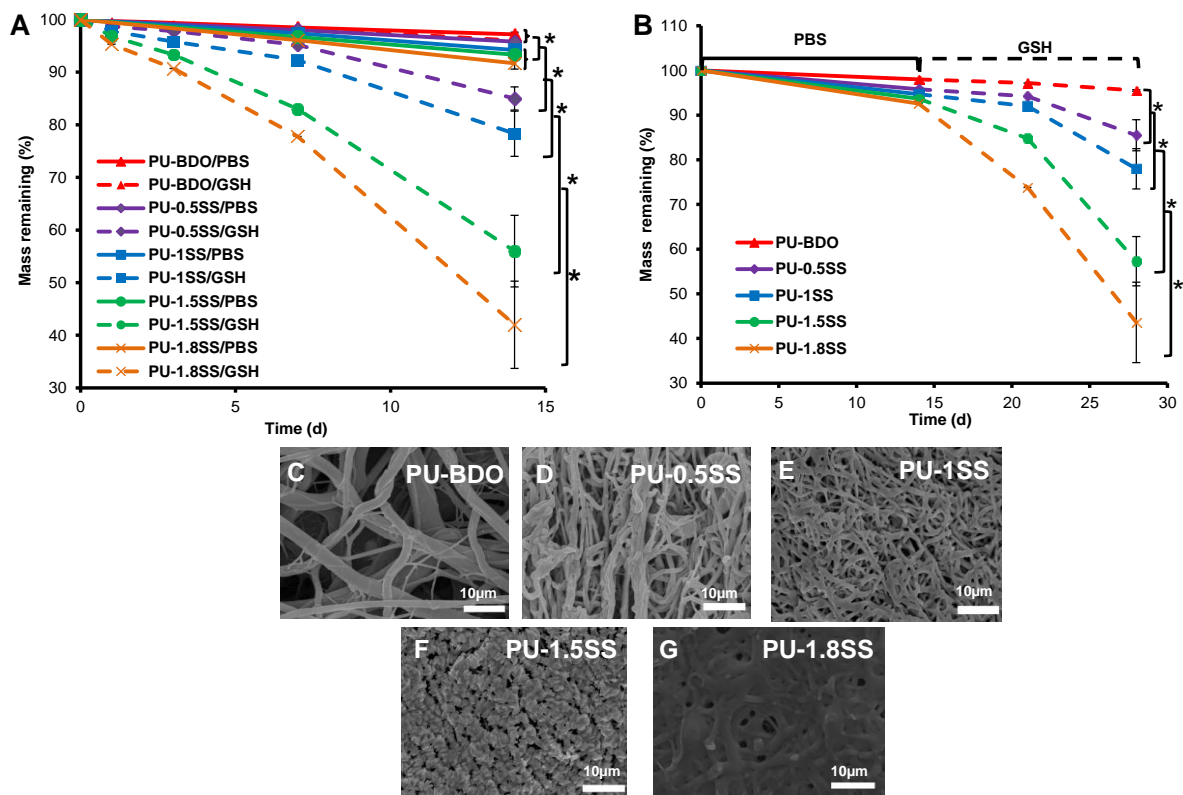


Figure 2.11 Scaffold degradation. (A) Mass remaining of fibrous scaffolds in GSH and PBS at 37°C. (B) Scaffold controllable degradation. Scaffolds were immersed in PBS for 14 d and then in 10 mM GSH for another 14 d. (C) PU-BDO, (D) PU-0.5SS, (E) PU-1SS, (F) PU-1.5SS and (G) PU-1.8SS scaffold morphology after 14 d immersion in 10 mM GSH solution. * represented significant different groups ($p < 0.05$).

2.3.7 *In vivo* cellular growth on the scaffolds

The mouse 3T3 fibroblasts proliferated on all scaffolds from 1d to 5d (Figure 2.12A). There were no significant differences in cell viability between all of the scaffolds and the TCPS at each time point. Typical cell morphologies on the scaffold (PU-1SS) were visualized (Figure 2.12B-D). At day 1, few of cells attached and spread on the fibrous scaffold (Figure 2.12B). At day 3, cell number obviously increased and partial cell confluence was observed (Figure 2.12C). At day 5, the complete cell confluence was observed on the scaffold surface (Figure 2.12D).

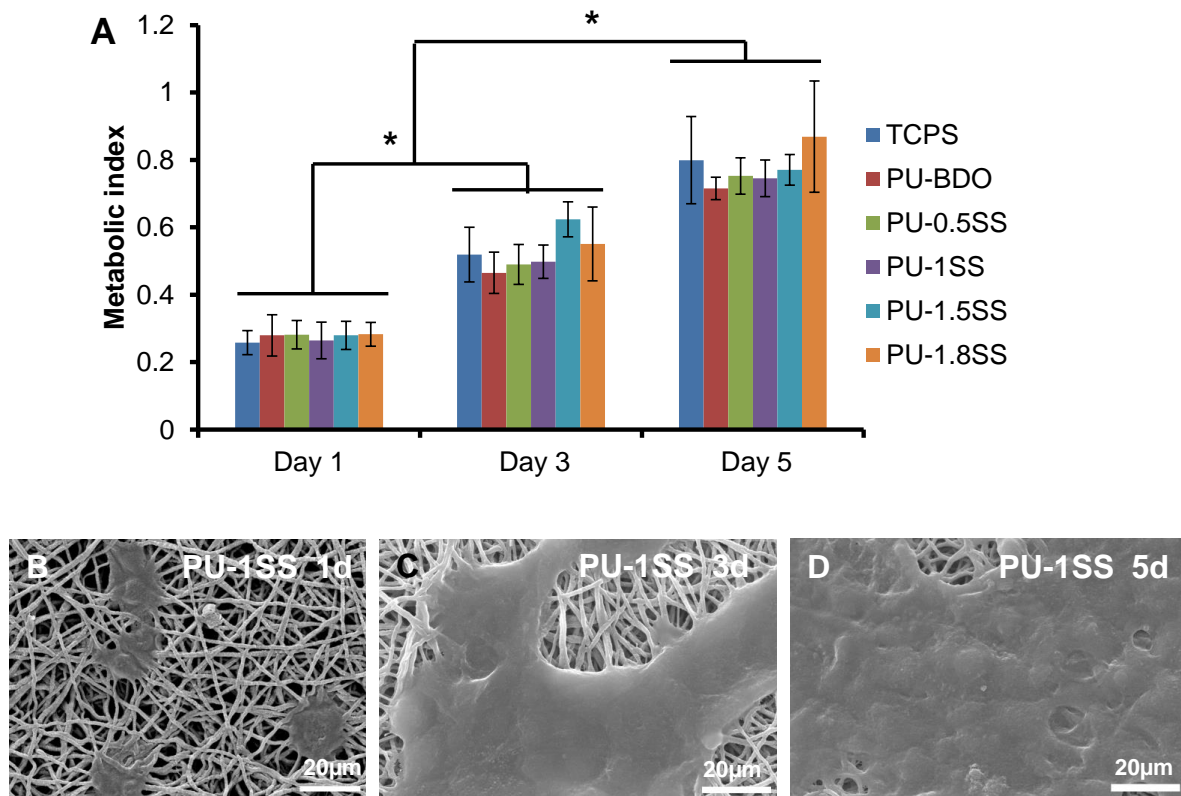


Figure 2.12 Cell growth on scaffolds. (A) Metabolic index to show the 3T3 fibroblast viability on the scaffold (TCPS as a control). SEM micrographs of 3T3 fibroblasts on

the surface of PU-1SS scaffold at (B) 1 d, (C) 3 d, and (D) 5 d.* represented significant different groups ($p<0.05$).

2.3.8 *In vivo* mouse subcutaneous implantation

To determine their *in vivo* degradation rates and tissue compatibility, PU-BDO, PU-1SS, and PU-1.8SS scaffolds were implanted subcutaneously on the backs of mice for a period of 1 and 2 months. We found very little inflammatory cell accumulation surrounding all implants at both time points (Figure 2.13A). Intensive cell infiltration was not found in all test materials. The scaffolds exhibited an increased trend of degradation rate with disulfide bond amount (Figure 2.13B). PU-1.8SS scaffolds showed significantly lower explant thickness than for PU-BDO at 2 month ($p<0.05$). The degradation rates of PU-1.8SS (34%) and PU-1SS (30%) were higher than that of PU-BDO (13%).

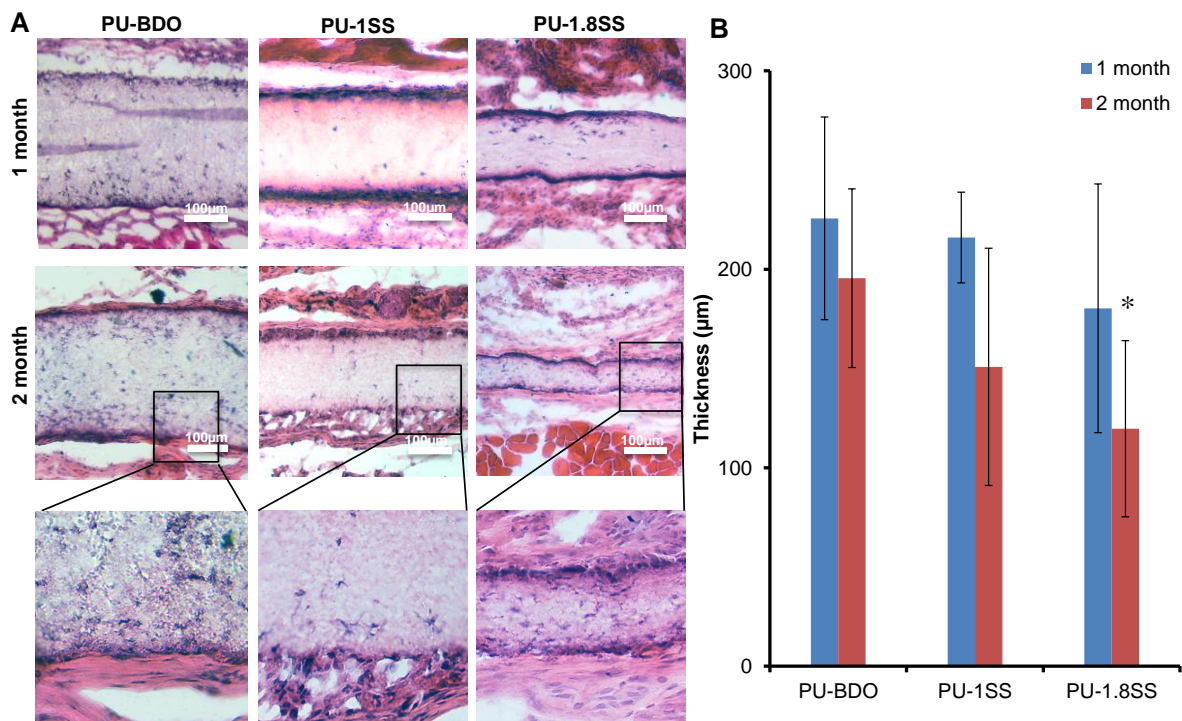


Figure 2.13 Histological evaluation of explanted scaffolds in a mouse subcutaneous model. (A) H&E staining were carried out on the scaffolds implanted in mice for 1 and 2 months. Red arrows indicate location of inflammatory cells at the tissue:implant interfaces. (B) Explanted scaffold thicknesses were measured after 1 and 2 month implantation. * : $p < 0.05$, PU-1.8SS compared with other groups at 1 month and 2 month.

2.4 Discussion

The bioreducible polyurethanes have been fabricated for gene delivery and drug control release.[201-204] For example, a targeting-clickable and tumor-cleavable polyurethane micelle has also been reported for multifunctional delivery of antitumor drugs. Those micelles contained redox-responsive disulfide bonds, which triggered the intracellular drug release under the reductive environment of tumor

tissue.[205] Furthermore, degradable cationic polyurethane micelles bearing redox-responsive disulfide linkages throughout the backbone were developed for magnetic resonance imaging (MRI) and drug delivery.[206] Finally, disulfide cross-linked micelles were fabricated by cross-linking of poly(ethylene glycol)/polyurethane block copolymers containing cyclic disulfide moieties via a thiol-disulfide exchange reaction to load anticancer drug for cancer therapy.[207] However, it is rarely reported that the polyurethanes containing disulfide bonds serve as scaffolds to provide temporary mechanical support for personalized tissue engineering. Recently, a reduction-sensitive polyurethane was synthesized from poly(ethylene glycol) (PEG) or PCL and HDI with cystine chain extender,[208, 209] but no further characterization was reported for tissue engineering scaffold use. In this project, elastomeric biodegradable polyurethanes containing disulfide bonds were synthesized by introducing HDS as a chain extender, and were further processed into fibrous scaffolds for *in vitro* and *in vivo* assessment.

The PCL, used as a soft segment for all synthesized polyurethanes, is a semicrystalline polymer with a T_g of -60° C and T_m of 59-64°C.[22] The low T_gs (<-50°C) of the polyurethanes were attributed to PCL soft segment, while the T_ms were attributed to PCL crystalline and the hard segment. The interaction between the PCL and hard segment reduces the PCL crystalline degree and hard segment phase, and then leads to the decrease of T_ms.[25] Thus, the polyurethanes (PU-BDO, PU-0.5SS and PU-1SS) with high PCL contents only present a single T_m at 30-40°C. With PCL content decrease and HDS content increase, two T_ms (PU-1.5SS) were observed and then a single high T_m (PU-1.8SS) was seen.

The initial modulus of the PU-SS films obviously increased with the increase of HDS content. The stiff hard segment increase is majorly attributed to HDS content increase, which leads to initial modulus increase. The tensile strengths of all polymers have no significant difference because the mechanical strength is dependent on molecular weight and phase separation as well as the hard/soft segment ratio. The elasticity of polyurethane is a result of the recoiling of the soft segment, while the permanent deformation is attributed to the plastic deformation of the hard segment phase, according to the strain-softening theory.[199] Since PU-1.8SS has the highest hard segment content, it exhibited higher irreversible deformation for 30% cyclic stretching than other polyurethanes with lower disulfide contents. Once the strain reached 300%, all hard segment phases might be deformed to produce the permanent deformation, which results in a large deformation of polyurethanes (~200%) without significant difference for all polyurethanes. The electrospun fibrous scaffolds showed consistent results with the films, but the mechanical strengths decreased due to the porous structure.[210]

The degradation of PU-SS polymers and scaffolds can be induced in a reductive environment. Their degradation rate can also be adjusted by altering the amount of the disulfide bond, which would compromise the mechanical properties of PU-SS polymers. The PCL is slowly degradable polyester,[211] and it would provide a relatively slow degradation before triggering fast degradation. Thus, in PBS, all materials showed slow degradation rates. The PUs with higher disulfide bond amounts exhibited faster degradation. It may be resulted from an increase in polymer hydrophilicity with an increase of disulfide bond amounts. When placed in GSH

solution, all polymers and scaffolds with disulfide bonds distinctly increased degradation rates, which verified the reductively triggered degradation of the PU-SS material. It is obvious that higher SS bond amounts in polymer result in higher sensitivity of polymer degradation to the reductive agent. Other reductive agents, such as dithiothreitol (DTT) and cysteine, are also workable to trigger the polymer degradation.[212-214] DTT has stronger reductive activity than GSH, and it induced much faster degradation of PU-SS material (Data not shown). However, DTT is toxic to the cells and tissues,[214] thus it is not suitable for our future biomedical use. GSH and cysteine are natural products and are compatible with cells and tissues, and have been administered into human via oral intake, inhalation, intravenous and intramuscular injection with no known toxicity and side-effect.[175, 176] Thus, high dosage of GSH could be used as a safe on-demand trigger via intramuscular injection to induce the fast degradation of the implant *in vivo*.

The synthesized PU-SS materials exhibited good cellular compatibility and tissue compatibility from the *in vitro* and *in vivo* assessments. The selected chemical components for PU-SS synthesis, including PCL, HDI, and BDO, have been applied for the materials of FDA-approved devices. The final degradation products also lacked cellular toxicity. The degradation products containing the thiol group (-SH) are non-toxic and have no effect on the pH value of the surrounding tissue.[215] The PU-SS films and scaffolds supported 3T3 fibroblast cells proliferation. *In vivo* subcutaneous implantation showed all implants had good biocompatibility with minor inflammation and without severe immune response, which further confirmed their safety for future use. The conventional electrospun scaffold is very dense, which

cannot allow a good cellular infiltration *in vitro* and *in vivo*.^[216] The fast degradation of the electrospun scaffolds can accelerate the cell infiltration.^[217] The PU-1.8SS scaffold had the fastest degradation, which may contribute to the enhanced cell infiltration *in vivo* as compared to PU-BDO and PU-1SS scaffolds. On the other hand, the reduction-induced degradation of the PU-SS polymer is not sensitive to the low GSH level in the tissue. The intracellular concentrations of GSH range from 0.5-10 mM,^[190] while the GSH concentrations in body fluids and extracellular matrices are relatively low (e.g., 2-20 μ M in plasma).^[218, 219] It was reported that the GSH concentration in rat subcutaneous tissue is \sim 4 μ M, which is much lower than the concentration (10 mM) used for *in vitro* degradation tests.^[220] Thus, SS amount in PU-SS scaffolds may not be high enough to respond to this low GSH concentration in subcutaneous tissue, which led to insignificantly different degradation rates between PU-BDO and PU-SS scaffolds in 1 month. However, the SS sensitivity of the PU-SS may be enhanced with time *in vivo*. In the 2nd month, the PU-1.8SS scaffolds with high amounts of SS obviously exhibited fast degradation *in vivo* compared with PU-BDO scaffolds.

The developed polyurethane family in this study showed good elasticity, robust mechanical properties, good biocompatibility, and tunable degradation behavior with sensitivity to GSH. It can be processed into nanofibrous scaffolds. As it is a linear thermoplastic polymer, the PU-SS would also be processed into porous scaffold using phase separation, salt leaching, and other technologies.^[37, 118, 216, 221, 222] PU-based scaffolds have been widely used for soft tissue engineering, such as myocardium,^[223, 224] blood vessels,^[225, 226] tendon,^[227] skin,^[228, 229]

corneal,[230] abdominal wall,[216] cartilage,[231] and hard tissue engineering, such as bone.[232] Scaffolds incorporating disulfide linkages are of particular interest when compared with the hydrolysis process, as the reductive degradation process can be performed relatively faster under physiological conditions by nontoxic reducing agents such as glutathione or cysteine.[233] Generally, *in vivo* degradation of scaffolds tends to weaken the tissue/scaffold system during tissue growth. However, it is necessary to provide sufficient mechanical support at least at the early stage of tissue growth. Thus, it is desirable to develop a slow degradation at an early stage and then an on-demand fast degradation process upon the end of tissue growth, which can be performed by disulfide-bond cleavage.[234] Thus, the PU-SS would be promising to find multiple opportunities for tissue repair and regeneration applications.

There are some limitations that should be mentioned. First, we only used 3T3 fibroblast cells for biological evaluation, and we had no specific application focus. In the future, for specific biomedical application, we will use the corresponding cell type to further evaluate the polymer. For example, for myocardium regeneration, cardiomyocytes or stem cells will be used. For blood vessel use, endothelial cells and vascular smooth muscle cells will be used, along with blood compatibility evaluation using human whole blood. Second, to accelerate scaffold degradation, GSH may be administered via direct injection to the implantation sites and/or surrounding tissue/muscles *in vivo*. However, the potential influence of GSH injection on wound healing process has yet to be determined. Third, there are many disulfide bonds-containing proteins in the blood and tissue. The influence of these disulfide bonds-containing proteins on polymer degradation remains to be evaluated. Finally, it is

possible that different degradation rates are needed for different phases of tissue regeneration. Further studies are needed to determine the optimal degradation scheme to achieve the best tissue regeneration outcomes.

2.5 Conclusion

A family of elastic polyurethanes with active inducible biodegradation property was synthesized by introducing disulfide bonds into the polymer backbone. Both PU-SS films and scaffolds had good elasticity and attractive mechanical properties. Their *in vitro* fast degradation can be actively triggered by GSH. The polymer degradation rate can be tuned by altering disulfide bond amounts in PU-SS backbone. The polymer films and scaffolds had good cellular compatibility to support cell growth without apparent cytotoxicity. The polymer scaffolds showed good tissue compatibility with minimal immune response in mouse subcutaneous models. These polyurethane elastomers possessed attractive mechanical properties, controllable degradation, and good biocompatibility, which would find opportunities to be applied as 3D scaffolds for tissue repair and regeneration.

CHAPTER 3
DEVELOPMENT OF ELECTROACTIVE, BIODEGRADABLE POLYURETHANE
ELASTOMERS

3.1

SYNTHESIS AND CHARACTERIZATION OF CONDUCTIVE, BIODEGRADABLE,
ELASTOMERIC POLYURETHANES FOR BIOMEDICAL APPLICATIONS

3.1.1 Introduction

Conductive polymer-based biomaterials have been used in a variety of biomedical fields.[47] For example, these polymers have been employed to control or regulate cellular behavior (e.g. cell proliferation, differentiation and metabolism) with/without electrical stimulation for tissue engineering applications.[235-237] Additionally, biomolecules entrapped within conductive polymers can be released with electrical stimulation.[238-240] They also can be utilized as bioactuators due to their redox activity[241, 242] and as biosensors by entrapping targeted molecules.[243, 244] However, current conductive polymer families have limitations to meet the needs of various biomedical applications. Specifically in soft tissue engineering, a conductive material with softness, elasticity (stretchability) and full degradation is expected. One major limitation of current conductive polymers is their poor flexibility.[164, 245-248] It creates difficulties in processing and it also results in high mechanical stiffness, which negatively influences the mechano–biological interactions between cells and polymers in soft tissue engineering.[125, 249]

Blending a soft elastomer with an intrinsically conductive polymer is simple and effective to improve its flexibility and stretchability,[250-253] which has also been utilized in tissue engineering application.[254-258]² For example, elastic poly(glycerol sebacate) or poly(L-lactide-co- ϵ -caprolactone) was blended with polyaniline as a soft conductive scaffold for cardiac or skeletal tissue repair.[254, 255] Polyurethane elastomer was also mixed with polypyrrole or polythiophene derivative to yield an electroactive composite with improved mechanical resilience for tissue engineering applications.[256-258] However, these non-biodegradable conductive polymers were dispersed in the insulating polymer matrices without covalent bonding, which may lead to poor controllability in mechanics and conductivity due to the possible immiscibility of two polymers. Furthermore, after degradation of the biodegradable polymer, the non-degradable conductive polymers still exist in the body, and may induce chronic inflammation and infection, then implant failure. Direct conjugation of appropriate conductive oligomers into polymer backbones may achieve a conductive elastomer with the desirable biodegradable, electrical and mechanical properties, which may address the above concerns.

In this study, we utilized polyurethane chemistry to combine biodegradable soft segments and conductive oligomers into a polymer chain using diisocyanate. Specifically, a biodegradable conductive polyurethane elastomer (CPU) was synthesized from biodegradable PCL and conductive aniline trimer with HDI. Linear polyurethane was selected because of its well-known flexibility, biocompatibility, biodegradability and processability.[25, 37] Aniline trimer has a well-defined electroactive structure, and it can easily be eliminated by macrophages *in vivo*. [259-

261] A common dopant, (1S)-(+)-10-camphorsulfonic acid (CSA), was used to dope the synthesized conductive polyurethane. The conductive polyurethane films were fabricated by solvent-evaporation, and their mechanical, electrical and biodegradable properties were characterized. Electrical stability of the films was assessed with degradation and in cell culture medium with long-time charging, respectively. Cytocompatibility evaluation of the conductive polyurethane film was conducted using mouse 3T3 fibroblasts.

3.1.2 Experimental section

3.1.2.1 Materials

PCL (number average molecular weight =2000, Sigma-Aldrich) was dried in a vacuum oven at 60 °C to remove residual water before use. Putrescine (Sigma) and HDI (Sigma) were purified by distillation prior to use. CSA (Sigma), Sn(Oct)₂ (Sigma), *p*-phenylenediamine (Sigma), 4-fluoronitrobenzene (Sigma), triethylamine (TEA, Sigma), tin granular (Sigma), ammonium persulfate (Sigma), hydrochloric acid (HCl, Sigma), NaOH (Sigma), DMSO (Sigma), acetone (Sigma), HFIP (Oakwood Product), dimethylformamide (DMF, Sigma), hexamethyldisilazane (HMDS, Sigma) and lipase from *Thermomyces lanuginosus* (≥100,000 U/g, Sigma) were used as received.

3.1.2.2 Synthesis of oxidized aniline trimer

p-Phenylenediamine (1.54 g, 14.2 mmol), 4-fluoronitrobenzene (5.06 g, 3.78 mL, 35.6 mmol), and triethylamine (2.88 g, 3.97 mL, 28.5 mmol), were initially mixed in a round-bottom flask containing DMSO at 125 °C for 3 days under an argon

atmosphere, then cooled to room temperature. Concentrated HCl was then quickly added and a red precipitate was formed. This precipitate was collected and subsequently dissolved in concentrated HCl along with granulated tin prior to refluxing for 5 h. After cooling to room temperature and washing in succession by concentrated HCl and 5 M NaOH, a whitish-blue solid was collected. This solid was then completely dissolved in ethanol/acetone (1/1, v/v) and 1 M HCl. Ammonium persulfate (1.98 g, 8.67 mmol) was added and stirred in a cold bath (-17 °C) for 10 min. The resultant blue precipitate was filtered, washed by deionized water and dried overnight resulting in pure oxidized aniline trimer (2.31 g, dark-blue solid).

Chemical structure characterization of the oxidized aniline trimer, possessing two NH₂ end groups, is as follows: ¹H NMR (DMSO, 500 MHz): δ = 5.43 (s, 4 H), 6.60-6.79 (m, 4 H), 6.89-7.05 (m, 4 H). ¹³C NMR (CDCl₃, 125 MHz): δ = 114.0, 123.0, 124.1, 124.3, 135.2, 136.8, 139.2, 139.3, 147.6, 147.8, 155.1. IR (neat, cm⁻¹): 3379, 3309, 3206, 1630, 1542, 1318, 1166, 984, 830, 699, 541, 506, 411. HRMS *m/z* (ESI) calculated for C₁₈H₁₇N₄⁺(M + H)⁺ 289.1448, found 289.1443.

3.1.2.3 Synthesis of CPU

The CPU polymer was synthesized using PCL, HDI and aniline trimer via a two-step process (Figure 3.1.1).[37] PCL (3.1 mmol) was dissolved initially in DMSO at 70° C in a 3-neck flask under N₂ protection. HDI (6.2 mmol) was then added into the flask, followed by 3 drops of Sn(Oct)₂ catalyst. After 3 h reaction at 70 °C, the prepolymer solution was cooled to room temperature, the aniline trimer/DMSO solution was then added dropwise to the prepolymer solution in the flask. The molar

ratio of PCL/HDI/aniline trimer was fixed as 1:2:1. The final polymer concentration was 4% (w/v). The reaction was carried out for 18 h at room temperature. The polymer was then precipitated in deionized water, rinsed with ethanol to remove unreacted components, and dried in a vacuum oven at 60 °C for 3 days. The yield of the conductive polyurethane was 96% of the total feeding amounts of PCL, HDI, and aniline trimer.

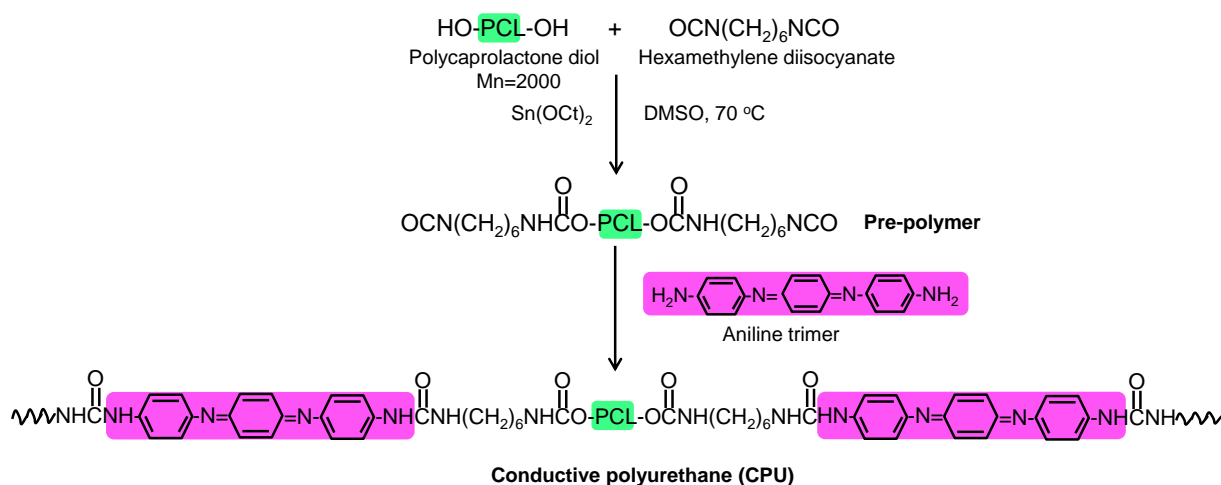


Figure 3.1.1 Synthesis of a biodegradable conductive polyurethane (CPU).

3.1.2.4 Fabrication of CSA-doped CPU films

The synthesized CPU polymer was dissolved in HFIP at a concentration of 2 % (w/v). The CSA dopant was mixed with the CPU polymer in HFIP at different molar ratios of 0.5/1, 1/1 and 1.5/1 (CSA:aniline trimer), which were referred as CPU0.5, CPU1 and CPU1.5, respectively (Table 3.1.1). The CPU/CSA/HFIP solution was then poured into a Teflon dish in the absence of bubble formation. After complete HFIP evaporation, the films were dried in a vacuum oven at 60°C for 3 days. The CPU film without CSA dopant was a control.

Table 3.1.1 Polymer film characterization*

Samples	Molar ratio of CSA:anilin e trimer	Water absorptio n (%)	Initial modulus (MPa)	Peak stress (MPa)	Breaking strain (%)	Instant recovery (%)	Conductivity (S/cm)	

							Dry state	Dry state
CPU	0:1	6±2 ^a	7±1 ^a	17.9±2.0 ^a	728±88 ^a	99±1	2.7±0.9 ×10 ^{-10 a}	4.2±0.5 ×10 ^{-8 a}
CPU0.5	0.5:1	9±1 ^b	13±6 ^b	7.3±1.0 ^b	288±37 ^b	98±1	4.0±0.7 ×10 ^{-9 b}	1.8±0.6 ×10 ^{-7 b}
CPU1	1:1	8±3 ^b	25±3 ^c	5.0±1.4 ^c	238±66 ^b	98±1	5.0±1.8 ×10 ^{-8 c}	5.5±1.9 ×10 ^{-6 c}
CPU1.5	1.5:1	11±2 ^c	35±11 ^c	3.1±0.3 ^d	75±18 ^c	97±2	4.4±0.6 ×10 ^{-7 d}	7.3±1.5 ×10 ^{-5 d}

*a, b, c, d represent significantly different groups for each characteristic.

3.1.2.5 CPU film characterization

FTIR spectra were recorded on a Nicolet 6700 (Thermo Scientific, Germany) spectrometer to verify the chemical structure of the CPU polymers. The UV-visible spectra of CPU in DMF were recorded on a UV-vis spectrometer (Perkin-Elmer Lambda 35). For water absorption, the weighed CPU films (W_0) were immersed in a PBS solution at 37°C. After 24 h, the films were weighed (W_1) after removal of the surface water by filter paper. The water absorption ($n=3$ for each CPU film) was calculated as $(W_1-W_0)/W_0 \times 100\%$. The surface morphologies of CPU films were observed using SEM (Hitachi S-4800 HRSEM). One-dimensional X-ray diffraction (1-D XRD) measurements of CPU films were carried out using a Bruker D8 Advance X-ray diffractometer.

3.1.2.6 Electrical conductivity and electrochemical measurements

The electrical conductivities of CPU films were measured in both dry and wet (24h PBS immersion) states at room temperature using a standard four-probe technique.[262] The various CPU films were placed under a home-made four-point probe and the corresponding voltage drops across the two inner probes were obtained under a direct current through the two outer probes. A PARSTAT 2273 potentiostat was employed for the measurement. The electrical conductivities (σ) of the samples were calculated using the equation: σ (S/cm) = $(\ln 2/\pi)(I/V)(1/t)$, [254, 263] where I is the current through the outer probes in ampere, V is the voltage drop across the inner probes in volt, and t is the sample thickness in cm. Four measurements were taken for each sample group.

The cyclic voltammogram (CV) of the CPU polymer was recorded using the potentiostat instrument (PARSTAT 2273) to characterize their electrochemical properties.[263] The CSA-doped CPU polymer was coated on a platinum sheet as the working electrode. A platinum mesh was employed as the auxiliary electrode. The reference electrode was Ag/AgCl in 1M H₂SO₄ solution. The scanning potential ranged from -0.1 to 1.3 V with a scan rate of 50 mV/s.

3.1.2.7 Mechanical testing

The uniaxial tensile mechanical properties of the strips (2x20 mm strips; n=6) cut from the CPU films were measured on a MTS Insight Testing System with a 500 N load cell and a cross head rate of 10 mm/min following ASTM D638-03 standard.[198] The initial modulus (E) was determined by the slope (strain < 10%) of

the stress-strain curve.[264] Instant recovery of CPU films was measured under the same conditions as described above. The strips (2 × 20 mm strips; n = 4) marked with two distal ends were stretched to 10% strain, held for 1 min, then released. The procedure was repeated 3 times. The instant strain recovery was calculated as $(1 - (L_1 - L_0)/L_0) \times 100\%$. For cyclic stretch testing, the samples (2 × 20 mm; n = 3) were stretched to a maximum strain of 30%, which was set because of the deformations (< 30%) of most tissues (e.g., cardiac muscle, bladder, and blood vessel) during normal activities,[127, 265, 266] then retracted back to the original length repeatedly for 10 cycles at a constant rate of 10 mm/min. The test was conducted on a uniaxial cyclic tensile test system as previously described with a 500 N load cell.[25, 267]

3.1.2.8 *In vitro* hydrolytic and enzymatic degradation

The *in vitro* degradation studies of the CPU films were carried out in 10 mL PBS, and in 2 mL PBS containing 100 U/mL lipase at 37°C, respectively.[25] The samples (n = 3) were cut from the CPU films and weighed (W_0), then immersed in PBS or lipase/PBS (refreshed every 3 days) at 37 °C. At each predetermined time point, the samples were picked and rinsed with deionized water, dried in a freeze-dryer for 3 days, then weighed (W_1). The mass remaining was calculated as $W_1/W_0 \times 100\%$.

The electrical conductivity changes of CPU films (n = 4) were measured after 3, 7, and 14 days degradation in 100 U/mL lipase/PBS solution at 37 °C. The degraded CPU films were rinsed with PBS solution, then their electrical conductivities in the wet state were measured using the four-probe technique as described above.

3.1.2.9 Electrical stability

To ascertain electrical stability under physiological conditions, the CPU1.5 film (n=3) was connected to an external power source (PARSTAT 2273) by NEM tape (Nisshin EM Co., Ltd) and immersed in DMEM (Sigma) containing 0.05% sodium azide (Sigma) to prevent bacterial growth.[246] Sample incubation was carried out for 150 h at 37 °C. A constant DC voltage of 100±2 mV was applied to the CPU1.5 film by a PARSTAT 2273 potentiostat, and the current-potential curve was recorded electronically. The measurement was undertaken in triplicate.

3.1.2.10 *In vitro* cellular growth on the CPU films

Mouse 3T3 fibroblasts (ATCC, Manassas, VA) were used to evaluate the cell compatibility of CPU films. The 6 mm CPU disks were punched from the CPU films using standard biopsy punches (6 mm, Miltex), and then sterilized by UV radiation for 1 h (two sides). The disks were rinsed 3 times with PBS prior to immersion in cell culture medium (DMEM supplemented with 10% fetal bovine serum, 100 U/mL penicillin, and 100 µg/mL streptomycin) overnight. The 3T3 fibroblasts (3 × 10³ cells per sample) were seeded on the disk surface in 96 well plates, then incubated at 37 °C for 1, 3, and 5 days. The cell culture medium was exchanged every 3 days. The cellular metabolic activity was measured using a MTT assay (Sigma) at each time point.[200] Five samples were used for each polymer group. TCPS was employed as a positive control. To verify the results qualitatively based on the MTT assay and observe the cell morphology on CPU films, the cell-seeded CPU disks were fixed in 4%

paraformaldehyde, dehydrated by an ascending gradient of ethanol (from 30% to 100%), and finally dried with HMDS. The cell morphology was observed using scanning electronic microscopy.

3.1.2.11 Statistical analysis

All data are presented as mean \pm standard deviation (SD). All data were analyzed by one-way ANOVA followed by a post-hoc Tukey-Kramer test. Repeated measures ANOVA was used for hydrolytic and enzymatic degradation of CPU films using the SAS. $P < 0.05$ was considered statistically significant.

3.1.3 Results

3.1.3.1 CPU characterization

The chemical structure of the CPU polymer was verified using ATR-FTIR (Figure 3.1.2). The urethane and urea groups were confirmed by specific peaks at 3320 cm^{-1} (N-H stretching of urethane and urea groups), 1720 cm^{-1} (C=O stretching of urethane and urea groups), and 2940 cm^{-1} and 2860 cm^{-1} (symmetric and asymmetric C-H stretching).[268] The specific peaks for aniline trimer were located at 1590 cm^{-1} and 1510 cm^{-1} (C=C stretching of quinoid and benzenoid rings), 1300 cm^{-1} (C-N stretching of aromatic amine), and 860 cm^{-1} (C-H bending in benzenoid rings).[269] For CSA-doped CPU films, there was an additional peak at 1040 cm^{-1} attributed to the asymmetrical stretching of the sulfonyl group interacting with aniline trimer in the polyurethane backbone, which is a characteristic of the doped form of polyaniline and its derivatives.[270]

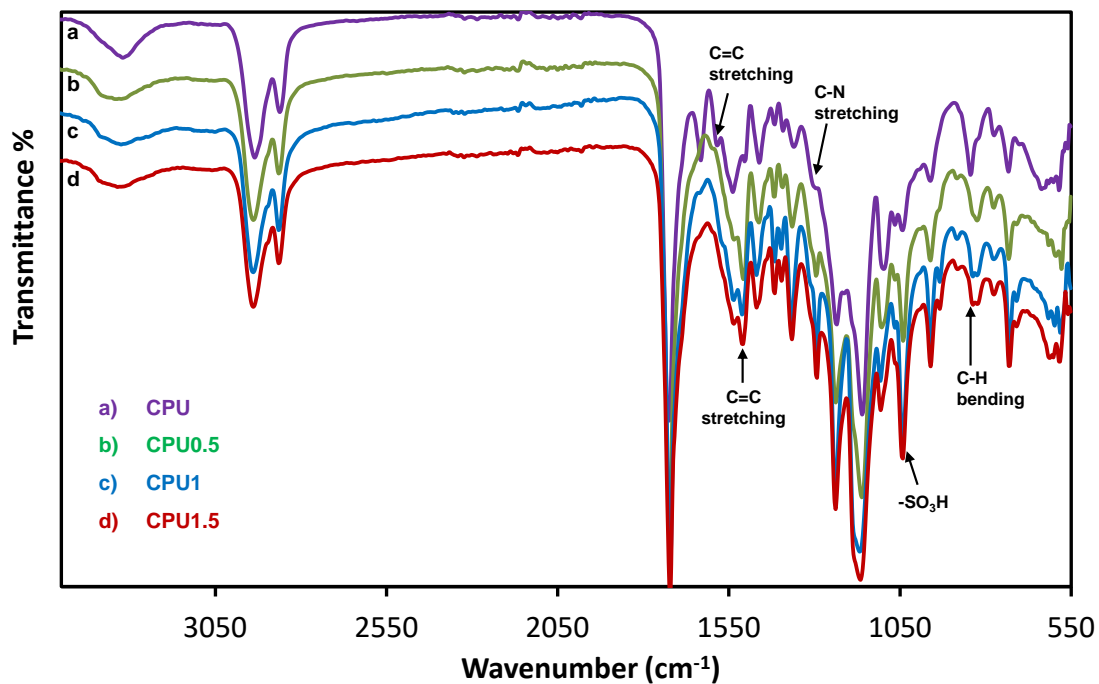


Figure 3.1.2 ATR-FTIR spectra of a) CPU, b) CPU0.5, c) CPU1, and d) CPU1.5.

The bulk hydrophilicity of CPU films was characterized by water absorption (Table 3.1.1). The water absorption of CPU films increased with increasing CSA content. The CPU film without CSA dopant had the lowest water absorption at $6 \pm 2\%$, while the CPU1.5 film had the highest water absorption at $11 \pm 2\%$ ($p < 0.05$). The undoped CPU film had a smooth surface and the CPU films with CSA dopant showed increased surface roughness (Figure 3.1.3). The XRD spectrum of CPU1.5 showed two characteristic peaks at $21.9 2\theta$ and $24.3 2\theta$ corresponding to the diffraction of the 110 and 200 lattice planes of the crystalline PCL (Figure 3.1.4).²⁹ However, the undoped CPU showed weaker and broader crystalline peaks for PCL, indicating lower crystallinity of undoped CPU compared with CPU1.5. In the UV-vis spectra of CPU and CPU1.5 (Figure 3.1.5A), the undoped CPU polymer had absorption peaks at 329 nm and 528 nm, resulting from the π - π^* transition in benzene rings and the π _b-

π_q transition from the benzene ring to the quinoid ring in the aniline trimer segment, respectively.[261] When CSA was added to the CPU polymer, the absorption peak at 528 nm disappeared and the absorption peak at 329 nm was blue-shifted to 303 nm. A shoulder band with a maximum at 492 nm from the polaron- π^* transition appeared, and a broad peak at 827 nm was observed due to the localization of radical polaron along the doped CPU backbone.[259, 271]

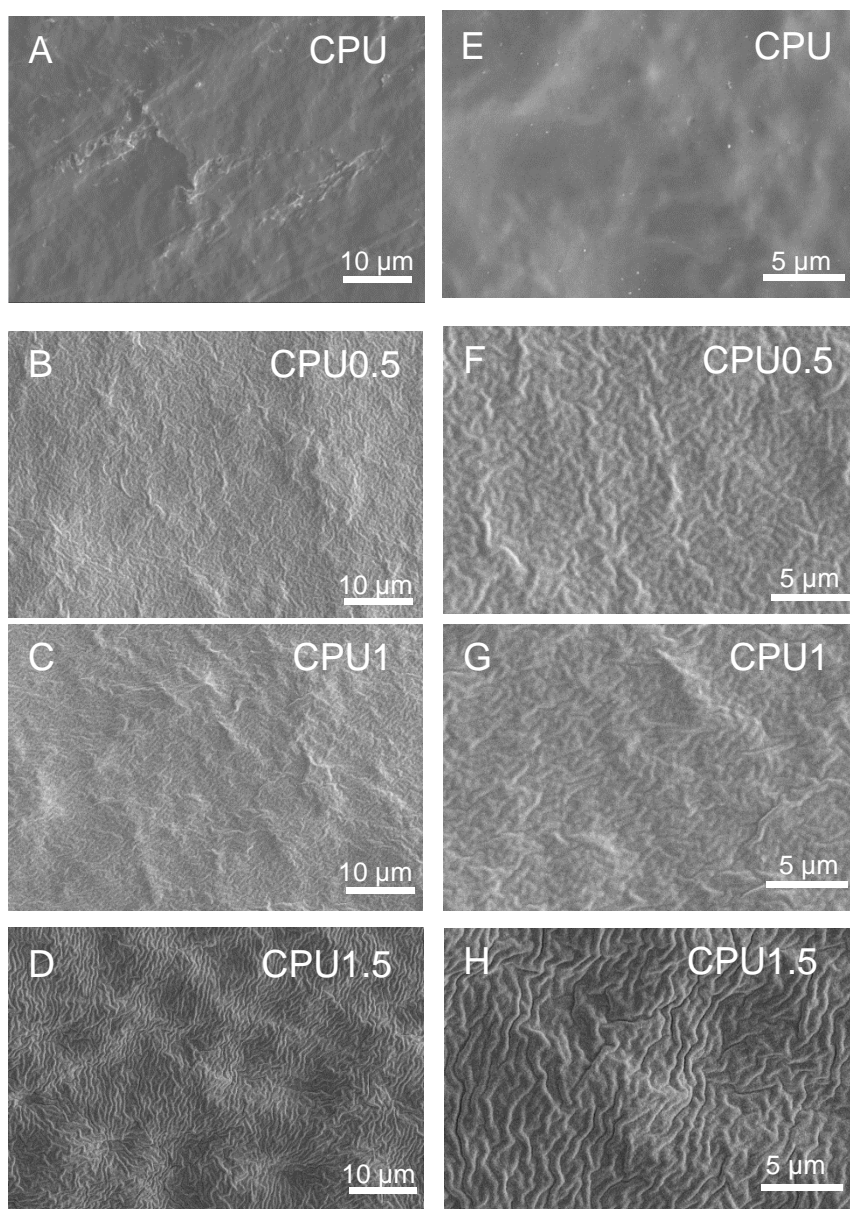


Figure 3.1.3 SEM images of CPU films at two levels of magnification, (A-D) at 2000x,

(E-H) at 5000x.

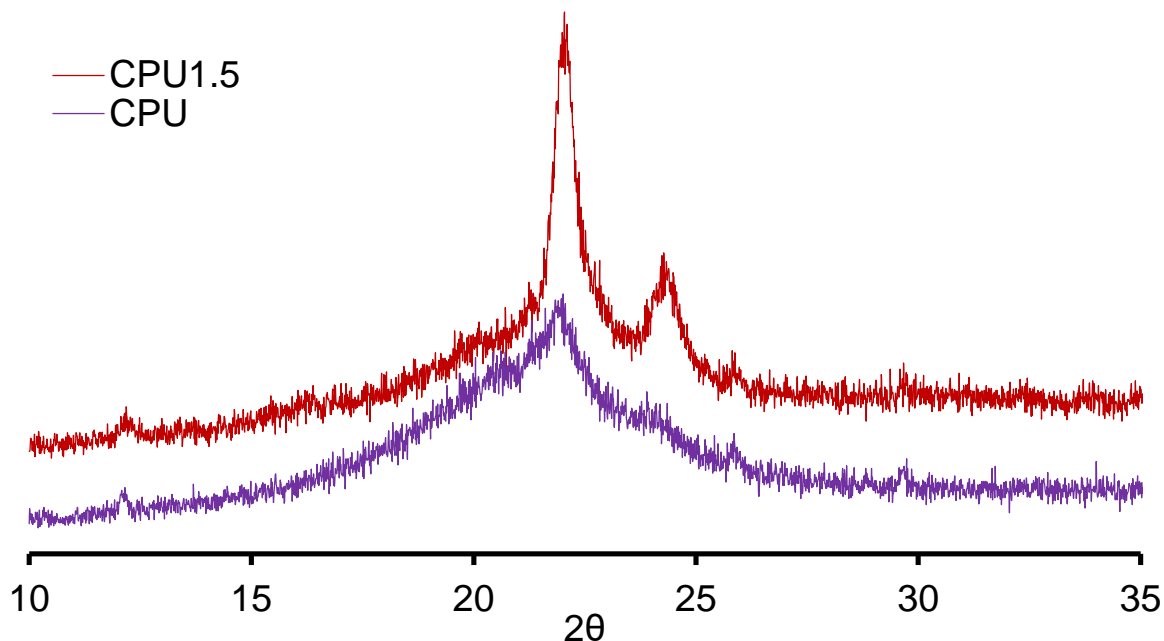


Figure 3.1.4 XRD spectra of a) CPU and b) CPU1.5.

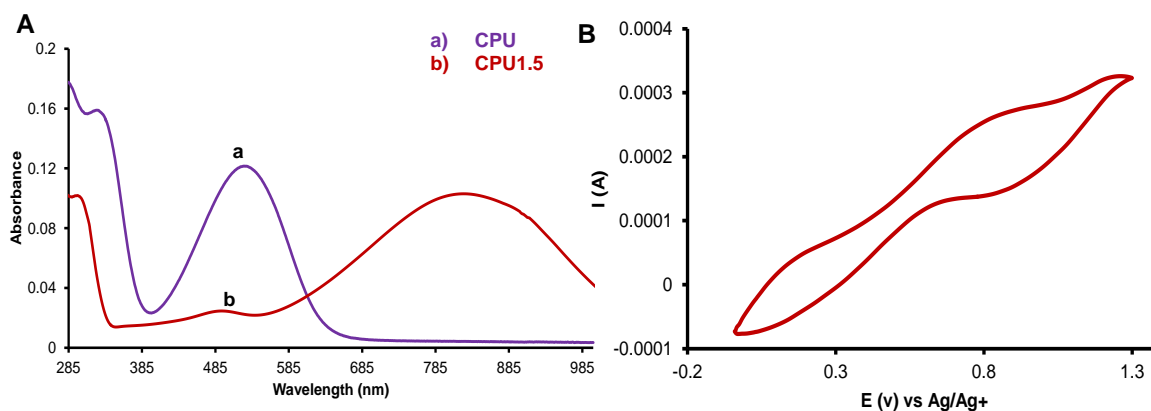


Figure 3.1.5 (A) UV-vis spectra of a) undoped CPU and b) CPU1.5 in DMF. (B) Cyclic voltammogram of CPU1.5 polymer on Pt electrode in 1.0 M H_2SO_4 using Ag/AgCl as reference at a scan rate of 50 mV/s.

3.1.3.2 Electrical and electrochemical properties

The conductivity of CPU films in the dry state ranged from $2.7 \pm 0.9 \times 10^{-10}$ to $4.4 \pm 0.6 \times 10^{-7}$ S/cm (Table 3.1.1). There was a clear trend toward increased conductivity of CPU films with increasing CSA content. Compared with the dry state, the wet CPU films (PBS immersion) showed markedly increased conductivities, ranging from $4.2 \pm 0.5 \times 10^{-8}$ to $7.3 \pm 1.5 \times 10^{-5}$ S/cm.

The cyclic voltammogram of the CPU1.5 polymer is shown in Figure 3.1.5B. The initial oxidation peak at 0.17 V corresponded to transition from the leucoemeraldine state to the emeraldine state, and the second oxidation peak at 0.82 V was attributed to the transition from the emeraldine state to the pernigraniline.[259] The well-defined redox peaks, corresponding to the transitions of three oxidation/reduction forms in CPU1.5, confirmed the good electroactivity of this composite polymer.

3.1.3.3 Mechanical properties

The stress-strain curves of the CPU films are presented in Figure 3.1.6A and their uniaxial mechanical properties are summarized in Table 3.1.1. The tensile strength of CPU films decreased from 17.9 ± 2.0 MPa to 3.1 ± 0.3 MPa with increased CSA content ($p < 0.05$). The same trend was seen for the ultimate elongation. The CPU had the highest ultimate elongation ($728 \pm 88\%$) while the CPU1.5 had the lowest ($75 \pm 18\%$) ($p < 0.05$). The initial moduli of the CPU films increased with increasing CSA content. The CPU1.5 film had the highest initial modulus (35 ± 11 MPa), and the CPU had the lowest initial modulus, at 7 ± 1 MPa (p

< 0.05). The instant recovery of all CPU films was $\geq 97\%$ after 3 cycles of stretching at 10% strain.

Cyclic stretching of CPU films at a maximum strain of 30% was performed to detect their resiliency (Figure 3.1.6B). A large hysteresis loop was observed in the first cycle for all the CPU films, followed by smaller hysteresis loops in the next nine cycles. All of the CPU films showed small irreversible deformations ($\sim 10\%$) at a maximum strain of 30%, except for the CPU1.5 film ($\sim 15\%$).

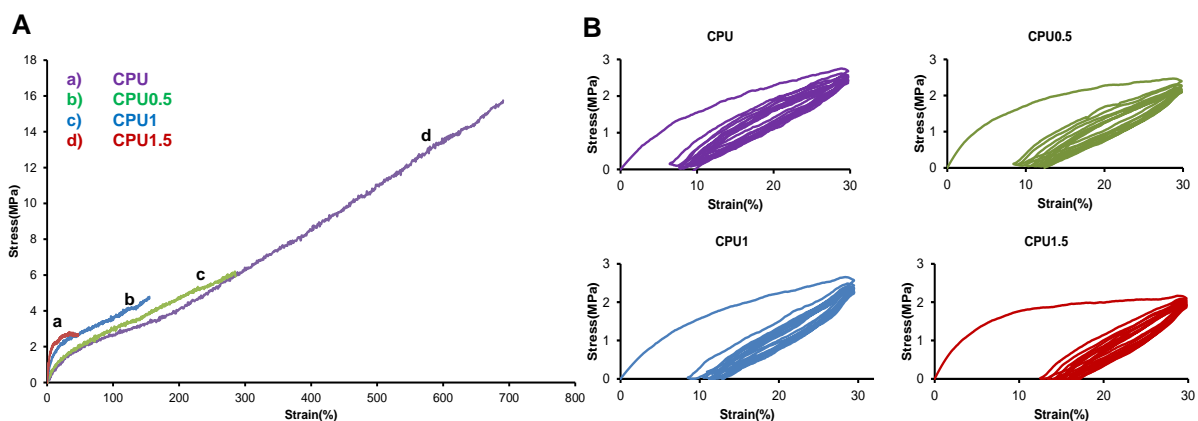


Figure 3.1.6 (A) Stress-strain curves of a) CPU, b) CPU0.5, c) CPU1, and d) CPU1.5 films. (B) Cyclic stretching curves of CPU films at 30% deformation.

The DM-ECMs were readily solubilized by pepsin and were capable of forming solid hydrogels within 30 min at physiological temperature. No significant difference was found in the gelation behaviors and fiber diameters of the hydrogels prepared from different DM-ECMs (Figure 3.8), indicating that the collagen was majorly contributed to the hydrogel formation.

3.1.3.4 *In vitro* degradation

In vitro hydrolytic and enzymatic degradation of the CPU films were carried out in PBS and lipase/PBS solutions at 37 °C, respectively (Figure 3.1.7A,B). The degradation rate of the CPU films is relevant to the CSA amount. After 8 weeks degradation in PBS (Figure 3.1.7A), the undoped CPU film maintained 98.6±0.4% of its initial weight, and the mass remaining of CPU0.5, CPU1 and CPU1.5 decreased from 97.8±0.2% to 96.6±0.4% ($p < 0.05$). In lipase/PBS solution (Figure 3.1.7B), the CPU films showed faster degradation than in PBS solution. Within 14 days, the undoped CPU film had the lowest degradation rate (93.3 ± 0.3% mass remaining), while the CPU1.5 film had the highest degradation rate (80 ± 1.8% mass remaining) ($p < 0.05$).

The electrical conductivity changes of CPU films with enzymatic degradation at days 3, 7 and 14 were shown in Figure 3.1.7C. The conductivity of the undoped CPU film did not significantly change within 14 days degradation in lipase/PBS solution ($4.2 \pm 0.5 \times 10^{-8}$ S/cm at day 0, $4.9 \pm 0.8 \times 10^{-8}$ S/cm at day 3, $4.0 \pm 0.3 \times 10^{-8}$ S/cm at day 7 and $3.6 \pm 0.8 \times 10^{-8}$ S/cm at day 14) ($p > 0.05$). However, the electrical conductivity of CSA-doped CPU films markedly decreased with enzymatic degradation. After 3 days, the electrical conductivities of the CPU0.5 ($1.8 \pm 0.6 \times 10^{-7}$ S/cm at day 0), CPU1 ($5.5 \pm 1.9 \times 10^{-6}$ S/cm at day 0) and CPU1.5 films ($7.3 \pm 1.5 \times 10^{-5}$ S/cm at day 0) were $5.2 \pm 1.1 \times 10^{-8}$, $1.2 \pm 0.3 \times 10^{-6}$ and $5.9 \pm 2.1 \times 10^{-6}$ S/cm, respectively. After 7 days, the conductivities of the CSA-doped CPU films had decreased to the same level as that of the undoped CPU film ($4.5 \pm 0.7 \times 10^{-8}$, $3.5 \pm 0.6 \times 10^{-8}$, and $4.2 \pm 1.1 \times 10^{-8}$ S/cm for the CPU0.5, CPU1 and CPU1.5 films,

respectively) ($p > 0.05$). After 14 days, the electrical conductivities of CSA-doped CPU films showed no significant difference from those after 7 days degradation ($p > 0.05$).

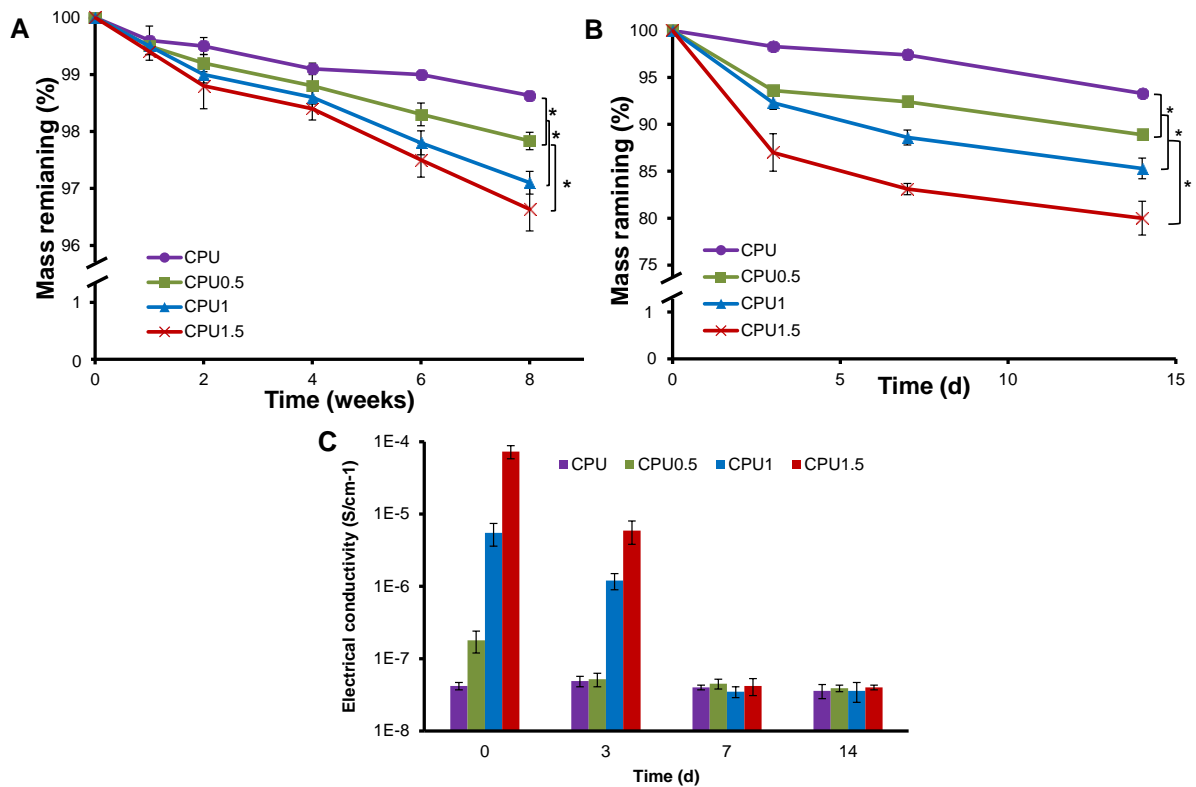


Figure 3.1.7 CPU film degradation. (A) Mass remaining of CPU films in PBS solution at 37 °C. (B) Mass remaining of CPU films in 100 U/mL lipase/PBS solution at 37 °C. (C) Changes in electrical conductivities of CPU films during degradation in lipase/PBS solution for 14 days. *represented significant different groups ($p < 0.05$).

3.1.3.5 Electrical stability

The current conductivity of the CPU1.5 film increased from 15.7 nA to 21.6 nA in the first 14.6 h in DMEM, followed by a relatively quick decrease to 15.1 nA at 67 h,

representing 96% of the initial current (Figure 3.1.8). After that, the conductivity slowly decreased to 13.6 nA at 150 h, which was 87% of the initial value.

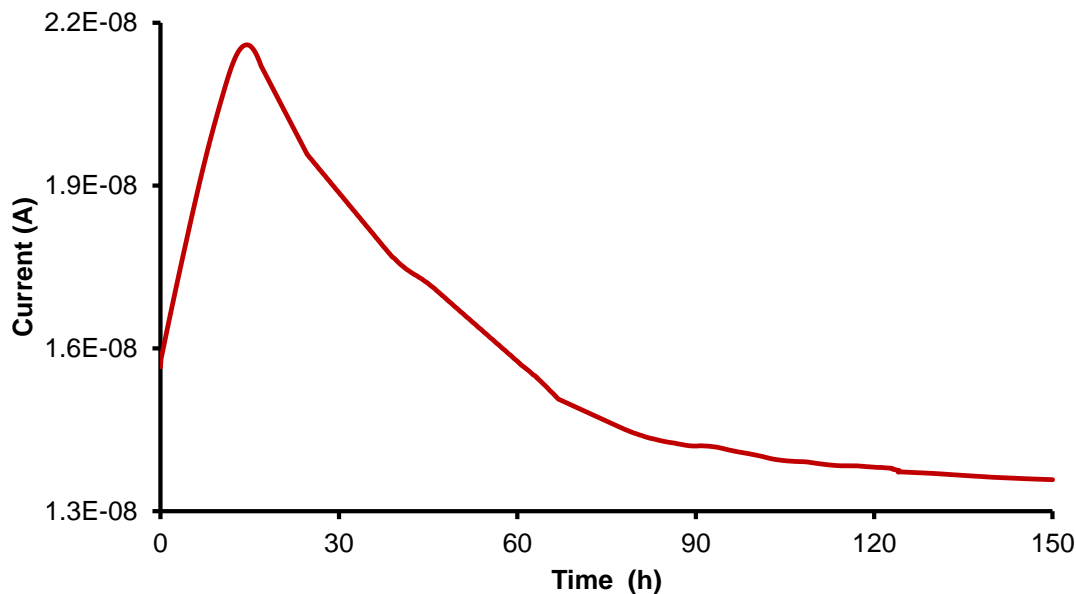


Figure 3.1.8 Electrical stability. Relationship between electrical current and incubation time of CPU1.5 film in cell culture medium charged with a fixed voltage

3.1.3.6 In vitro cellular growth on the CPU films

The cell viability of the 3T3 fibroblasts seeded on the CPU films and the control TCPS increased from day 1 to day 5 ($p < 0.05$) (Figure 3.1.9A). There were no significant differences in cell proliferation between the CPU films and TCPS within 5 days of incubation ($p > 0.05$), except for the CPU1.5 film. The CPU1.5 film showed less cell viability than other samples and TCPS at day 3 and day 5 ($p < 0.05$). The SEM images of 3T3 fibroblasts cultured on CPU films at day 5 are shown in Figure 3.1.9B. The cells with clear pseudopods spread on the CPU films. However, the cells

on the CPU1.5 film had relatively lower density than those on the other CPU films, which was consistent with the cell viability results.

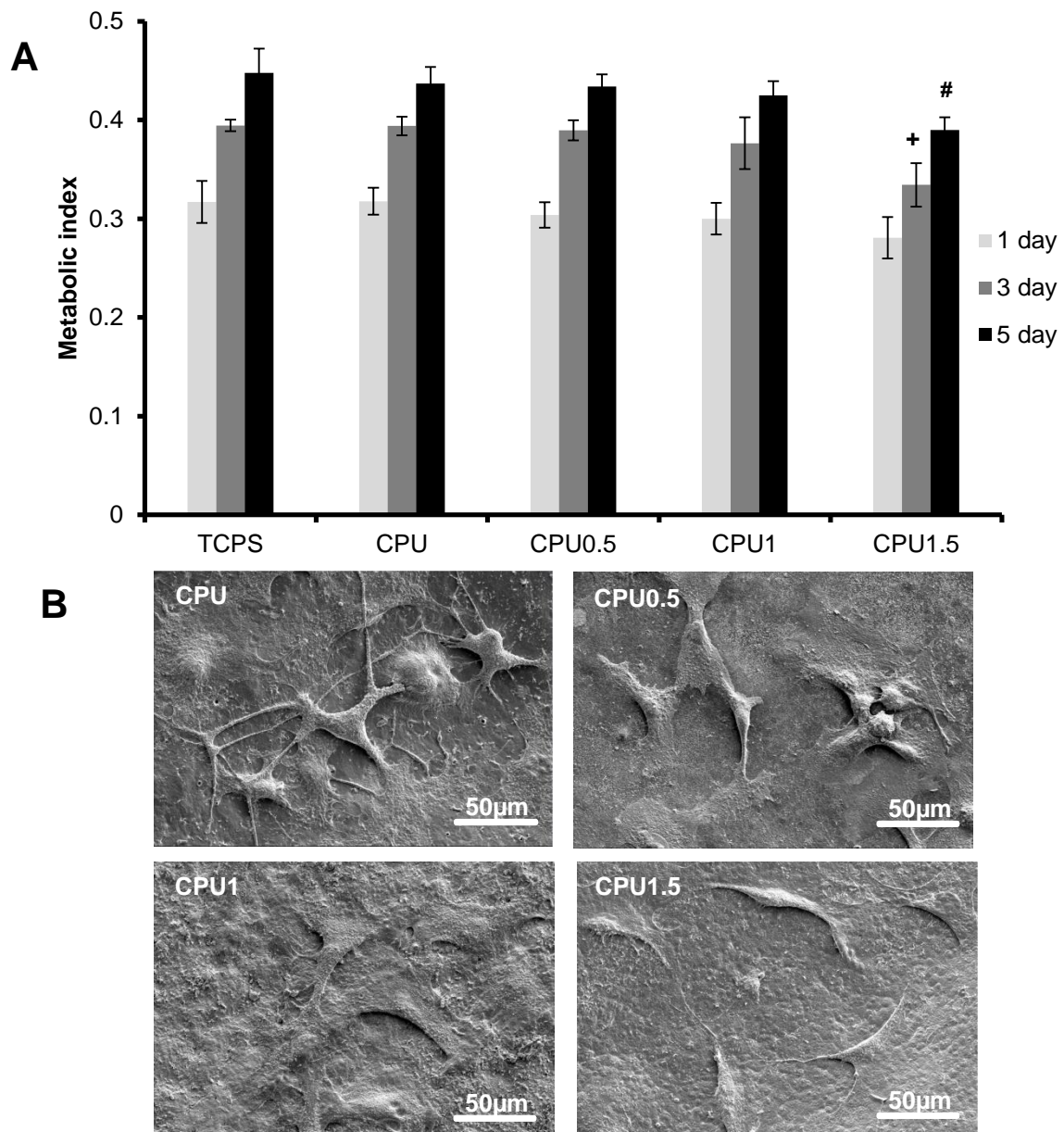


Figure 3.1.9 Cytocompatibility of CPU films. (A) Metabolic index of mouse 3T3 fibroblasts seeded on polymer films (TCPS as a control) at days 1, 3 and 5. +, #: $p < 0.05$, CPU1.5 compared with other groups at days 3 and 5, respectively. (B) SEM images of mouse 3T3 fibroblasts cultured on the polymer films at day 5.

3.1.4 Discussion

Biodegradable elastomeric polyurethane has been employed for biomedical applications due to its tunable mechanical properties, processability, biodegradability, and good biocompatibility.[25, 37] It has been processed into films,[108, 272] electrospun fibers,[107, 273] and porous scaffold,[37, 118] for tissue engineering application as well as nano/micro particulates,[206, 207, 274] membranes,[275, 276] and matrices[168] for controlled drug release. The biodegradable polyurethane has also been combined with traditional conductive polymers or organic additives to form PU-based conductive composites for tissue engineering.[55, 159, 256-258] However, few studies were reported to combine conductive segments with a PU backbone to form a PU-based conductive polymer. In one relatively complicated synthesis process, a conductive polyurethane was synthesized based on PEG, PCL, IPDI and aniline pentamer via 3 steps (isocyanate-terminated prepolymer, aniline-dimer-ended polyurethane, then polyurethane containing aniline pentamer).[133, 134] The PU containing the pentamer could not be directly processed into a film due to its poor solubility,[164] and it had to be blended with other polymers, as a dispersed additive, in the film or scaffold for further use.[164] In contrast to these prior studies, a typical two-step PU synthesis process was used to synthesize an elastomeric biodegradable polyurethane containing aniline trimer. Importantly, the resulting films exhibited good mechanical (soft and elastic) and electrical properties, and did not require a secondary polymer.

The conductivity of CPU films increased exponentially with increased amounts of CSA dopant, which was consistent with previous studies.[277, 278] It can be

attributed to the increased concentration of carriers hopping between polymer chains available for electrical conduction.[279] The conductivities of the synthesized CPU films in this study were comparable with polyurethane-siloxane-aniline tetramer (6.5×10^{-11} - 1.3×10^{-5} S/cm),[261] and had relatively lower conductivities than those of the polyurethane-aniline pentamer (on the order of 10^{-5} S/cm).[133] The relatively lower conductivity was attributed to a small number of aniline repeat units and the low content of the aniline trimer segment in the CPU backbone. The electrical conductivity of oligomers with 7 or 8 aniline repeat units can be equal to that of pure polyaniline.[280, 281] The higher content of aniline oligomer in polymer can also enhance its conductivity due to better π - π stacking of the conductive moieties.[263, 282] However, high molecular weight and content of aniline oligomer would make the polymer mechanically rigid, brittle and insoluble,[164, 254, 255, 281] which would be hard to be processed into implants with desirable morphology to meet the needs for biomedical applications. The conductivities of wet CPU films were in the range of semiconductor materials (~ 1 - 10^{-8} S/cm),[283] that are similar to those of human physiological environments. The semiconductor range of conductivity is sufficient for tissue engineering and regeneration use because of the low micro-current intensity present in human bodies.[60, 284] For example, a porous conductive scaffold based on polyurethane and PCL with conductivity at around 10^{-5} S/cm has shown the ability to improve the cardiomyocyte adhesion, growth and cardiac gene expression without external electrical stimulation.[134]

The CPU film possessed good elasticity and robust mechanical properties. The elasticity of polyurethane is related to its chemical structure, including a hard segment,

soft segment, and chain extender. Linear aliphatic HDI was employed as the hard segment to impart more flexibility to the CPU polymer than aromatic diisocyanates (e.g., methylene diphenyl diisocyanate and alicyclic diisocyanates (e.g. IPDI)), due to the inherent rigidity of the latter.[285, 286] Linear PCL is semicrystalline and has often been used as a soft segment in polyurethane synthesis.[25, 37, 108, 273] The current initial moduli of the polymer solid films are higher than those of soft tissues (e.g. human heart (0.01-0.5 MPa) and skin (0.1-2 MPa)), [249, 287] When the solid polymer is processed into a porous scaffold, the initial modulus of the polymer would be significantly reduced,[273] and may match with the mechanics of the native tissue. Furthermore, the soft segment can also be replaced by softer polymer diols, such as PTMC[199] and PVCL,[25] which can reduce the initial modulus of the CPU . The chain extender aniline trimer, which has the minimum number of aniline repeat units, has fewer negative impacts on polymer flexibility than aniline oligomers with higher molecular weights (e.g. tetramer and pentamer).[281] However, the CPU conductivity is reduced because of the small number of aniline repeat units. Thus, it is necessary to consider the elasticity and conductivity of the polyurethane comprehensively. Additionally, the dopant involvement greatly affects the material mechanical properties. The incorporation of CSA dopant led to an increased initial modulus with decreased tensile strength and ultimate elongation of the CPU films, which might result from the interaction between CSA and the aniline oligomer segment. As the charge donors, the dopants can introduce charge carrier between polymer chains,[164, 279] thus, there is an electrical interaction between polymer chains and dopants.[288] This limits the mobility of CPU polymer chains, which reduces the

elasticity of doped CPU films while increasing their initial moduli. Furthermore, the doped polyaniline showed higher crystalline at higher doping levels,[289, 290] which was confirmed by the XRD spectra of CPU and CPU1.5. Thus, it also reduced the elasticity of the doped CPU films compared with the undoped CPU film.

The conductivities of CPU films decreased with degradation. During the degradation of CPU polymers in lipase/PBS solution, the dopant CSA gradually leached out within 7 days, which resulted in an obvious reduction in conductivity.[291] A similar test conducted on a poly(glycerol-sebacate)/polyaniline composite in PBS solution showed that within 4 days, the conductivities of the composites decreased by around an order of magnitude.[254] Importantly, the enzymatic degradation of the polymer is much faster than its hydrolytic degradation in PBS. Thus, the conductivity of the CPU films may persist for a long term in a physiological condition, which also was evidenced in the conductivity stability testing of the CPU in cell culture medium. The CPU1.5 film retained 87% of its initial conductivity in cell culture medium after 150 h of immersion. The change of the current is directly responsible for the change of film conductivity under a fixed voltage. The slightly reduced conductivity of the CPU1.5 film is primarily attributed to dedoping and deprotonation under the synergic action of the cell medium and the current.[292] Because of the wet environment in biomedical applications, long-term electrical stability of the conductive polymers is required for practical purposes.[246] The good electrical stability of the CPU1.5 film exhibited the potential to be appropriate for biomedical applications.

The CPU film has good cell compatibility, which was evidenced by cell proliferation on the film surface. The traditional conductive polymers (e.g., polyaniline)

have been proved to support the growth of various cell types.[164] But dopant toxicity and polymer surface morphology have a significant impact on cell adhesion, proliferation and differentiation.[291] Further, the diffusion of the dopant into the cell culture medium may induce cytotoxicity.[293] When CSA was incubated with rat thymocytes, it resulted in significant toxicity at a high concentration (50 $\mu\text{g/mL}$).[294] Thus, at high dosages. CSA may exhibit toxicity to the cells during the culture. In addition, the leaching out of CSA can cause a pH value drop in the cell culture medium, which also might influence cell growth.[254] These factors may result in CPU1.5 having less cell proliferation than other samples. In future studies, a dopant with less toxicity may be employed to substitute CSA to achieve better cytocompatibility.

The CPU may have broad applications in the biomedical field, not limited to the tissue engineering. The repair and regeneration of some tissues, such as myocardium, nerve, muscle, skin and bone, respond positively to the presence of electrical fields, which makes conductive polymers attractive as tissue-engineered scaffolds.[47] The CPU exhibits good elasticity and electrical conductivity with biodegradable ability. It can be processed into tissue engineering scaffolds because the developed CPU can be dissolved in organic solvent, which is convenient for various scaffold processing approaches. In addition, drug release may be precisely controlled under applied electrical current or potential stimulus on drug-loaded conductive polyurethane through a de-doping procedure. For example, the conductive composites, such as polypyrrole/ poly[(D,L-lactic acid)-co-(glycolic acid)]-b-poly(ethylene oxide)-b-poly[(D,L-lactic acid)-co-(glycolic acid)] (PLGA-PEG-PLGA)

composite,[295] PEDOT/poly(vinyl alcohol) (PVA) composite,[296] and polyaniline/PVA composite,[297] carried drugs during the doping process, and then released them with electrical stimuli, suggesting the potential application of the CPU as a smart drug carrier. Furthermore, the synthesized CPU may also find opportunities for biodegradable, soft/wearable, and stretchable electronics use because of its biodegradability, conductivity, flexibility, and elasticity.

3.1.5 Conclusion

A biodegradable conductive polyurethane containing aniline trimer has been synthesized. These CPU films with CSA dopant exhibited good elasticity and increased initial moduli with increasing amounts of CSA. The electrical conductivities of wet CPU films are in the range of semiconductive materials. The CPU films exhibited good electroactivity and electrical stability under a physiological condition. All CPU films had good cytocompatibility to support cell growth on their surfaces. These results show that the conductive polyurethanes offer opportunities to be applied for tissue engineering, smart drug delivery, and electronics.

3.2

DEVELOPMENT OF DOPANT-FREE CONDUCTIVE BIOELASTOMERS

3.2.1 Introduction

A biodegradable conductive polyurethane, CPU, was synthesized previously by covalently conjugating conductive segments in the biodegradable polymer backbone and then doped with CSA. Some other conductive polymers have been also reported, such as polylactide-aniline pentamer-polylactide (PLA-AP-PLA)[259], polypyrrole-co-polycaprolactone (PPy-PCL)[298], and hyperbranched ductile polylactide (HPLA)-co-aniline tetramer (AT) (HPLAAT)[235], which all require mixing with dopants for conductivity. A dopant is required for conventional conductive polymers in the composites and the biodegradable conductive polymers to achieve high conductivity[278].^[164] They are used to dope the polymer via physical mixture, and they can leach with time or electrical stimulus. This behavior not only deteriorates the electrical properties (e.g., conductivity and electrical stability) of conductive polymers but also their cytotoxicity[299].^{[164],[246, 300]} Furthermore, the addition of dopants could influence other material properties of the conductive polymers[164]. For example, their mixture can increase the stiffness of conductive material, and negatively affect the material flexibility and elasticity, which could limit their application in soft tissue repair and regeneration and in soft/stretchable electronics[278].^[125, 291, 300] An alternative approach to avoiding the dopant mixture is to covalently bind the dopants into a polymer constituent and then dope the conductive polymers[301, 302]. A hybrid conductive hydrogel without the need for

mobile doping ions was prepared with PEDOT evenly distributed in poly(vinyl alcohol) (PVA)/ heparin methacrylate (Hep-MA) hydrogel. Heparin was covalently bound to the PVA backbone and doped the PEDOT[301]. The conductive hydrogel exhibited superior mechanical stability and retained superior electroactivity compared to metal electrodes. Unfortunately, the lack of biodegradability could limit the use of these hybrids in tissue engineering application. To overcome these drawbacks, we have developed a biodegradable conductive polymer with desirable electrical (stable electrochemical performance) and mechanical (robust, soft and elastic) properties without dopant mixture.

In this study, we have designed a dopant-free conductive polyurethane (DCPU) by chemically linking biodegradable segments, conductive segments, and dopant molecules into one polymer chain. Specifically, a biodegradable PCL, conductive aniline trimer, and dopant DMPA were linked into a polyurethane chain through HDI. The electrical, mechanical and biodegradable properties of the conductive polyurethane films were characterized. The electrical stability was evaluated under physiological conditions. Cytotoxicity of the conductive polyurethane degradation products and the cytocompatibility of the conductive films were assessed using mouse 3T3 fibroblasts. Furthermore, the dopant-free conductive polyurethane was processed into porous scaffolds using salt-leaching, and then implanted into a mouse subcutaneous model for *in vivo* biocompatibility evaluation.

3.2.2 Experimental section

3.2.2.1 Materials

PCL (average number molecular weight=2000, Sigma) was dried in a vacuum oven at 60°C to remove residual water before synthesis. HDI (Sigma) and putrescine (Sigma) were purified by distillation before use. DMPA (Sigma), Sn(Oct)₂ (Sigma), 4-fluoronitrobenzene (Sigma), *p*-phenylenediamine (Sigma), triethylamine (TEA, Sigma), tin granular (Sigma), ammonium persulfate (Sigma), hydrochloric acid (HCl, Sigma), NaOH (Sigma), CSA (Sigma), DMSO (Sigma), acetone (Sigma), HFIP (Oakwood Product), HMDS (Sigma) and lipase from *Thermomyces lanuginosus* (≥100,000 U/g, Sigma) were used as received.

3.2.2.2 Synthesis of oxidized aniline trimer with two amine end groups

All chemicals were purchased from Sigma-Aldrich. A round-bottomed flask equipped with a magnetic stirrer and an argon inlet was charged with *p*-phenylenediamine (1.54 g), 4-fluoronitrobenzene (5.06 g), and triethylamine (2.88 g) in anhydrous dimethyl sulfoxide (DMSO). The reaction lasted 3 days at 125 °C, then was cooled to room temperature, followed by the addition of concentrated HCl, then a red precipitate was formed. The collected red precipitate was subsequently dissolved in concentrated HCl along with granulated tin prior to refluxing for 5 h. A whitish-blue solid was further collected after the addition of concentrated HCl and 5 M NaOH. The solid was then dissolved in ethanol/acetone (1/1, v/v) and 1 M HCl completely, followed by the addition of ammonium persulfate (1.98 g), and stirred in a cold bath for 10 min. The formed blue precipitate was then filtered, washed with an excess

amount of distilled water, and dried overnight for the collection of pure oxidized aniline trimer (2.31 g, dark-blue solid). Chemical structure characterization of the oxidized aniline trimer, possessing two NH₂ end groups, is as follows: ¹H NMR (500 MHz, DMSO-*d*₆, δ): 5.43 (s, 4 H), 6.60–6.79 (m, 4 H), 6.89–7.05 (m, 4 H). ¹³C NMR (125 MHz, CDCl₃, δ): 114.0, 123.0, 124.1, 124.3, 135.2, 136.8, 139.2, 139.3, 147.6, 147.8, 155.1. IR (neat): 3379, 3309, 3206, 1630, 1542, 1318, 1166, 984, 830, 699, 541, 506, 411 cm⁻¹. HRMS (ESI) *m/z* calcd for C₁₈H₁₇N₄⁺(M + H)⁺ 289.1448; found, 289.1443.

3.2.2.3 Synthesis of DCPU

The conductive polyurethanes were synthesized from PCL, DMPA, HDI, and a chain extender aniline trimer. PCL and DMPA were dissolved in DMSO at 70 °C in a three-neck flask under N₂ protection with stirring, followed by the addition of HDI and 3 drops of catalyst Sn(Oct)₂. After 3 h of reaction, the prepolymer solution was cooled to room temperature. The aniline trimer/DMSO solution was added dropwise into the pre-polymer solution. The reaction then continued for 18 h at room temperature. The resulting polymer was precipitated in distilled water, washed by ethanol, and then dried in a vacuum oven at 60 °C for 3 days. The molar ratios of PCL:DMPA:HDI:trimer were set as 1:0:2:1, 0.9:0.1:2:1, 0.8:0.2:2:1, and 0.7:0.3:2:1, which were referred to as PU-trimer, DCPU-0.1/1, DCPU-0.2/1, and DCPU-0.3/1, respectively. Polyurethane with a chain extender putrescine (PU-COOH) was used as a control. The molar ratio of PCL:DMPA:HDI:putrescine was 0.7:0.3:2:1. The yields of all final products were above 85%.

3.2.2.4 Fabrication of DCPU films

The synthesized DCPU polymers were dissolved in HFIP at a concentration of 2% (wt/v), followed by pouring into a Teflon dish. After the complete evaporation of HFIP, the conductive polymer films were dried in a vacuum oven at 60 °C for 3 days.

3.2.2.5 Polymer characterization

FTIR spectra were obtained using a Nicolet 6700 spectrometer (Thermo Scientific, Germany) to verify the chemical structure of DCPU. Thermal properties were characterized by DSC (Shimadzu DSC-60) at a scanning rate of 10°C min⁻¹ ranging from -100 to 200 °C with a nitrogen flow. UV-visible spectra of DCPU solutions in DMSO were recorded on a UV-vis spectrometer (PerkinElmer, Lambda 35). For water absorption, the weighted polymer films (W_0) were incubated in a phosphate buffer solution (PBS, Sigma) at 37 °C. The films were weighted (W_1) after removing surface water using filter paper. The water absorption was calculated using equation (1):

$$\text{Water absorption (\%)} = \frac{W_1 - W_0}{W_0} \times 100\% \quad (1)$$

Three parallel samples were tested for each group. The polymer inherent viscosity (IV) associated with molecular weight was measured using an Ubbelohde viscometer[199]. Each sample was dissolved in 15 mL HFIP at a concentration of 0.1 g dL⁻¹ and then filtered by a 1.2 µm glass-fiber filter. Each sample was tested five times at room temperature. The IV was calculated using equation (2):

$$IV = \frac{\ln\left(\frac{t_p}{t_s}\right)}{C_p} \quad (2)$$

$\ln(t_p/t_s)/C_p$, where t_p is the time for the polymer solution flowing through the capillary; t_s is the time for the solvent HFIP flowing through the capillary; and C_p is the polymer concentration.

3.2.2.6 Electrical conductivity and electrochemical measurements

The electrical conductivity (σ , $S\text{ cm}^{-1}$) of the DCPU films was measured using the four-point probe technique at both dry and wet states at room temperature[254].^[303] A direct current (DC) was supplied to pass through the outer probes, and voltage was induced in the inner two probes. The four-point probe was homemade, and the instrument for current supply and voltage measurement was a PARSTAT 2273 potentiostat. The electrical conductivities of the samples were calculated by equation (3):

$$S = (\ln 2 / \rho) (I / V) (1 / t) \quad (3)$$

where σ represents the electrical conductivity; I is the current in ampere; V is the voltage in volts; and t is the sample thickness in cm. Four measurements were taken for each group. The electrochemical properties of DCPU were assessed by cyclic voltammetric (CV) analysis using the same potentiostat instrument (PARSTAT 2273) as above[263]. A three-electrode system was involved, consisting of a platinum working sheet electrode coated with the conductive polymer, a platinum-mesh auxiliary electrode, and an Ag/AgCl reference electrode. The CV was recorded at a

scan rate of 50 mV s⁻¹ in 1 M H₂SO₄ solution with scanning potential between -1 and 1.3 V.

3.2.2.7 Mechanical testing

The mechanical properties of the samples (2 × 20 mm strips; n = 5) were measured on an MTS Insight Testing System with a 500-N load cell and a crosshead rate of 10 mm min⁻¹ according to ASTM D638-03[198]. For conductivity-strain measurements, DCPU films (n = 3) were stretched in the uniaxial direction at room temperature, and then their electrical conductivities at 30%, 70%, and 100% strains were measured using the four-point probe technique, as described above. The instant strain recovery was measured under the same conditions as described above. Two distal ends of the samples were marked, and the samples were stretched to 10% strain, held for 1 min, and released. This stretch cycle was repeated three times. The original length (L₀) and the length after stretching (L₁) were measured using a caliper. The instant strain recovery was calculated using equation (4):

$$\text{Instant recovery (\%)} = \left(1 - \frac{L_1 - L_0}{L_0} \right) \times 100\% \quad (4)$$

Cyclic stretch testing was conducted by stretching the strips (2 × 20 mm; n = 3) to a maximum strain of 30% or 300%, respectively, and then releasing them back to 0% strain. The stretch cycle was repeated 10 times at a rate of 10 mm min⁻¹ [273].

3.2.2.8 Polymer degradation

To study the *in vitro* hydrolytic and enzymatic degradation profile of synthesized polymers, the weighted samples (W_0) were immersed in 10 mL PBS or in 2 mL of PBS containing 100 U mL⁻¹ lipase solution at 37°C[25]. The lipase/PBS solution was changed every 3 days. At a predetermined time point, the samples were rinsed three times with deionized water, dried in a freeze-dryer for 3 days, and then weighed (W_1). The mass remaining was calculated by equation (5) below. Three parallel samples were used for each group at each time point.

$$\text{Mass remaining(\%)} = \frac{W_1}{W_0} \times 100\% \quad (5)$$

The mechanical properties of the DCPU films (n=4) after enzymatic degradation were measured as described above.

3.2.2.9 Electrical stability of DCPU films

The conductivity changes of the DCPU films (n = 3) were recorded in 100 U mL⁻¹ lipase/PBS solution after 7 and 14 days of degradation at 37°C. At each time point, the degraded DCPU films were taken out and rinsed by PBS to remove the attached enzymes on the film surface. Their conductivities in the wet state were then measured by the four-probe technique, as described above. The electrical stability of the DCPU film was measured in a cell culture medium (Eagle's medium containing 0.05% sodium azide to prevent bacterial growth) under a constant DC voltage of 100 ± 2 mV provided by a PARSTAT 2273 potentiostat[246]. The incubation lasted for 150 h at 37°C. The measurement was undertaken in triplicate. PU-trimer doped with CSA (the molar ratio of CSA:aniline trimer was set as 1.5:1) during the film fabrication

process as described above was used as a control group. Conductivity changes during enzymatic degradation and electrical stability of the control group (PU-trimer doped with CSA) were measured via the same processes as those of the DCPU films.

3.2.2.10 Cytotoxicity of DCPU degradation products

The DCPU polymers (100 mg) were placed in 1 M NaOH solution at 37 °C for 1 week to achieve complete degradation[16]. The degradation solution was neutralized using 10 M HCl solution to pH = 7 and sterilized by a 0.22 µm membrane filter. Mouse 3T3 fibroblasts (ATCC, Manassas, VA) were seeded in 24-well cell culture plates at a density of 1.6×10^4 cells per well in cell culture medium of DMEM, which was supplemented with 10% fetal bovine serum, 100 U mL⁻¹ penicillin, and 100 µg mL⁻¹ streptomycin. After 1 day of incubation, the neutralized degradation solution diluted by the DMEM medium at a final concentration of 0.1, 0.01, and 0.001 mg mL⁻¹ was then added to each well. The DMEM medium was used as the control group. After 24 h cell culture, the cell viability (n = 4) was measured using a MTT assay (Sigma), and an optical microscope was used to observe cell morphology.

3.2.2.11 *In vitro* biocompatibility of polymer films

The polymer films were punched into 6 mm diameter disks using standard biopsy punches (6 mm, Miltex) and sterilized using 70% ethanol solution and UV irradiation for 30 min each, and then they were rinsed by PBS three times. Prior to cell seeding, the sterilized disks were placed in a cell culture medium overnight. Mouse 3T3 fibroblasts were seeded on the sample surface with a seeding density of

3×10^3 per well in 96-well plates. The cell medium was exchanged every 2 days. The MTT assay was used to evaluate the cellular activity ($n = 4$) at 1, 3, and 5 days. The tissue culture polystyrene (TCPS) was used as a positive control. To qualitatively verify the MTT results and visualize the 3T3 fibroblasts on the films, the cell-seeded films at 1 and 5 days were fixed in 4% paraformaldehyde and dehydrated in graded ethanol solutions (30%, 50%, 70%, 80%, 90%, 95%, and 100%), treated with HMDS, and dried at room temperature. The treated films were observed under SEM (Hitachi S-4800 HRSEM) to visualize the cell morphologies on polymer films.

3.2.2.12 Porous scaffold fabrication and characterization

For porous scaffold fabrication, the DCPU-0.3/1 polymer was completely dissolved in HFIP at a concentration of 6% (wt/v). Salt particles (NaCl, Sigma) with sizes ranging from 100 to 150 μm were obtained by American standard sieves. The salt particles (5 g) were uniformly mixed with 1 mL of DCPU/HFIP solution. The DCPU/salt mixture was then placed in a cylinder glass mold and exposed to the air for HFIP evaporation. After complete HFIP evaporation, the scaffold was immersed in DI water for 3 days to remove salt particles. The porous scaffold was eventually obtained after lyophilization for 3 days. The morphology of the porous scaffold was observed under SEM. The scaffold porosity was measured by ethanol displacement[304]. The scaffold sample was immersed in a measurement cylinder containing a known volume of pure ethanol (V_1). After 5 min, the total volume of ethanol and ethanol-impregnated scaffold was recorded as V_2 . After removing the

ethanol-impregnated scaffold from the cylinder, the residual ethanol volume was recorded as V_3 . The scaffold porosity was calculated by equation (6):

$$\text{Porosity} = \frac{V_1 - V_3}{V_2 - V_3} \quad (6)$$

3.2.2.13 Mouse subcutaneous implantation model

In vivo study was carried out in accordance with National Institutes of Health (NIH) guidelines for animal care and was approved by the Institutional Animal Care and Use Committee of the University of Texas at Arlington. Female Balb/C mice (20–25 grams, purchased from Taconic Farms, Germantown, NY) were utilized for this study. Porous scaffolds made from DCPU-0.3/1 and PCL (a positive control, average $M_n=80,000$, Sigma) (4 mm diameter \times 2 mm thickness) were implanted subcutaneously on the back of animals. After implantation for 2 and 4 weeks, these mice were sacrificed, and then the implants along with their surrounding tissues were collected and frozen in OCT. For histological analysis of tissue compatibility, 8- μ m sections from frozen samples were made using Leica Cryostat (CM1850, Leica 247 Microsystem, Wetzlar, Germany), followed by staining with H&E. In addition, 4,6-diamidino-2-phenylindole (DAPI) staining was also performed to assess the extent of cell infiltration in DCPU and PCL porous scaffolds.

3.2.2.14 Statistical analysis

All results are presented as mean \pm standard deviation. All data were analyzed by one-way ANOVA followed by a post-hoc Tukey-Kramer test. Repeated-measure

ANOVA was used for hydrolytic and enzymatic degradation of conductive polymer films using SAS. $p < 0.05$ was considered a significant difference.

3.2.3 Results and discussion

3.2.3.1 Characterization of the DCPU

DCPU was synthesized from PCL (biodegradable segment), aniline trimer with two amine end groups (conductive segment), and DMPA (dopant molecule) with HDI using two-step solvent polymerization (Figure 3.2.1A). The PCL:DMPA:HDI:aniline trimer feeding ratios were varied as 0.9:0.1:2:1, 0.8:0.2:2:1, and 0.7:0.3:2:1, which were referred to as DCPU-0.1/1, DCPU-0.2/1, and DCPU-0.3/1 (Table 3.2.1). Electroactive DCPU films with high elasticity and flexibility were then obtained (Figure 3.2.1B). Polyurethane without DMPA (PU-trimer) and polyurethane without aniline trimer (PU-COOH) were two control groups. The chemical structure of the DCPU was verified by FTIR (Figure 3.2.2). The urethane and urea groups were confirmed by specific peaks at 3340 cm^{-1} (N-H stretching of urethane and urea groups), 2940 cm^{-1} and 2860 cm^{-1} (symmetric and asymmetric C-H stretching), 1720 cm^{-1} (C=O stretching of urethane and urea groups)[268]. The specific peaks for aniline trimer were located at 1600 cm^{-1} and 1510 cm^{-1} (C=C stretching of quinoid and benzenoid rings), and 820 cm^{-1} (C-H bending in benzenoid rings)[269].[263].

The DCPU polymers had low glass transition temperatures (T_g s) below $-60\text{ }^\circ\text{C}$ (Table 3.2.1), which were attributed to PCL soft segment. The T_g decreased by reducing the PCL amount in DCPU backbone. The melting temperatures (T_m s) of DCPU resulted from the semicrystalline PCL segment, and decreased from $29\text{ }^\circ\text{C}$ to

24 °C with decreased PCL amount in DCPU backbone. The inherent viscosities of DCPU ranged from 1.20 (DCPU-0.3/1) to 2.32 dL/g (DCPU-0.1/1; Table 3.2.1). The water absorption increased with the increasing DMPA amount in DCPU, which was contributed to the hydrophilic carboxyl group on DMPA (Table 3.2.1). DCPU-0.1/1 had the lowest water absorption at $8 \pm 1\%$, while DCPU-0.3/1 had the highest water absorption at $15 \pm 2\%$.

The UV-vis spectra of PU-trimer, DCPU-0.3/1, and PU-COOH, shown in Figure 3.2.3A show their electroactivities and the effects of the conjugated proton donor (DMPA) on DCPU electroactivity. The PU-trimer had two typical absorption peaks at 526 nm (π_b - π_q transition from the benzene ring to the quinoid ring) and 323 nm (π - π^* transition in the benzene ring), which were routinely observed for the emeraldine base form of polyaniline derivatives[261, 305]. After introducing DMPA into the DCPU backbone, the absorption peak at 526 nm shifted to 578 nm, and a small shoulder band at 438 nm appeared, representing the delocalized polaron peak arising from the polaron- π^* transition[259, 271]. However, the PU-COOH showed no absorption peaks in the wavelength range from 300 nm to 1,000 nm due to the absence of aniline trimer in the polyurethane backbone.

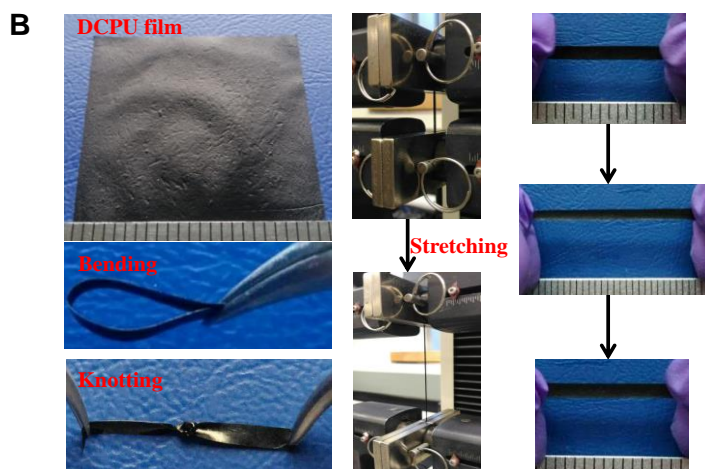
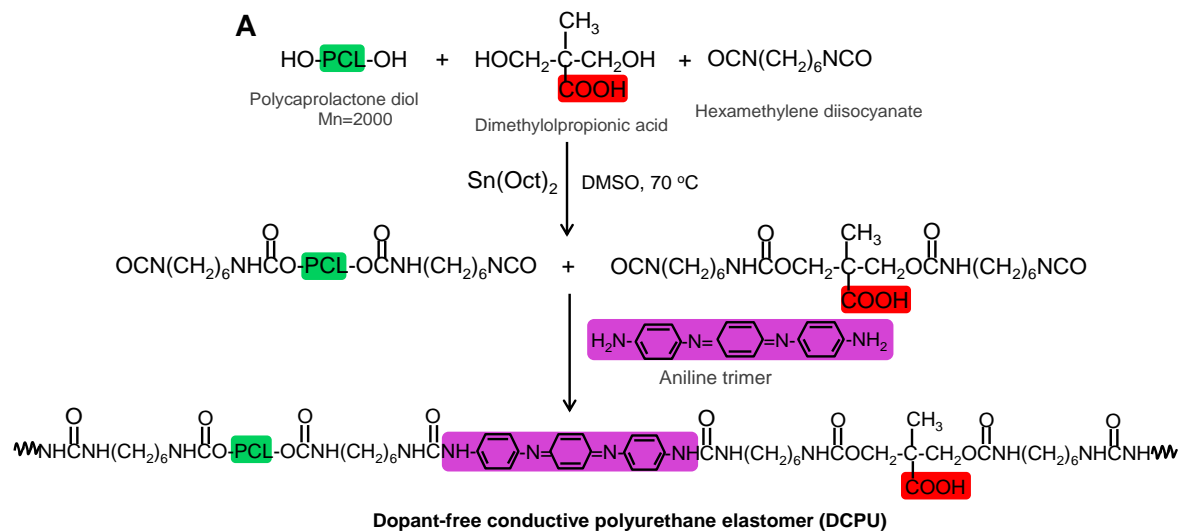


Figure 3.2.1 Dopant-free conductive polyurethane elastomer (DCPU) synthesis. (A) Synthetic scheme of DCPU. (B) Biodegradable DCPU film and its high elasticity presented by bending, knotting, stretching and recoiling.

Table 3.2.1 Polymer film characterization

Samples	Molar ratio of PCL:DMPA:H DI:trimer	T _g (°C)	T _m (°C)	Water absorption (%)	Inherent viscosity (dL/g)	Conductivity (S/cm)		Tensile strength (MPa)	Initial modulus (MPa)	Breaking strain (%)	Instant recovery (%)
						Dry state	Wet state				
PU-trimer	1:0:2:1	-60	32	6±2 ^a	2.54	2.7±0.9 ×10 ⁻¹⁰	4.2±0.5 ×10 ⁻⁸	17.9±2.0 ^a	7.2±0.8 ^a	728±88	99±1
DCPU-0.1/1	0.9:0.1:2:1	-61	29	8±1 ^b	2.32	5.5±0.7 ×10 ⁻⁸	4.4±0.4 ×10 ⁻⁷	12.6±2.3 ^b	5.2±1.1 ^b	695±96	100±2
DCPU-0.2/1	0.8:0.2:2:1	-62	28	9±1 ^c	1.37	4.6±0.4 ×10 ⁻⁷	2.1±0.3 ×10 ⁻⁵	10.9±1.5 ^b	3.6±0.4 ^c	825±198	99±1
DCPU-0.3/1	0.7:0.3:2:1	-67	24	15±2 ^d	1.20	1.2±0.3 ×10 ⁻⁵	4.7±0.8 ×10 ⁻³	9.6±1.2 ^c	3.0±0.6 ^c	695±104	99±1
PU-COOH	0.7:0.3:2:0 [#]	-64	30	19±2 ^e	1.23	5.5 ± 1.2 × 10 ⁻¹²	9.7±0.4 ×10 ⁻⁸	20.3±5.3 ^a	16.5±3.1 ^d	839±275	99±1

*a, b, c, d, e represent significantly different groups for each characteristic; # Chain extender is putrescine in PU-COOH.

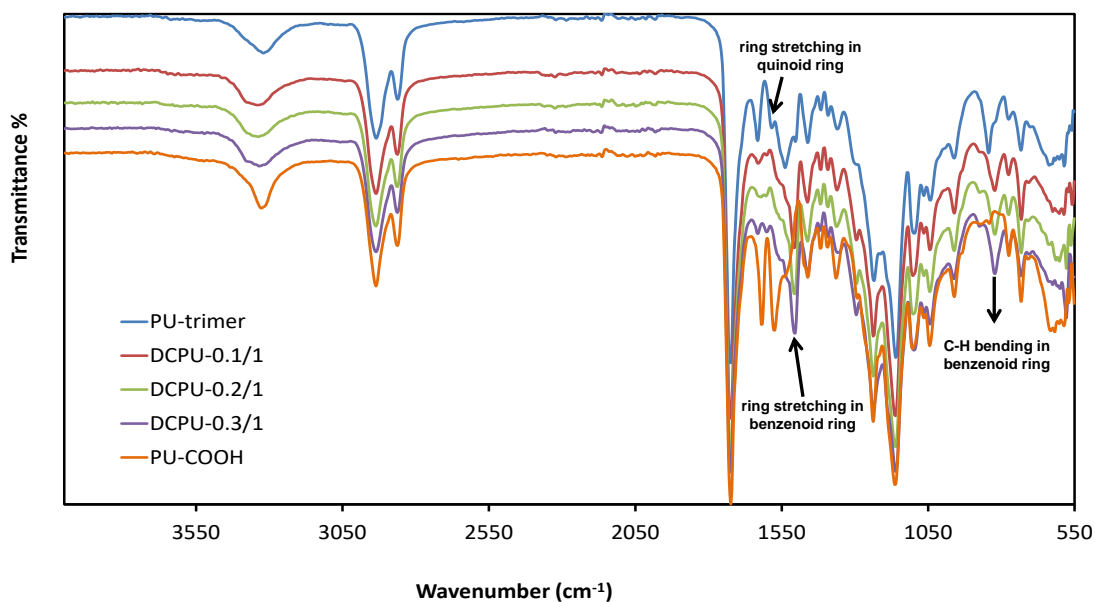


Figure 3.2.2 FTIR spectra of DCPU

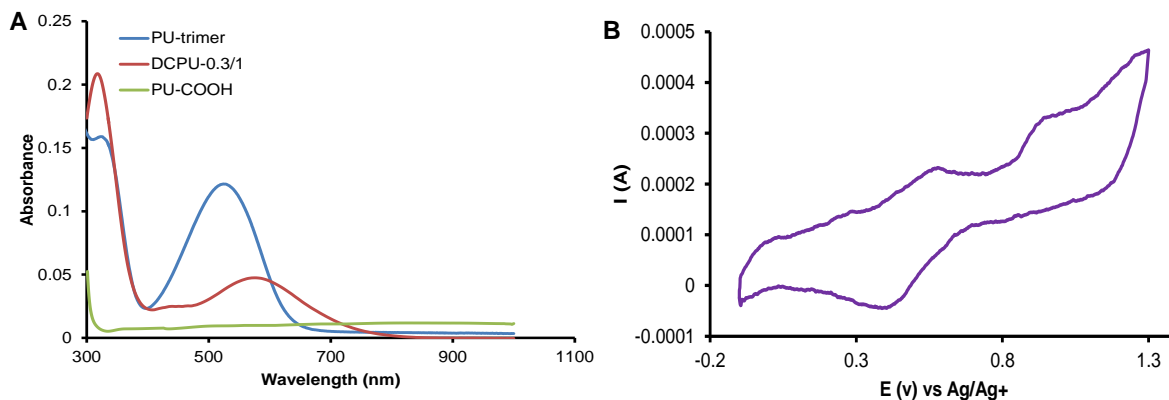


Figure 3.2.3 Electroactivity of DCPU. (A) UV-vis spectra PU-trimer, DCPU-0.3/1 and PU-COOH in DMF. (B) Cyclic voltammogram of DCPU-0.3/1 polymer on Pt electrode in 1.0 M H_2SO_4 using Ag/AgCl as reference with scan rate of 50 mV s^{-1} .

3.2.3.2 Electrical and electrochemical properties of DCPU

The electrical conductivity of DCPU films in dry and wet states is summarized in Table 3.2.1. The conductivities of DCPUs in the dry state ranged from $5.5 \pm 0.7 \times 10^{-8}$ to $1.2 \pm 0.3 \times 10^{-5} \text{ S cm}^{-1}$. With fixed aniline trimer content, the conductivity of the DCPU rose with an increasing DMPA amount in the polyurethane backbone. The PU-trimer without a dopant possessed very low conductivity at $2.7 \pm 0.9 \times 10^{-10} \text{ S cm}^{-1}$, and the PU-COOH without aniline trimer showed a conductivity value close to 0 S cm^{-1} . The conductivities of DCPUs in the wet state (phosphate buffer solution (PBS) immersion) markedly increased compared to those in the dry state, ranging from $4.4 \pm 0.4 \times 10^{-7}$ to $4.7 \pm 0.8 \times 10^{-3} \text{ S cm}^{-1}$. These conductivity values of DCPUs in the wet state showed the same trend as those in the dry state (Table 3.2.1). The conductivity of wet PU-COOH was $9.7 \pm 0.4 \times 10^{-8} \text{ S cm}^{-1}$. This increase was

attributed to the absorbed PBS in the polymer matrix associated with its bulk hydrophilicity (Table 3.2.1). The conductivities of DCPUs were lower than the conductivities of polyaniline (5 S cm^{-1})[299] and some reported biodegradable conductive materials, such as a polythiophene-based multilayer film ($2.7 \times 10^{-2} \text{ S cm}^{-1}$)[306] and a polypyrrole-*b*-polycaprolactone (PPy-PCL) copolymer ($10\text{-}20 \text{ S cm}^{-1}$)[298]. However, the conductivities of DCPUs in wet state (from $4.4 \pm 0.4 \times 10^{-7}$ to $4.7 \pm 0.8 \times 10^{-3} \text{ S cm}^{-1}$) are also comparable to or higher than some reported conductive biomaterials, which have been applied for neural and myocardial repair[133, 134, 307-309]. For example, a blended scaffold of conductive polyurethane containing aniline pentamer and PCL ($10 \times 10^{-5} \pm 0.09 \text{ S cm}^{-1}$) was capable of improving the adhesion and proliferation of rat neonatal cardiomyocytes[133, 134]. Polypyrrole-containing nanofibrous scaffolds (1.3×10^{-5} to $3.7 \times 10^{-4} \text{ S cm}^{-1}$) promoted cardiomyocyte attachment, proliferation and interaction as well as cardiac-specific protein expression [307]. Three-dimensional engineered cardiac tissues (ECTs) from single walled carbon nanotubes (SWNTs) and gelatin hydrogels ($\sim 10^{-3} \text{ S/cm}$) [308] enhanced *in vitro* cardiac contraction and the expression of electrochemical associated proteins, and also structurally integrated with the host myocardium and improved heart function in rats [308]. Furthermore, a biodegradable conductive composite made of polypyrrole (2.5% w/w) and chitosan (97.5% w/w) ($1.3 \pm 0.1 \times 10^{-3} \text{ S cm}^{-1}$) supported the adhesion, spreading and proliferation of olfactory ensheathing cells with or without electrical stimulation[309]. Thus, it is plausible that the electrical conductivities of DCPU polymers would be sufficient to pass the low

micro-current in human bodies and positively affect the cell behaviors such as cell adhesion, proliferation and differentiation. [60, 283, 284]

In the cyclic voltammogram of DCPU-0.3/1 (Figure 3.2.3B), the first redox peak at 550 mV represented the reversible redox process from the leucoemeraldine form to the emeraldine form. With higher potentials, the second peak at 930 mV corresponded to the transition from the emeraldine form to the pernigraniline form. However, the PU-trimer and PU-COOH displayed undetectable electrochemical signals due to their poor conductivities (data not shown). The obvious redox peaks corresponding to the transitions of the three oxidation/reduction forms in DCPU-0.3/1 revealed good electroactivity of the DCPU polymer.

3.2.3.3 Mechanical properties of DCPU films

The DCPU films exhibited robust mechanical properties with softness and high elasticity. The digital images show the attractive mechanical properties of the DCPU polymer, including bending, knotting, stretching, and recoiling (Figure 3.2.1B). The stress-strain curves of these synthesized polyurethanes showed the typical “S” shape (Figure 3.2.4A), and the tensile strengths and initial moduli of the DCPU films ranged from 9.6 ± 1.2 to 12.6 ± 2.3 MPa and from 3.0 ± 0.6 to 5.2 ± 1.1 MPa, respectively (Table 3.2.1). The tensile strengths and initial moduli decreased with increased DMPA content in the DCPU backbone. This might be attributed to the decreased semicrystalline PCL content in the polyurethane backbone, along with reduced PCL crystallinity, which was consistent with the DSC results (Table 3.2.1). The breaking strain of the DCPU films ranged from $685 \pm 104\%$ to $825 \pm 198\%$, with no significant

difference between each group ($p > 0.05$). The instant recovery of all DCPU films was $\geq 99\%$ after three cycles of stretching at 10% strain (Table 3.2.1).

The conductivity change of DCPU-0.3/1 was monitored at various uniaxial strains (30%, 70%, and 100% strain) at room temperature (Figure 3.2.4B). There was a slight conductivity increase of the DCPU-0.3/1 film from $1.2 \pm 0.3 \times 10^{-5} \text{ S cm}^{-1}$ (unstretched) to $3.2 \pm 0.8 \times 10^{-5} \text{ S cm}^{-1}$ at a strain of 30%, followed by a sharp rise to $6.4 \pm 0.6 \times 10^{-4} \text{ S cm}^{-1}$ at 100% strain, which was a 43-fold increase compared with that of unstretched DCPU-0.3/1 film. The conductivity increase of the DCPU film by applied strains (from 30% to 100%) was primarily due to the oriented polymer chains along the stretched direction[310].

To study the resilience of DCPU films, cyclic stretching was performed at a maximum strain of 30% and 300% (Figure 3.2.4C). All the polymers had a large hysteresis loop in the first cycle, followed by smaller hysteresis loops in the next nine cycles. All the samples showed small irreversible deformations ($< 10\%$) at a maximum strain of 30%. With the maximum strain of 300%, the irreversible deformations became larger for all polymer samples ($\sim 200\%$). These results verified that DCPUs are robust, elastic, and flexible, which is promising for soft tissue repair and stretchable soft electronics use.

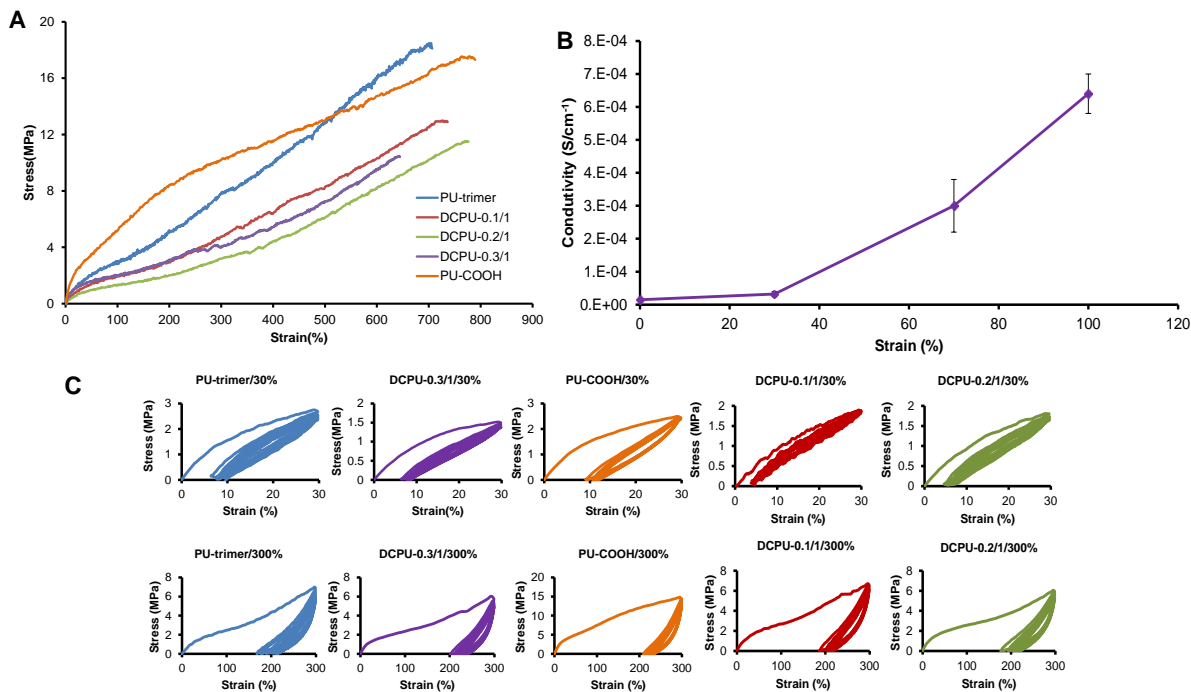


Figure 3.2.4. Mechanical properties of DCPU films. (A) Stress-strain curves of DCPU films. (B) Dependence of electrical conductivity of DCPU-0.3/1 on applied strains varied from 30% to 100%. (C) Cyclic stretching of PU-trimer, DCPU-0.1/1, DCPU-0.2/1 and DCPU-0.3/1 at 30% and 300% deformations.

3.2.3.4 *In vitro* degradation of DCPU films

DCPUs could be degraded by hydrolysis and enzymes (Figure 3.2.5A and B). For hydrolytic degradation in PBS (Figure 3.2.5A), DCPU polymers showed low degradation rates in 8 weeks with mass remaining ranging from $96.6 \pm 0.5\%$ (DCPU-0.3/1) to $98.2 \pm 0.2\%$ (DCPU-0.1/1; $p < 0.05$). The degradation rates of DCPUs increased with an increasing DMPA amount in the DCPU backbone, which resulted from the hydrophilic carboxyl groups in the polyurethane backbone. The higher carboxyl group content allowed more water penetration into the polyurethane film,

which then led to faster hydrolysis^[311]. Besides, many enzymes exist in the human body that can accelerate the degradation of the polymer *in vivo*^[312]. In lipase/PBS solution (Figure 3.2.5B), all polymers degraded faster than in PBS solution. Within 14 days, the polymer degradation behavior showed similar trends as that of DCPUs in PBS. DCPU-0.1/1 had the lowest degradation rate ($92.4 \pm 0.6\%$ mass remaining), whereas DCPU-0.3/1 had the highest degradation rate ($75.8 \pm 2.6\%$ mass remaining).

The changes in mechanical property of DCPU films with degradation time were characterized after 3, 7, and 14 days of degradation in lipase/PBS solution (Figure 3.2.5C-E). The tensile strengths of the DCPU films decreased with increasing degradation time. The tensile strength reductions increased with increased hydrophilicity of DCPU polymers. The DCPU-0.3/1 had the highest tensile strength reduction ($68.2 \pm 4.2\%$ at day 14), and the DCPU-0.1/1 had the lowest tensile strength reduction ($57.9 \pm 7.1\%$ at day 14). The initial moduli of DCPU films eventually showed a decreasing trend after 14 days of degradation with a temporary increase at the beginning of the degradation period. A possible explanation for this phenomenon could be that at an early stage of enzymatic degradation, soft segment degradation starts earlier and is faster while hard segment degradation may not begin or be slower. This result was comparable to a previous study on the hydrolytic degradation of polyurethanes (PU) synthesized from PCL, 1,4-butanediisocyanate and 1,4-butanediol in PBS at 37 °C over 400 days [313]. It was observed that the Young's modulus of PU-2300 (containing PCL with molecular weight at 2300 g/mol) increased up to 300 days and then decreased, which was related to the crystallinity changes with time. In addition, the breaking strains of the DCPU films decreased with the

enzymatic degradation time without significant difference between each sample ($p > 0.05$).

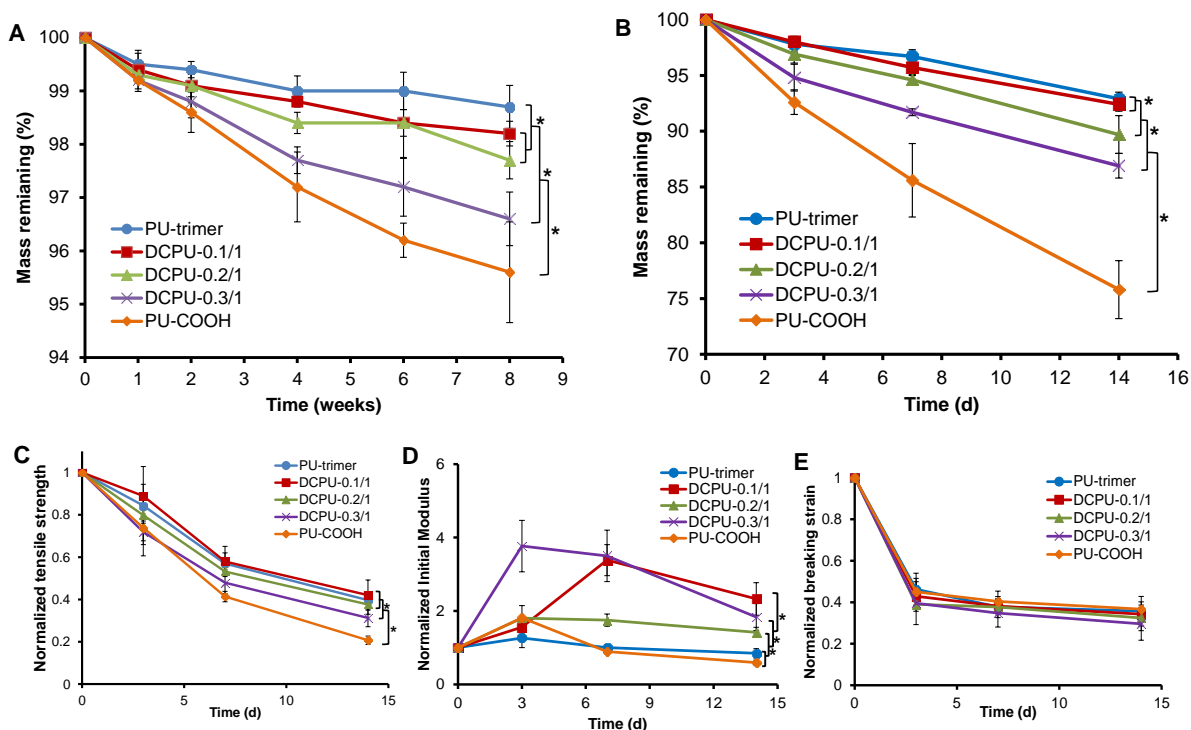


Figure 3.2.5 DCPU film degradation. (A) Mass remaining for DCPU in PBS at 37 °C. (B) Mass remaining for DCPU in 100 U mL⁻¹ lipase in PBS solution at 37 °C. The changes of (C) tensile strengths, (D) initial moduli and (E) breaking strains of DCPU films with enzymatic degradation at 37 °C. * represented significant different groups ($p < 0.05$).

3.2.3.5 Electrical stability of DCPU

The electrical conductivity changes of DCPU films with enzymatic degradation up to day 14 are shown in Figure 3.2.6A. The conductivities of DCPU-0.2/1 and

DCPU-0.3/1 were slightly reduced from $2.1 \pm 0.3 \times 10^{-5} \text{ S cm}^{-1}$ at day zero to $1.2 \pm 0.3 \times 10^{-5} \text{ S cm}^{-1}$ at day 14, and from $4.7 \pm 0.8 \times 10^{-3} \text{ S cm}^{-1}$ at day zero to $1.3 \pm 0.3 \times 10^{-3} \text{ S cm}^{-1}$ at day 14, respectively ($p < 0.05$). Although the conductivities of DCPU-0.2/1 and DCPU-0.3/1 decreased, the values did not fall below more than an order of magnitude over 14 days of enzymatic degradation. Similar testing was carried out by immersing poly(glycerol-sebacate)/polyaniline composites in PBS solution and recording their conductivity changes every 24 h for a period of 4 days[254]. The conductivities of those composites decreased with time and eventually fell by around an order of magnitude. It must be noted that the enzymatic degradation of polymer in lipase/PBS solution was much faster than the hydrolytic degradation in PBS. Thus, DCPUs may be able to maintain their conductivities for a longer time in a physiological environment, which was further proved by the electrical stability testing of DCPU.

The electrical stability of DCPU-0.3/1 film was conducted in the cell culture medium with a long-term charge of a fixed voltage (Figure 3.2.6B). The detected current changes directly reflected the changes in film conductivity. The current in Figure 3.2.6B was normalized against the initial value at time zero. When the DCPU-0.3/1 film was immersed in the cell culture medium, the current doubled in the first 22 h and then gradually increased. At 150 h, the current reached up to 264% of the initial value. To further demonstrate the good electrical stability of DCPUs, PU-trimer doped with (1S)-(+)-10-camphorsulfonic acid (CSA; the molar ratio of CSA:aniline trimer was set as 1.5:1) was treated under the same conditions (Figure 3.2.6B). After 150 h of charge, the CSA-doped PU-trimer retained only 88% of its initial conductivity. The

proton donor (DMPA) was covalently conjugated into the polyurethane backbone, which made the proton donor more difficult to leach out with time or electrical stimulus compared with those free dopants physically mixed in conductive polymers. Furthermore, because of the water absorption ability of DCPU-0.3/1 ($15 \pm 2\%$), shown in Table 1, the absorbed cell culture medium with a large amount of electrolytes diffused in polymer matrix made DCPU-0.3/1 possess almost triple conductivity after 150 h of immersion in cell culture medium (264% of initial conductivity)[314].

The conductive stability of the conductive material is very significant for *in vitro* cell culture and *in vivo* implantation. Conductivity normally decreases with degradation, dopant leaching, and electrical charge (de-doping)[164, 246, 254]. For DCPU, the dopant was covalently linked with the polymer, which significantly reduced dopant leaching and de-doping and gave the polymer good conductive stability. Because of the unavoidable wet environment during biomedical applications[292], DCPUs with good electrical stability have great potential application as electroactive biomaterials.

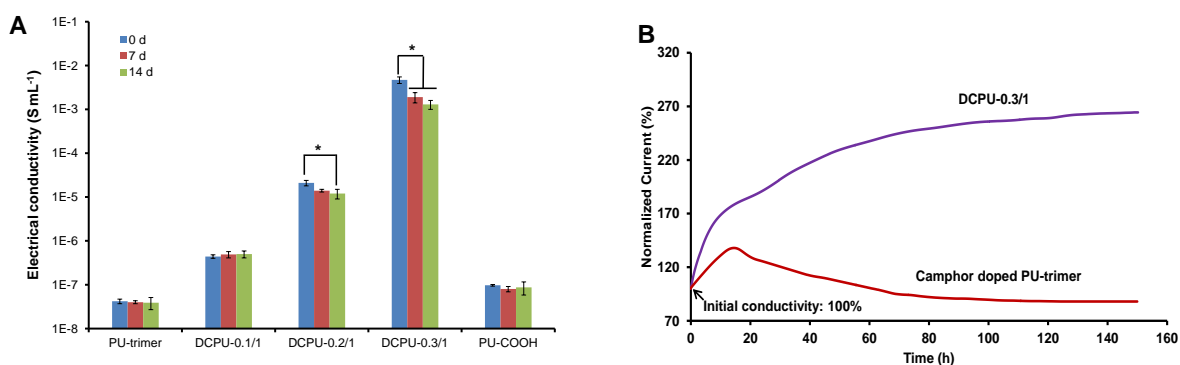


Figure 3.2.6 Electrical stability of DCPU. (A) Changes in electrical conductivities of DCPU films in lipase/PBS solution within 14 d. (B) Relationship between electrical current and incubation time in the electrical stability test of DCPU-0.3/1 film in cell culture medium. Camphor doped PU-trimer film was used as a control.

3.2.3.6 Cytotoxicity and cytocompatibility of DCPUs

The cytocompatibility of DCPU films and the cytotoxicity of their degradation products were evaluated using mouse 3T3 fibroblasts (Figure 3.2.7). The cell viability of all DCPU polymers showed no significant difference from that of the Dulbecco's modified Eagle's medium (DMEM) control when the concentration of polymer degradation products was $\leq 0.1 \text{ mg mL}^{-1}$ ($p > 0.05$; Figure 3.2.7A). There was no statistical difference between each DCPU polymer group at the same concentration of polymer degradation products ($p > 0.05$). This trend was further visualized by the optical images of 3T3 fibroblasts exposed to different concentrations of DCPU degradation products (Figure 3.2.7B).

Regarding the cytocompatibility of DCPU films (Figure 3.2.7C), the 3T3 fibroblasts proliferated on both DCPU film surfaces and TCPS from 1 to 5 days ($p < 0.05$) with no significant difference between the polymer films and TCPS during 5 days of incubation ($p > 0.05$). The cell morphologies on the DCPU films were visualized by SEM (Figure 3.2.7D). The cells spread on the polymer films and formed a confluent layer covering the surface of the DCPU films. The magnified SEM image of the single-cell spread on DCPU-0.3/1 film with clear pseudopods is shown in Figure 3.2.7D. The results indicate the good cytocompatibility of DCPU films. We are aware that 3T3 fibroblasts are robust clonal cell line and may have higher tolerance of

material toxicity. Future studies should be carried out using specialized and perhaps primary cells to better assess the potential tissue- and cell-specific toxicity of DCPU polymers.

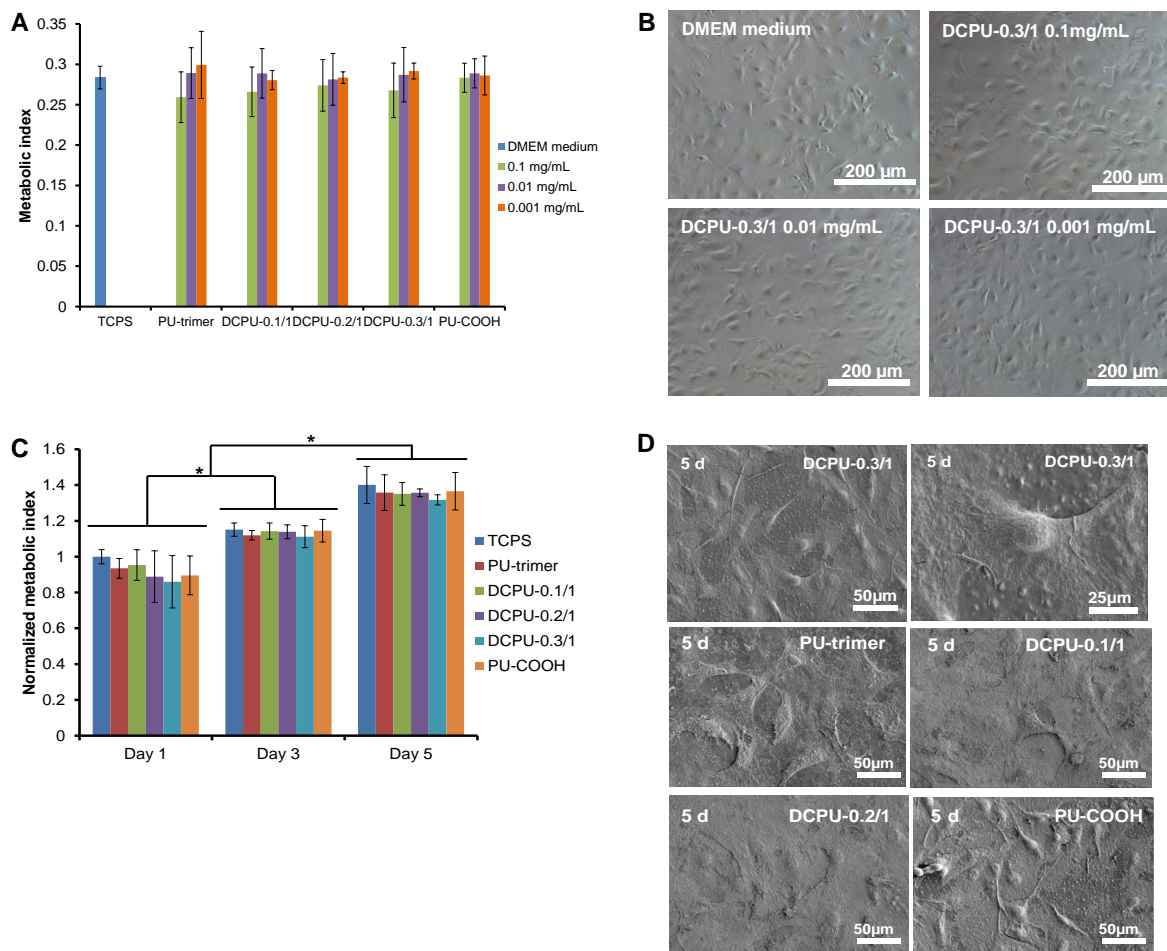


Figure 3.2.7 *In vitro* DCPU cytotoxicity and cytocompatibility. (A) Metabolic index of mouse 3T3 fibroblasts cultured with DMEM medium mixed with DCPU degradation products at concentrations of 1, 0.1, 0.01 and 0.001 mg mL⁻¹. (B) Optical microscopy images of mouse 3T3 fibroblasts cultured with DMEM medium mixed with DCPU-0.3/1 degradation products at concentrations of 0.1, 0.01 and 0.001 mg mL⁻¹. DMEM

medium was used as the control. (C) Metabolic index of mouse 3T3 fibroblasts seeded on polyurethane films (TCPS as a control) at days 1, 3 and 5. (D) Scanning electron micrographs of mouse 3T3 fibroblasts cultured on the DCPU-0.3/1 (500 × and 1000× magnification), PU-trimer, DCPU-0.1/1, DCPU-0.2/1 and PU-COOH films at day 5. *represented significant different groups ($p < 0.05$).

3.2.3.7 Fabrication and characterization of porous DCPU scaffold

DCPU can be processed into porous scaffolds using the salt leaching technique (Figure 3.2.8A), which is a convenient way to obtain porous scaffolds with controllable pore size and porosity[37, 134]. The morphology of DCPU porous scaffolds was observed by SEM (Figure 3.2.8B). The salt particle shaped pores were obvious and interconnected. The pore size and porosity of the DCPU scaffolds were $116 \pm 25 \mu\text{m}$ and $86 \pm 4\%$, respectively. The poor processability of conventional conductive polymers has limited their biomedical applications due to their poor solubility and flexibility[164]. A conductive polyurethane with aniline pentamer had to be a diffusive additive to blend with PCL to form a film and a porous scaffold because of the poor solubility of this conductive polyurethane, and it still required mixing with a dopant[133, 134]. However, DCPU as a single-component conductive polymer can be processed into porous conductive scaffolds with flexibility and elasticity without adding extra additives and dopants. This unique property may facilitate the preparation of scaffolds with good material stability and controllability.

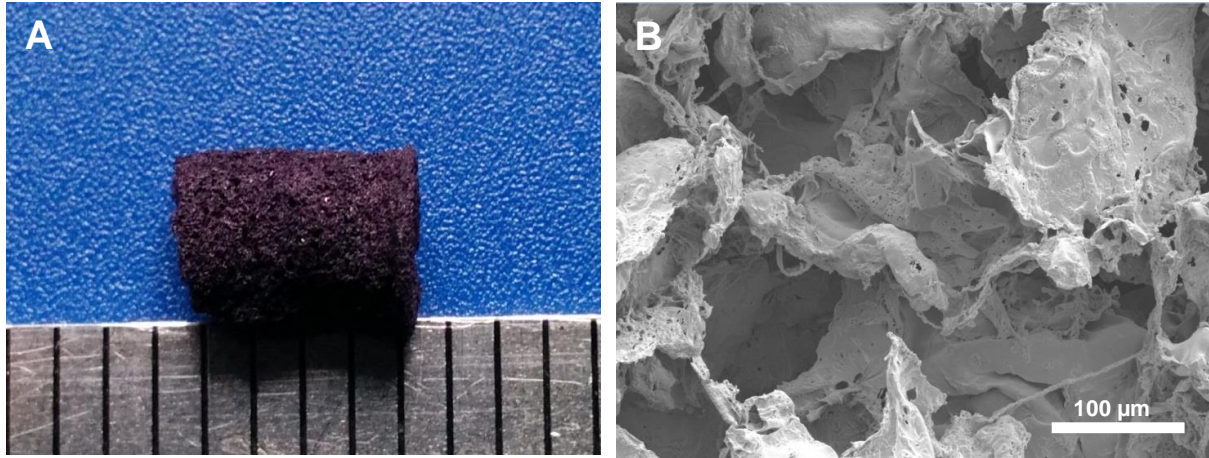


Figure 3.2.8 Porous DCPU scaffold. (A) Digital image and (B) SEM image of porous DCPU-0.3/1 scaffold fabricated by salt leaching.

3.2.3.8 *In vivo* mouse subcutaneous implantation

In vivo tissue compatibility of DCPU porous scaffold was evaluated utilizing subcutaneous implantation in mice model for 2 and 4 weeks. Porous scaffold fabricated using PCL, which has excellent tissue biocompatibility and has been used in fabrication of FDA-approved devices, was chosen as a positive control [273, 315-318]. The implants and surrounding tissues were stained with H&E and DAPI (nuclei) staining to reflect the extent of tissue compatibility and cell infiltration, respectively (Figure 3.2.9A-H). H&E staining showed that tissue responses to DCPU scaffolds were comparable to those to PCL scaffolds and only small number of inflammatory cells were found at the interface between tissue and both scaffolds at Week 2 (Figure 3.2.9A vs. E) and Week 4 (Figure 3.2.9C vs. G). Similarly, we found that both PCL scaffolds and DCPU scaffolds were infiltrated with large number of host cells (stained with DAPI) after implantation for 2 weeks (Figure 3.2.9B vs. F) and 4 weeks (Figure 3.2.9D vs. H). The *in vivo* results support that DCPU scaffolds have good tissue/cells

compatibility while facilitating cell infiltration at the extent similar to PCL scaffolds. Our results support that DCPU possesses excellent cell and tissue compatibility suitable for the fabrication of a variety of tissue engineering scaffolds, medical implants and bioelectronics.

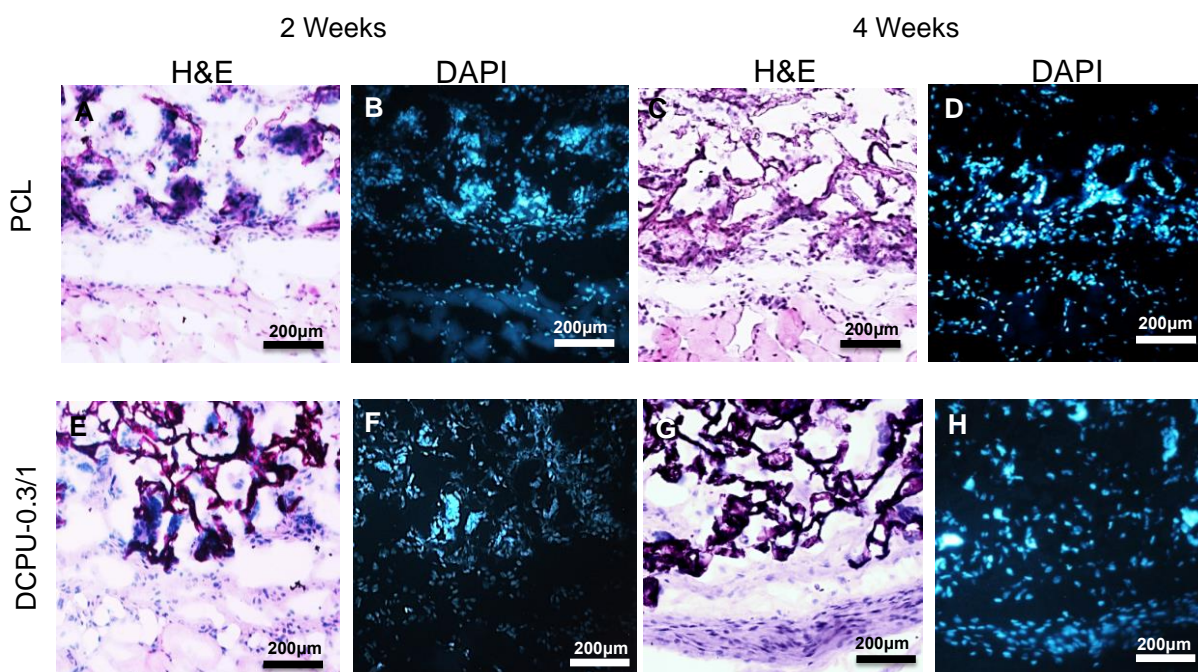


Figure 3.2.9 *In vivo* biocompatibility of DCPU porous scaffolds in a mouse subcutaneous model. H&E (A, C, E and G) and DAPI (B, D, F and H) staining of the tissue surrounding PCL (A-D) and DCPU-0.3/1 (E-H) porous scaffolds which were implanted for 2 weeks (A, B, E and F) and 4 weeks (C, D, G and H). PCL scaffolds were used as a positive control.

3.2.4 Conclusion

A biodegradable dopant-free conductive polymer with good elasticity and flexibility was synthesized. Compared to existing biodegradable conductive materials, DCPU is a unicomponent biodegradable elastomer with good electroactivity and

electric stability and processability. It also exhibits good cytocompatibility and *in vivo* biocompatibility. The DCPUs may find opportunities to be utilized in tissue repair and regeneration, and other biomedical-related application. This simple and effective methodology can also be utilized to develop serials of novel dopant-free conductive polymers.

CHAPTER 4
BIODEGRADABLE POLYURETHANE SCAFFOLDS MECHANICALLY MATCHING
WITH NATIVE MYOCARDIUM

4.1

SYNTHESIS AND CHARACTERIZATION OF LOW-INITIAL-MODULUS
BIODEGRADABLE POLYURETHANE ELASTOMERS

4.1.1 Introduction

Mechanically matched scaffold with host tissues has been one of the primary considerations in tissue engineering and regenerative medicine.[319] Repairing different host tissues requires biodegradable scaffolds with distinct biomechanics, such as load bearing, force generation, and transmission.[125] The mechanical mismatch between the scaffolds and host tissues would trigger foreign body reactions and/or cause implantation failure. For example, the mechanical mismatch between the rigid implant materials and soft brain tissue would stimulate neuroinflammatory response.[320] The mechanical mismatch between vascular graft and human artery would result in intimal hyperplasia and thrombosis.[321] The mechanical mismatch between the synthetic cardiac patch and the host myocardium would lead to abnormal cardiac functions, such as arrhythmia.[126] Generally, most of the soft elastic tissues showed a typical J-shaped stress-strain curve with relatively low elastic moduli, such as 0.1–2 MPa for skin,[322] 0.002–0.1 MPa for aortic valve leaflet,[323,

324] and 0.02–0.5 MPa for heart muscle.[287, 325]Therefore, it is crucial to develop biodegradable robust polymers with low initial modulus for soft tissue engineering.

Biodegradable polyurethanes have been of great interest in soft tissue engineering due to their good biocompatibility, and strong and resilient mechanical properties similar to the soft tissues. Variety of biodegradable polyurethanes have been investigated to repair soft tissues, such as abdominal wall,[216]heart and blood vessels,[326-328]adipose,[329]and skin.^[330]Polyurethanes are usually synthesized from three “blocks”: soft segment, hard segment, and chain extender. The mechanical properties of polyurethanes can be flexibly tuned by altering these three blocks.[19, 25, 331] For example, a biodegradable polyurethane from a soft segment PVCL (molecular weight = 6000) diol and hard segment BDI with a chain extender putrescine had an initial modulus of 2.8 ± 1.3 MPa (film) in dry state, which has markedly lower initial modulus than a polyurethane (12.1 ± 2.5 MPa) based on the semicrystalline PCL, BDI and putrescine.[25]However, the value still is higher than those of soft tissues. To further reduce the initial moduli of polyurethanes under a physiological condition, one promising strategy is to incorporate hydrophilic PEG into the soft segment.[32] The incorporation of PEG can markedly enhance the water absorption ability of polymers.[332] The absorbed water in “bound state” can attach to polymer chains via hydrogen bonding and work as a plasticizer, which can reduce initial modulus.[333, 334]

In this work, we designed a series of biodegradable elastic polyurethanes with low initial moduli through designing a novel soft segment, which can be used to engineer the low-moduli soft elastic scaffold to mechanically match with soft tissues.

We firstly synthesized new triblock copolymer PVCL-PEG-PVCL with various PEG molecular weights and total molecular weights, where the PVCL block is random with VL/CL molar ratio of 50/50 to maximally reduce crystallinity. The polyurethanes were then synthesized from the new complex triblock PVCL-PEG-PVCL as a soft segment, HDI as a hard segment and putrescine chain extender. The polyurethanes synthesized from copolymer PVCL diols without PEG block were set as controls. The chemical structure, thermal properties, *in vitro* degradation, and cytocompatibility of polyurethane films were studied. The mechanical properties were measured in dry and wet states. The selected polyurethanes were then processed into porous scaffolds using TIPS, and the porous scaffolds were characterized mechanically in dry and wet states. Mouse subcutaneous implantation was utilized to evaluate *in vivo* tissue compatibility and cell infiltration ability of the scaffolds to verify their potential applications for soft tissue engineering. .

4.1.2 Experimental section

4.1.2.1 Materials

All chemicals were purchased from Sigma unless otherwise noted. VL, putrescine and HDI were purified through vacuum distillation ahead of use. Diethylene glycol (DEG) was vacuum dried at 60°C overnight prior to use. Caprolactone (CL), PEG (MW=1000 and 2000), Sn(Oct)₂, diethyl ether, anhydrous dichloromethane (DCM), HFIP (Oakwood Product), DMSO, PBS, lipase from *Thermomyceslanuginosus* (≥100,000 U/g) and HMDS were used as received.

4.1.2.2. Synthesis of PVCL copolymer diols and PVCL-PEG-PVCL triblock copolymer diols

Random copolymer PVCL and triblock copolymer PVCL-PEG-PVCL diols were obtained from VL and CL by ring-opening polymerization with $\text{Sn}(\text{Oct})_2$ as the catalyst and DEG (for PVCL synthesis) or PEG (molecular weight=1000 and 2000) as an initiator (Figure 4.1.1A).[25, 335] VL, CL and DEG or PEG were mixed in a flask (250 mL), and reacted at 120 °C under N_2 protection with $\text{Sn}(\text{Oct})_2$. After 24 h, the synthesized polymer diols were dissolved in DCM and then precipitated in cold diethyl ether. The obtained polymer diols were dried at 60°C for 3 days in a vacuum oven for further polyurethane synthesis. The molar ratio of VL/CL was fixed as 50/50.

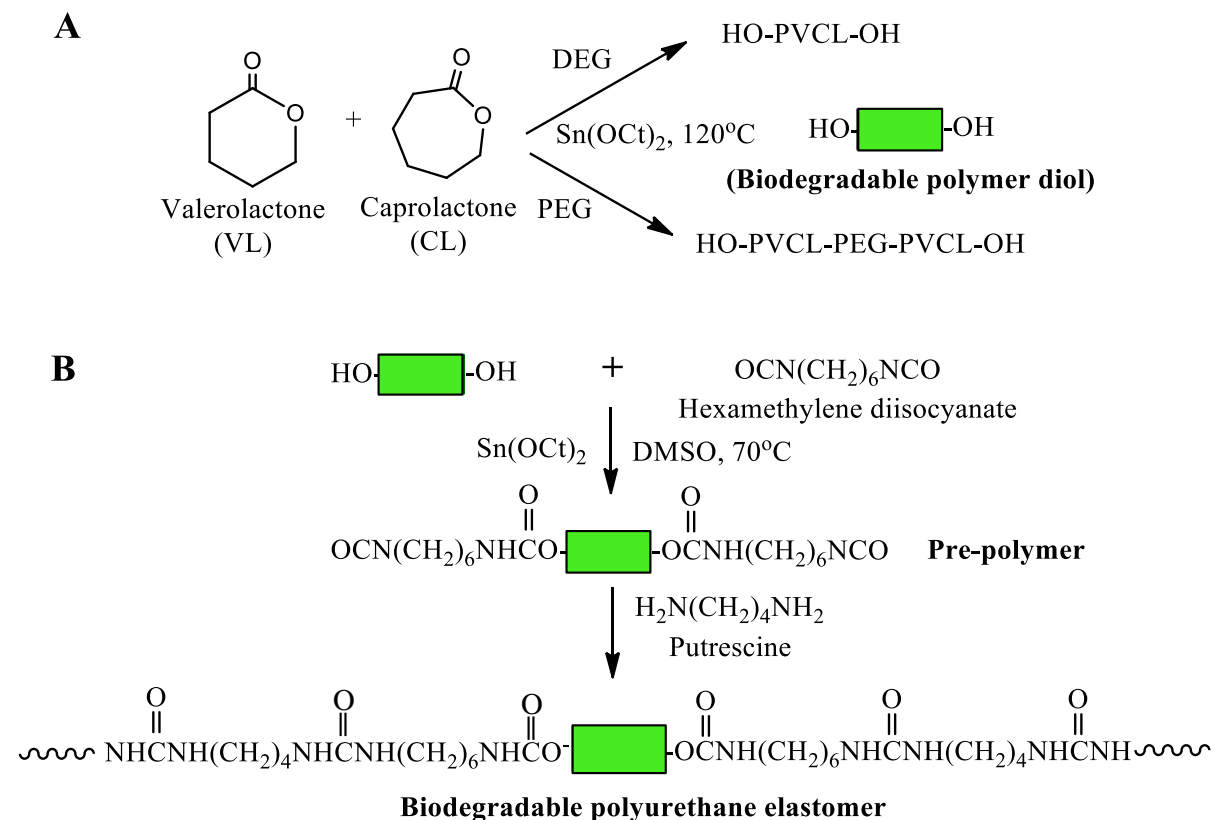


Figure 4.1.1 Synthetic scheme of (A) PVCL or PVCL-PEG-PVCL copolymer diols and (B) polyurethanes.

4.1.2.3 Synthesis of polyurethanes

Polyurethanes (PU) were synthesized from PVCL or PVCL-PEG-PVCL diols, HDI and putrescine via a two-step solution method (Figure 4.1.1B).[273] Polymer diols and HDI with Sn(Oct)₂ were reacted in DMSO at 70°C in a glass flask with N₂ input and stirring for 3 h. The putrescine/DMSO mixture was then added into the prepolymer solution at room temperature. After 18h, the polymer was precipitated by use of deionized water and purified in 2-propanol. The obtained polyurethane was vacuum-dried at 60 °C for 2 days. The molar ratio of polymer diol/HDI/putrescine was set as 1:2:1. The yields of all products were above 90%. The polyurethane products were named as PU-PEG_x-PVCL_y, where x and y denote the molecular weight of PEG and PVCL, respectively. Polyurethane films were prepared by a solvent casting method. The solvent is HFIP. The obtained films were further dried at 60 °C in a vacuum oven for 3 days.[37]

4.1.2.4 Polymer characterization

The chemical structure and relative component molecular weight of PVCL and PVCL-PEG-PVCL diols were characterized by ¹H nuclear magnetic resonance (¹H-NMR, JEOL ECX 300 MHz) with CD₃Cl as a solvent. The block length of the copolymer diols can be calculated from NMR spectra by the integrals of specific peaks from DEG or PEG segments and those from PVCL segments. FTIR (Nicolet 6700, Thermo Electron Corporation) was used to verify chemical structures of polyurethanes.

DSC-60 differential scanning calorimetry (Shimazu) was used to characterize the film thermal properties from -100 to 200 °C with 10°C/min heating rate and nitrogen flow. A sessile drop method was utilized to measure water contact angle on the film surface (n=8) in air on a contact angle instrument (FTA-1000B, First Ten Angstroms). For water absorption, the weighed PU films (W_0 , n=3) were immersed in PBS at 37 °C. After 24h, the samples were weighed (W_1) after removal of the surface residual water. The water absorption ratio was computed as $[(W_1-W_0)/W_0] \times 100\%$.

Inherent viscosity (IV) of the polyurethanes was measured on a Ubbelohde viscometer for polymer molecular weight characterization because polyurethanes may damage gel-permeation chromatographic (GPC) columns by their strong hydrogen bonding.[199] Each polymer solution (0.1g/dL) in HFIP was filtered using a 1.2 μm glassfiber filter. The measurement was conducted at 25°C and repeated five times. The IV was calculated as $\ln(t_p/t_s)/C_p$, where t_p is the time for polymer solution flowing through the glass capillary, t_s is the time for HFIP solvent alone, and C_p is the concentration of polymer solution.

4.1.2.5 Uniaxial mechanical properties

Stripes of 2x20 mm (n=6) were cut from the PU films and were tested on a MTS Insight Testing System (500 N loading cell) with a 10mm/min cross-head rate at room temperature. The measured samples were tested in both dry and wet states. Instant strain recovery (n=3) was measured by stretching the stripe at 10% strain and 10 mm/min stretching rate, holding for 1 min, and then releasing; this cycle was repeated three times. Instant strain recovery was computed from the formula $[1-(L_1-$

$L_0/L_0 \times 100\%$, where L_0 is the original length of the stripe and L_1 is the final length after three cycles. Cyclic stretch testing was conducted by stretching the stripes (2x20 mm, n=3) to strain at 30% or 300% and then releasing back to 0% strain.[25] This measurement was repeated for 10 cycles at fixed rate of 10 min/min.

4.1.2.6 *In vitro* degradation

The weighed polymer films (W_0) were immersed in PBS (10 mL, hydrolytic degradation) or 100 units/mL lipase/PBS solution (2 mL, enzymatic degradation) at 37 °C.[336] The lipase/PBS solution was refreshed every 3 days. Samples (n=3 for each sample at each time point) were weighed (W_1) after a deionized water rinse and lyophilization. The mass remaining was calculated as $W_1/W_0 \times 100\%$.

4.1.2.7 *In vitro* cytocompatibility of polyurethane films

Polyurethane disk (6 mm diameter) were obtained from the films by use of standard biopsy punches (6 mm, Miltex). UV irradiation (1 h, 30 min for each side) was used to sterilize the disks. Before cell seeding, the sterilized disks were rinsed three times with sterilized PBS solution and then immersed in DMEM supplemented with 10% fetal bovine serum, 100 units/mL penicillin, and 100 µg/mL streptomycin for 24 h. Mouse 3T3 fibroblasts (2×10^3) (ATCC, Manassas, VA) were seeded on each disk surface. The cell culture medium was changed every 3 days. A MTT assay was used to detect cell metabolic activity (n = 5) at days 1, 3, and 5. The 3T3 fibroblast-seeded films were fixed by use of 2.5% glutaraldehyde solution at 4 °C to observe cell morphology. The samples were then dehydrated in a series of ethanol solutions,

immersed in HMDS, and dried in air. The 3T3 fibroblast morphology on the films was recorded under SEM (Hitachi S-4800 HRSEM).

4.1.2.8 Porous scaffold fabrication

Polyurethane scaffolds were fabricated via TIPS technique according to a previous study.[118] A 5% (w/v) polymer solution in DMSO was poured into a glass cylinder mold at 80 °C. The mold was then immediately placed in an –80 °C freezer. After 3 h, the mold was immersed in a 70% ethanol bath at 4 °C for 3 days to completely remove DMSO. The scaffold removed from the mold was then immersed in a large amount of deionized water to extract ethanol. The porous scaffold was frozen and lyophilized for further measurements.

4.1.2.9 Scaffold characterization

The scaffold morphology was observed under SEM, and the pore size was measured by use of ImageJ software (National Institutes of Health, UIH). The scaffold porosity was tested by ethanol displacement.[304, 337] Mechanical properties of the porous scaffolds were measured by use of the same protocols as for polymer films at room temperature. For suture retention strength, porous scaffolds were cut into 5×20 mm strips. A single loop of 4-0 silk braided suture (Ethicon, Inc.) was created 5 mm from distal of the strip. Samples (n=4 for each group) were then tested as described above for the tensile testing of the polyurethane films. The suture retention strength was calculated as load force (newton)/ (suture diameter[millimeters] × sample thickness [millimeters]).[138]

4.1.2.10 Mouse subcutaneous implantation

All experimental designs for animal study were reviewed and approved by the University of Texas at Arlington Institutional Animal Care and Use Committee (IACUC) according to NIH guidelines for the use of laboratory animals. Female Balb/c mice (20–25 g; Taconic Farms, Germantown, NY) were used. Disk-shaped scaffolds (6 mm diameter by 300 μ m thickness, two implants per animal) were placed in the mouse dorsal subcutaneous area. After 2 weeks, the implants and surrounding tissues were explanted for cryosection and hematoxylin and eosin (H&E) staining. The extent of inflammatory cell recruitment and infiltration around and in the implants was then calculated by use of ImageJ software.

4.1.2.11 Statistical analysis

All results are exhibited as mean \pm standard deviation. One-way analysis of variance (ANOVA) with a posthoc Tukey–Kramer test was used for all data analysis. For polyurethane film degradation, a repeated measure ANOVA was conducted with the SAS. Significant differences were considered when $p < 0.05$.

4.1.3 Results

4.1.3.1 Synthesis and characterization of PVCL and PVCL-EPG-PVCL diols

$^1\text{H-NMR}$ spectra confirmed the chemical structure of synthesized PVCL copolymer diols (Figure 4.1.2A) and PVCL-PEG-PVCL triblock copolymer diols (Figure 4.1.2B). The specific peaks of methyl protons of the PVCL blocks (in the region between 1.34 to 4.06 ppm in Figure 4.1.2A and B) were demonstrated in both

PVCL and PVCL-PEG-PVCL copolymer diols. The ethylene oxide protons of the PEG block in PVCL-PEG-PVCL triblock copolymer diols were assigned to δ 3.66 ppm, δ 4.35 ppm and δ 4.23 ppm (Figure 4.1.2B). The block lengths of PVCL and PVCL-PEG-PVCL in calculation were close to those in theory. Specifically, the calculated block molecular weight of PVCL_{2K} and PVCL_{6K} were 1936 and 5576, respectively. The theoretical molecular weights of PVCL blocks ranged from 500 to 3000 in PVCL-PEG-PVCL triblock copolymer diols, which were practically distributed as 493-1000-493 in PEG_{1K}-VCL_{1K}, 2763-1000-2763 in PEG_{1K}-VCL_{6K}, and 2873-2000-2873 in PEG_{2K}-VCL_{6K} (Table 4.1.1).

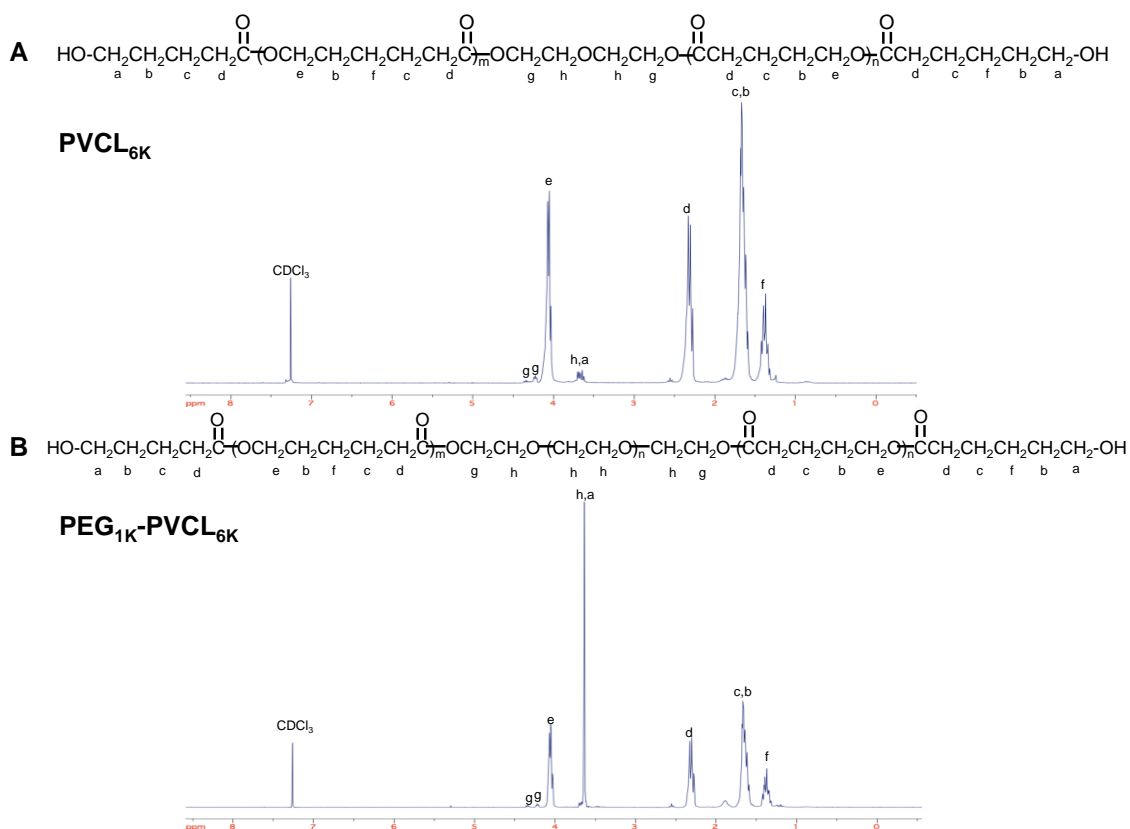


Figure 4.1.2 ¹H-NMR spectra of (A) PVCL and (B) PVCL-PEG-PVCL copolymer diols.

Table 4.1.1 Block length of polyurethane soft segment

Polyurethane soft segment	Theoretical molar ratio of CL/VL	Calculated molar ratio of CL/VL	Theoretical block length of PVCL or PVCL-PEG-PVCL	Calculated block length of PVCL or PVCL-PEG-PVCL
PVCL _{2K}	50/50	58/42	2000	1936
PVCL _{6K}	50/50	53/47	6000	5576
PEG _{1k} -PVCL _{1K}	50/50	57/43	500-1000-500	493-1000-493
PEG _{1k} -PVCL _{6K}	50/50	51/49	3000-1000-3000	2763-1000-2763
PEG _{2k} -PVCL _{6K}	50/50	58/42	3000-2000-3000	2873-2000-2873

4.1.3.2 Synthesis and characterization of polyurethanes

In FTIR spectra (Figure 4.1.3), the soft segments in polyurethanes are mainly related to the asymmetrical and symmetrical stretching of the methyl and methylene groups between 2800 and 3000 cm^{-1} . The hard segments in polyurethanes are primarily characterized by the absorption peaks from urethane groups: N-H stretching between 3300 and 3500 cm^{-1} , C=O stretching at 1730 cm^{-1} , C-N stretching and N-H symmetrical bending between 1530 and 1580 cm^{-1} . The intensity ratio of hard segment absorption peaks at 3300–3500 cm^{-1} to soft segment absorption peaks at 2800-3000 cm^{-1} can reflect the content ratio of hard segments to soft segments in polymers. Polyurethanes with higher molecular weight of soft segments and lower content of hard segments showed lower absorption peaks at 3300–3500 cm^{-1} . The absorbance at 1100 cm^{-1} was mainly attributed to the ether groups in soft segments, and also corresponded to the C-O-C stretching absorptions from urethane groups.[268] The intensities of the C-O-C stretching absorption peak at 1100 cm^{-1} in

PU-PVCL_{2K} and PU-PVCL_{6K} were relatively lower than those in polyurethanes containing PEG segments with abundant ether groups.

All polyurethanes had glass transition temperatures (T_gs) lower than -55°C (Table 4.1.2). The T_g decreased with increasing soft segment molecular weights. Comparing the polyurethanes (PU-PVCL_{6K}, PU-PEG_{1K}-PVCL_{6K}, and PU-PEG_{2K}-PVCL_{6K}) with the same PVCL block length and different PEG molecular weights, the introduction of PEG segment decreased the T_g. All the polymers showed melting temperatures (T_ms) below room temperature from -7 °C to 9 °C, suggesting that none of the polyurethanes had crystalline domains at room or body temperature. Polymer inherent viscosities ranged from 1.42 to 2.17 dL/g (Table 4.1.2).

The surface and bulk hydrophilicity of polyurethane films were characterized by water contact angle and water absorption (Table 4.1.2), respectively. The decrease of PVCL block length and the increase of PEG block length in soft segments led to an increase of surface hydrophilicity of polyurethanes, which was related to the decreasing water contact angle ($p < 0.05$). The water absorption decreased with increasing PVCL molecular weight ($p < 0.05$). The incorporation of the PEG component into the polymer backbone increased the hydrophilicity of polyurethanes, which was associated with an increase of water absorption ($p < 0.05$). The increasing PEG content in the soft segments from 14 % (PU-PEG_{1K}-PVCL_{6K}) to 50 % (PU-PEG_{1K}-PVCL_{1K}) resulted in the increase of water absorption from 23±3% (PU-PEG_{1K}-PVCL_{6K}) to 65±5% (PU-PEG_{1K}-PVCL_{1K}).

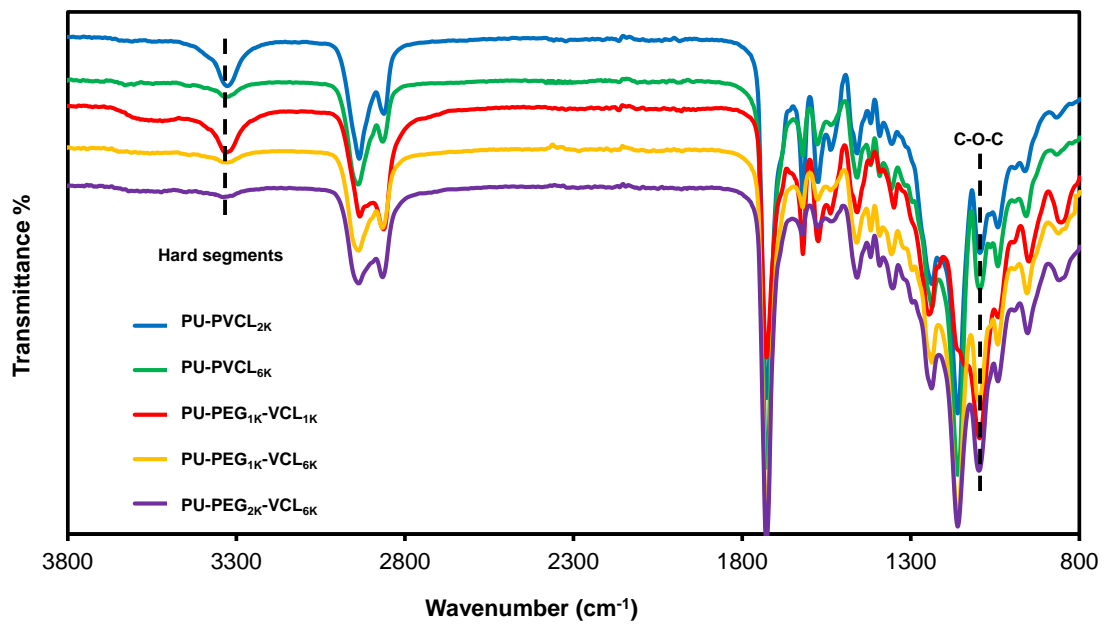


Figure 4.1.3 FTIR spectra of polyurethane.

Table 4.1.2 Polymer film characterization*

Samples	Tg (°C)	Tm (°C)	Inherent viscosity (dL/g)	Contact angle (°)	Water Absorption (%)	Tensile strength (MPa)		Initial modulus (MPa)		Breaking strain (%)		Instant recovery (%)
						Dry state	Wet state	Dry state	Wet state	Dry state	Wet state	
PU- PVCL _{2K}	-59	9	1.42	65±4 ^a	24±2 ^a	14.4±1.8 ^a	13.4±1.5 ^a	17.3±1.9 ^a	16.7±1.5 ^a	1212±245 ^a	1050±178 ^a	99±1
PU- PVCL _{6K}	-64	6	1.98	79±5 ^b	12±3 ^b	10.6±1.7 ^a	13.3±0.9 ^a	3.1±0.6 ^b	3.8±0.5 ^b	1588±65 ^b	1785±165 ^b	100±1
PU- PEG _{1K} - PVCL _{1K}	-63	-7	1.49	28±3 ^c	65±5 ^c	12.2±1.3 ^a	8.2±0.9 ^b	18.6±0.7 ^a	9.1±0.5 ^c	855±204 ^c	808±60 ^a	100±1
PU- PEG _{1K} -	-66	7	2.05	69±2 ^{a,d}	23±3 ^a	6.4±0.4 ^b	4.3±0.3 ^c	3.5±0.4 ^b	2.3±0.6 ^d	1629±249 ^b	1470±229 ^c	100±2
PU- PEG _{2K} - PVCL _{6K}	-67	8	2.17	61±3 ^{a,e}	41±7 ^d	1.1±0.2 ^c	0.7±0.1 ^d	2.2±0.3 ^b	0.9±0.3 ^e	296±59 ^d	244±35 ^d	99±1

*a, b, c, d, e represent significerences for each group and each characteristic.

4.1.3.3 Mechanical properties of polymer films

Mechanical properties of polyurethane films in dry and wet states were summarized in Table 4.1.2, and the typical stress-strain curves of polymer films were shown in Figure 4.1.4. In dry state, the tensile strengths of the polyurethane films ranged from 1.1 ± 0.2 to 14.4 ± 1.8 MPa, the initial moduli from 2.2 ± 0.3 to 18.6 ± 0.7 MPa, and the breaking strains from 296 ± 59 to $1629\pm 249\%$. The tensile strength and initial modulus were associated with the molecular weight of soft segments, which markedly decreased with the increasing molecular weight of soft segments ($p < 0.05$). The PU-PEG_{2K}-PVCL_{6K} with the highest molecular weight of soft segments showed the lowest initial modulus (2.2 ± 0.3 MPa) and tensile strength (1.1 ± 0.2 MPa) in dry state. The instant recovery of all polyurethane films was $\geq 99\%$ after repeatedly stretching for 3 cycles at 10% strain.

The introduction of PEG block into soft segments had great effects on the mechanical properties of polyurethanes in wet state, compared to those polyurethanes in dry state (Table 4.1.2). For the polyurethanes incorporated with PEG segments (PU-PEG_{1K}-PVCL_{1K}, PU-PEG_{1K}-PVCL_{6K}, and PU-PEG_{2K}-PVCL_{6K}), the initial modulus and tensile stress reduced greatly from dry state to wet state ($p < 0.05$). The initial modulus of PU-PEG_{1K}-PVCL_{6K} decreased from 3.5 ± 0.4 to 2.3 ± 0.6 MPa, and its tensile strength decreased from 6.4 ± 0.4 to 4.3 ± 0.3 MPa. However, for the PU-PVCL_{2K} and PU-PVCL_{6K} without PEG segment in the backbone, the mechanical properties showed no significant difference between the dry and wet states ($p > 0.05$). There was no significant difference on the breaking strain between the dry and wet states, with or without PEG segments ($p > 0.05$).

To further study the elasticity of the polyurethanes, the cyclic stretching was performed with a maximum strain of 30% and 300% in dry and wet states (Figure 4.1.5). Most of the polymers had a large hysteresis loop in the first cycle, followed by smaller hysteresis loops in the next nine cycles. With a maximum strain of 30%, most of the samples showed small irreversible deformations (~5%) (Figure 4.1.5A–D, and a–d), except for the PU-PEG_{2K}-PVCL_{6K} (10%-15%) (Figure 4.1.5E and e). With a maximum strain of 300%, the irreversible deformations became appreciable (50%-100%) (Figure 4.1.5F–I, and f–i). The cyclic stretching curves of the PU-PEG_{2K}-PVCL_{6K} film were not obtained at 300% deformation in both dry and wet states because of its low breaking strain ($296\pm59\%$ in dry state and $244\pm35\%$ in wet state).

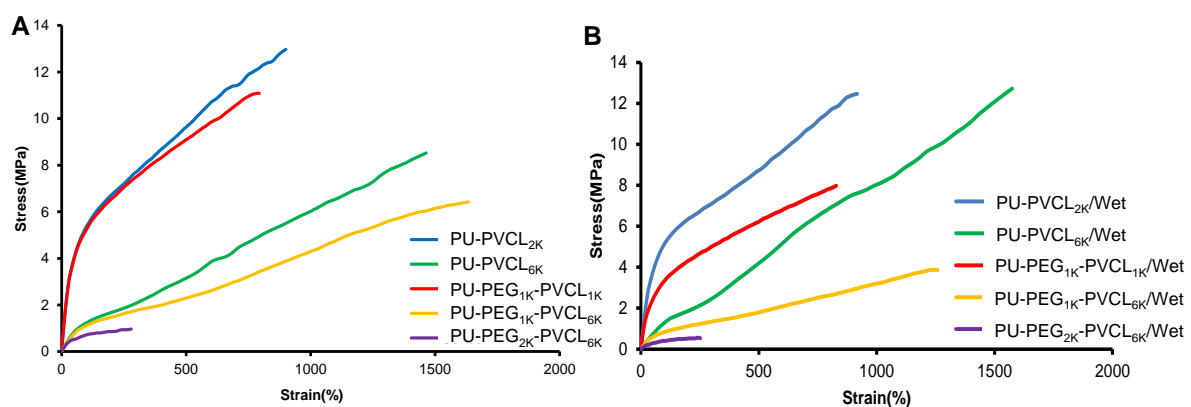


Figure 4.1.4 Typical stress-strain curves of polyurethane films in (A) dry and (B) wet states.

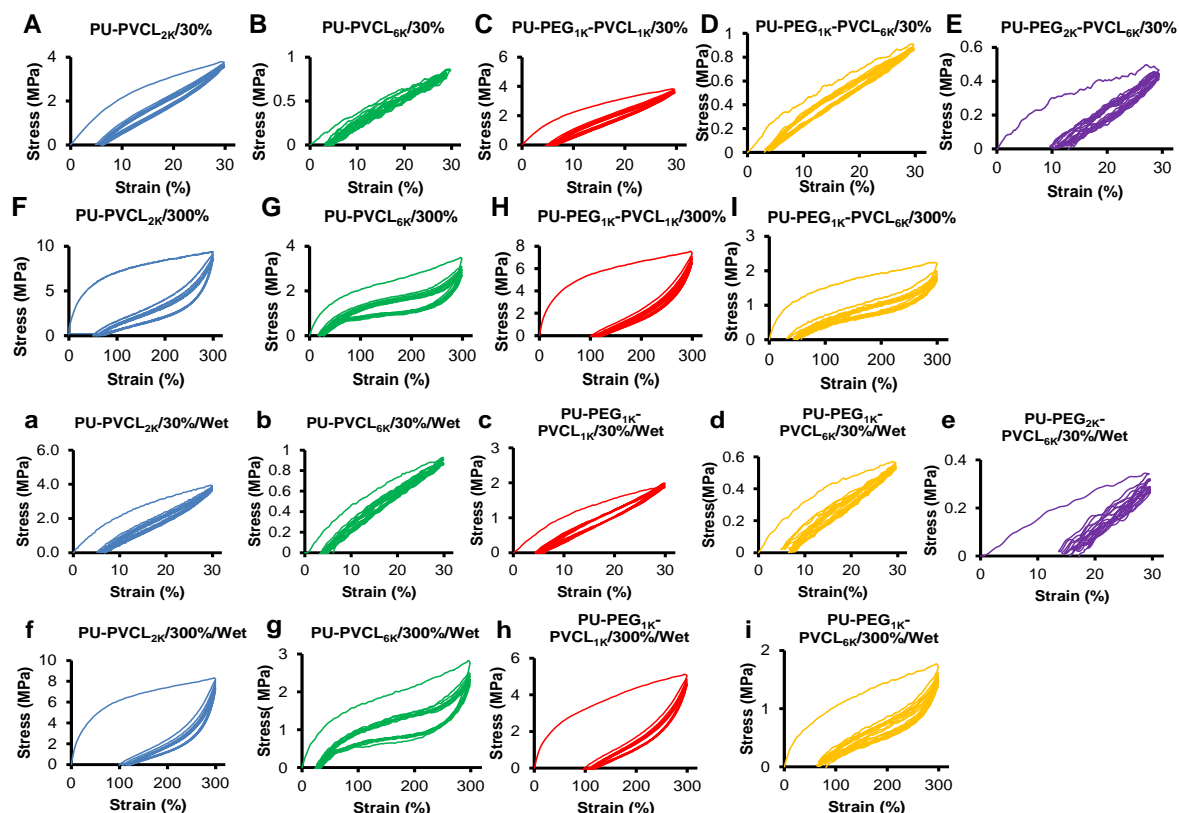


Figure 4.1.5 Cyclic stretching of polyurethane films in dry state with (A-E) 30% and (F-I) 300% strains and in wet state with (a-e) 30% and (f-i) 300% strains. The PU-PEG_{2K}-PVCL_{6K} film is too weak to obtain cyclic stretching curves at 300% deformation in both dry and wet states.

4.1.3.4 *In vitro* degradation of polyurethane films

The hydrolytic and enzymatic degradation of polyurethane films were evaluated in both PBS and 100 U/mL lipase/PBS solutions at 37 °C (Figure 4.1.6). The hydrolytic degradation rate of polyurethane films significantly increased with the increasing PEG molecular weight in soft segments and the decreasing PVCL block length (Figure 4.1.6A; $p < 0.05$). The PU-PVCL_{6K} had the lowest degradation rate

(93.8±1.3% mass remaining at 8 weeks), whereas the PU-PEG_{1K}-PVCL_{1K} had the highest degradation rate (75.5±1.3% mass remaining at 8 weeks; $p < 0.05$).

For enzymatic degradation in lipase/PBS solution (Figure 4.1.6B), the polyurethanes without PEG segments showed remarkably higher degradation amounts than in PBS. After 14 d of degradation, the degradation amounts of PU-VCL_{2K} and PU-VCL_{6K} reached 85.8±2.4% and 96.8±1.6%. For the polyurethanes incorporated with PEG block in soft segments, small degradation amounts were observed after 14 d of enzymatic degradation. The degradation amounts of PU-PEG_{1K}-PVCL_{1K}, PU-PEG_{1K}-PVCL_{6K}, and PU-PEG_{2K}-PVCL_{6K} within 14 d of degradation in lipase/PBS solution were only 5.7±0.4%, 16.8±2.3% and 11.2±1.3%, respectively, which were much smaller than those of PU-VCL_{2K} (85.8±2.4%) and PU-VCL_{6K} (96.8±1.6%) ($p < 0.05$).

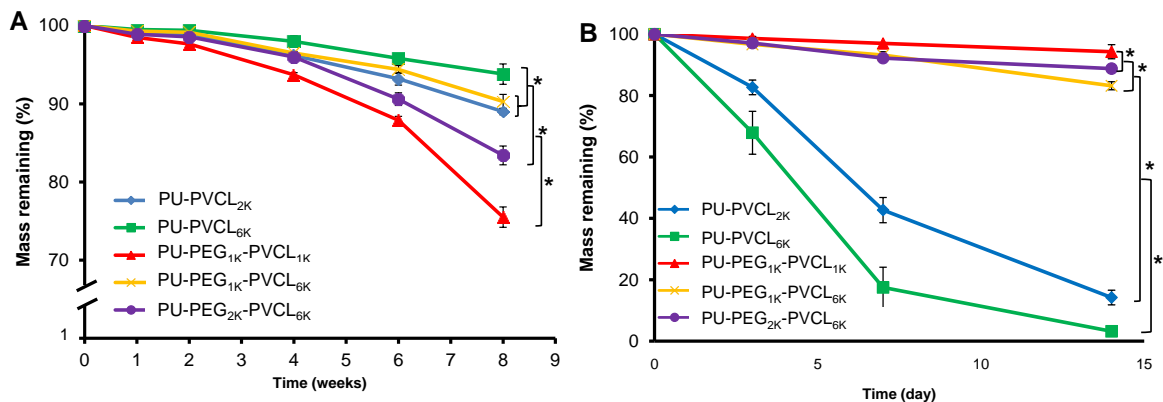


Figure 4.1.6 Mass remaining for polyurethane films in (A) PBS and (B) 100 units/mL lipase/PBS at 37 °C.

4.1.3.5 *In vitro* cytocompatibility of polyurethane films

The cell compatibility of PU-PEG-VCL films was evaluated by measuring the survival of mouse 3T3 fibroblasts seeded on the materials for different durations of time (1-5 d) (Figure 4.1.7). The cell viability increased from 1 d to 5 d on both TCPS and polymer films ($p < 0.05$). No significant difference was existed between TCPS and polymer films within 5 d culture ($p > 0.05$), except for the PU-PEG_{1K}-PVCL_{1K} films which showed fewer cell numbers than other films ($p < 0.05$) at 1, 3 and 5 d. The cell numbers on PU-PEG_{2K}-PVCL_{6K} were higher than PU-PEG_{1K}-PVCL_{1K} but lower than PU-VCL_{2K} and TCPS at 3 and 5 d ($p < 0.05$). The electron micrographs (Figure 4.1.7B) of 3T3 fibroblasts seeded on polyurethane films at day 5 were taken to qualitatively confirm the cell proliferation measured by the MTT method. In addition, 3T3 fibroblasts on most of the polyurethane films had a high cell density and formed a confluent cell monolayer, except for the PU-PEG_{1K}-PVCL_{1K}.

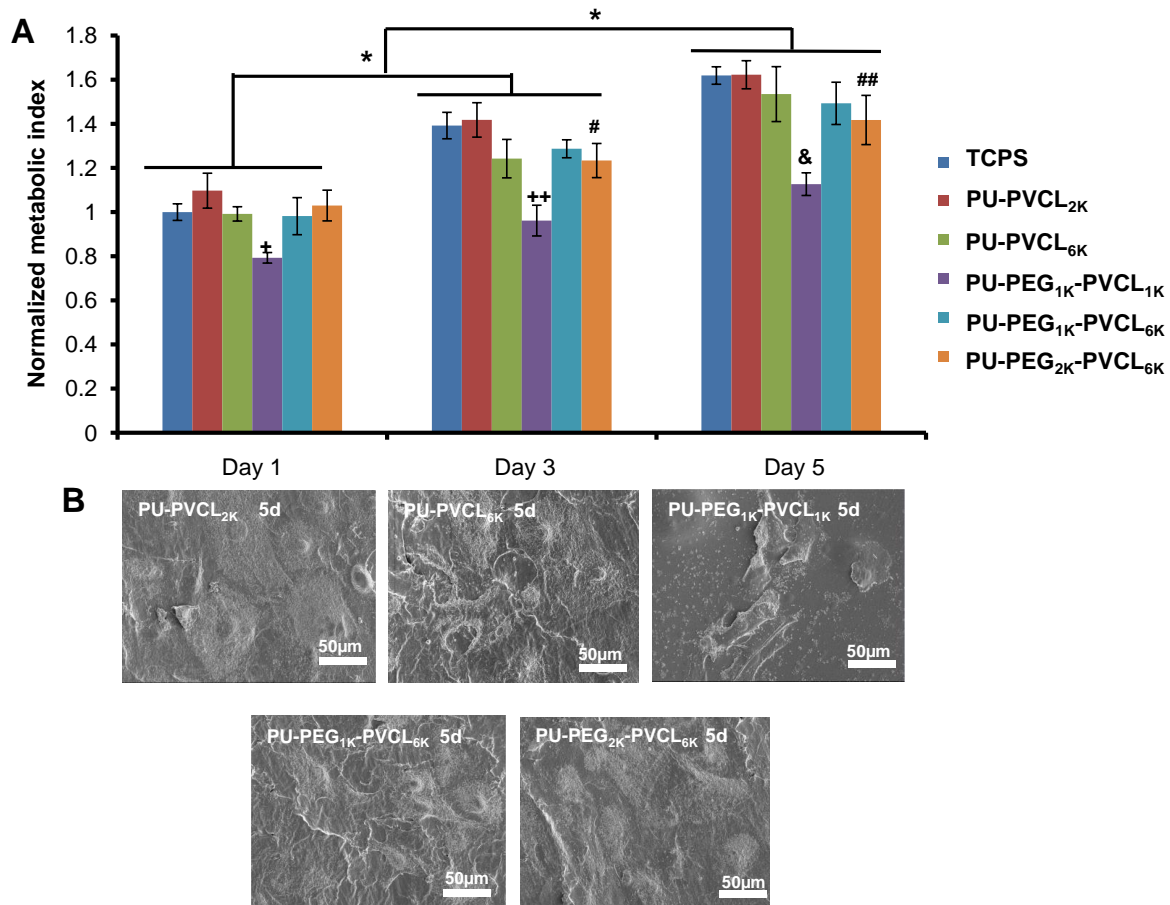


Figure 4.1.7 Cell compatibility of polyurethane films. (A) Metabolic index of 3T3 fibroblasts cultured on polyurethane films. Tissue cultured polystyrene (TCPS) was a positive control. (+) $p < 0.0003$, PU-PEG_{1K}-PVCL_{1K} compared to other groups at day 1. (++) and (&) $p < 0.0001$, PU-PEG_{1K}-VCL_{1K} compared with other groups at day 3 and day 5, respectively. (# and ##) $p < 0.05$, PU-PEG_{2K}-PVCL_{6K} compared with other groups at days 3 and 5, respectively. (B) Electron micrographs of the PU-PEG-PVCL films seeded with 3T3 fibroblasts at 5 days.

4.1.3.6 Porous scaffold characterization

The cross-sectional morphologies of porous scaffolds prepared by TIPS technique were shown in Figure 4.1.8A–C. The interconnected porous structure was observed. The pore sizes of porous scaffolds ranged from 58 ± 34 to 64 ± 39 μm with porosities above 90% (Table 4.1.3).

The mechanical parameters of PU-VCL_{6K}, PU-PEG_{1K}-PVCL_{6K} and PU-PEG_{2K}-PVCL_{6K} in both dry and wet states were obtained from the typical tensile stress-strain curves (Figure 4.1.8D and E) and summarized in Table 4.1.3. The tensile strengths and initial moduli of porous scaffolds increased from 0.42 ± 0.05 (PU-PEG_{2K}-PVCL_{6K}) to 2.13 ± 0.20 MPa (PU-PVCL_{6K}) and 1.19 ± 0.33 (PU-PEG_{2K}-PVCL_{6K}) to 3.14 ± 0.52 MPa (PU-PVCL_{6K}) in dry state, respectively, with the decreased molecular weight of soft segments in the polyurethane backbone. After immersion in PBS for 24 h, both of the tensile strengths and initial moduli of PU-PEG_{1K}-PVCL_{6K} and PU-PEG_{2K}-PVCL_{6K} scaffolds decreased markedly (Table 4.1.3). The tensile strengths of PU-PEG_{1K}-PVCL_{6K} and PU-PEG_{2K}-PVCL_{6K} scaffolds decreased from 1.08 ± 0.16 MPa and 0.42 ± 0.05 MPa in dry state to 0.31 ± 0.03 MPa and 0.07 ± 0.01 MPa in wet state, and the initial moduli of those decreased from 1.91 ± 0.13 MPa and 1.19 ± 0.33 MPa in dry state to 0.60 ± 0.14 MPa and 0.19 ± 0.08 MPa in wet state, respectively. The mechanical properties of PU-PVCL_{6K} scaffold in wet state (2.50 ± 0.36 MPa of tensile strength and 3.47 ± 0.24 MPa of initial modulus) showed no significant difference with those in dry state (2.13 ± 0.20 MPa of tensile strength and 3.14 ± 0.52 MPa of initial modulus). The instant recoveries for all polyurethane scaffolds had no significant difference ($p>0.05$).

The cyclic stretches of scaffolds at a maximum strain of 30% in dry and wet states were shown in Figure 4.1.9. All the scaffolds showed a larger hysteresis loop in the first cycle than in the following 9 cycles. Small permanent deformations were observed among all three groups (~10%) in dry state (Figure 4.1.9A–C). However, in wet state, only the PU-PVCL_{6K} showed a small irreversible deformation (~5%) (Figure 4.1.9D). The irreversible deformations of PU-PEG_{1K}-PVCL_{6K} and PU-PEG_{2K}-PVCL_{6K} were at around 15% (Figure 4.1.9E and F).

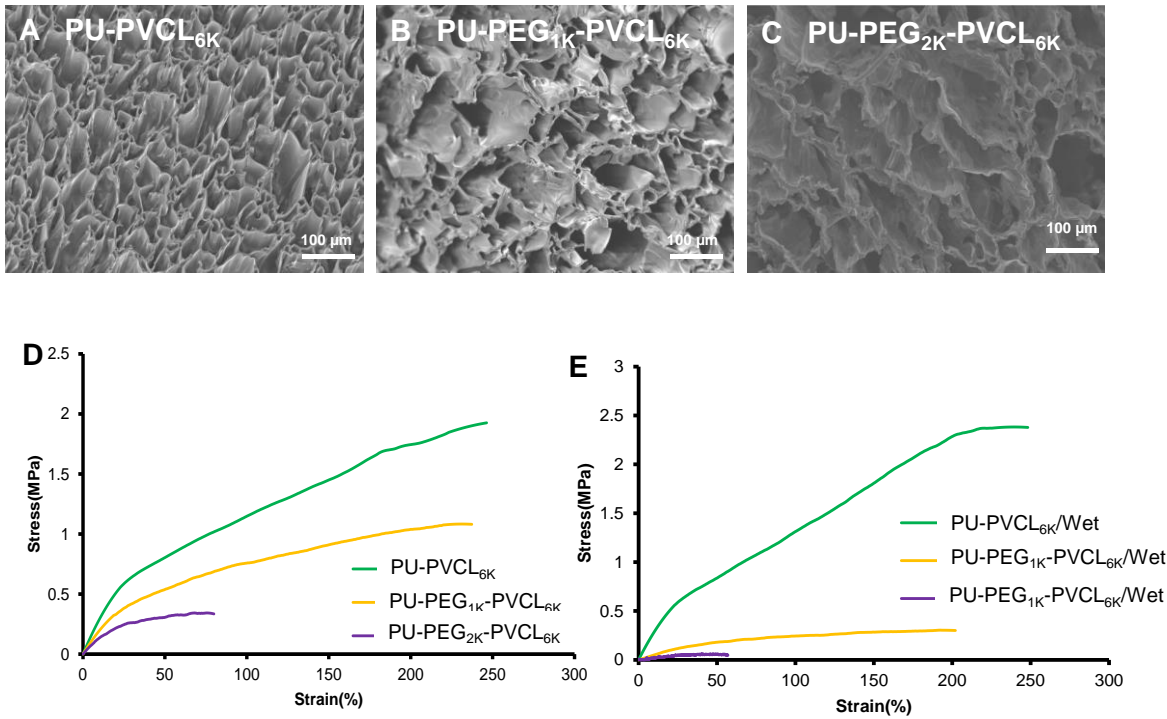


Figure 4.1.8 Porous scaffold characterization. (A-C) Electron micrographs of (A) PU-PVCL_{6K}, (B) PU-PEG_{1K}-PVCL_{6K} and (C) PU-PEG_{2K}-PVCL_{6K} porous scaffolds. (D, E) Typical stress-strain curves of PU-PVCL_{6K}, PU-PEG_{1K}-PVCL_{6K} and PU-PEG_{2K}-PVCL_{6K} porous scaffolds in (D) dry and (E) wet states.

Table 4.1.3 Scaffold characterization*

Samples	Porosity (%)	Pore size (μm)	Tensile strength (MPa)		Initial modulus (MPa)		Strain at peak stress (%)		Instant recovery (%)
			Dry state	Wet state	Dry state	Wet state	Dry state	Wet state	
PU-PVCL _{6K}	90 \pm 2	58 \pm 34	2.13 \pm 0.20 ^a	2.50 \pm 0.36 ^a	3.14 \pm 0.52 ^a	3.47 \pm 0.24 ^a	219 \pm 24 ^a	250 \pm 13 ^a	100 \pm 1
PU-PEG _{1K} -PVCL _{6K}	93 \pm 2	54 \pm 26	1.08 \pm 0.16 ^b	0.31 \pm 0.03 ^b	1.91 \pm 0.13 ^b	0.60 \pm 0.14 ^b	253 \pm 13 ^a	209 \pm 36 ^a	100 \pm 1
PU-PEG _{2K} -PVCL _{6K}	94 \pm 3	64 \pm 39	0.42 \pm 0.05 ^c	0.07 \pm 0.01 ^c	1.19 \pm 0.33 ^c	0.19 \pm 0.08 ^c	82 \pm 25 ^b	91 \pm 32 ^b	98 \pm 1

*a, b, c, d, e represent significances for each group and each characteristic

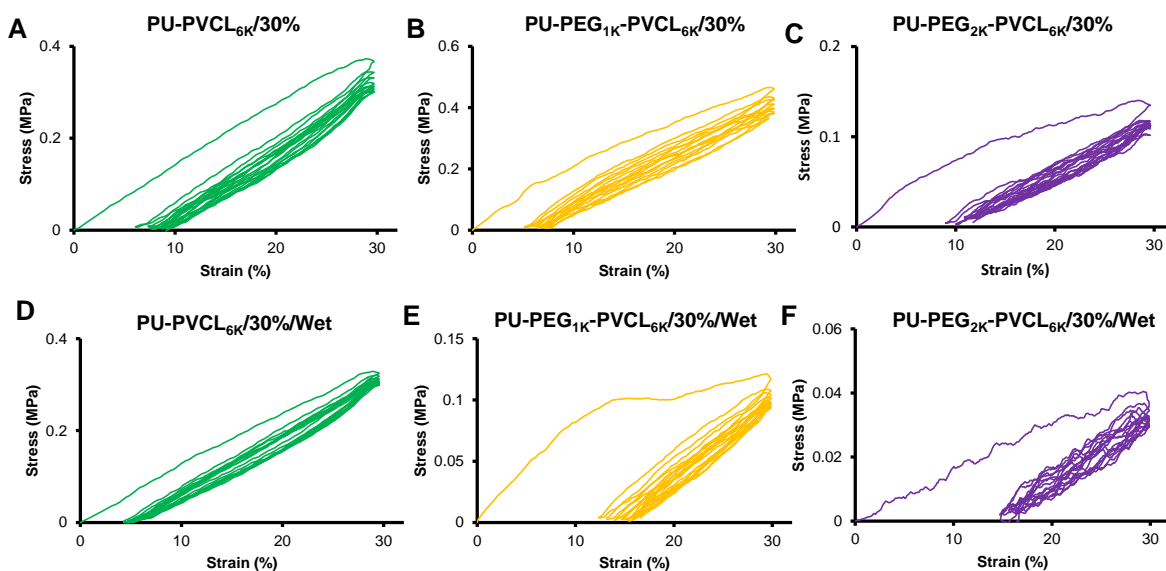


Figure 4.1.9 Cyclic stretching curves of PU-PVCL_{6K}, PU-PEG_{1K}-PVCL_{6K} and PU-PEG_{2K}-PVCL_{6K} porous scaffolds at 30% deformation in (A-C) dry and (D-F) wet states.

4.1.3.7 Mouse subcutaneous implantation of scaffolds

To investigate *in vivo* cell penetration and tissue compatibility, PU-PVCL_{6K}, PU-PEG_{1K}-VCL_{6K}, and PU-PEG_{2K}-VCL_{6K} scaffolds were implanted for 2 weeks. The implant and surrounding tissues were sectioned and H&E stained. H&E images showed minimal inflammatory cells (granulocytes) accumulated at the implant sites (**Figure 4.1.10A**). In addition, significant cell infiltration and cell attachment surrounding and inside all tested materials were observed (**Figure 4.1.10A**). The number of infiltrating cells in PU-PEG_{1K}-VCL_{6K} (189 ± 8.8) was higher than that in PU-PVCL_{6K} (142 ± 8.5) and PU-PEG_{2K}-VCL_{6K} (132 ± 6.9) ($p < 0.05$) (**Figure 4.1.10B**). We also noticed that the degradation rate of PU-PEG_{2K}-VCL_{6K} was faster than those of the other two materials. The results from the animal study demonstrated that PU-

PVCL_{6K}, PU-PEG_{1K}-VCL_{6K}, and PU-PEG_{2K}-VCL_{6K} scaffolds have good tissue compatibility and also facilitate cell infiltration.

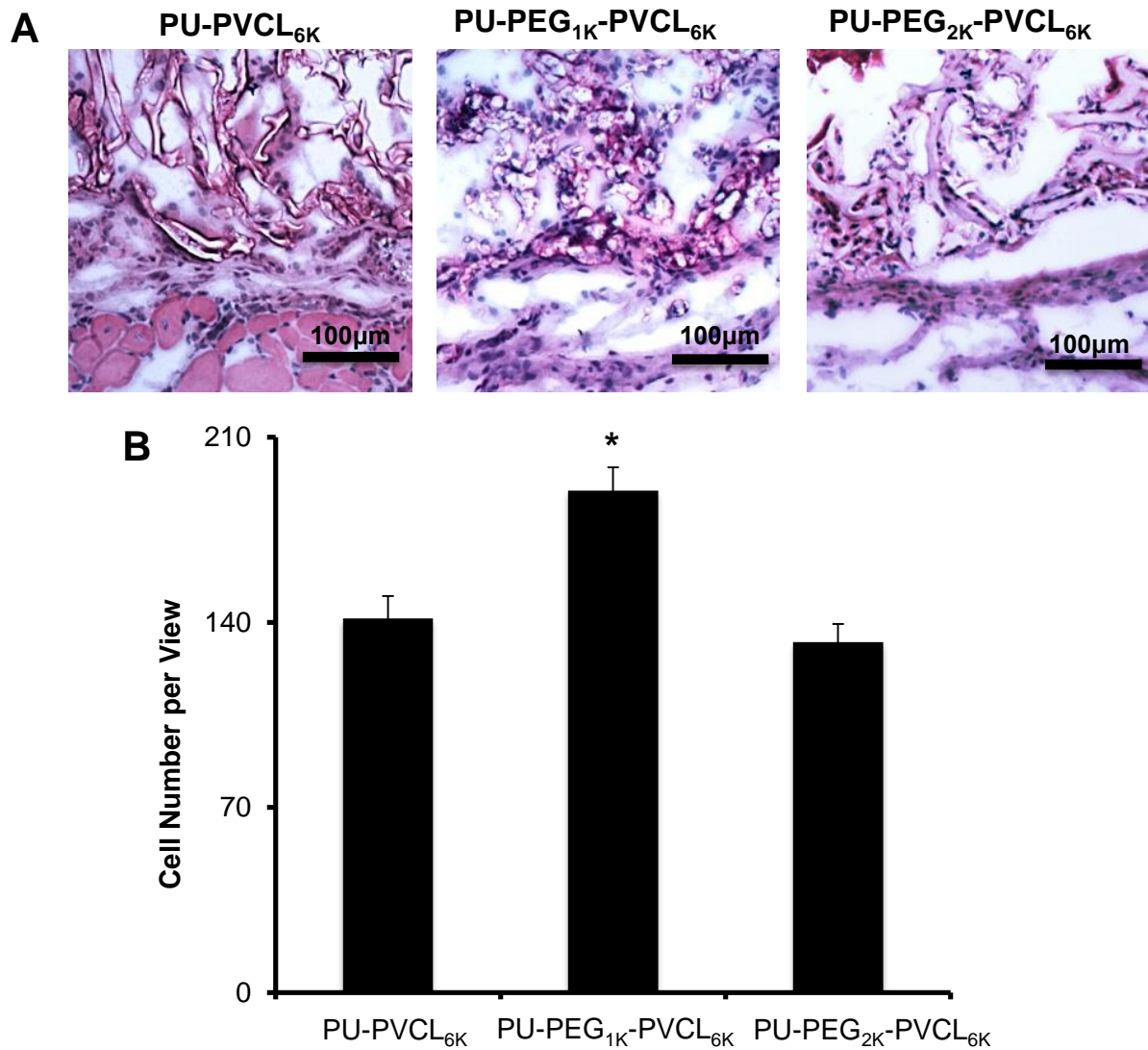


Figure 4.1.10 Histological analysis of tissue responses to subcutaneous implanted scaffolds made of PU-PVCL_{6K}, PU-PEG_{1K}-VCL_{6K}, or PU-PEG_{2K}-VCL_{6K}. (A) Representative images of H/E stains of implants and surrounding tissue at 2 weeks reveal mild inflammatory cell accumulation at the implant-tissue interface (200× magnification). Significant cell infiltration was also found inside all scaffolds. (B) Cell

number per area on the implants was quantified and statistically analyzed with Student's t-test (mean \pm SD, * $p < 0.05$).

4.1.4 Discussion

Biodegradable polyurethanes using polyesters[19, 25, 32, 327] or polycarbonates[25, 35, 37] as the soft segment exhibit robust mechanical properties and high elasticity. To achieve the desired properties of polyurethanes, altering segmented components, especially the soft segments in polyurethane, is a relatively easy and efficient approach.[34] In previous studies, a variety of macrodiols have been used as the single component in soft segment, such as PCL,[273, 338]PLA,[339] PHB[340] and PTMC.[25] To further control the mechanical behavior and degradation profile of polyurethanes, copolymer diols have been developed for the soft segment in polyurethane backbone, such as PCL-co-PVL,[25] PCL-PEG-PCL,[32, 341]PEO-PPO-PEO,[34] and PTMC-PEO-PPO-PEO-PTMC.[35]To obtain polyurethanes with lower initial moduli, we designed a new triblock copolymer diol (PVCL-PEG-PVCL) as the soft segment in polyurethanes, including random copolymer PVCL block and hydrophilic segment PEG. The mechanical properties of polyurethanes under physiological conditions can be manipulated by altering the chemical components, molecular weights and hydrophilicities of the soft segments.

PCL, PVL and PEG (MW=1000, 2000) showed T_g s lower than $-60\text{ }^\circ\text{C}$.[25, 342]The low T_g s of the polyurethanes (below -55°C) were attributed to the soft segments. The T_g s of the polyurethanes decreased with increasing PEG contents in soft segments, which was attributed to the lower T_g of PEG ($-79\text{ }^\circ\text{C}$ and $-76\text{ }^\circ\text{C}$ for

PEG1000 and PEG2000, respectively) than PCL (-63°C) and PVL (-72°C).[25, 342]The low Tms of the polyurethanes (-7 to 9 °C) were mainly attributed to the soft segment crystallinity. The random polymerization of VL and CL increased the irregular arrangement of polymer chains, and subsequently reduced the polymer crystallization. When the molar ratio of CL to VL was 50/50, the polymer chain structure reached the maximum randomness, which maximally reduced crystalline compared to the semicrystalline PCL (Tm=61 °C).[25]

The mechanical properties of the synthesized polyurethanes can be tuned by altering the molecular weights and hydrophilicities of the soft segments in polyurethane backbone to match the variable mechanical properties of native soft tissues. The observed decrease of tensile strength and initial modulus with the increasing molecular weight of soft segments (Table 4.1.2) is consistent with the rubber thermodynamic theory, which claims that the initial modulus of an elastomer increases with the decrease of its average molecular weight between cross-link points.[25, 36]Incorporation of PEG into the soft segments greatly reduced the tensile strength and initial modulus of the polyurethanes in wet state (Table 4.1.2) due to the hydrophilicity of PEG. After the polymers were immersed in the water, the water molecules penetrated into the polymer and attached to the hydrophilic groups on polymer chains, and then the hydrogen-bonds were established between water and polymer. The bound water was primarily responsible for the plasticization of the polymer, thus reducing the mechanical strength and modulus of polymer.[334, 343]The synthesized polyurethanes showed good elasticity with small irreversible deformations (<10%) at 30% maximum strain. When the strain reached up to 300%,

all the hard segment domains were reorganized to form permanent deformations, which resulted in a large deformation of all polyurethanes (50%–100%). The polyurethane porous scaffolds showed consistent results with the polyurethane films, but the mechanical strength decreased due to the porous structure.[210] The developed polyurethane porous scaffolds possessed attractive low initial modulus for soft tissue scaffolds. For example, the initial modulus of PU-PEG_{1K}-PVCL_{6K} (0.60 ± 0.14 MPa) in wet state is comparable with that of native human heart muscle (0.02 – 0.50 MPa).[287] The initial moduli of PU-PEG_{1K}-PVCL_{6K} (0.60 ± 0.14 MPa) and PU-PEG_{2K}-PVCL_{6K} (0.19 ± 0.08 MPa) in wet state are similar with that of skin (0.1 – 2.0 MPa).[322]

Hydrolytic degradation in PBS for the polyurethanes was influenced by both the hydrophilic PEG block and hydrophobic and degradable polyester block of PVCL in the polyurethane backbone. The higher mass loss of polyurethanes was associated with increased PEG molecular weight and decreased PVCL block length. The ester bonds which mainly existed in the PVCL segment were considered as the initial cleavage position in poly(ester urethane)s during the hydrolysis.[311] The PEG segment that allowed the high penetration of water molecules into the polyurethane matrix structure could lead to a high hydrolysis rate.[311] The trend of polyurethane degradation behavior suggests that the greater water penetration and access to the labile ester bonds is more important than the density of ester bonds in the PVCL segments, which is consistent with the previous report.[32] The enzymatic degradations of the polyurethanes in lipase solution were faster than those in PBS, which was attributed to the ester bond sensitive to the lipase.[327, 344] The

degradation rate of the polyurethanes without PEG content (PU-VCL_{2K} and PU-VCL_{6K}) in lipase solution was higher compared with the polyurethanes containing PEG segment (PU-PEG_{1K}-PVCL_{1K}, PU-PEG_{1K}-PVCL_{6K}, and PU-PEG_{2K}-PVCL_{6K}). Two main reasons may lead to this phenomenon. Firstly, the hydrolase lipase is used as the catalyst of ester-bond cleavage with hydrolysis,[327, 344] whereas the ether bond is not as sensitive to the lipase as the ester bond. It was reported that the polyester based polyurethanes were much more susceptible to fungal degradation than polyether based polyurethanes.[42] Secondly, the surface hydrophobicity of polymer was reported to be beneficial to the protein adsorption,[43, 345] further accelerating the polymer enzymatic degradation which occurred preferentially on the polymer surface.[42] In terms of the water contact angles of the polyurethanes (Table 4.1.2), introducing PEG segments into the polyurethane backbone led to an increase of polymer surface hydrophilicity, which would result in less protein adsorption and might compromise the polyurethane enzymatic degradation. In a similar study, this phenomenon was found for the degradation of poly(ether urethane) in a polyester hydrolase of cholesterol esterase(CE) .[38] Only a small loss in polyurethane films was observed after 36 days of enzymatic degradation in CE. Therefore, the involvement of PEG segment in the polyurethane backbone can promote the polymer hydrolysis but cannot accelerate the enzymatic degradation of the polyurethanes.

The synthesized polyurethanes exhibited good cytocompatibility and tissue compatibility via *in vitro* and *in vivo* assessments. The chemical components of the synthesized polyurethane, including PCL, PVL, PEG, and HDI, have been used in FDA-approved devices.[273] These ensure the good biocompatibility of the

polyurethanes. The lower cell viability on PU-PEG_{1K}-PVCL_{1K} film compared with TCPS and other groups ($p < 0.05$) was primarily due to its high hydrophilicity. It may decrease protein adsorption onto the hydrophilic polyurethanes and induce less cell adhesion.[32] Many studies have proven the good *in vivo* biocompatibility of polyurethane scaffolds.[37, 273, 346] The good long-term tissue compatibility of a polyurethane based on poly(DL-lactide/ ϵ -caprolactone), 1,4-butanediisocyanate, and 1,4-butanediol was concluded by a 3-year *in vivo* subcutaneous implantation study in both rat and rabbit.[346] Polyurethane scaffolds based on poly(ester carbonate urethane)urea (PECUU) and polyurethanes with disulfide bonds (PU-SS) also had good tissue response in rat and mouse subcutaneous models after 8-week implantation, respectively.[37, 273] Similar with above biodegradable polyurethanes, the *in vivo* mouse subcutaneous implantation (2 weeks) showed PU-PVCL_{6K}, PU-PEG_{1K}-VCL_{6K}, and PU-PEG_{2K}-VCL_{6K} scaffolds have good tissue compatibility with good cell infiltration, which indicated that the polyurethane scaffolds could be safely used as biodegradable implants.

Some limitations in this study should be mentioned. First, although the mechanical testing has confirmed the low initial moduli of the new polymers and scaffolds, other mechanical testing, such as biaxial mechanical testing and ball burst testing,[347, 348] can be used to further evaluate the polyurethane scaffold biomechanics under physiological conditions in the future. Second, the mechanical properties of the scaffold were tuned by altering polymer types. The mechanical properties of the polyurethane scaffolds fabricated using TIPS can also be optimized by altering other parameters, such as polymer concentration and quenching

temperature, to obtain scaffolds with variable mechanical properties.[118, 349, 350]Third, the 2-week examination period of subcutaneous implantations is common to initially evaluate the scaffold short-term immune response and cell infiltration. But it can be further extended to study the *in vivo* degradation behavior of the scaffolds, and their long-term tissue response.

4.1.5 Conclusion

A series of biodegradable copolymer diols based on PVCL and PEG were synthesized as soft segments for polyurethane synthesis. The mechanical properties of these biodegradable polyurethanes can be manipulated by varying the molecular weight and hydrophilicity of the copolymer diols. These synthesized polyurethane elastomers showed strong and flexible mechanical properties with low initial modulus. Further, the polymers were processed into porous scaffolds with comparable initial modulus to the soft tissues. The polymer films and porous scaffolds showed good cellular compatibility *in vitro* and tissue compatibility *in vivo*. These biodegradable polyurethanes would have the potential for soft tissues repair and regeneration.

4.2

OPTIMIZING ANISOTROPIC POLYURETHANE SCAFFOLDS TO MECHANICALLY MATCH WITH THE NATIVE MYOCARDIUM

4.2.1 Introduction

Myocardial infarction (MI) is a leading cause of death of the cardiovascular diseases in the world. Approximately every 43 seconds, an American will have an MI according to the American Heart Association computation.[351] The in-hospital mortality rate for US MI patients is approximately 5%.[352] As the common end-point of MI, congestive heart failure (CHF) is a life-threatening condition in which the infarcted heart cannot provide sufficient pumping efficiency to meet the body's needs. Most current therapies for CHF, such as medications, biventricular pacing implantation, coronary artery bypass grafting, and valve repair or replacement, have limited applications because they do little to restore the size or shape of the infarcted myocardium in CHF.[353] Heart transplantation is also not the first choice for each patient due to the shortage of donors, pulmonary hypertension, chronic organ failure of the recipient and societal limitations in some parts of the world.[354, 355] Surgical ventricular restoration (SVR) has been reported as a promising therapy to treat post-infarction heart failure since 1990s. Most SVR, such as endoventricular circular patch plasty (EVCPP, Dor procedure),[356] and septal anterior ventricular exclusion (SAVE),[357, 358] involves a procedure to place a synthetic cardiac patch, such as polytetrafluoroethylene (PTFE) and Dacron,[355, 358] to restore/remodel the heart to a more normal size and shape to improve function. These non-biodegradable patches

usually trigger the foreign body reaction, form fibrous capsule and end up in failure to restore heart function.[359, 360] Hence, new cardiac patches served for SVR to structurally and functionally restore the infarcted myocardium are required.

In recent years, tissue engineered cardiac patches have gained many research interests and shown promising improvements in cardiac function and remodeling after MI.[361, 362] [363, 364] The ideal cardiac patch should mimic the morphologies of the native myocardium and possess comparable physiological and functional properties to the native heart tissue, such as biocompatibility, biodegradation, bioabsorption at a rate compatible with repair process, mechanically matching with native heart tissue, and high bioactivity to promote cell recruitment, migration, proliferation and differentiation.[360, 363, 365] Currently, either synthetic polymers, such as poly(glycerol sebacate) (PGS),[287, 366] PLGA,[367, 368] poly(glycolide-co-caprolactone) (PGCL),[369] and PCL,[370, 371] or natural biomaterials, such as collagen,[372, 373] alginate,[374, 375] fibrin,[376, 377] Matrigel,[378] small intestinal submucosa (SIS)[379] and urinary bladder matrix (UBM)[380] have been intensively investigated as tissue engineered cardiac patch. However, only a few of them have emphasized the significance of mechanical properties in tissue engineered cardiac patch. The cardiac patches should replace the heart infarct with its stiffness and elasticity exactly matching that of native left ventricle wall.[381] Mechanical mismatch between the tissue engineered cardiac patch and the native myocardium would result in abnormal cardiac functions, and eventually lead to implantation failure.[126] Natural biomaterials usually possess low elastic modulus and low tensile strength, which cannot provide sufficient mechanical

support to restore heart functions. Moreover, most of the synthetic polymers have stiffness many fold higher than the native heart tissue. Hence, there is a necessity to develop a biodegradable polymer with low initial modulus, appropriate tensile strength and sufficient elasticity to engineer soft native myocardium.

Biodegradable polyurethanes have been known as elastomeric biomaterials with tunable mechanical properties and good processability, and have been used cardiac patches for infarcted heart treatment.[382-384] But it still needs efforts to further improve their mechanical properties to match with the myocardium mechanics through PU molecular design and scaffold processing. In our previous work, biodegradable elastomeric polyurethanes (PU-PEG-PVCL) were synthesized based on a soft segment, a triblock copolymer of poly(ethylene glycol) (PEG) and random copolymers of ϵ -caprolactone (CL) and δ -valerolactone (VL), which showed low initial moduli (film, 0.9 ± 0.3 to 9.1 ± 0.5 MPa) comparable to the initial moduli of the human myocardium (0.02-0.50 MPa).[385] In this study, the synthesized PU-PEG-PVCL polymers were further processed into anisotropic porous scaffolds using thermally induced phase separation (TIPS) technique because of the anisotropic heart muscle, and their biomechanical properties including ball burst, suture retention, and biaxial mechanics, were optimized to mechanically match the native human myocardium.[287] To further improve the bioactivity of the PU-PEG-PVCL anisotropic scaffolds, a myocardium-derived extracellular matrix hydrogel was combined with the PU-PEG-PVCL scaffolds to form a biohybrid scaffold. Their morphologies and mechanical properties were characterized with comparison to the PU-PEG-PVCL

scaffold alone. A Lewis rat subcutaneous model was used to evaluate the *in vivo* bioactivity of the biohybrid scaffold.

4.2.2 Experimental section

4.2.2.1 Materials

All chemicals were purchased from Sigma. VL, HDI were distilled before use. DEG, CL, PEG (MW=1000 and 2000) were dried in vacuum oven at 60 °C before use. Sn(Oct)₂, putrescine, DMSO, sodium dodecyl sulfate (SDS), pepsin, PBS, concentrated hydrogen chloride (HCl), NaOH were used as received.

4.2.2.2 PU-PEG-PVCL polymer synthesis and anisotropic scaffold fabrication

PU-PEG-PVCL was synthesized according to our previous report.[385] Briefly, diblock copolymer diols (PVCL) and triblock copolymer diols (PVCL-PEG-PVCL) were synthesized by ring-opening polymerization based on DEG (as initiator for PVCL synthesis) or PEG, CL and VL. Then, the PU-PEG-PVCL polymer was prepared from the PVCL or PVCL-PEG-PVCL diols (soft segment), hexamethylene diisocyanate (HDI; hard segment) and putrescine (chain extender). The final products were named as PU-PEG_x-PVCL_y, where x and y are the block length of PEG and PVCL.

The anisotropic scaffolds were fabricated via TIPS following a previous report (**Figure 4.2.1**).[118] PU-PVCL_{6K}, PU-PEG_{1K}-PVCL_{6K} and PU-PEG_{2K}-PVCL_{6K} polymers were thoroughly dissolved in anhydrous dimethyl sulfoxide (DMSO) at 80 °C to reach predetermined concentrations(5%, 8% and 10%). The polymer/DMSO solution at 80 °C was then poured into a cylinder glass mold and then transferred to a -80 °C freezer immediately. After 3 h, the mold was placed in a 70% ethanol solution

at 4 °C for 4 d to remove DMSO, followed by immersion in deionized water to exchange ethanol for 3 d. The anisotropic scaffold was obtained after lyophilization for further characterization.

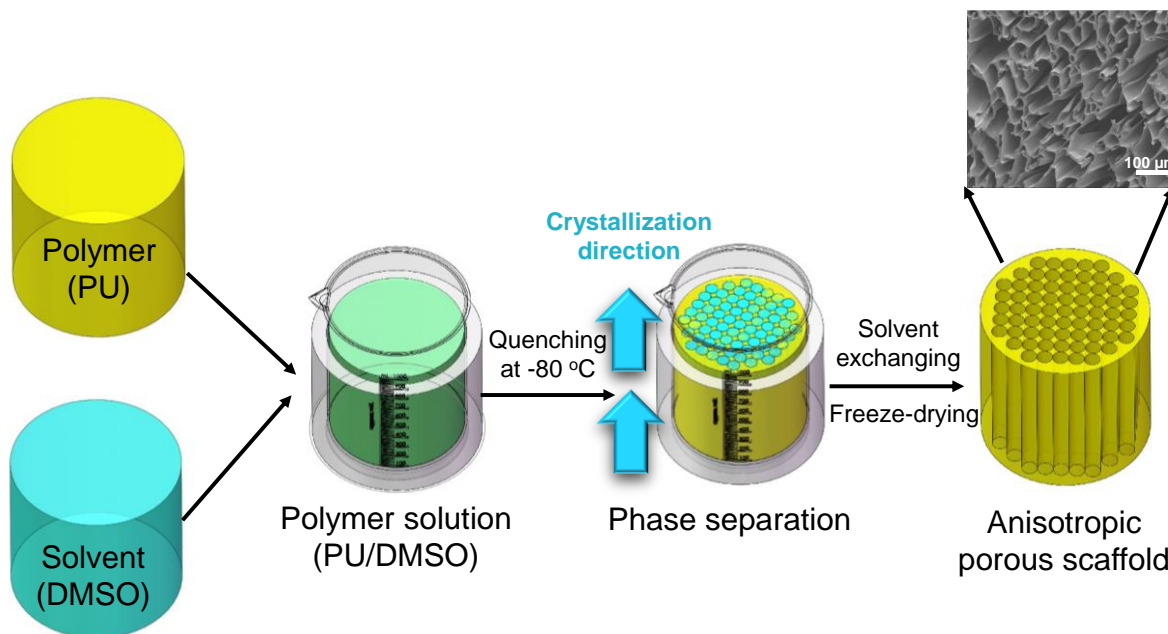


Figure 4.2.1 Anisotropic polyurethane porous scaffold fabrication by thermally induced phase separation (TIPS).

4.2.2.3 Scaffold characterization

The morphologies of the anisotropic scaffolds were observed by SEM (Hitachi S-4800 HRSEM) after sputter coating with silver. Pore sizes were determined by the SEM images using ImageJ software (National Institutes of Health, NIH). Porosity of the anisotropic scaffolds (n=3) was determined via ethanol displacement method.[118, 386]

4.2.2.4 Scaffold uniaxial mechanical properties

The uniaxial mechanical properties of the anisotropic scaffolds were measured in longitudinal and transversal directions, respectively, under both dry and wet states. Strips (2×20 mm, n=6) cut from the scaffolds along longitudinal and transversal directions were tested on a MTS Insight Testing System using 500 N loading cell at 10 mm/min under room temperature according to ASTM D638-03.[198] The instant recovery (n=3) was measured under the same condition as described above. The two distal ends of the strips were marked, then stretched to 10% strain, held for 1 min and then released. The whole process was repeated for 3 times. The instant recovery was calculated according to the formula $[1-(L_1-L_0)/L_0] \times 100\%$, where L_0 referring to the original length of the strips, and L_1 referring to the eventual length right after stretching/releasing for 3 cycles. Cyclic stretching to characterize material elasticity was performed at 30% strain for 10 cycles at 10 mm/min.[273] Three samples were tested for each group.

4.2.2.5 Biomechanical measurement

Suture retention strength was measured using a 4-0 silk braided suture (Ethicon, Inc.) under the same conditions as the uniaxial mechanical testing.[216] One suture loop was threaded through a distal end of the strip (5×20 mm, n=6) and fixed on the upper clamp. The calculation of the suture retention strength at the point of tearing followed the formula $\text{suture load}/(\text{suture diameter} \times \text{strip thickness})$.

Ball-burst strength of the anisotropic scaffold (n=4) was assessed by a ball-burst test, following the *Standard Test Method for Bursting Strength of Knitted Goods*,

Constant-Rate-of-Transverse (CRT) Ball-burst Test (ASTM D 3797-89).[348, 387]

The MTS Insight Testing machine was equipped with a ball-burst cage in which a 10 mm polished steel ball was pushed at a constant rate (10 mm/min) against the test material. The ball-burst strength was defined as the force required rupturing the test material when an applied stress is perpendicular to the plane of the material. The porcine native left ventricles (LV) were excised as the control group.

Biaxial mechanical testing was performed to obtain the mechanical behavior of the material and tissue. The principles, setup, and testing protocols of the system were based on a previous design.[388] A custom made biaxial mechanical testing system was used to capture the tissue behavior under physiologically-relevant loading conditions. Biaxial testing is well known for its sensitivity to detect tension-stretch (stress-stretch) behavior alterations due to subtle tissue microstructural changes.[389-391] PU-PEG_{1K}-VCL_{6K}-5% and PU-PEG_{1K}-VCL_{6K}-10% were tested. One axis of each square sample (~ 20 mm × 20 mm × 1 mm) was aligned with the cross-fiber direction (CD) and the other with the fiber-preferred direction (LD) (n=5). Accurate dimensions of each sample were measured using a digital caliper before mounting to the biaxial machine as conditioning parameters. Each side of the square sample was mounted onto four stainless steel hooks that are attached to two loops of 000 polyester sutures. Four fiducial graphite markers, affixed to the center of the square sample with cyanoacrylate adhesive, were monitored via a CCD camera to capture the real time stretch ratios. The sample was preconditioned biaxially by imposing 10 cycles of 25 N/m maximum Lagrangian membrane tension as the

physiological range [389]. After preconditioning, an equi-biaxial tension protocol of $T_{CD}:T_{LD} = 25:25$ N/m was performed to capture the biaxial behavior.

4.2.2.6 Biohybrid scaffold fabrication and characterization

The decellularized porcine cardiac extracellular matrix (ECM) was prepared and processed into a solubilized preparation as previous reports.[392, 393] Briefly, intact hearts were freshly harvested from adult pigs from a local abattoir and kept in an ice bath. The hearts were sliced into thin pieces (2-mm in thickness) and washed with deionized water to thoroughly eliminate the blood. The cardiac slices were stirred in 1% (wt/v) sodium dodecyl sulfate (SDS) for 3-4 days until the slices became white. The samples were rinsed with deionized water overnight to remove the residual chemical, lyophilized to obtain the decellularized cardiac ECM and milled into fine powders.

The obtained powder ECM was sterilized by exposure to UV light for 30 min, then digested in pepsin/0.01 M HCl solution with stirring under room temperature, where the ratio of pepsin:matrix was 1:10. After 2 days, the decellularized cardiac tissue was thoroughly solubilized, followed by neutralization using 0.1 M NaOH and 10× PBS, and then diluted by 1× PBS to reach predetermined concentration. The final solution was sealed and kept in an ice bath until use.

The anisotropic scaffolds were cut into circular patches with 6 mm diameter and 400 μ m thickness using standard biopsy punches (6 mm, Miltex) and microtome blade (Thermo Scientific). The patches were sterilized by immersion in 70% ethanol for 1 h, followed by placing in PBS solution to exchange the ethanol for another 1 h.

The sterile patches were placed in a 0.22 μm bottle top filter (Corning) connected to a receiving flask.[394] The prepared decellularized cardiac ECM solution was injected onto the surface of the scaffold patches, and then absorbed into the patches using a low vacuum through the receiving flask. The patch/ECM solution complex was put into a 37 °C incubator for 30 min to allow the injected ECM solution gelation to obtain the biohybrid scaffold. The biohybrid scaffold morphology was observed with SEM after sputtering coating of silver. The uniaxial mechanical testing of the biohybrid scaffold (n=4) was performed in wet state using the same protocol as the synthetic anisotropic scaffold.

4.2.2.7 Rat subcutaneous implantation

All experimental designs for this animal study was reviewed and approved by the University of Texas at Arlington Animal Care and Use Committee (IACUC) following the National Institutes of Health guidelines for the use of laboratory animals. Two Rats were implanted with two different (synthetic and biohybrid scaffolds) subcutaneous implants (one in each side of the pelvis) with one sacrificed on the 2nd week and the other on the 4th week post-implantation with the tissue containing the implants excised for further studies. Tissue sections (10 μm thickness) were taken with a Leica Cryostat (CM1850, Leica Microsystem, Wetzlar, Germany) after fixing in OCT embedding medium, frozen, and mounted on glass slides. Multiple tissues from different samples were imaged with light microscopy after hematoxylin-eosin (H&E) staining and were used for cell infiltration assessment.

4.2.2.8 Statistical analysis

All results are presented as mean \pm standard deviation. One-way ANOVA with Tukey-Kramer's post-hoc test was used to analyze all the mechanical property parameters. $p \leq 0.05$ was considered as significant difference.

4.2.3 Results

4.2.3.1 Anisotropic scaffold characterization

The anisotropic porous structure of the PU-PEG-PVCL scaffolds was shown in Figure 4.2.2. In transversal direction, the scaffolds possessed honeycomb-like pores (Figure 4.2.2.2A, 2C and 2E). In longitudinal direction, aligned pores were observed on the scaffolds (Figure 4.2.2B, 2D and 2F). The PU-PVCL_{6K}(5%), PU-PEG_{1K}-PVCL_{6K}(5%), and PU-PEG_{2K}-PVCL_{6K}(5%) had pore sizes at $66 \pm 26 \mu\text{m}$, $91 \pm 57 \mu\text{m}$ and $123 \pm 70 \mu\text{m}$, respectively, with porosities of $93\% \pm 2\%$ to $97\% \pm 2\%$ (Table 4.2.1).

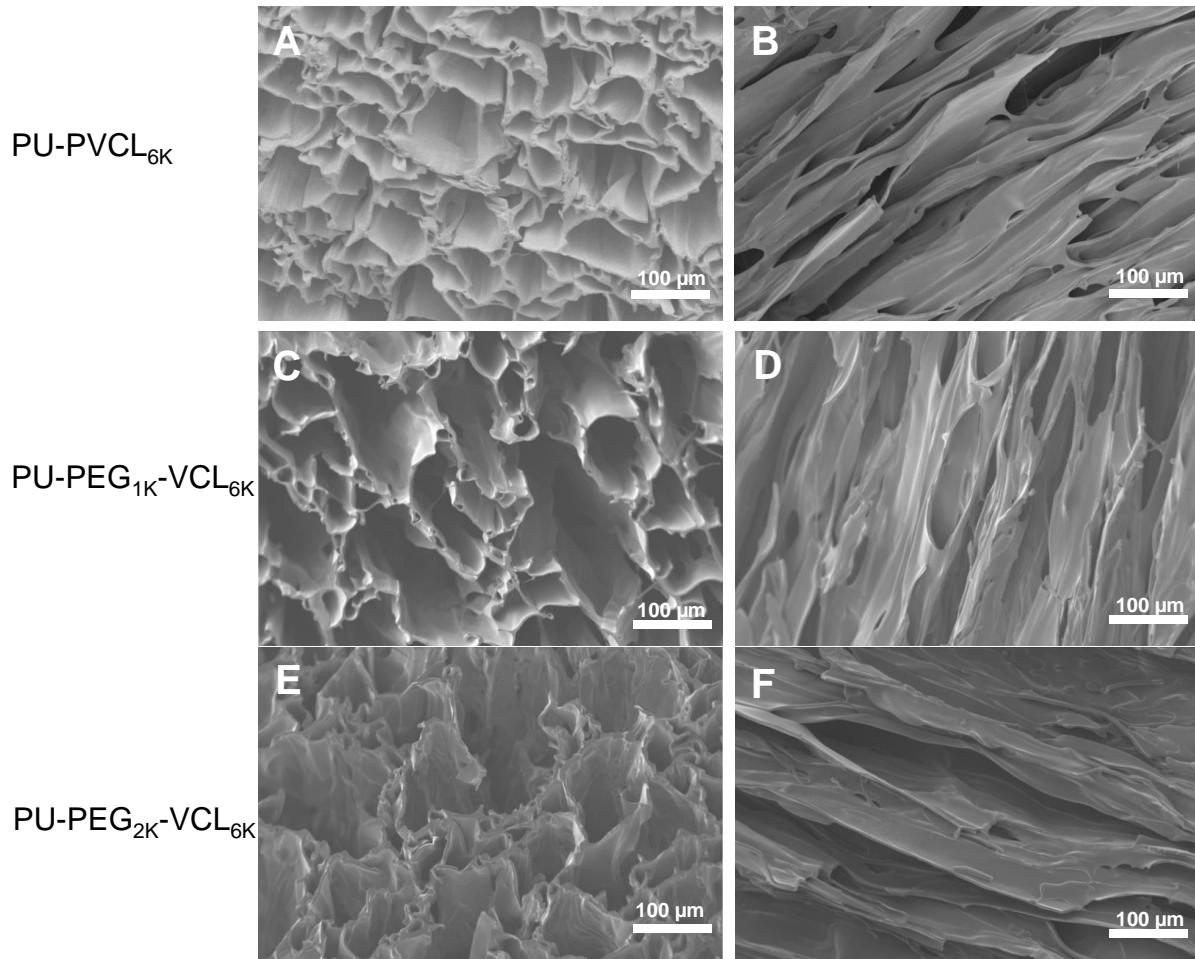


Figure 4.2.2 Electron micrographs of anisotropic porous scaffolds prepared from 5% polymer concentrations at -80 °C quenching temperature. (A-B) PU-PVCL_{6K}(5%) in transversal (A) and longitudinal (B) directions. (C-D) PU-PEG_{1K}-VCL_{6K}(5%) in transversal (C) and longitudinal (D) directions. (E-F) PU-PEG_{2K}-VCL_{6K}(5%) in transversal (E) and longitudinal (F) directions.

Table 4.2.1 Anisotropic porous scaffold characterization in dry state

c	Peak stress (MPa)		Initial modulus (MPa)		Breaking strain (%)		Suture retention (N/mm ²)	Instant recovery (%)	Pore size (μm)	Porosity (%)
	L ⁺	T [#]	L	T	L	T				
PU-PVCL _{6K} (5%)	2.3±0.4 ^a	1.16±0.30 ^a	2.3±0.6 ^a	2.53±0.45 ^a	404±86 ^a	131±23 ^a	55±14 ^a	100±1	66±26	93±2
PU-PEG _{1K} -VCL _{6K} (5%)	1.0±0.2 ^b	0.27±0.04 ^b	1.3±0.1 ^b	1.64±0.42 ^b	445±130 ^a	51±13 ^b	27±8 ^b	100±2	91±57	96±3
PU-PEG _{2K} -VCL _{6K} (5%)	0.3±0.1 ^c	0.13±0.02 ^c	0.8±0.2 ^c	0.67±0.30 ^c	53±18 ^b	27±6 ^c	4±1 ^c	98±1	123±70	97±2

+ and # represent longitudinal direction and transversal direction, respectively.

* a, b and c represent significantly different groups for each characteristic.

4.2.3.2 Scaffold mechanical properties

Figure 4.2.3 showed the typical stress-strain curves of the PU-PVCL_{6K}(5%), PU-PEG_{1K}-PVCL_{6K}(5%), and PU-PEG_{2K}-PVCL_{6K}(5%) anisotropic scaffolds in longitudinal and transversal directions under dry and wet states. The scaffold tensile properties were summarized in Table 4.2.1 (dry state) and Table 4.2.2 (wet state). In dry state (Table 4.2.1), the peak stresses and initial moduli of the anisotropic scaffolds decreased with increasing soft segment molecular weight ($p < 0.05$). The peak stresses ranged from 0.3 ± 0.1 MPa [PU-PEG_{2K}-PVCL_{6K}(5%)] to 2.3 ± 0.4 [PU-PVCL_{6K}(5%)] longitudinally, and from 0.13 ± 0.02 MPa [PU-PEG_{2K}-PVCL_{6K}(5%)] to 1.16 ± 0.30 [PU-PVCL_{6K}(5%)] transversally. The initial moduli were from 0.8 ± 0.2 MPa [PU-PEG_{2K}-PVCL_{6K}(5%)] to 2.3 ± 0.6 [PU-PVCL_{6K}(5%)] in longitudinal direction, and from 0.67 ± 0.30 MPa [PU-PEG_{2K}-PVCL_{6K}(5%)] to 2.53 ± 0.45 [PU-PVCL_{6K}(5%)] in transversal direction. The breaking strains also showed the same trends, decreasing from 404 ± 86 % [PU-PVCL_{6K}(5%)] to 53 ± 18 % [PU-PEG_{2K}-PVCL_{6K}(5%)] longitudinally, and from 131 ± 23 % [PU-PVCL_{6K}(5%)] to 27 ± 6 % [PU-PEG_{2K}-

PVCL_{6K}(5%)] transversally. The instant recovery for all anisotropic scaffolds in longitudinal direction was $\geq 98\%$.

In wet state (Table 4.2.2), the incorporation of PEG segment into the polyurethane backbone significantly affected the scaffold mechanical behaviors. The peak stresses and the initial moduli of the PU-PEG_{1K}-PVCL_{6K}(5%), and PU-PEG_{2K}-PVCL_{6K}(5%) anisotropic scaffolds decreased obviously from dry state to wet state ($p < 0.05$). For example, the peak stresses of the PU-PEG_{1K}-PVCL_{6K}(5%) reduced from 1.0 ± 0.2 to 0.43 ± 0.13 MPa longitudinally, and from 0.27 ± 0.04 to 0.17 ± 0.01 MPa transversally. The initial moduli of the PU-PEG_{1K}-PVCL_{6K}(5%) decreased from 1.3 ± 0.1 to 0.56 ± 0.11 MPa longitudinally, and from 1.64 ± 0.42 to 0.51 ± 0.14 MPa transversally. However, for the PU-PVCL_{6K}(5%) anisotropic scaffold without PEG segment in the polymer chain, there were no significant differences on the peak stress and initial modulus between dry and wet states ($p > 0.05$).

To evaluate the scaffold dynamic elasticity, the cyclic stretching of the PU-PVCL_{6K}(5%), PU-PEG_{1K}-PVCL_{6K}(5%), and PU-PEG_{2K}-PVCL_{6K}(5%) at 30% deformation in longitudinal and transversal directions was performed under dry and wet states (Figure 4.2.4). All the scaffolds exhibited a large hysteresis loop in the first cycle, followed by nine smaller loops. The PU-PVCL_{6K}(5%) and PU-PEG_{1K}-PVCL_{6K}(5%) exhibited small irreversible deformations ($\leq 10\%$) in two directions under dry and wet states (Figure 4.2.4A, 4B, 4D-4G, 4I, and 4J). The PU-PEG_{2K}-PVCL_{6K}(5%) showed larger permanent deformations ($\sim 15\%$) longitudinally in dry and wet states (Figure 4.2.4C and 4H). The cyclic stretching testing of the PU-PEG_{2K}-

PVCL_{6K}(5%) scaffold in transversal direction cannot be carried out due to its low breaking strain (27 ± 6 % in dry state and 28 ± 6 % in wet state, transversally).

Suture retention for the PU-PVCL_{6K}(5%), PU-PEG_{1K}-PVCL_{6K}(5%), and PU-PEG_{2K}-PVCL_{6K}(5%) anisotropic scaffolds decreased with increasing soft segment molecular weight ($p < 0.05$) (Table 4.2.1). The PU-PVCL_{6K}(5%) had the highest suture retention at 55 ± 14 N/mm², and the PU-PEG_{2K}-PVCL_{6K}(5%) had the lowest suture retention at 4 ± 1 N/mm².

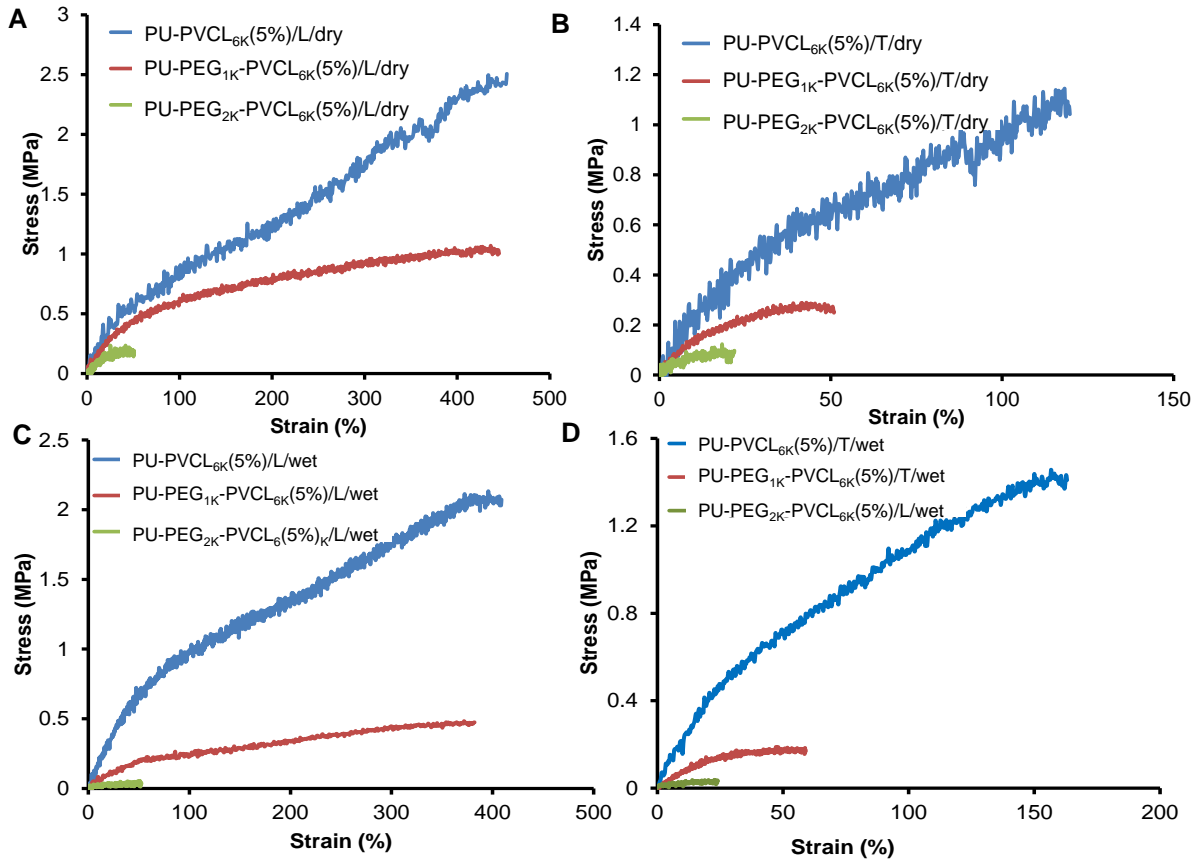


Figure 4.2.3 Stress-strain curve of anisotropic porous scaffolds in (A) longitudinal direction and (B) transversal direction at dry state; (C) longitudinal direction and (D) transversal direction at wet state.

Table 4.2.2 Anisotropic porous scaffold characterization in wet state

Samples	Peak stress (MPa)		Initial modulus (MPa)		Breaking strain (%)	
	L ⁺	T [#]	L	T	L	T
PU-PVCL _{6K} (5%)	2.30±0.23 ^a	1.21±0.40 ^a	1.90±0.24 ^a	1.92±0.37 ^a	356±81 ^a	142±36 ^a
PU-PEG _{1K} -VCL _{6K} (5%)	0.43±0.13 ^b	0.17±0.01 ^b	0.56±0.11 ^b	0.51±0.14 ^b	246±88 ^a	61±12 ^b
PU-PEG _{2K} -VCL _{6K} (5%)	0.05±0.02 ^c	0.03±0.01 ^c	0.16±0.06 ^c	0.16±0.07 ^c	45±8 ^b	28±6 ^c

+ and # represent longitudinal direction and transversal direction, respectively.

* a, b and c represent significantly different groups for each characteristic.

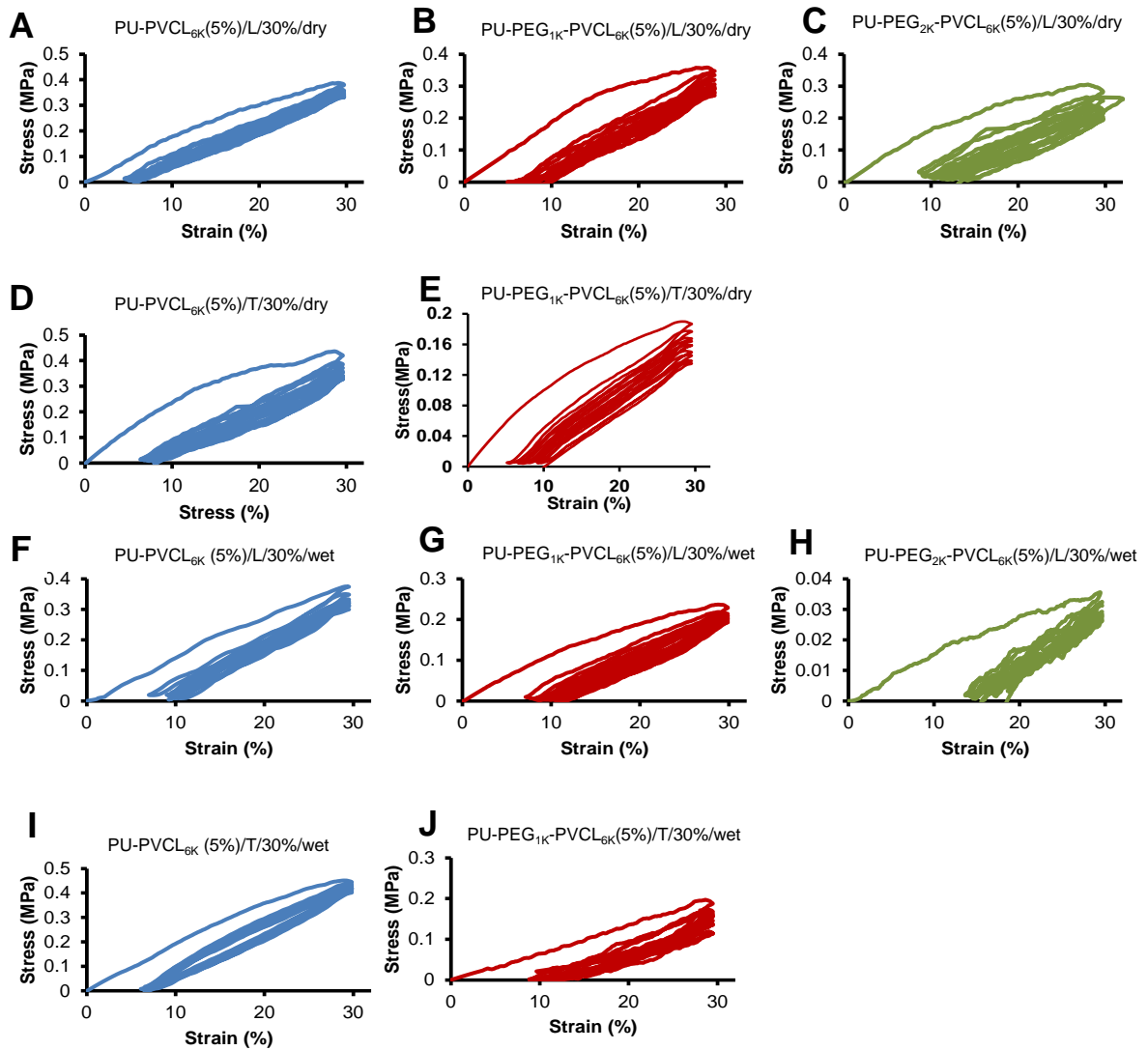


Figure 4.2.4 Cyclic stretch of anisotropic porous scaffolds at 30% deformation. (A), (B), (C) in dry state in longitudinal direction; (D) and (E) in dry state in transversal direction; (F), (G), (H) in wet state in longitudinal direction; (I) and (J) in wet state in transversal direction.

4.2.3.3 PU-PEG_{1K}-PVCL_{6K} scaffold mechanical properties

The PU-PEG_{1K}-PVCL_{6K}-5%, PU-PEG_{1K}-PVCL_{6K}-8% and PU-PEG_{1K}-PVCL_{6K}-10% scaffolds (PU-PEG_{1K}-PVCL_{6K} scaffolds made from three different polymer concentrations, 5%, 8%, and 10%) had regular pore structures in transversal (Figure 4.2.5A, 5C and 5E) and longitudinal (Figure 4.2.5B, 5D and 5F) cross-sections. The average pore sizes and porosities of the PU-PEG_{1K}-PVCL_{6K} scaffolds decreased with increasing polymer concentration (Table 4.2.3), although this trend was not statistically significant ($p > 0.05$). The PU-PEG_{1K}-PVCL_{6K}-5% had the highest average pore size and porosity at 91 μm and 96%, respectively. The PU-PEG_{1K}-PVCL_{6K}-10% had the lowest average pore size and porosity at 51 μm and 90%, respectively.

The typical stress-strain curves of the scaffolds made from different concentrations in transversal directions under dry and wet states were shown in Figure 4.2.6. Generally, the scaffold made from higher polymer concentration had greater peak stress, initial modulus and breaking strains in two directions under both dry and wet states ($p < 0.05$) (Table 4.2.3 and Table 4.2.4). For example, in dry state (Table 4.2.3), the initial modulus increased from 1.3 ± 0.1 (PU-PEG_{1K}-PVCL_{6K}-5%) to 3.0 ± 0.3 MPa (PU-PEG_{1K}-PVCL_{6K}-10%) longitudinally, and from 1.64 ± 0.42 (PU-PEG_{1K}-PVCL_{6K}-5%) to 2.60 ± 0.34 MPa (PU-PEG_{1K}-PVCL_{6K}-10%) transversally. In wet state (Table 4.2.4), the PU-PEG_{1K}-PVCL_{6K}-5% scaffold had the lowest initial modulus at 0.56 ± 0.11 MPa (longitudinally) and 0.61 ± 0.14 MPa (transversally). The PU-PEG_{1K}-PVCL_{6K}-10% had the highest initial modulus at 1.07 ± 0.20 MPa (longitudinally) and 0.91 ± 0.21 MPa (transversally). The instant recovery for the PU-

PEG_{1K}-PVCL_{6K} scaffolds made from 5%, 8% and 10% polymer concentrations in longitudinal direction was $\geq 99\%$.

The results of the ball burst test of all the anisotropic scaffolds were shown in Figure 4.2.7. The PU-PEG_{1K}-PVCL_{6K}-10% had the highest ball burst strength at 20.7 ± 1.5 N, which showed no significant difference between the native LV (20.4 ± 6.0 N) ($p > 0.05$). The PU-PVCL_{6K}(5%), PU-PEG_{1K}-PVCL_{6K}-8%, PU-PEG_{1K}-PVCL_{6K}-5%, and PU-PEG_{2K}-PVCL_{6K}(5%) had ball burst strengths at 15.0 ± 2.4 N, 10.5 ± 1.9 N, 7.7 ± 0.6 N and 1.4 ± 0.1 N, respectively, which were statistically lower than that of the native LV ($p < 0.05$).

The biaxial behaviors of PU-PEG_{1K}-PVCL_{6K}-10% scaffold was evaluated in Figure 4.2.8 and compared with that of the native porcine myocardium.[389] The PU-PEG_{1K}-PVCL_{6K}-5% was ruptured when the tension reached 15 N/m (data not shown). Along both the CD and LD directions, the stiffness of the PU-PEG_{1K}-PVCL_{6K}-10% scaffold was comparable to that of the native myocardium. The anisotropy of the PU-PEG_{1K}-PVCL_{6K}-10% scaffold was similar to that of the native myocardium where the extensibilities in CD direction were larger than those in LD direction under equal tension of 25:25 N/m. The PU-PEG_{1K}-PVCL_{6K}-10% were more extensible along both CD and LD directions than those of the native myocardium at the maximum tension of 25 N/m in two directions.

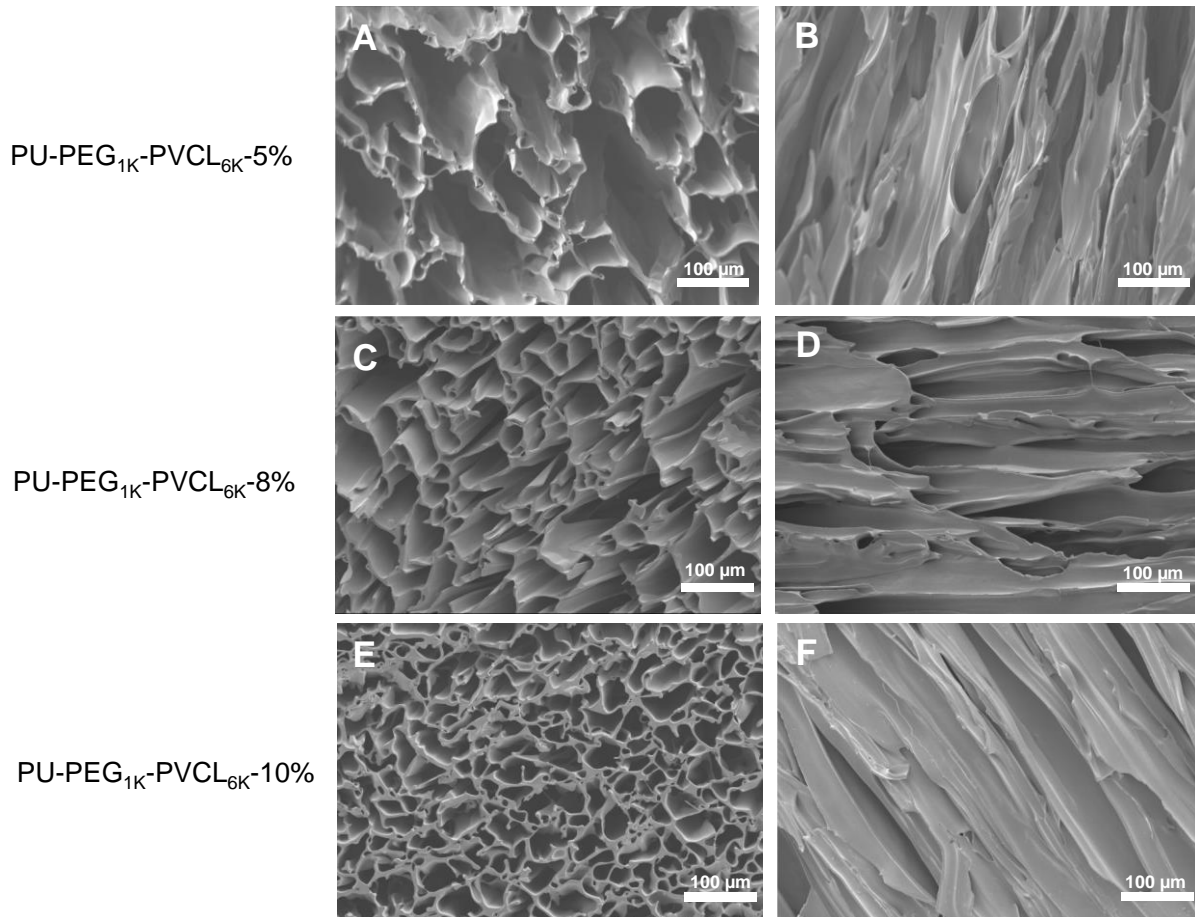


Figure 4.2.5 Electron micrographs of PU-PEG_{1K}-PVCL_{6K} anisotropic porous scaffolds prepared from 5%, 8% and 10% polymer concentrations at -80 °C quenching temperature. (A-B) PU-PVCL_{6K}-5% in transversal (A) and longitudinal (B) directions. (C-D) PU-PEG_{1K}-VCL_{6K}-8% in transversal (C) and longitudinal (D) directions. (E-F) PU-PEG_{2K}-VCL_{6K}-10% in in transversal (E) and longitudinal (F) directions.

Table 4.2.3 PU-PEG_{1K}-VCL_{6K} anisotropic porous scaffold characterization in dry state

Samples	Peak stress (MPa)		Initial modulus (MPa)		Breaking strain (%)		Instant recovery (%)	Pore size (µm)	Porosity (%)
	L ⁺	T [#]	L	T	L	T			
PU-PEG _{1K} -VCL _{6K} -5%	1.0±0.2 ^a	0.27±0.04 ^a	1.3±0.1 ^a	1.64±0.42 ^a	445±130 ^a	51±13 ^a	99±1	91±57	96±3 ^a
PU-PEG _{1K} -VCL _{6K} -8%	1.9±0.2 ^b	0.60±0.05 ^b	2.2±0.2 ^b	1.99±0.33 ^b	470±80 ^a	107±23 ^b	99±1	61±34	93±1 ^a
PU-PEG _{2K} -VCL _{6K} -10%	3.1±0.2 ^c	1.23±0.16 ^c	3.0±0.3 ^c	2.60±0.34 ^c	701±99 ^b	146±46 ^c	100±2	51±28	90±1 ^b

+ and # represent longitudinal direction and transversal direction, respectively.
 * a, b and c represent significantly different groups for each characteristic.

Table 4.2.4 PU-PEG_{1K}-VCL_{6K} anisotropic porous scaffold characterization in wet state

Samples	Peak stress (MPa)		Initial modulus (MPa)		Breaking strain (%)	
	L ⁺	T [#]	L	T	L	T
PU-PEG _{1K} -VCL _{6K} -5%	0.43±0.13 ^a	0.17±0.01 ^a	0.56±0.11 ^a	0.61±0.14 ^a	246±88 ^a	61±12 ^a
PU-PEG _{1K} -VCL _{6K} -8%	0.56±0.07 ^b	0.31±0.08 ^b	0.93±0.22 ^b	0.85±0.15 ^b	250±49 ^a	97±24 ^b
PU-PEG _{2K} -VCL _{6K} -10%	0.83±0.15 ^c	0.52±0.11 ^c	1.07±0.20 ^b	0.91±0.21 ^b	344±43 ^b	121±36 ^c

+ and # represent longitudinal direction and transversal direction, respectively.
 * a, b and c represent significantly different groups for each characteristic.

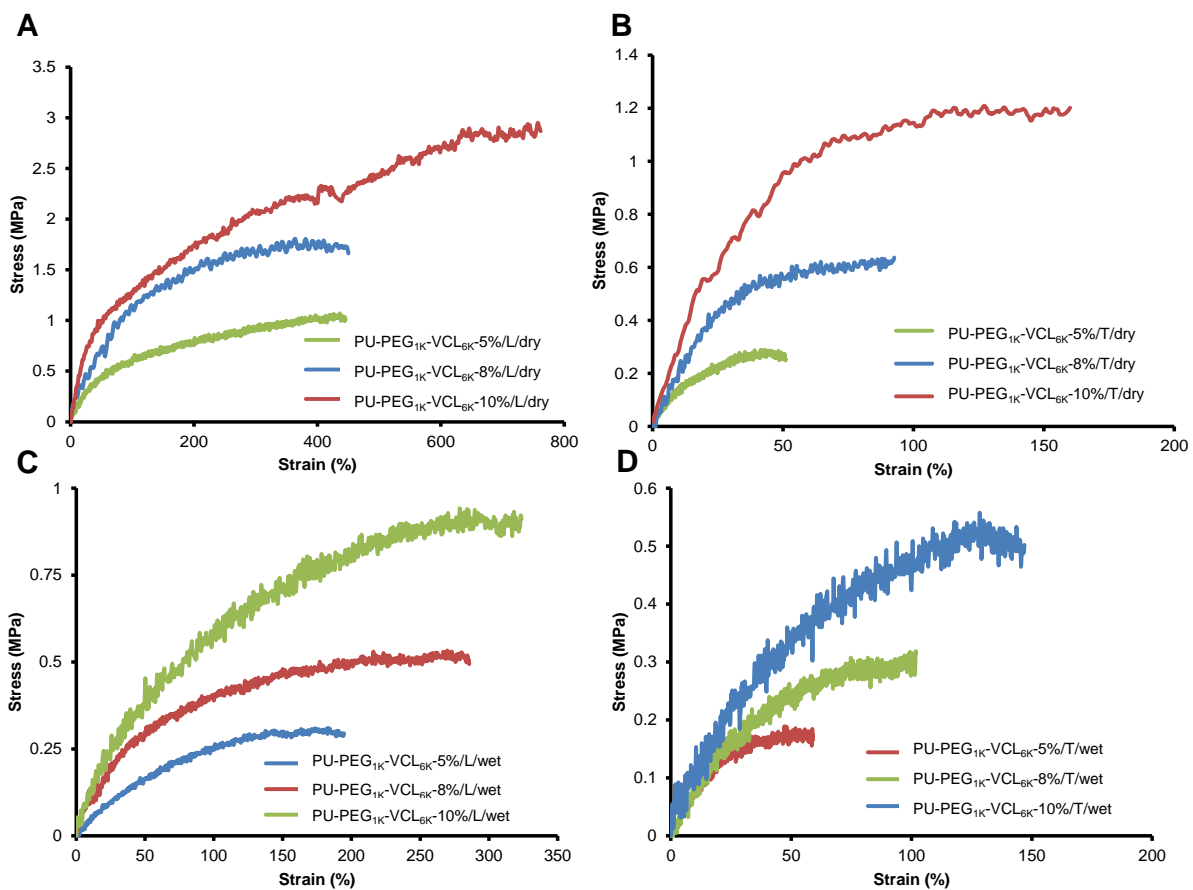


Figure 4.2.6 Stress-strain curve of PU-PEG_{1K}-VCL_{6K} anisotropic porous scaffolds in (A) longitudinal direction and (B) transversal direction at dry state; (C) longitudinal direction and (D) transversal direction at wet state.

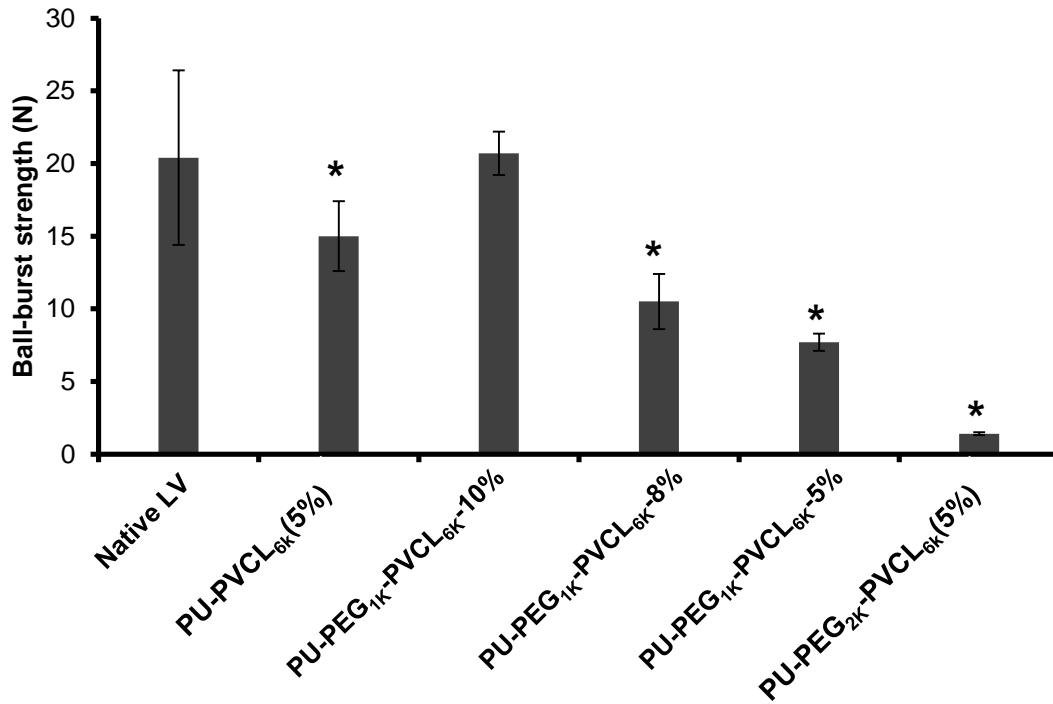


Figure 4.2.7 Ball-burst test results for all anisotropic porous scaffolds. Native left ventricle (LV) was used as the control group. *represents statistically different from the native LV group.

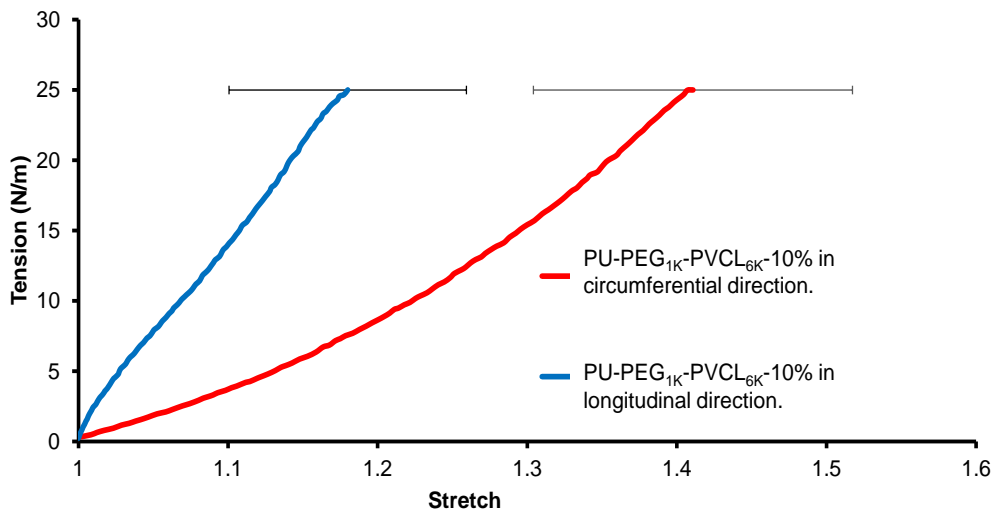


Figure 4.2.8 Biaxial testing of PU-PEG_{1K}-PVCL_{6K}-10% in cross-fiber direction (CD) and fiber-preferred direction (LD).

4.2.3.4 Biohybrid scaffold characterization

The longitudinal and transversal cross-section views of the biohybrid scaffolds were shown in Figure 4.2.9. The fibrous myocardium ECM distributed on the surface of the biohybrid scaffolds and inside their aligned pores.

The mechanical properties of the biohybrid scaffolds and the corresponding synthetic scaffolds (PU-PEG_{1K}-PVCL_{6K}-5%, PU-PEG_{1K}-PVCL_{6K}-8%, and PU-PEG_{1K}-PVCL_{6K}-10%) in wet state were summarized and compared in Table 4.2.5. There was no significant difference between the biohybrid scaffold and its corresponding synthetic scaffold on peak stress, initial modulus and breaking strain ($p > 0.05$).

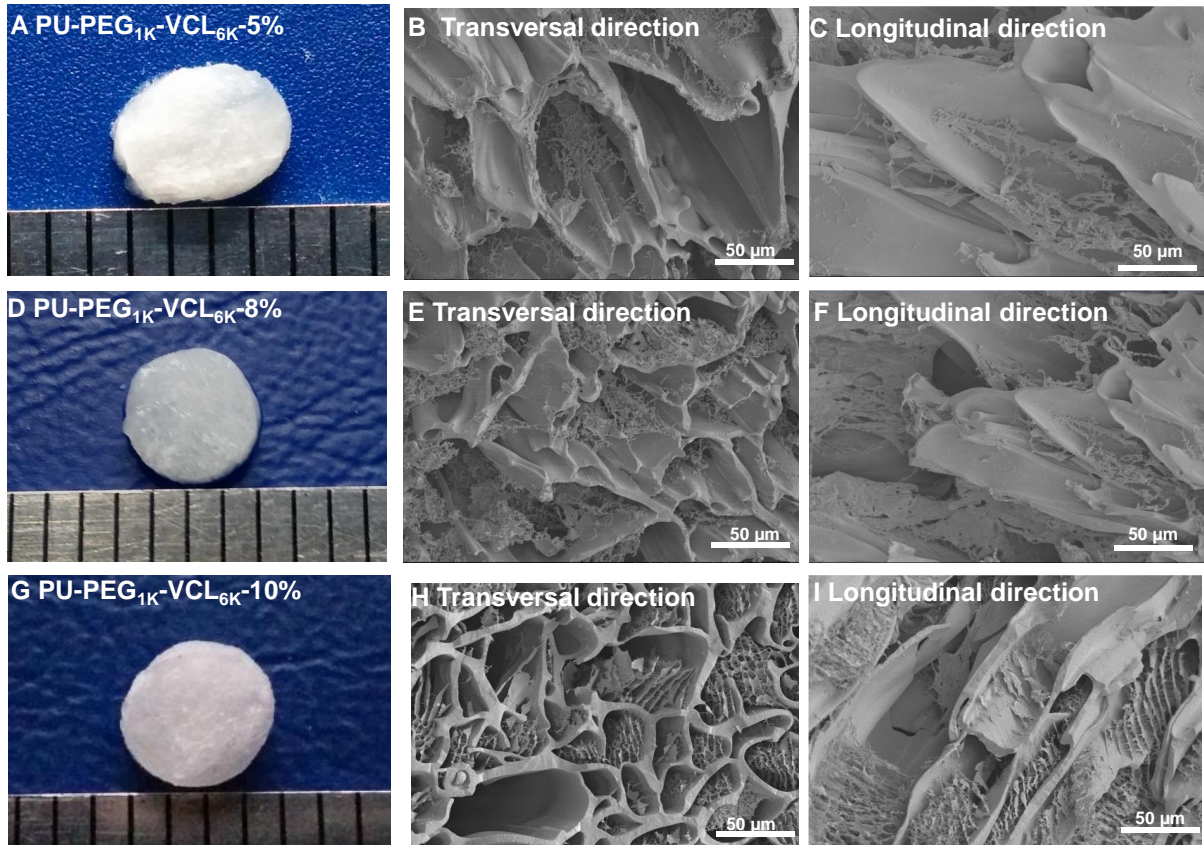


Figure 4.2.9 Biohybrid scaffolds fabricated by combining PU-PEG_{1K}-VCL_{6K} anisotropic scaffolds (5%,8% and 10% w/v) with myocardium-derived hydrogel. (A), (D) and (G) Digital images of PU-PEG_{1K}-VCL_{6K}-5%, PU-PEG_{1K}-VCL_{6K}-8% and PU-PEG_{1K}-VCL_{6K}-10%. (B), (E), and (H) electron micrographs of PU-PEG_{1K}-VCL_{6K}-5%, PU-PEG_{1K}-VCL_{6K}-8% and PU-PEG_{1K}-VCL_{6K}-10% biobybrid scaffolds in transversal direction. (C), (F), and (I) electron micrographs of PU-PEG_{1K}-VCL_{6K}-5%, PU-PEG_{1K}-VCL_{6K}-8% and PU-PEG_{1K}-VCL_{6K}-10% biobybrid scaffolds in longitudinal direction

Table 4.2.5 Mechanical properties of PU-PEG1K-VCL6K-5%, 8% and 10% scaffold with or without ECM in wet state*

Samples	Peak stress (MPa)				Initial modulus (MPa)				Breaking strain (%)			
	Composite		Without ECM		Composite		Without ECM		Composite		Without ECM	
	L ⁺	T [#]	L	T	L	T	L	T	L	T	L	T
PU-PEG _{1K} -VCL _{6K} -5%	0.36±0.05 ^a	0.19±0.02 ^a	0.43±0.13 ^a	0.17±0.01 ^a	0.64±0.11 ^a	0.60±0.15 ^a	0.56±0.11 ^a	0.61±0.14 ^a	255±33 ^a	66±15 ^a	246±88 ^a	61±12 ^a
PU-PEG _{1K} -VCL _{6K} -8%	0.62±0.05 ^b	0.35±0.05 ^b	0.56±0.07 ^b	0.31±0.08 ^b	0.85±0.19 ^{a,b}	0.78±0.17 ^b	0.93±0.22 ^b	0.85±0.15 ^b	276±32 ^a	88±27 ^a	250±49 ^a	97±24 ^b
PU-PEG _{1K} -VCL _{6K} -10%	0.78±0.10 ^c	0.56±0.08 ^c	0.83±0.15 ^c	0.52±0.11 ^c	1.08±0.14 ^b	0.85±0.20 ^b	1.17±0.20 ^c	0.91±0.21 ^b	363±52 ^c	132±25 ^c	344±43 ^b	121±36 ^c

+ and # represent longitudinal direction and transversal direction, respectively.

* a, b and c represent significantly different groups for each characteristic.

4.2.3.5 Rat subcutaneous implantation

To investigate the *in vivo* cell penetration and tissue compatibility, anisotropic synthetic (PU-PEG_{1K}-PVCL_{6K}-10%) and biohybrid scaffolds were implanted for 2 and 4 weeks, and then excised with the surrounding tissue after animal sacrifice. Many inflammatory cells were seen to surround the implants (Figure 4.2.10A). Significant polymer cell infiltration and attachment was observed in all the tested materials with more occurring in the biohybrid samples with an increase in the number of cells penetrating deep into the sample by the 4th week shown with H&E staining (Figure 4.2.10A). The average number of cells infiltrating the implants were about 146±65 (synthetic in 2wks), 241±64 (synthetic in 4wks), 205±41 (biohybrid in 2wks), and 318±35 (biohybrid in 4wks). Taking a crop from the surface to deeper portions of the implant on different locations and dividing them into 3 zones, and the cells counted, the results were as follows (Figure 4.2.10B): for the 2wk sample of the synthetic scaffold, the outer zone had 210±24 cells which reduced to 147±20 cells for the middle zone and then 80±7 cells for the inner zone. For the 4wk sample of the synthetic scaffold, the outer zone had an increased number of cells which was 313±63 cells which reduced to 217±28 cells for the middle zone and then 192±50 cells for the inner zone. For the 2wk sample of the biohybrid scaffold, the outer zone had 252±49 cells which reduced to 185±33 cells for the middle zone and then 177±47 cells for the inner zone. For the 4wk sample of the biohybrid scaffold, the cells were generally increased and were for 358±63 cells the outer zone, which reduced to 294±82 cells for the middle zone and then increased marginally to 301±82 cells for the inner zone. Biohybrid degradation was observed within 4 weeks of implantation.

Histological study showed that biohybrid scaffolds have great biocompatibility, cell attachment and significant cell infiltration compared to the synthetic scaffold.

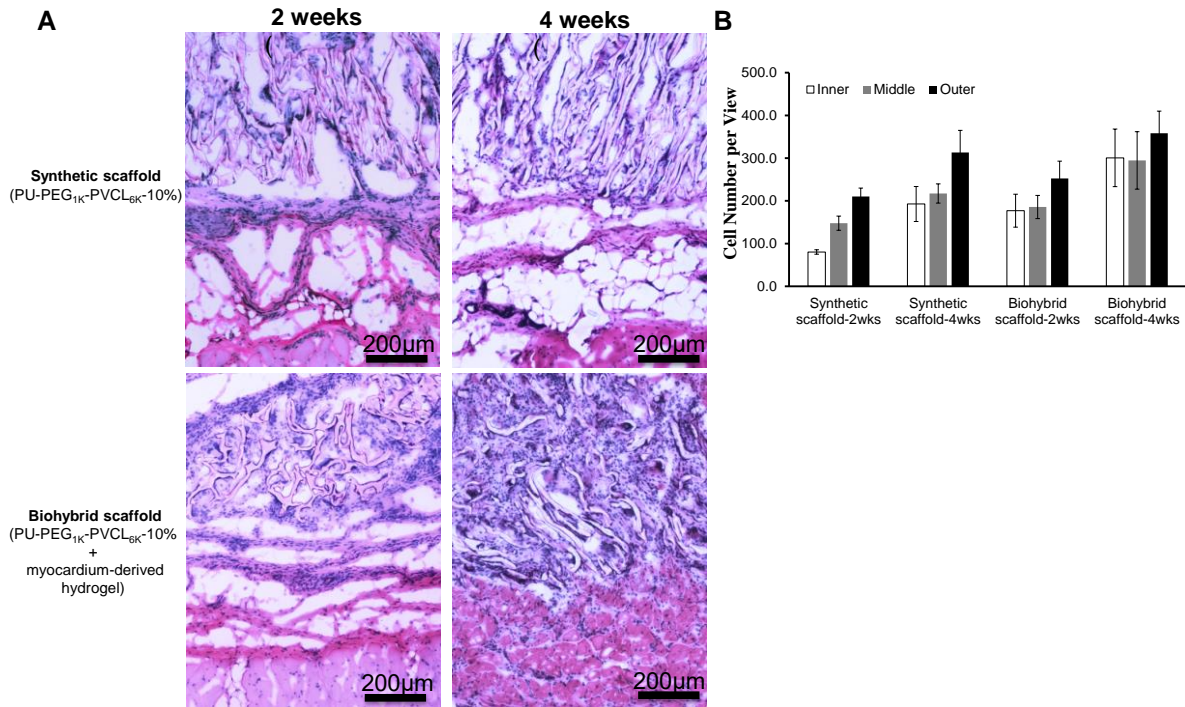


Figure 4.2.10 *In vivo* tissue compatibility of biohybrid scaffolds (PU-PEG_{1K}-VCL_{6K}-10% combined with myocardium-derived hydrogel) in a rat subcutaneous model. (A) H&E staining of the implanted scaffolds and surrounding tissues after 2 and 4 weeks of implantation; (B) Cell number in inner, middle, and outer area on the implants was quantified.

4.2.4 Discussion

Bio-hybridization of the tissue-derived biomaterials and synthetic polymers is an efficient method to fabricate new tissue-engineered biomaterials, which can benefit from the advantages of the tissue-derived (preservation of the native ECM

composition and biological activity)[395] and synthetic polymers (strong mechanical properties and durability), while minimize their weaknesses.[363, 396] Currently, the biohybrid tissue engineered scaffolds have been primarily achieved by co-electrospinning a blend solution of synthetic polymers (e.g., polyurethanes and PCL) and tissue-derived biomaterials (e.g., dermal ECM, SIS, and UBM),[216, 217, 397, 398] and concurrently electrospinning polymer solution and electrospaying dermal ECM hydrogel[399]. None of the above biohybrid scaffolds were specifically designed to be applied as tissue engineered cardiac patches. Besides, those methods to fabricate the biohybrid scaffolds involved various organic solvents (e.g., hexafluoroisopropanol, dichloromethane, and dimethylformamide), which might adversely impact the bioactivity of the tissue-derived biomaterials.[399] In our study, the biohybrid scaffolds were fabricated by injecting the cardiac ECM into the pores of the prepared PU-PEG-PVCL anisotropic scaffolds, and then solidified the hydrogel, which completely prevented the direct contact between the organic solvent and the cardiac ECM. Hence, we fabricated a novel biohybrid cardiac patch which not only structurally and mechanically mimic the native myocardium, but also possess high bioactivity originating from the blended cardiac ECM.

The ideal tissue engineered cardiac patch should mechanically match the native myocardium and have sufficient elasticity to synchronously contract and relax with native heart cycle. The cardiac patch stiffness significantly impairs the phenotype maintenance of the cardiomyocytes, subsequently weakens their functional abilities (e.g., cell striation loss, beating frequency decreasing, and the reduced fraction of beating cells).[381, 400] The increasing stiffness value is directly associated with the

healing degree of the myocardial infarct tissue, which is significantly greater than the non-infarcted myocardium.[401] Hence, the tissue engineered cardiac patch should replace the abnormal infarct stiffness with low initial modulus which is comparable to that of the native non-infarcted myocardium ($E=0.02-0.5$ MPa).[287, 381, 402] Most natural biomaterial based scaffolds, such as fibrin matrices ($E=2.4-3.7 \times 10^{-5}$ MPa),[403] Matrigel ($E=4.5 \times 10^{-4}$ MPa),[404] and alginate hydrogel ($E=1.8 \times 10^{-4}$ to 2.0×10^{-2} MPa),[405] have lower Young's moduli than that of the human myocardium. However, most synthetic polymer based scaffolds, such as PLGA nanofibers ($E=80$ MPa),[406] PCL nanofibers ($E=8.84$ MPa),[407] poly(L-lactide-co- ϵ -caprolactone) nanofibers (PLCL; $E=0.8-14.2$ MPa)[408] and poly(ester urethane)urea nanofibers (PEUU; $E=3$ MPa)[216] are stiffer than the human myocardium. In our study, the initial moduli of the anisotropic PU-PEG-PVCL scaffolds can be tuned by changing the conjugated block length of the soft segments in the polyurethane backbone, in which the initial moduli of the anisotropic PU-PEG_{1K}-PVCL_{6K}(5%) scaffold (0.56 ± 0.11 MPa in longitudinal direction, and 0.51 ± 0.14 MPa in transversal direction in wet state) were comparable to that of the native heart tissue. Besides, the PU-PEG_{1K}-PVCL_{6K}(5%) scaffold had suture retention strength at 27 ± 8 N/mm² which is comparable to that of expanded poly(tetrafluoroethylene) (23 N/mm²) used clinically.[399] Hence, the PU-PEG_{1K}-PVCL_{6K}(5%) scaffold with soft segment block length (3000-1000-3000) was promising for further mechanical optimization through scaffold geometry approach using TIPS technique.

To engineer a cardiac patch mechanically matching the native myocardium, the PU-PEG_{1K}-PVCL_{6K} anisotropic scaffolds made from different polymer

concentrations (5%, 8% and 10%) by TIPS were not only compared with the native heart tissue on the stiffness, but also on ball-burst strength and biaxial mechanical properties which can reflect the scaffold behavior under physiologically-relevant loading conditions. Few literatures have compared both the stiffness of the synthetic cardiac patches and their biomechanics (e.g., suture retention, ball-burst strength and biaxial mechanical properties) with the native myocardium.[383] There was a predictable increase in initial moduli of the PU-PEG_{1K}-PVCL_{6K} scaffolds with increased polymer concentration. The tissue engineered cardiac patch is required to possess sufficient ball-burst strength to prevent rupture or bleeding around the patch during the heart beating.[409] As the data shown in Figure 4.2.7, the PU-PEG_{1K}-PVCL_{6K}-10% apparently had the highest ball burst strength at 20.7 ± 1.5 N, which was the closest to the of the native heart tissue (20.4 ± 6.0 N). In biaxial testing (Figure 4.2.8), PU-PEG_{1K}-PVCL_{6K}-10% scaffold can be stretched to a tension at 25 N/m as the native myocardium, while the PU-PEG_{1K}-PVCL_{6K}-5% scaffold was too weak to be stretched to the tension at 25 N/m (ruptured at 15 N/m). Besides, the PU-PEG_{1K}-PVCL_{6K}-10% scaffold had comparable anisotropy and stiffness to those of the native porcine myocardium and larger extensibilities in both CD and LD directions than the native myocardium. Hence, according to the results from ball burst test and biaxial testing, the PU-PEG_{1K}-PVCL_{6K}-10% scaffold showed more comparable biaxial behaviors to the native myocardium than the PU-PEG_{1K}-PVCL_{6K}-5% and PU-PEG_{1K}-PVCL_{6K}-8% scaffolds.

The biohybrid scaffolds consisting of synthetic PU-PEG_{1K}-PVCL_{6K}-10% scaffold and myocardium-derived hydrogel had similar morphologies to the

decellularized porcine myocardial scaffold. Moreover, from the data in Table 4.2.5, the combination of the myocardium-derived hydrogel with the synthetic PU-PEG_{1K}-PVCL_{6K}-10% scaffold had no effects on the mechanical properties of the synthetic polymer scaffolds. Hence, the biohybrid scaffolds can maintain the optimized mechanical properties of the synthetic scaffolds, in the meanwhile, benefit from the high bio-functional abilities of the myocardium-derived hydrogel. To our knowledge, it is the first time to combine the myocardium-derived hydrogel with synthetic polymer scaffolds to fabricate tissue engineered cardiac patch for potential SVR use. However, the promotion of the tissue-derived biomaterials on bioactivity of the synthetic polymer scaffolds has been reported by a few studies.[216, 217, 399] For example, the electrospun polyurethane/UBM hybrid scaffold showed greater amount of cellular infiltration than the synthetic polyurethane scaffold after 28 days of implantation in a rat subcutaneous model.[217] The electrospun polyurethane/dermal ECM patch was implanted in a rat full-thickness abdominal wall replacement model for 8 weeks and its explant showed higher wall thickness and greater expression of associated smooth muscle actin–positive staining cells.[216] The polyurethane/dermal ECM scaffold fabricated by electrospinning and electro spraying was implanted into a rat abdominal wall defect model. More extensive cellular infiltration was observed in the hybrid scaffold than the polyurethane scaffold.[399] Similarly, our biohybrid scaffold showed no severe immune response after 4 weeks of implantation and exhibited higher cell penetration than the synthetic scaffold, indicating its good tissue compatibility and high bioactivity to recruit surrounding cells and promote tissue repair.

4.2.5 Conclusion

A series of anisotropic polyurethane porous scaffolds were fabricated by TIPS technique. Their mechanical properties, including uniaxial mechanical properties, suture retention strength, ball-burst strength and uniaxial mechanical properties were optimized to mechanically match the human myocardium. Furthermore, the optimized polyurethane scaffold was combined with the porcine myocardium-derived hydrogel to form the biohybrid scaffold. The biohybrid scaffold had similar morphologies to the acellular porcine myocardial scaffold and exhibited high bioactivity without affecting the optimal mechanical properties from the synthetic polyurethane scaffold. The biohybrid scaffold with optimized mechanical properties may find opportunities to be applied as a cell-free cardiac patch for CHF treatment.

CHAPTER 5

CONCLUSION AND FUTURE WORK

5.1 Conclusions

Biodegradable polyurethanes have been widely used as scaffolds in tissue repair and regeneration. Their mechanical, biological, and physio-chemical properties can be tailored by varying the three blocks, diisocyanates, diols and chain extenders in the polymer backbone. A variety of functionalized polyurethanes, such as conductive, shape memory, waterborne, amino-acid-based, antibacterial and nonthrombogenic polyurethanes have been designed to meet the demands of facilitating tissue regeneration. Biodegradable polyurethane based tissue engineered scaffolds have been applied in a variety of tissue engineering fields, such as cardiovascular, musculoskeletal, neural and wound healing fields.

In this thesis, we seek to develop functionalized biodegradable polyurethanes and process them into tissue engineered scaffolds for cardiac tissue repair and regeneration. The design of functionalized biodegradable polyurethanes is from three different aspects: 1) degradation controllability, 2) electroactivity, and 3) mechanical match with native myocardium, were performed accordingly from Chapter 2 to 4.

In Chapter 2, we synthesized reduction-sensitive biodegradable elastomeric polyurethanes containing disulfide bonds in which degradation can be initiated and accelerated with the supplement of a biological product: antioxidant-GSH. The scaffold degradation plays an important role in tissue repair and regeneration. Fast degradation would induce mechanical failure while slow degradation would lead to inappropriate tissue growth. Furthermore, in vivo tissue development is individually

different, especially for aged persons and children, which requires scaffold having tunable degradation behavior specifically for individual. Thus, it is very promising to develop a new material with controllable degradation to meet individual requirement for personalized medicine. The disulfide linkage exists in the proteins of human body and can be cleaved under a mild reductive environment,[410] hence, it can be used a safe trigger for material degradation control. The synthesized reduction-sensitive polyurethanes exhibited robust mechanical properties and high elasticity. Accelerated degradation of the materials was observed in the presence of GSH, and the rate of such degradation depends on the amount of disulfide present in the polymer backbone. The polymers and their degradation products exhibited no apparent cell toxicity while the electrospun scaffolds supported fibroblast growth *in vitro*. The *in vivo* subcutaneous implantation model showed that the polymers prompt minimal inflammatory responses, and as anticipated, the polymer with the higher disulfide bond amount had faster degradation *in vivo*. This new family of polyurethanes offers tremendous potential for directed scaffold degradation to promote maximal tissue regeneration.

In Chapter 3, we developed series of electroactive biodegradable polyurethanes. Biodegradable conductive materials have promises to be applied for myocardium, nerve, muscle and bone tissue repair. The conductive hydrogel promoted growth and maturation of cardiac cells, and enhanced the electrical and mechanical coupling and contractile properties.[48] The conductive material also improved neurite outgrowths from the nerve cells by integrating biochemical and electrical stimulations.[411] However, biodegradable conductive elastomer was rarely reported. To address this

limitation, we firstly designed an electrically conductive polyurethane (CPU) was synthesized from polycaprolactone diol, hexadiisocyanate, and aniline trimer and subsequently doped with CSA. All CPU films showed good elasticity within 30% strain range, and their initial moduli increased with increasing CSA content. The roughness of CPU films increased with increasing CSA amount. The electrical conductivity of CPU films also enhanced with increasing CSA dopant amount, ranging from $1.8 \pm 0.6 \times 10^{-7}$ to $7.3 \pm 1.5 \times 10^{-5}$ S/cm in wet state, which were in the semiconductive region. The redox peaks (0.17 V and 0.82 V) of CPU1.5 film (molar ratio of CSA:aniline trimer was 1.5:1) in cyclic voltammogram indicated its good electroactivity. The doped CPU film exhibited excellent electrical stability (91% of initial conductivity after 150 h charge) in cell culture medium. The degradation of CPU films became faster with increasing CSA dopant amount in either PBS or lipase/PBS solutions. After 7 d of enzymatic degradation, all CSA doped CPU films lost their conductivity. Their conductivities were similar to that of the undoped CPU film, which may attribute to the dopant leaching during degradation. The 3T3 fibroblasts proliferated and spread on all CPU films. There was no significantly difference on cell proliferation between CPU films and the tissue culture polystyrene, except for the CPU1.5 film. The CPU1.5 film having the highest dopant content showed less cell viability within 5 d incubation, which may be resulted from the rough surface and leached dopant. Because the addition of dopant, CSA, increased the polymer stiffness and deteriorated the electrical stability of the CPU due to the dopant leaching-out, we improved our design by introducing the dopant molecule into the polyurethane backbone via covalent bonding to form a biodegradable, dopant-free

conductive polyurethane (DCPU) without adding extra dopant, which possessed improved mechanical properties, electrical conductivity and conductive stability, compared with the CPU polymer. The electrical conductivities of DCPUs increased with increasing dopant DMPA amounts, ranging from $4.4 \pm 0.4 \times 10^{-7}$ to $4.7 \pm 0.8 \times 10^{-3}$ S/cm in wet state, which were higher than those of CPU polymers doped with different amounts of CSA (ranging from $1.8 \pm 0.6 \times 10^{-7}$ S/cm to $7.3 \pm 1.5 \times 10^{-5}$ S/cm in wet state). The redox peaks (550 mV and 930 mV) of DCPU-0.3/1 film in cyclic voltammogram indicated its good electroactivity. The DCPU film showed excellent electrical stability (264% of initial conductivity after 150h charge) under a physiological condition. In comparison, the CPU1.5 film (molar ratio of CSA:aniline trimer was 1.5:1) only retained 87% of its initial conductivity under the same conditions. The initial moduli of CPU films ranged from 3.0 ± 0.6 MPa to 5.2 ± 1.1 MPa with decreasing DMPA content, which were lower than those of CPU films (increasing from 7 ± 1 MPa to 35 ± 11 MPa with increased CSA amount). This conductive elastomer also exhibits robust mechanical properties with high elasticity and flexibility. Mouse 3T3 fibroblasts proliferated on these films exhibiting good cytocompatibility. DCPU can also be processed into a porous scaffold using salt leaching. *In vivo* mouse subcutaneous model exhibited good tissue compatibility with extensive cell infiltration over 4 weeks of the DCPU scaffold compared to polycaprolactone porous scaffold. Such biodegradable DCPU with good flexibility and elasticity, processability, and electrical stability would find opportunities to be applied as tissue engineered scaffolds, for example, cardiac patch, smart drug release carriers and bioelectronics.

In Chapter 4, we developed biodegradable polyurethane-based tissue engineered cardiac patch with high bioactivity and comparable mechanical properties to the native myocardium. The mechanical match between synthetic scaffold and host tissue remains challenging in tissue regeneration. The elastic soft tissues exhibit low initial moduli with a J-shaped tensile curve. Suitable synthetic polymer scaffolds require low initial modulus and elasticity. To achieve these requirements, we firstly synthesized a triblock copolymer (PVCL-PEG-PVCL) based on random copolymers PVCL and hydrophilic PEG, and then synthesized biodegradable elastomeric polyurethanes (PU-PEG-PVCL) using a soft segment PVCL-PEG-PVCL, a hard segment HDI and a chain extender putrescine. The mechanical properties of polyurethanes in dry and wet states can be tuned by altering the molecular weights and hydrophilicities of the soft segments. Increasing the length of either PVCL or PEG in the soft segments reduced initial moduli of the polyurethane films and scaffolds in dry and wet states. The polymer films are found to have good cell compatibility and to support fibroblast growth in vitro. Selected PU-PEG-PVCL polymers were processed into anisotropic porous scaffolds by TIPS technique, and their mechanical properties (e.g. uniaxial mechanics, ball burst, suture retention, and biaxial mechanics) were optimized to mechanically match the native myocardium. Furthermore, the optimized synthetic polyurethane scaffold was combined with myocardium-derived hydrogel to form a biohybrid scaffold to improve its bioactivity. The biohybrid scaffold had morphologies similar to the decellularized porcine myocardial scaffold. The mechanical testing results showed the combination of the myocardium-derived hydrogel with the synthetic polyurethane scaffold did not affect

the optimal mechanical properties of the synthetic scaffold. In vivo rat subcutaneous implantation of the biohybrid scaffold showed minimal immune response and exhibited higher cell penetration than the synthetic polyurethane scaffold, indicating its good tissue compatibility and high bioactivity. This newly-developed biohybrid scaffold with mechanics and bioactivity mimicking the native myocardium would have great potential to be applied as cardiac patch for end-stage congestive heart failure treatment.

5.2 Future work

Different functionalized biodegradable polyurethanes have been developed in this thesis offering great potential for cardiac tissue repair and regeneration. Those developed polyurethanes with controllable degradation behavior, electroactivity, or comparable mechanical properties to the native myocardium have good biocompatibility, elasticity, processability and show potential to regulate cell growth. Future work will be discussed in this chapter.

5.2.1 Further characterization of reduction-sensitive polyurethane

In chapter 2, we synthesized a series of reduction-sensitive polyurethanes containing various amount of disulfide bonds which can be mildly cleaved by the naturally existed reducing agent, GSH in human body. The in vitro controllable degradation of the polyurethane scaffold has been studied. However, the in vivo controllable degradation study has yet to be carried out, in which the GSH will be injected directly into the implantation sites or surrounding tissues to accelerate the

scaffold degradation on demand. Besides its tissue engineering applications, the reduction-sensitive polyurethane can also be used as the drug carrier for cancer treatment because the GSH concentration in cancer cells was found to be several times higher than that in normal cells.[412, 413]

5.2.2 Further characterization and improvement of electroactive polyurethane

In chapter 3, we have developed a family of dopant-free, electroactive, biodegradable polyurethane elastomers with good cell and tissue compatibility. Our future work will focus on exploring their effect on cell proliferation and differentiation. C2C12 cells have been cultured on the DCPU films and the abilities of this electroactive polymer to support cell proliferation, promote myogenic differentiation and maturation, and induce cell-to-cell interactions are studied at present. Later, cardiomyocytes and neural cells will also be seeded on the conductive polyurethane films to study its ability to enhance heart and nerve regeneration. Besides, further improvement of the electroactive polyurethane will be made, for example, hydrophilic segment will be incorporated into the polyurethane backbone to improve its solubility in organic solvents and thus, further enhance its processability.

Besides the application as tissue engineering scaffold, the DCPU can also be used as smart drug carrier because of the ability of CPs to entrap the biomolecules through doping process and electrically controlled release of biomolecules via electrochemical reduction/oxidation process.[47] For example, a conductive composite, PLGA-PEG-PLGA as the hydrogel matrix combined with polypyrrole (PPy) nanoparticles were loaded with fluorescein or daunorubicin as the model drugs.[414] The chemical synthesis produced negatively charged fluorescein or positively

charged daunorubicin incorporated into the PPy nanoparticles. Under applied electric field, the fluorescein was released upon reduction, while the oxidation reaction could promote the release of daunorubicin. The amount of drug released increased with increasing electrical potential.

5.2.3 Further optimization of polyurethane cardiac patch

In chapter 4, we have developed a series of low-initial-modulus biodegradable polyurethanes and then fabricated them into anisotropic porous scaffolds. The mechanical properties of those scaffolds have been optimized to mimic native myocardium. Porcine heart ECM was then combined with the optimized anisotropic scaffold to form biohybrid scaffold with high bioactivity. Our next work is optimizing the mechanical properties of the anisotropic porous scaffolds by further altering the block lengths of the soft segments in the polyurethane backbone and the parameters during the porous scaffold fabrication process by TIPS (e.g., quenching temperature and polymer solution concentration). This obtained biohybrid scaffold with tunable mechanical properties and high bioactivity can not be only used for cardiac tissue engineering, but also for other soft tissue engineering, such as skin, skeletal muscle, and nerve.

5.2.4 Combination of all the functionalized polyurethanes

So far, we have developed three different series of functionalized polyurethanes with controllable degradation behavior, electroactivity and comparable mechanical properties to native myocardium, respectively. Since all of these attractive

functions are desirable as tissue engineered scaffolds, it will be promising to develop a polyurethane combining all of these functions together to form a degradation-controllable, electroactive biodegradable polyurethane with tunable mechanical properties and high bioactivities, which may find great opportunities for soft tissue repair and regeneration.

Appendix A
Related Publications

Journal Articles

1. Xu, C.; Hong, Y. Rational design and synthesis of biodegradable polyurethanes for tissue repair and regeneration. In preparation
2. Xu, C.; Huang, Y.; Shi, X.; Wu, J.; Liao, J.; Tang, L.; Hong, Y. Optimizing anisotropic polyurethane scaffolds to mechanically match with the native myocardium. In preparation.
3. Xu, C.; Dai, G.; Hong, Y. Recent Advances of robust elastic hydrogel for 3D printing in biomedical application. In submission.
4. Xu C.; Kuriakose E.; Truong D.; Punnakitikashem P.; Nguyen K.; Hong Y. Enhancing anti-thrombogenicity of biodegradable polyurethanes through drug molecule incorporation. *J. Mater. Chem. B.* 2018, DOI: 10.1039/C8TB01582A.
5. Xu, C.; Lee, W.; Dai, G.; Hong, Y. A highly elastic biodegradable single-network hydrogel for cell printing. *ACS Appl Mater Interfaces.* 2018; 10: 9969-9979.
6. Pandey, N.; Hakamivala, A.; Xu, C.; Hariharan, P.; Radionov, B.; Huang, Z.; Tang, L.; Zimmern, P.; Nguyen, K. T.; Hong, Y. Biodegradable nanoparticles enhanced adhesiveness of mussel-like hydrogels at tissue interface. *Adv Healthc Mater.* 2017; 1701069.
7. Anand, S.; Desai, V.; Alsmadi, N.; Kanneganti, A.; Nguyen, D. H.; Tran, M.; Patil, L.; Vasudevan, S.; Xu, C.; Hong, Y.; Cheng, J.; Keefer, E.; Romero-Ortega, M. I. Asymmetric sensory-motor regeneration of transected peripheral nerves using molecular guidance cues. *Sci Rep.* 2017; 7: 14323.

8. Dorsey, T. B.; Grath, A.; Xu, C.; Hong, Y.; Dai, G. Patterning bioactive proteins or peptides on hydrogel using photochemistry for biological applications. *J Vis Exp.* 2017; 127: e55873.
9. Dorsey, T. B.; Grath, A.; Wang, A.; Xu, C.; Hong, Y.; Dai, G. Evaluation of photochemistry reaction kinetics to pattern bioactive proteins on hydrogels for biological applications. *Bioact. Mater.* 2017; 1-10.
10. Xu, C.; Huang, Y.; Tang, L.; Hong, Y. Low initial modulus biodegradable polyurethane elastomers for soft tissue regeneration. *ACS Appl Mater Interfaces.* 2017; 9: 2169-2180.
11. Yu, S.; Cheng, B.; Yao, T.; Xu, C.; Nguyen, K.; Hong, Y.; Yuan, B. New generation ICG-based contrast agents for ultrasound-switchable fluorescence imaging. *Sci Rep.* 2016; 6: 35942.
12. Xu, C.; Huang, Y.; Yepez, G.; Wei, Z.; Liu, F.; Bugarin, A.; Tang, L.; Hong, Y. Development of dopant-free conductive bioelastomers. *Sci Rep.* 2016; 6: 34451.
13. Xu, C.; Yepez, G.; Wei, Z.; Liu, F.; Bugarin, A.; Hong, Y. Synthesis and characterization of conductive, biodegradable, elastomeric polyurethanes for biomedical applications. *J. Biomed. Mater. Res. Part A.* 2016, 104, 2305-2314.
14. Xu, C.; Huang, Y.; Wu, J.; Tang, L.; Hong, Y. Triggerable degradation of polyurethanes for tissue engineering applications. *ACS Appl. Mater. Interfaces.* 2015, 7, 20377-20388.

Conference Abstracts

1. Xu, C.; Lee, W.; Dai, G.; Hong, Y. Highly elastic, biodegradable hydrogel with shear-thinning properties for bioprinting. In: Society for Biomaterials; 2019 Apr 3-6; Seattle, Washington. In submission.
2. Xu, C.; Kuriakose, E.; Truong, D.; Punnakitikashem, P.; Nguyen, K.; Hong, Y. Biodegradable, elastic polyurethane with enhanced anti-thrombogenicity as blood-contacting biomaterials. In: Society for Biomaterials; 2019 Apr 3-6; Seattle, Washington. In submission.
3. Xu, C.; Lee, W.; Dai, G.; Hong, Y. Shear-thinning biodegradable hydrogel with high elasticity for 3D bioprinting. In: Biomedical Engineering Society; 2018 Oct 17-20; Atlanta, Georgia.
4. Xu, C.; Kuriakose, E.; Truong, D.; Punnakitikashem, P.; Nguyen, K.; Hong, Y. Non-thrombogenic, biodegradable elastomeric polyurethane for blood contacting applications. In: Biomedical Engineering Society; 2018 Oct 17-20; Atlanta, Georgia.
5. Xu, C.; Lee, W.; Dai, G.; Hong, Y. Highly elastic biodegradable hydrogel for cell printing. In: Society for Biomaterials; 2018 Apr 11-14; Atlanta, GA.
6. Xu, C.; Lee, W.; Dai, G.; Hong, Y. A single-network, biodegradable hydrogel with high elasticity for bioprinting. In: 5th TERMIS World Congress; 2018 Sep 4-7; Kyoto, Japan.
7. Xu, C.; Huang, Y.; Yopez, G.; Wei, Z.; Liu, F.; Bugarin, A.; Tang, L.; Hong, Y. Biodegradable conductive elastomers with improved conductive stability. In: Biomedical Engineering Society; 2017 Oct 11-14; Phoenix, Arizona.

8. Xu, C.; Huang, Y.; Yopez, G.; Wei, Z.; Liu, F.; Bugarin, A.; Tang, L.; Hong, Y. Development of conductive biodegradable elastomeric polyurethane. In: 254th American Chemical Society National Meeting & Exposition; 2017 Aug 20-24; Washington, DC.
9. Xu, C.; Huang, Y.; Wu, J.; Liao, J.; Tang, L.; Hong, Y. Biodegradable polyurethane cardiac patch mechanically matching with native myocardium. In: Society for Biomaterials; 2017 Apr 5-8; Minneapolis, Minnesota.
10. Xu, C.; Huang, Y.; Wu, J.; Liao, J.; Tang, L.; Hong, Y. Optimizing anisotropic polyurethane scaffolds to mechanically match with the native myocardium. In: Biomedical Engineering Society; 2016 Oct 5-8; Minneapolis, Minnesota.
11. Xu, C.; Liu, F.; Bugarin, A.; Hong, Y. Synthesis and characterization of a conductive, biodegradable polyurethane elastomer. In: 10th World Biomaterial Congress; 2016 May 17-22; Montreal, Canada.
12. Xu, C.; Brazile, B.; Nguyen, K.; Liao, J.; Tang, L.; Hong, Y. Biodegradable elastomeric polyurethane scaffolds mechanically matching with native heart muscle. In: Basic Cardiovascular Sciences Scientific Sessions; 2015 July 13-16; New Orleans, LA.
13. Xu, C.; Hong Y. Development of biodegradable elastomeric polyurethanes with low initial moduli. In: Society for Biomaterials; 2015 Apr 15-18; Charlotte, NC.
14. Xu, C.; Hong, Y. Reduction induced biodegradable polyurethane elastomers for biomedical applications. In: Biomedical Engineering Society; 2014 Oct 22-25; San Antonio, TX.

Appendix B
Abbreviations

Abbreviations

PU	Polyurethane
PLA	Poly(lactic acid)
PCL	Polycaprolactone
PGA	Poly(glycolide)
PHA	Polyhydroxyalkanoates
T _g	Glass-transition temperature
T _m	Melting temperature
MDI	4,4'-Methylenebis(phenylisocyanate)
TDI	Toluene diisocyanate
BDI	1,4-Butane diisocyanate
HDI	1,6-Hexamethylene diisocyanate
LDI	Lysine-based diisocyanate
IPDI	Sophorone diisocyanate
HMDI	4,4'- Methylene bis(cyclohexyl isocyanate)
PEO	Poly(ethylene oxide)
PPO	Poly(propylene oxide)
BDO	1,4-Butanediol
EG	Ethylene glycol
ED	Ethylenediamine
BDA	1,4-Butanediamine
VL	δ-valerolactone
CL	ε-caprolactone

PEDOT	Poly(3,4-ethylenedioxythiophene)
PDMS	Polydimethylsiloxane
SMP	Shape memory polymers
WBPU	Waterborne polyurethanes
DMPA	2,2-bis(Hydroxymethyl)propionic acid
MSCs	Mesenchymal stem cells
HUVECS	Human umbilical vein endothelial cells
PC	Phosphorylcholine
TIPS	Thermally-induced phase separation
NO	Nitric oxide
ELP	Elastin-like peptide
DPA	Dipyridamole
VEGF	Vascular endothelial growth factor
PHB	Poly[(R)-3-hydroxybutyrate]
CSA	(1S)-(+)-10-Camphorsulfonic acid
GSH	Glutathione
Sn(Oct) ₂	Stannous octoate
HFIP	1,1,1,3,3,3-Hexafluoroisopropanol
NaOH	Sodium hydroxide
DMSO	Anhydrous dimethyl sulfoxide
HDS	Hydroxyethyl disulfide
FTIR	Fourier transform infrared spectrometer
PBS	Phosphate buffer solution

GPC	Gel-permation chromatographic
SEM	Scanning electronic microscope
DMEM	Dulbecco's modified eagle's medium
DTT	Dithiothreitol
TEA	Triethylamine
DMF	Dimethylformamide
HMDS	Hexamethyldisilazane
HCl	Hydrochloric acid
CV	Cyclic voltammogram
PLGA	Poly[(D,L-lactic acid)-co-(glycolic acid)]
PVA	Poly(vinyl alcohol)
IV	Inherent viscosity
DSC	Differential scanning calorimetry
MI	Myocardial infarction
PGS	Poly(glycerol sebcate)
SIS	Small intestinal submucosa
UBM	Urinary bladder matrix
SDS	Sodium dodecyl sulfata

References

- 1 J. A., and Mauck R. L. In *Biomaterials for Tissue Engineering Applications: A Review of the Past and Future Trends*, 1st ed.; Springer wien: New York, 2011; p 181
- 2 O'brien F. J. *Biomaterials & scaffolds for tissue engineering*. *Materials today* 2011;14(3):88-95.
- 3 Yang S., Leong K. F., Du Z., and Chua C. K. The design of scaffolds for use in tissue engineering. Part I. Traditional factors. *Tissue engineering* 2001;7(6):679-689.
- 4 Lamba N. M., Woodhouse K. A., and Cooper S. L. *Polyurethanes in biomedical applications*. CRC press: Boca Raton, FL, 1998.
- 5 Zhang C., Wen X., Vyavahare N. R., and Boland T. Synthesis and characterization of biodegradable elastomeric polyurethane scaffolds fabricated by the inkjet technique. *Biomaterials* 2008;29(28):3781-3791.
- 6 Pavlova M., and Draganova M. Biocompatible and biodegradable polyurethane polymers. *Biomaterials* 1993;14(13):1024-1029.
- 7 Gentile P., Chiono V., Carmagnola I., and Hatton P. V. An overview of poly (lactic-co-glycolic) acid (PLGA)-based biomaterials for bone tissue engineering. *International journal of molecular sciences* 2014;15(3):3640-3659.
- 8 Gupta B., Revagade N., and Hilborn J. Poly (lactic acid) fiber: an overview. *Progress in Polymer Science* 2007;32(4):455-482.
- 9 Labet M., and Thielemans W. Synthesis of polycaprolactone: a review. *Chemical Society Reviews* 2009;38(12):3484-3504.
- 10 Bassas-Galià M., Gonzalez A., Micaux F., Gaillard V., Piantini U., Schintke S. *et al.* Chemical modification of polyhydroxyalkanoates (PHAs) for the preparation of hybrid biomaterials. *CHIMIA International Journal for Chemistry* 2015;69(10):627-630.
- 11 Guelcher S. A. Biodegradable polyurethanes: synthesis and applications in regenerative medicine. *Tissue Engineering Part B: Reviews* 2008;14(1):3-17.
- 12 Gunatillake P. A., Adhikari R., and Felton G. Biodegradable polyurethanes: design, synthesis, properties and potential applications. *Biodegradable Polymers: Processing, Degradation and Applications* 2011;431-470.

- 13 Chu B., Gao T., Li Y., Wang J., Desper C. R., and Byrne C. A. Microphase separation kinetics in segmented polyurethanes: effects of soft segment length and structure. *Macromolecules* 1992;25(21):5724-5729.
- 14 Sobczak M. Biodegradable polyurethane elastomers for biomedical application-synthesis methods and properties. *Polymer-Plastics Technology and Engineering* 2015;54(2):155-172.
- 15 Krol P. Synthesis methods, chemical structures and phase structures of linear polyurethanes. Properties and applications of linear polyurethanes in polyurethane elastomers, copolymers and ionomers. *Progress in materials science* 2007;52(6):915-1015.
- 16 Zhou L., Yu L., Ding M., Li J., Tan H., Wang Z. *et al.* Synthesis and characterization of pH-sensitive biodegradable polyurethane for potential drug delivery applications. *Macromolecules*;44(4):857-864.
- 17 Thomas S., Datta J., Haponiuk J., and Reghunadhan A. *Polyurethane Polymers: Composites and Nanocomposites*. Elsevier: Amsterdam, 2017; 634 p.
- 18 Reed A. M., Potter J., and Szycher M. A solution grade biostable polyurethane elastomer: ChronoFlex AR. *Journal of biomaterials applications* 1994;8(3):210-236.
- 19 Guelcher S. A., Gallagher K. M., Didier J. E., Klinedinst D. B., Doctor J. S., Goldstein A. S. *et al.* Synthesis of biocompatible segmented polyurethanes from aliphatic diisocyanates and diurea diol chain extenders. *Acta biomaterialia* 2005;1(4):471-484.
- 20 Ratner B. D., Hoffman A. S., Schoen F. J., and Lemons J. E., *Biomaterials science: an introduction to materials in medicine*: Elsevier: San Diego, CA, ed. 2, 2004.
- 21 Sawhney A. S., and Hubbell J. A. Rapidly degraded terpolymers of DL-lactide, glycolide, and ϵ -caprolactone with increased hydrophilicity by copolymerization with polyethers. *Journal of Biomedical Materials Research Part A* 1990;24(10):1397-1411.
- 22 Woodruff M. A., and Hutmacher D. W. The return of a forgotten polymer-polycaprolactone in the 21st century. *Progress in Polymer Science* 2010;35(10):1217-1256.

- 23 De Groot J., De Vrijer R., Wildeboer B., Spaans C., and Pennings A. New biomedical polyurethane ureas with high tear strengths. *Polymer Bulletin* 1997;38(2):211-218.
- 24 Martina M., and Hutmacher D. W. Biodegradable polymers applied in tissue engineering research: a review. *Polymer International* 2007;56(2):145-157.
- 25 Ma Z., Hong Y., Nelson D. M., Pichamuthu J. E., Leeson C. E., and Wagner W. R. Biodegradable polyurethane ureas with variable polyester or polycarbonate soft segments: effects of crystallinity, molecular weight, and composition on mechanical properties. *Biomacromolecules* 2011;12(9):3265-3274.
- 26 Barikani M., Honarkar H., and Barikani M. Synthesis and characterization of polyurethane elastomers based on chitosan and poly (ϵ -caprolactone). *Journal of applied polymer science* 2009;112(5):3157-3165.
- 27 Chan-Chan L., Vargas-Coronado R., Cervantes-Uc J., Cauich-Rodríguez J., Rath R., Phelps E. *et al.* Platelet adhesion and human umbilical vein endothelial cell cytocompatibility of biodegradable segmented polyurethanes prepared with 4, 4-methylene bis (cyclohexyl isocyanate), poly (caprolactone) diol and butanediol or dithioerythritol as chain extenders. *Journal of biomaterials applications* 2013;28(2):270-277.
- 28 Zhang J.-Y., Beckman E. J., Hu J., Yang G.-G., Agarwal S., and Hollinger J. O. Synthesis, biodegradability, and biocompatibility of lysine diisocyanate-glucose polymers. *Tissue engineering* 2002;8(5):771-785.
- 29 Hassan M. K., Mauritz K. A., Storey R. F., and Wiggins J. S. Biodegradable aliphatic thermoplastic polyurethane based on poly (ϵ -caprolactone) and L-lysine diisocyanate. *Journal of Polymer Science Part A: Polymer Chemistry* 2006;44(9):2990-3000.
- 30 Hettrich W., and Becker R. New isocyanates from amino acids. *Polymer* 1997;38(10):2437-2445.
- 31 Takahara A., Hadano M., Yamaguchi T., Otsuka H., Kidoaki S., Matsuda T. *et al.*, "Biodegradation behavior of segmented polyurethanes prepared from amino acid-based diisocyanate."
- 32 Guan J., Sacks M. S., Beckman E. J., and Wagner W. R. Biodegradable poly (ether ester urethane) urea elastomers based on poly (ether ester) triblock copolymers and putrescine: synthesis, characterization and cytocompatibility. *Biomaterials* 2004;25(1):85-96.

- 33 Cohn D., Stern T., González M. F., and Epstein J. Biodegradable poly (ethylene oxide)/poly (ϵ -caprolactone) multiblock copolymers. *Journal of Biomedical Materials Research Part A* 2002;59(2):273-281.
- 34 Korley L. T. J., Pate B. D., Thomas E. L., and Hammond P. T. Effect of the degree of soft and hard segment ordering on the morphology and mechanical behavior of semicrystalline segmented polyurethanes. *Polymer* 2006;47(9):3073-3082.
- 35 Wang F., Li Z., Lannutti J. L., Wagner W. R., and Guan J. Synthesis, characterization and surface modification of low moduli poly (ether carbonate urethane) ureas for soft tissue engineering. *Acta biomaterialia* 2009;5(8):2901-2912.
- 36 Kloczkowski A. Application of statistical mechanics to the analysis of various physical properties of elastomeric networks-a review. *Polymer* 2002;43(4):1503-1525.
- 37 Hong Y., Guan J., Fujimoto K. L., Hashizume R., Pelinescu A. L., and Wagner W. R. Tailoring the degradation kinetics of poly (ester carbonate urethane) urea thermoplastic elastomers for tissue engineering scaffolds. *Biomaterials*;31(15):4249-4258.
- 38 Christenson E. M., Patel S., Anderson J. M., and Hiltner A. Enzymatic degradation of poly (ether urethane) and poly (carbonate urethane) by cholesterol esterase. *Biomaterials* 2006;27(21):3920-3926.
- 39 Ashton J. H., Mertz J. A., Harper J. L., Slepian M. J., Mills J. L., McGrath D. V. *et al.* Polymeric endoaortic paving: Mechanical, thermoforming, and degradation properties of polycaprolactone/polyurethane blends for cardiovascular applications. *Acta biomaterialia* 2011;7(1):287-294.
- 40 Zhang Z., Kuijter R., Bulstra S. K., Grijpma D. W., and Feijen J. The in vivo and in vitro degradation behavior of poly (trimethylene carbonate). *Biomaterials* 2006;27(9):1741-1748.
- 41 Tokiwa Y., and Suzuki T. Hydrolysis of polyesters by lipases. *Nature* 1977;270(5632):76.
- 42 Kim Y. D., and Kim S. C. Effect of chemical structure on the biodegradation of polyurethanes under composting conditions. *Polymer degradation and stability* 1998;62(2):343-352.

- 43 Pringle J. H., and Fletcher M. Influence of substratum wettability on attachment of freshwater bacteria to solid surfaces. *Applied and Environmental Microbiology* 1983;45(3):811-817.
- 44 Tatai L., Moore T. G., Adhikari R., Malherbe F. o., Jayasekara R., Griffiths I. *et al.* Thermoplastic biodegradable polyurethanes: the effect of chain extender structure on properties and in-vitro degradation. *Biomaterials* 2007;28(36):5407-5417.
- 45 Dahiyat B., Posadas E., Hirosue S., Hostin E., and Leong K. Degradable biomaterials with elastomeric characteristics and drug-carrier function. *Reactive Polymers* 1995;25(2-3):101-109.
- 46 Guan J., and Wagner W. R. Synthesis, characterization and cytocompatibility of polyurethaneurea elastomers with designed elastase sensitivity. *Biomacromolecules* 2005;6(5):2833-2842.
- 47 Guimard N. K., Gomez N., and Schmidt C. E. Conducting polymers in biomedical engineering. *Progress in Polymer Science* 2007;32(8-9):876-921.
- 48 Dvir T., Timko B. P., Brigham M. D., Naik S. R., Karajanagi S. S., Levy O. *et al.* Nanowired three-dimensional cardiac patches. *Nature nanotechnology* 2011;6(11):720.
- 49 Hirata E., Uo M., Takita H., Akasaka T., Watari F., and Yokoyama A. Multiwalled carbon nanotube-coating of 3D collagen scaffolds for bone tissue engineering. *Carbon* 2011;49(10):3284-3291.
- 50 Durgam H., Sapp S., Deister C., Khaing Z., Chang E., Luebben S. *et al.* Novel degradable co-polymers of polypyrrole support cell proliferation and enhance neurite out-growth with electrical stimulation. *Journal of Biomaterials Science, Polymer Edition* 2010;21(10):1265-1282.
- 51 Chen M.-C., Sun Y.-C., and Chen Y. H. Electrically conductive nanofibers with highly oriented structures and their potential application in skeletal muscle tissue engineering. *Acta biomaterialia* 2013;9(3):5562-5572.
- 52 Jiang S., Zhang H., Song S., Ma Y., Li J., Lee G. H. *et al.* Highly stretchable conductive fibers from few-walled carbon nanotubes coated on poly (m-phenylene isophthalamide) polymer core/shell structures. *ACS nano* 2015;9(10):10252-10257.

- 53 Li P., Sun K., and Ouyang J. Stretchable and Conductive polymer films prepared by solution blending. *ACS applied materials & interfaces* 2015;7(33):18415-18423.
- 54 Ma R., Kang B., Cho S., Choi M., and Baik S. Extraordinarily high conductivity of stretchable fibers of polyurethane and silver nanoflowers. *ACS nano* 2015;9(11):10876-10886.
- 55 Sirivisoot S., and Harrison B. S. Skeletal myotube formation enhanced by electrospun polyurethane carbon nanotube scaffolds. *International journal of nanomedicine* 2011;6:2483.
- 56 Seil J. T., and Webster T. J. Decreased astroglial cell adhesion and proliferation on zinc oxide nanoparticle polyurethane composites. *International journal of nanomedicine* 2008;3(4):523.
- 57 Kai D., Tan M. J., Prabhakaran M. P., Chan B. Q. Y., Liow S. S., Ramakrishna S. *et al.* Biocompatible electrically conductive nanofibers from inorganic-organic shape memory polymers. *Colloids and Surfaces B: Biointerfaces* 2017;148:557-565.
- 58 Yang H. S., Lee B., Tsui J. H., Macadangdang J., Jang S. Y., Im S. G. *et al.* Electroconductive nanopatterned substrates for enhanced myogenic differentiation and maturation. *Advanced healthcare materials* 2016;5(1):137-145.
- 59 Wu Y., Wang L., Guo B., Shao Y., and Ma P. X. Electroactive biodegradable polyurethane significantly enhanced Schwann cells myelin gene expression and neurotrophin secretion for peripheral nerve tissue engineering. *Biomaterials* 2016;87:18-31.
- 60 Niple J., Daigle J., Zaffanella L., Sullivan T., and Kavet R. A portable meter for measuring low frequency currents in the human body. *Bioelectromagnetics* 2004;25(5):369-373.
- 61 Bao M., Lou X., Zhou Q., Dong W., Yuan H., and Zhang Y. Electrospun biomimetic fibrous scaffold from shape memory polymer of PDLLA-co-TMC for bone tissue engineering. *ACS applied materials & interfaces* 2014;6(4):2611-2621.
- 62 Lendlein A., and Langer R. Biodegradable, elastic shape-memory polymers for potential biomedical applications. *Science* 2002;296(5573):1673-1676.

- 63 Yakacki C. M., Shandas R., Lanning C., Rech B., Eckstein A., and Gall K. Unconstrained recovery characterization of shape-memory polymer networks for cardiovascular applications. *Biomaterials* 2007;28(14):2255-2263.
- 64 Schmidt A. M. Electromagnetic activation of shape memory polymer networks containing magnetic nanoparticles. *Macromolecular Rapid Communications* 2006;27(14):1168-1172.
- 65 Szabo D., Szeghy G., and Zrinyi M. Shape transition of magnetic field sensitive polymer gels. *Macromolecules* 1998;31(19):6541-6548.
- 66 Ji S., Fan F., Sun C., Yu Y., and Xu H. Visible light-induced plasticity of shape memory polymers. *ACS applied materials & interfaces* 2017;9(38):33169-33175.
- 67 Lendlein A., Jiang H., Jünger O., and Langer R. Light-induced shape-memory polymers. *Nature* 2005;434(7035):879.
- 68 Bao M., Zhou Q., Dong W., Lou X., and Zhang Y. Ultrasound-modulated shape memory and payload release effects in a biodegradable cylindrical rod made of chitosan-functionalized PLGA microspheres. *Biomacromolecules* 2013;14(6):1971-1979.
- 69 Bao M., Tu H., Zhou Q., Dong W., and Zhang Y. Ultrasound-mediated release of lysozyme from biodegradable shape-memory polymeric rods prepared from microspheres. *Journal of Controlled Release* 2013;1(172):e110-e111.
- 70 Venkatraman S. S., Tan L. P., Joso J. F. D., Boey Y. C. F., and Wang X. Biodegradable stents with elastic memory. *Biomaterials* 2006;27(8):1573-1578.
- 71 Ortega J. M., Small W., Wilson T. S., Benett W. J., Loge J. M., and Maitland D. J. A shape memory polymer dialysis needle adapter for the reduction of hemodynamic stress within arteriovenous grafts. *IEEE Transactions on Biomedical Engineering* 2007;54(9):1722-1724.
- 72 Small IV W., Wilson T. S., Benett W. J., Loge J. M., and Maitland D. J. Laser-activated shape memory polymer intravascular thrombectomy device. *Optics Express* 2005;13(20):8204-8213.
- 73 Sokolowski W., Metcalfe A., Hayashi S., Yahia L. H., and Raymond J. Medical applications of shape memory polymers. *Biomedical Materials* 2007;2(1):S23.

- 74 Xie R., Hu J., Hoffmann O., Zhang Y., Ng F., Qin T. *et al.* Self-fitting shape memory polymer foam inducing bone regeneration: A rabbit femoral defect study. *Biochim Biophys Acta Gen Subj.* 2018;1862(4):936-945.
- 75 Yu J., Xia H., Teramoto A., and Ni Q. Q. Fabrication and characterization of shape memory polyurethane porous scaffold for bone tissue engineering. *Journal of Biomedical Materials Research Part A* 2017;105(4):1132-1137.
- 76 Kai D., Prabhakaran M. P., Chan B. Q. Y., Liow S. S., Ramakrishna S., Xu F. *et al.* Elastic poly (ϵ -caprolactone)-polydimethylsiloxane copolymer fibers with shape memory effect for bone tissue engineering. *Biomedical Materials* 2016;11(1):015007.
- 77 Ping P., Wang W., Chen X., and Jing X. Poly (ϵ -caprolactone) polyurethane and its shape-memory property. *Biomacromolecules* 2005;6(2):587-592.
- 78 Liu C., Qin H., and Mather P. Review of progress in shape-memory polymers. *Journal of Materials Chemistry* 2007;17(16):1543-1558.
- 79 Deng Z., Guo Y., Zhao X., Li L., Dong R., Guo B. *et al.* Stretchable degradable and electroactive shape memory copolymers with tunable recovery temperature enhance myogenic differentiation. *Acta biomaterialia* 2016;46:234-244.
- 80 Tsai M. C., Hung K. C., Hung S. C., and Hsu S. H. Evaluation of biodegradable elastic scaffolds made of anionic polyurethane for cartilage tissue engineering. *Colloids and Surfaces B: Biointerfaces* 2015;125:34-44.
- 81 Xu F., Wang Y., Jiang X., Tan H., Li H., and Wang K. J. Effects of different biomaterials: Comparing the bladder smooth muscle cells on waterborne polyurethane or poly-lactic-co-glycolic acid membranes. *The Kaohsiung journal of medical sciences* 2012;28(1):10-15.
- 82 Hao H., Deng Y., Wu Y., Liu S., Lin W., Li J. *et al.* Synthesis of biodegradable waterborne phosphatidylcholine polyurethanes for soft tissue engineering applications. *Regenerative biomaterials* 2017;4(2):69-79.
- 83 Hsu S. H., Chang W. C., and Yen C. T. Novel flexible nerve conduits made of water-based biodegradable polyurethane for peripheral nerve regeneration. *Journal of Biomedical Materials Research Part A* 2017;105(5):1383-1392.

- 84 Hsu S., Hung K. C., Lin Y. Y., Su C. H., Yeh H. Y., Jeng U. S. *et al.* Water-based synthesis and processing of novel biodegradable elastomers for medical applications. *Journal of Materials Chemistry B* 2014;2(31):5083-5092.
- 85 Jiang X., Li J., Ding M., Tan H., Ling Q., Zhong Y. *et al.* Synthesis and degradation of nontoxic biodegradable waterborne polyurethanes elastomer with poly (ϵ -caprolactone) and poly (ethylene glycol) as soft segment. *European Polymer Journal* 2007;43(5):1838-1846.
- 86 Jiang X., Wang K., Ding M., Li J., Tan H., Wang Z. *et al.* Quantitative grafting of peptide onto the nontoxic biodegradable waterborne polyurethanes to fabricate peptide modified scaffold for soft tissue engineering. *Journal of Materials Science: Materials in Medicine* 2011;22(4):819-827.
- 87 Deming T. J. Synthetic polypeptides for biomedical applications. *Progress in Polymer Science* 2007;32(8-9):858-875.
- 88 Lanza R., Langer R., and Vacanti J. P., *Principles of tissue engineering*: Academic press: 2011.
- 89 Wang D., Ji J., Sun Y.-h., Shen J., Feng L., and Elisseeff J. H. In situ immobilization of proteins and RGD peptide on polyurethane surfaces via poly (ethylene oxide) coupling polymers for human endothelial cell growth. *Biomacromolecules* 2002;3(6):1286-1295.
- 90 Krijgsman B., Seifalian A. M., Salacinski H. J., Tai N. R., Punshon G., Fuller B. J. *et al.* An assessment of covalent grafting of RGD peptides to the surface of a compliant poly (carbonate-urea) urethane vascular conduit versus conventional biological coatings: its role in enhancing cellular retention. *Tissue engineering* 2002;8(4):673-680.
- 91 Anderheiden D., Klee D., Höcker H., Heller B., Kirkpatrick C., and Mittermayer C. Surface modification of a biocompatible polymer based on polyurethane for artificial blood vessels. *Journal of Materials Science: Materials in Medicine* 1992;3(1):1-4.
- 92 Jun H. W., and West J. L. Modification of polyurethaneurea with PEG and YIGSR peptide to enhance endothelialization without platelet adhesion. *Journal of Biomedical Materials Research Part B: Applied Biomaterials* 2005;72(1):131-139.
- 93 Han J., Cao R. W., Chen B., Ye L., Zhang A. Y., Zhang J. *et al.* Electrospinning and biocompatibility evaluation of biodegradable

- polyurethanes based on L-lysine diisocyanate and L-lysine chain extender. *Journal of Biomedical Materials Research Part A* 2011;96(4):705-714.
- 94 Shah P. N., and Yun Y. H. Cellular interactions with biodegradable polyurethanes formulated from L-tyrosine. *Journal of biomaterials applications* 2013;27(8):1017-1031.
- 95 Lin H. B., García-Echeverría C., Asakura S., Sun W., Mosher D. F., and Cooper S. L. Endothelial cell adhesion on polyurethanes containing covalently attached RGD-peptides. *Biomaterials* 1992;13(13):905-914.
- 96 Jayakumar R., Prabakaran M., Kumar P. S., Nair S., and Tamura H. Biomaterials based on chitin and chitosan in wound dressing applications. *Biotechnology advances* 2011;29(3):322-337.
- 97 Lakshman L. R., Shalumon K., Nair S. V., Jayakumar R., and Nair S. Preparation of silver nanoparticles incorporated electrospun polyurethane nano-fibrous mat for wound dressing. *Journal of Macromolecular Science, Part A: Pure and Applied Chemistry* 2010;47(10):1012-1018.
- 98 Hong S. M., Kim J. W., Knowles J. C., and Gong M. S. Facile preparation of antibacterial, highly elastic silvered polyurethane nanofiber fabrics using silver carbamate and their dermal wound healing properties. *Journal of biomaterials applications* 2017;31(7):1026-1038.
- 99 Lee S. J., Heo D. N., Moon J. H., Park H. N., Ko W. K., Bae M. S. *et al.* Chitosan/polyurethane blended fiber sheets containing silver sulfadiazine for use as an antimicrobial wound dressing. *Journal of nanoscience and nanotechnology* 2014;14(10):7488-7494.
- 100 Tran P. L., Hamood A. N., Souza A., Schultz G., Liesenfeld B., Mehta D. *et al.* A study on the ability of quaternary ammonium groups attached to a polyurethane foam wound dressing to inhibit bacterial attachment and biofilm formation. *Wound Repair and Regeneration* 2015;23(1):74-81.
- 101 Shababdoust A., Ehsani M., Shokrollahi P., and Zandi M. Fabrication of curcumin-loaded electrospun nanofibrous polyurethanes with anti-bacterial activity. *Progress in biomaterials* 2018;7(1):23-33.
- 102 Chen X., Zhao R., Wang X., Li X., Peng F., Jin Z. *et al.* Electrospun mupirocin loaded polyurethane fiber mats for anti-infection burn wound dressing application. *Journal of Biomaterials Science, Polymer Edition* 2017;28(2):162-176.

- 103 Li P., Poon Y. F., Li W., Zhu H.-Y., Yeap S. H., Cao Y. *et al.* A polycationic antimicrobial and biocompatible hydrogel with microbe membrane suctioning ability. *Nature materials* 2011;10(2):149.
- 104 Ziegler K., Görl R., Effing J., Ellermann J., Mappes M., Otten S. *et al.* Reduced cellular toxicity of a new silver-containing antimicrobial dressing and clinical performance in non-healing wounds. *Skin Pharmacology and Physiology* 2006;19(3):140-146.
- 105 Yari A., Yeganeh H., Bakhshi H., and Gharibi R. Preparation and characterization of novel antibacterial castor oil-based polyurethane membranes for wound dressing application. *Journal of Biomedical Materials Research Part A* 2014;102(1):84-96.
- 106 Luo C., Liu W., Luo B., Tian J., Wen W., Liu M. *et al.* Antibacterial activity and cytocompatibility of chitooligosaccharide-modified polyurethane membrane via polydopamine adhesive layer. *Carbohydrate polymers* 2017;156:235-243.
- 107 Hong Y., Ye S. H., Nieponice A., Soletti L., Vorp D. A., and Wagner W. R. A small diameter, fibrous vascular conduit generated from a poly (ester urethane) urea and phospholipid polymer blend. *Biomaterials* 2009;30(13):2457-2467.
- 108 Hong Y., Ye S. H., Pelinescu A. L., and Wagner W. R. Synthesis, characterization, and paclitaxel release from a biodegradable, elastomeric, poly (ester urethane) urea bearing phosphorylcholine groups for reduced thrombogenicity. *Biomacromolecules* 2012;13(11):3686-3694.
- 109 Soletti L., Nieponice A., Hong Y., Ye S. H., Stankus J. J., Wagner W. R. *et al.* In vivo performance of a phospholipid-coated bioerodable elastomeric graft for small-diameter vascular applications. *Journal of Biomedical Materials Research Part A* 2011;96(2):436-448.
- 110 Ye S. H., Hong Y., Sakaguchi H., Shankarraman V., Luketich S. K., D'Amore A. *et al.* Nonthrombogenic, biodegradable elastomeric polyurethanes with variable sulfobetaine content. *ACS applied materials & interfaces* 2014;6(24):22796-22806.
- 111 Yuan J., Lin S., and Shen J. Enhanced blood compatibility of polyurethane functionalized with sulfobetaine. *Colloids and Surfaces B: Biointerfaces* 2008;66(1):90-95.
- 112 Francolini I., Crisante F., Martinelli A., D'Ilario L., and Piozzi A. Synthesis of biomimetic segmented polyurethanes as antifouling biomaterials. *Acta biomaterialia* 2012;8(2):549-558.

- 113 Silver J. H., Hart A. P., Williams E. C., Cooper S. L., Charef S., Labarre D. *et al.* Anticoagulant effects of sulphonated polyurethanes. *Biomaterials* 1992;13(6):339-344.
- 114 Wang H., Feng Y., Zhao H., Fang Z., Khan M., and Guo J. A potential nonthrombogenic small-diameter vascular scaffold with polyurethane/poly (ethylene glycol) hybrid materials by electrospinning technique. *Journal of nanoscience and nanotechnology* 2013;13(2):1578-1582.
- 115 Martin J. R., Gupta M. K., Page J. M., Yu F., Davidson J. M., Guelcher S. A. *et al.* A porous tissue engineering scaffold selectively degraded by cell-generated reactive oxygen species. *Biomaterials* 2014;35(12):3766-3776.
- 116 Zhu N., and Chen X. Biofabrication of tissue scaffolds. Chapter 12. In: *Advances in biomaterials science and biomedical applications*. Rijeka, Croatia : InTech, 2013; 315–328.
- 117 Laschke M., Strohe A., Menger M., Alini M., and Eglin D. In vitro and in vivo evaluation of a novel nanosize hydroxyapatite particles/poly (ester-urethane) composite scaffold for bone tissue engineering. *Acta biomaterialia* 2010;6(6):2020-2027.
- 118 Guan J., Fujimoto K. L., Sacks M. S., and Wagner W. R. Preparation and characterization of highly porous, biodegradable polyurethane scaffolds for soft tissue applications. *Biomaterials* 2005;26(18):3961-3971.
- 119 Jiang X., Yu F., Wang Z., Li J., Tan H., Ding M. *et al.* Fabrication and characterization of waterborne biodegradable polyurethanes 3-dimensional porous scaffolds for vascular tissue engineering. *Journal of Biomaterials Science, Polymer Edition* 2010;21(12):1637-1652.
- 120 Wong C. S., Liu X., Xu Z., Lin T., and Wang X. Elastin and collagen enhances electrospun aligned polyurethane as scaffolds for vascular graft. *Journal of Materials Science: Materials in Medicine* 2013;24(8):1865-1874.
- 121 Jing X., Mi H. Y., Salick M. R., Cordie T. M., Peng X. F., and Turng L. S. Electrospinning thermoplastic polyurethane/graphene oxide scaffolds for small diameter vascular graft applications. *Materials Science and Engineering: C* 2015;49:40-50.
- 122 Amoroso N. J., D'Amore A., Hong Y., Rivera C. P., Sacks M. S., and Wagner W. R. Microstructural manipulation of electrospun scaffolds for specific bending stiffness for heart valve tissue engineering. *Acta biomaterialia* 2012;8(12):4268-4277.

- 123 Holzapfel G. A., and Ogden R. W., Biomechanics of soft tissue in cardiovascular systems. Wien: Springer-Verlag; 2003.
- 124 Kucinska-Lipka J., Gubanska I., Janik H., and Sienkiewicz M. Fabrication of polyurethane and polyurethane based composite fibres by the electrospinning technique for soft tissue engineering of cardiovascular system. *Materials Science and Engineering: C* 2015;46:166-176.
- 125 Guilak F., Butler D. L., Goldstein S. A., and Baaijens F. P. Biomechanics and mechanobiology in functional tissue engineering. *Journal of biomechanics* 2014;47(9):1933-1940.
- 126 Xu B., Li Y., Fang X., Thouas G. A., Cook W. D., Newgreen D. F. *et al.* Mechanically tissue-like elastomeric polymers and their potential as a vehicle to deliver functional cardiomyocytes. *Journal of the mechanical behavior of biomedical materials* 2013;28:354-365.
- 127 Soletti L., Hong Y., Guan J., Stankus J. J., El-Kurdi M. S., Wagner W. R. *et al.* A bilayered elastomeric scaffold for tissue engineering of small diameter vascular grafts. *Acta biomaterialia* 2010;6(1):110-122.
- 128 Tajaddini A., Kilpatrick D. L., Schoenhagen P., Tuzcu E. M., Lieber M., and Vince D. G. Impact of age and hyperglycemia on the mechanical behavior of intact human coronary arteries: an ex vivo intravascular ultrasound study. *American Journal of Physiology-Heart and Circulatory Physiology* 2005;288(1):H250-H255.
- 129 Blit P. H., Battiston K. G., Yang M., Santerre J. P., and Woodhouse K. A. Electrospun elastin-like polypeptide enriched polyurethanes and their interactions with vascular smooth muscle cells. *Acta biomaterialia* 2012;8(7):2493-2503.
- 130 Chen R., Qiu L., Ke Q., He C., and Mo X. Electrospinning thermoplastic polyurethane-contained collagen nanofibers for tissue-engineering applications. *Journal of Biomaterials Science, Polymer Edition* 2009;20(11):1513-1536.
- 131 Lisi A., Briganti E., Ledda M., Losi P., Grimaldi S., Marchese R. *et al.* A combined synthetic-fibrin scaffold supports growth and cardiomyogenic commitment of human placental derived stem cells. *PLoS One* 2012;7(4):e34284.
- 132 Martins A. M., Eng G., Caridade S. G., Mano J. F., Reis R. L., and Vunjak-Novakovic G. Electrically conductive chitosan/carbon scaffolds for cardiac tissue engineering. *Biomacromolecules* 2014;15(2):635-643.

- 133 Baheiraei N., Yeganeh H., Ai J., Gharibi R., Azami M., and Faghihi F. Synthesis, characterization and antioxidant activity of a novel electroactive and biodegradable polyurethane for cardiac tissue engineering application. *Materials Science and Engineering: C* 2014;44:24-37.
- 134 Baheiraei N., Yeganeh H., Ai J., Gharibi R., Ebrahimi-Barough S., Azami M. *et al.* Preparation of a porous conductive scaffold from aniline pentamer-modified polyurethane/PCL blend for cardiac tissue engineering. *Journal of Biomedical Materials Research Part A*; 2015;103(10):3179-3187.
- 135 Jun H. W., Taite L. J., and West J. L. Nitric oxide-producing polyurethanes. *Biomacromolecules* 2005;6(2):838-844.
- 136 Taite L. J., Yang P., Jun H. W., and West J. L. Nitric oxide-releasing polyurethane-PEG copolymer containing the YIGSR peptide promotes endothelialization with decreased platelet adhesion. *Journal of Biomedical Materials Research Part B: Applied Biomaterials* 2008;84(1):108-116.
- 137 Major T. C., Brisbois E. J., Jones A. M., Zanetti M. E., Annich G. M., Bartlett R. H. *et al.* The effect of a polyurethane coating incorporating both a thrombin inhibitor and nitric oxide on hemocompatibility in extracorporeal circulation. *Biomaterials* 2014;35(26):7271-7285.
- 138 Punnakitikashem P., Truong D., Menon J. U., Nguyen K. T., and Hong Y. Electrospun biodegradable elastic polyurethane scaffolds with dipyridamole release for small diameter vascular grafts. *Acta biomaterialia* 2014;10(11):4618-4628.
- 139 Del Gaudio C., Ercolani E., Galloni P., Santilli F., Baiguera S., Polizzi L. *et al.* Aspirin-loaded electrospun poly (ϵ -caprolactone) tubular scaffolds: potential small-diameter vascular grafts for thrombosis prevention. *Journal of Materials Science: Materials in Medicine* 2013;24(2):523-532.
- 140 Davoudi P., Assadpour S., Derakhshan M. A., Ai J., Solouk A., and Ghanbari H. Biomimetic modification of polyurethane-based nanofibrous vascular grafts: A promising approach towards stable endothelial lining. *Materials Science and Engineering: C* 2017;80:213-221.
- 141 Ding X., Chin W., Lee C. N., Hedrick J. L., and Yang Y. Y. Peptide-functionalized polyurethane coatings prepared via grafting-to strategy to selectively promote endothelialization. *Advanced healthcare materials*. 2018;7(5). doi: 10.1002/adhm.201700944.

- 142 Engler A. J., Griffin M. A., Sen S., Bönnemann C. G., Sweeney H. L., and Discher D. E. Myotubes differentiate optimally on substrates with tissue-like stiffness: pathological implications for soft or stiff microenvironments. *J Cell Biol* 2004;166(6):877-887.
- 143 Vannozzi L., Ricotti L., Santaniello T., Terencio T., Oropesa-Nunez R., Canale C. *et al.* 3D porous polyurethanes featured by different mechanical properties: Characterization and interaction with skeletal muscle cells. *Journal of the mechanical behavior of biomedical materials* 2017;75:147-159.
- 144 Liao I. C., Liu J. B., Bursac N., and Leong K. W. Effect of electromechanical stimulation on the maturation of myotubes on aligned electrospun fibers. *Cellular and molecular bioengineering* 2008;1(2-3):133-145.
- 145 Andriani Y., Chua J. M. W., Chua B. Y., Phang I. Y., Shyh-Chang N., and Tan W. S. Polyurethane acrylates as effective substrates for sustained in vitro culture of human myotubes. *Acta biomaterialia* 2017;57:115-126.
- 146 Chen J., Dong R., Ge J., Guo B., and Ma P. X. Biocompatible, biodegradable, and electroactive polyurethane-urea elastomers with tunable hydrophilicity for skeletal muscle tissue engineering. *ACS applied materials & interfaces* 2015;7(51):28273-28285.
- 147 Nagamine K., Sato H., Kai H., Kaji H., Kanzaki M., and Nishizawa M. Contractile skeletal muscle cells cultured with a conducting soft wire for effective, selective stimulation. *Scientific reports* 2018;8(1):2253.
- 148 Cha S. H., Lee H. J., and Koh W. G. Study of myoblast differentiation using multi-dimensional scaffolds consisting of nano and micropatterns. *Biomaterials research* 2017;21(1):1.
- 149 Riboldi S. A., Sadr N., Pignini L., Neuenschwander P., Simonet M., Mognol P. *et al.* Skeletal myogenesis on highly orientated microfibrillar polyurethane scaffolds. *Journal of Biomedical Materials Research Part A* 2008;84(4):1094-1101.
- 150 Shen J. Y., Chan-Park M. B. E., Feng Z. Q., Chan V., and Feng Z. W. UV-embossed microchannel in biocompatible polymeric film: Application to control of cell shape and orientation of muscle cells. *Journal of Biomedical Materials Research Part B: Applied Biomaterials* 2006;77(2):423-430.
- 151 Dhollander A., Verdonk P., and Verdonk R. Treatment of painful, irreparable partial meniscal defects with a polyurethane scaffold: midterm clinical

- outcomes and survival analysis. *The American journal of sports medicine* 2016;44(10):2615-2621.
- 152 Schüttler K. F., Haberhauer F., Gesslein M., Heyse T. J., Figiel J., Lorbach O. *et al.* Midterm follow-up after implantation of a polyurethane meniscal scaffold for segmental medial meniscus loss: maintenance of good clinical and MRI outcome. *Knee Surgery Sports Traumatology Arthroscopy* 2016;24(5):1478-1484.
- 153 Monllau J. C., Poggioli F., Erquicia J., Ramírez E., Pelfort X., Gelber P. *et al.* Magnetic resonance imaging and functional outcomes after a polyurethane meniscal scaffold implantation: minimum 5-year follow-up. *Arthroscopy*. 2018;34(5):1621-1627.
- 154 Marzec M., Kucińska-Lipka J., Kalaszczyńska I., and Janik H. Development of polyurethanes for bone repair. *Materials Science and Engineering: C* 2017;80:736-747.
- 155 Thoma R., Hung T., Nyilas E., Haubold A., and Phillips R., "Metal ion complexation of poly (ether) urethanes," *Advances in Biomedical Polymers*, pp. 131-145: Springer, 1987.
- 156 Liu K. L., Choo E. S. G., Wong S. Y., Li X., He C. B., Wang J. *et al.* Designing poly [(R)-3-hydroxybutyrate]-based polyurethane block copolymers for electrospun nanofiber scaffolds with improved mechanical properties and enhanced mineralization capability. *The Journal of Physical Chemistry B* 2010;114(22):7489-7498.
- 157 Gogolewski S., and Gorna K. Biodegradable polyurethane cancellous bone graft substitutes in the treatment of iliac crest defects. *Journal of Biomedical Materials Research Part A* 2007;80(1):94-101.
- 158 Aryal S., Bhattarai S. R., KC R. B., Khil M. S., Lee D. R., and Kim H. Y. Carbon nanotubes assisted biomimetic synthesis of hydroxyapatite from simulated body fluid. *Materials Science and Engineering: A* 2006;426(1-2):202-207.
- 159 Zawadzak E., Bil M., Ryszkowska J., Nazhat S. N., Cho J., Bretcanu O. *et al.* Polyurethane foams electrophoretically coated with carbon nanotubes for tissue engineering scaffolds. *Biomedical Materials* 2008;4(1):015008.
- 160 González-Paz R. J., Lligadas G., Ronda J. C., Galià M., Ferreira A. M., Boccafoschi F. *et al.* Enhancement of fatty acid-based polyurethanes cytocompatibility by non-covalent anchoring of chondroitin sulfate. *Macromolecular bioscience* 2012;12(12):1697-1705.

- 161 Tetteh G., Khan A., Delaine-Smith R., Reilly G., and Rehman I. Electrospun polyurethane/hydroxyapatite bioactive Scaffolds for bone tissue engineering: The role of solvent and hydroxyapatite particles. *Journal of the mechanical behavior of biomedical materials* 2014;39:95-110.
- 162 Yang W., Both S. K., Zuo Y., Birgani Z. T., Habibovic P., Li Y. *et al.* Biological evaluation of porous aliphatic polyurethane/hydroxyapatite composite scaffolds for bone tissue engineering. *Journal of Biomedical Materials Research Part A* 2015;103(7):2251-2259.
- 163 Li B., Yoshii T., Hafeman A. E., Nyman J. S., Wenke J. C., and Guelcher S. A. The effects of rhBMP-2 released from biodegradable polyurethane/microsphere composite scaffolds on new bone formation in rat femora. *Biomaterials* 2009;30(35):6768-6779.
- 164 Balint R., Cassidy N. J., and Cartmell S. H. Conductive polymers: towards a smart biomaterial for tissue engineering. *Acta biomaterialia* 2014;10(6):2341-2353.
- 165 Demir U. S., Shahbazi R., Calamak S., Ozturk S., Gultekinoglu M., and Ulubayram K. Gold nano-decorated aligned polyurethane nanofibers for enhancement of neurite outgrowth and elongation. *Journal of Biomedical Materials Research Part A*. 2018;106(6):1604-1613.
- 166 Javadi M., Gu Q., Naficy S., Farajikhah S., Crook J. M., Wallace G. G. *et al.* Conductive tough hydrogel for bioapplications. *Macromolecular bioscience*; 2018;18(2). doi: 10.1002/mabi.201700270.
- 167 Unnithan A. R., Gnanasekaran G., Sathishkumar Y., Lee Y. S., and Kim C. S. Electrospun antibacterial polyurethane-cellulose acetate-zein composite mats for wound dressing. *Carbohydrate polymers* 2014;102:884-892.
- 168 Li B., Brown K. V., Wenke J. C., and Guelcher S. A. Sustained release of vancomycin from polyurethane scaffolds inhibits infection of bone wounds in a rat femoral segmental defect model. *Journal of Controlled Release* 2010;145(3):221-230.
- 169 Unnithan A. R., Barakat N. A., Pichiah P. T., Gnanasekaran G., Nirmala R., Cha Y. S. *et al.* Wound-dressing materials with antibacterial activity from electrospun polyurethane-dextran nanofiber mats containing ciprofloxacin HCl. *Carbohydrate polymers* 2012;90(4):1786-1793.

- 170 Hensley K., Robinson K. A., Gabbita S. P., Salsman S., and Floyd R. A. Reactive oxygen species, cell signaling, and cell injury. *Free Radical Biology and Medicine* 2000;28(10):1456-1462.
- 171 Cui H., Cui L., Zhang P., Huang Y., Wei Y., and Chen X. In situ electroactive and antioxidant supramolecular hydrogel based on cyclodextrin/copolymer inclusion for tissue engineering repair. *Macromolecular bioscience* 2014;14(3):440-450.
- 172 Shiekh P. A., Singh A., and Kumar A. Engineering bioinspired antioxidant materials promoting cardiomyocyte functionality and maturation for tissue engineering application. *ACS applied materials & interfaces*. 2018;10(4):3260-3273.
- 173 Gizdavic-Nikolaidis M., Travas-Sejdic J., Bowmaker G. A., Cooney R. P., and Kilmartin P. A. Conducting polymers as free radical scavengers. *Synthetic Metals* 2004;140(2-3):225-232.
- 174 Gharibi R., Yeganeh H., Rezapour-Lactoe A., and Hassan Z. M. Stimulation of wound healing by electroactive, antibacterial, and antioxidant polyurethane/siloxane dressing membranes: in vitro and in vivo evaluations. *ACS applied materials & interfaces* 2015;7(43):24296-24311.
- 175 Lomaestro B. M., and Malone M. Glutathione in health and disease: pharmacotherapeutic issues. *Annals of Pharmacotherapy* 1995;29(12):1263-1273.
- 176 Go Y. M., and Jones D. P. Cysteine/cystine redox signaling in cardiovascular disease. *Free Radical Biology and Medicine* 2011;50(4):495-509.
- 177 Hamburg M. A., and Collins F. S. The path to personalized medicine. *New England Journal of Medicine* 2010;363(4):301-304.
- 178 Wu G., Mikhailovsky A., Khant H. A., Fu C., Chiu W., and Zasadzinski J. A. Remotely triggered liposome release by near-infrared light absorption via hollow gold nanoshells. *Journal of the American Chemical Society* 2008;130(26):8175-8177.
- 179 Nazemi A., Schon T. B., and Gillies E. R. Synthesis and degradation of backbone photodegradable polyester dendrimers. *Organic letters* 2013;15(8):1830-1833.

- 180 Epstein-Barash H., Orbey G., Polat B. E., Ewoldt R. H., Feshitan J., Langer R. *et al.* A microcomposite hydrogel for repeated on-demand ultrasound-triggered drug delivery. *Biomaterials* 2010;31(19):5208-5217.
- 181 Kost J., Leong K., and Langer R. Ultrasound-enhanced polymer degradation and release of incorporated substances. *Proceedings of the National Academy of Sciences* 1989;86(20):7663-7666.
- 182 El-Sayed M. E., Hoffman A. S., and Stayton P. S. Rational design of composition and activity correlations for pH-responsive and glutathione-reactive polymer therapeutics. *Journal of Controlled Release* 2005;104(2):417-427.
- 183 Li C., Madsen J., Armes S. P., and Lewis A. L. A new class of biochemically degradable, stimulus-responsive triblock copolymer gelators. *Angewandte Chemie International Edition* 2006;45(21):3510-3513.
- 184 Gunawan S. T., Kempe K., Such G. K., Cui J., Liang K., Richardson J. J. *et al.* Tuning Particle Biodegradation through Polymer-Peptide Blend Composition. *Biomacromolecules* 2014;15(12):4429-4438.
- 185 De La Rica R., Aili D., and Stevens M. M. Enzyme-responsive nanoparticles for drug release and diagnostics. *Advanced drug delivery reviews* 2012;64(11):967-978.
- 186 Kratz K., Habermann R., Becker T., Richau K., and Lendlein A. Shape-memory properties and degradation behavior of multifunctional electro-spun scaffolds. *The International journal of artificial organs* 2011;34(2):225-230.
- 187 Martin R. A., Yue S., Hanna J. V., Lee P., Newport R. J., Smith M. E. *et al.* Characterizing the hierarchical structures of bioactive sol-gel silicate glass and hybrid scaffolds for bone regeneration. *Phil. Trans. R. Soc. A* 2012;370(1963):1422-1443.
- 188 Hakimi O., Mouthuy P. A., and Carr A. Synthetic and degradable patches: an emerging solution for rotator cuff repair. *International journal of experimental pathology* 2013;94(4):287-292.
- 189 Fu H. L., Hong Y., Little S. R., and Wagner W. R. Collagenase-labile polyurethane urea synthesis and processing into hollow fiber membranes. *Biomacromolecules* 2014;15(8):2924-2932.

- 190 Wu G., Fang Y. Z., Yang S., Lupton J. R., and Turner N. D. Glutathione metabolism and its implications for health. *The Journal of nutrition* 2004;134(3):489-492.
- 191 Cai J., Chen Y., Seth S., Furukawa S., Compans R. W., and Jones D. P. Inhibition of influenza infection by glutathione. *Free Radical Biology and Medicine* 2003;34(7):928-936.
- 192 Arjinpathana N., and Asawanonda P. Glutathione as an oral whitening agent: a randomized, double-blind, placebo-controlled study. *Journal of Dermatological Treatment* 2012;23(2):97-102.
- 193 Witschi A., Reddy S., Stofer B., and Lauterburg B. The systemic availability of oral glutathione. *European journal of clinical pharmacology* 1992;43(6):667-669.
- 194 Bardellini E., Bindi P., Borzone S., Cagliaris S., Dagnino F., and Testa R. The effect of high doses of reduced glutathione on hepatic clearances and fibrogenetic activity in patients with chronic alcoholic liver disease. *Advances in Therapy* 1992;9(2):116-122.
- 195 Lenzi A., Culasso F., Gandini L., Lombardo F., and Dondero F. Andrology: Placebo-controlled, double-blind, cross-over trial of glutathione therapy in male infertility. *Human Reproduction* 1993;8(10):1657-1662.
- 196 Borok Z., Buhl R., Hubbard R., Holroyd K., Roum J., Czerski D. *et al.* Effect of glutathione aerosol on oxidant-antioxidant imbalance in idiopathic pulmonary fibrosis. *The Lancet* 1991;338(8761):215-216.
- 197 Guan J., Sacks M. S., Beckman E. J., and Wagner W. R. Synthesis, characterization, and cytocompatibility of elastomeric, biodegradable poly (ester-urethane) ureas based on poly (caprolactone) and putrescine. *Journal of Biomedical Materials Research Part A* 2002;61(3):493-503.
- 198 Chuang T. W., and Masters K. S. Regulation of polyurethane hemocompatibility and endothelialization by tethered hyaluronic acid oligosaccharides. *Biomaterials* 2009;30(29):5341-5351.
- 199 Asplund J. B., Bowden T., Mathisen T. r., and Hilborn J. n. Synthesis of highly elastic biodegradable poly (urethane urea). *Biomacromolecules* 2007;8(3):905-911.

- 200 Twentyman P. R., and Luscombe M. A study of some variables in a tetrazolium dye (MTT) based assay for cell growth and chemosensitivity. *British journal of cancer* 1987;56(3):279.
- 201 Saito G., Swanson J. A., and Lee K. D. Drug delivery strategy utilizing conjugation via reversible disulfide linkages: role and site of cellular reducing activities. *Advanced drug delivery reviews* 2003;55(2):199-215.
- 202 Choh S. Y., Cross D., and Wang C. Facile synthesis and characterization of disulfide-cross-linked hyaluronic acid hydrogels for protein delivery and cell encapsulation. *Biomacromolecules* 2011;12(4):1126-1136.
- 203 Blacklock J., Handa H., Manickam D. S., Mao G., Mukhopadhyay A., and Oupický D. Disassembly of layer-by-layer films of plasmid DNA and reducible TAT polypeptide. *Biomaterials* 2007;28(1):117-124.
- 204 Blacklock J., You Y. Z., Zhou Q. H., Mao G., and Oupický D. Gene delivery in vitro and in vivo from bioreducible multilayered polyelectrolyte films of plasmid DNA. *Biomaterials* 2009;30(5):939-950.
- 205 Song N., Ding M., Pan Z., Li J., Zhou L., Tan H. *et al.* Construction of targeting-clickable and tumor-cleavable polyurethane nanomicelles for multifunctional intracellular drug delivery. *Biomacromolecules* 2013;14(12):4407-4419.
- 206 Ding M., Zeng X., He X., Li J., Tan H., and Fu Q. Cell internalizable and intracellularly degradable cationic polyurethane micelles as a potential platform for efficient imaging and drug delivery. *Biomacromolecules* 2014;15(8):2896-2906.
- 207 Yu S., Ding J., He C., Cao Y., Xu W., and Chen X. Disulfide cross-linked polyurethane micelles as a reduction-triggered drug delivery system for cancer therapy. *Advanced healthcare materials* 2014;3(5):752-760.
- 208 Lu H., Sun P., Zheng Z., Yao X., Wang X., and Chang F. C. Reduction-sensitive rapid degradable poly (urethane-urea)s based on cystine. *Polymer degradation and stability* 2012;97(4):661-669.
- 209 Wang J., Zheng Z., Chen L., Tu X., and Wang X. Glutathione-responsive biodegradable poly (urea-urethane)s containing L-cystine-based chain extender. *Journal of Biomaterials Science, Polymer Edition* 2013;24(7):831-848.

- 210 Charriere E., Lemaitre J., and Zysset P. Hydroxyapatite cement scaffolds with controlled macroporosity: fabrication protocol and mechanical properties. *Biomaterials* 2003;24(5):809-817.
- 211 Vert M. Degradable and bioresorbable polymers in surgery and in pharmacology: beliefs and facts. *Journal of Materials Science: Materials in Medicine* 2009;20(2):437-446.
- 212 Kim T., Lee M., and Kim S. W. A guanidinylated bioreducible polymer with high nuclear localization ability for gene delivery systems. *Biomaterials* 2010;31(7):1798-1804.
- 213 Li C. Y., Wang H. J., Cao J. M., Zhang J., and Yu X. Q. Bioreducible cross-linked polymers based on G1 peptide dendrimer as potential gene delivery vectors. *European journal of medicinal chemistry* 2014;87:413-420.
- 214 Matsusaki M., Yoshida H., and Akashi M. The construction of 3D-engineered tissues composed of cells and extracellular matrices by hydrogel template approach. *Biomaterials* 2007;28(17):2729-2737.
- 215 Yoshida H., Klinkhammer K., Matsusaki M., Möller M., Klee D., and Akashi M. Disulfide-crosslinked electrospun poly (gamma-glutamic acid) nonwovens as reduction-responsive scaffolds. *Macromolecular bioscience* 2009;9(6):568-574.
- 216 Hong Y., Takanari K., Amoroso N. J., Hashizume R., Brennan-Pierce E. P., Freund J. M. *et al.* An elastomeric patch electrospun from a blended solution of dermal extracellular matrix and biodegradable polyurethane for rat abdominal wall repair. *Tissue Engineering Part C: Methods* 2012;18(2):122-132.
- 217 Stankus J. J., Freytes D. O., Badylak S. F., and Wagner W. R. Hybrid nanofibrous scaffolds from electrospinning of a synthetic biodegradable elastomer and urinary bladder matrix. *Journal of Biomaterials Science, Polymer Edition* 2008;19(5):635-652.
- 218 Jones D. P., "[11] Redox potential of GSH/GSSG couple: Assay and biological significance," *Methods in enzymology*, pp. 93-112: Elsevier, 2002.
- 219 Griffith O. W. Biologic and pharmacologic regulation of mammalian glutathione synthesis. *Free Radical Biology and Medicine* 1999;27(9-10):922-935.
- 220 Wan H. L., Tsai P. J., Chiang M. J., Wu J. P., Liu L., Tsai W. J. *et al.* Effect of acute skin thermal injury on subcutaneous glutathione, ascorbic acid and

- hydroxyl radical concentrations in anesthetized rats. *Redox Report* 1996;2(4):267-272.
- 221 Liu S. Q., and Kodama M. Porous polyurethane vascular prostheses with variable compliances. *Journal of Biomedical Materials Research Part A* 1992;26(11):1489-1502.
- 222 Fromstein J., and Woodhouse K. Elastomeric biodegradable polyurethane blends for soft tissue applications. *Journal of Biomaterials Science, Polymer Edition* 2002;13(4):391-406.
- 223 Siepe M., Giraud M. N., Liljensten E., Nydegger U., Menasche P., Carrel T. *et al.* Construction of skeletal myoblast-based polyurethane scaffolds for myocardial repair. *Artificial organs* 2007;31(6):425-433.
- 224 Fromstein J. D., Zandstra P. W., Alperin C., Rockwood D., Rabolt J. F., and Woodhouse K. A. Seeding bioreactor-produced embryonic stem cell-derived cardiomyocytes on different porous, degradable, polyurethane scaffolds reveals the effect of scaffold architecture on cell morphology. *Tissue Engineering Part A* 2008;14(3):369-378.
- 225 Fujimoto K., Minato M., Miyamoto S., Kaneko T., Kikuchi H., Sakai K. *et al.* Porous polyurethane tubes as vascular graft. *Journal of Applied Biomaterials* 1993;4(4):347-354.
- 226 Kowligi R., Von Maltzahn W., and Eberhart R. Fabrication and characterization of small-diameter vascular prostheses. *Journal of Biomedical Materials Research Part A* 1988;22(S14):245-256.
- 227 Ruzzini L., Longo U. G., Campi S., Maffulli N., Muda A. O., and Denaro V. Adhesion and collagen production of human tenocytes seeded on degradable poly (urethane urea). *Knee Surgery, Sports Traumatology, Arthroscopy* 2013;21(8):1834-1840.
- 228 Adolph E. J., Pollins A. C., Cardwell N. L., Davidson J. M., Guelcher S. A., and Nanney L. B. Biodegradable lysine-derived polyurethane scaffolds promote healing in a porcine full-thickness excisional wound model. *Journal of Biomaterials Science, Polymer Edition* 2014;25(17):1973-1985.
- 229 Heo D. N., Yang D. H., Lee J. B., Bae M. S., Kim J. H., Moon S. H. *et al.* Burn-wound healing effect of gelatin/polyurethane nanofiber scaffold containing silver-sulfadiazine. *Journal of biomedical nanotechnology* 2013;9(3):511-515.

- 230 Chirila T. V. First development of a polyurethane keratoprosthesis and its Australian connection: an unbeknown episode in the history of artificial cornea. *Clinical & experimental ophthalmology* 2006;34(5):485-488.
- 231 Reyes R., Delgado A., Solis R., Sanchez E., Hernandez A., Roman J. S. *et al.* Cartilage repair by local delivery of transforming growth factor-1 or bone morphogenetic protein-2 from a novel, segmented polyurethane/polylactic-co-glycolic bilayered scaffold. *Journal of Biomedical Materials Research Part A* 2014;102(4):1110-1120.
- 232 Mi H. Y., Palumbo S., Jing X., Turng L. S., Li W. J., and Peng X. F. Thermoplastic polyurethane/hydroxyapatite electrospun scaffolds for bone tissue engineering: effects of polymer properties and particle size. *Journal of Biomedical Materials Research Part B: Applied Biomaterials* 2014;102(7):1434-1444.
- 233 Wang L., Li C., Ryan A. J., and Armes S. P. Synthesis and peptide-induced degradation of biocompatible fibers based on highly branched poly (2-hydroxyethyl methacrylate). *Advanced Materials* 2006;18(12):1566-1570.
- 234 Dispinar T., Van Camp W., De Cock L. J., De Geest B. G., and Du Prez F. E. Redox-responsive degradable PEG cryogels as potential cell scaffolds in Tissue Engineering. *Macromolecular bioscience* 2012;12(3):383-394.
- 235 Xie M., Wang L., Guo B., Wang Z., Chen Y. E., and Ma P. X. Ductile electroactive biodegradable hyperbranched polylactide copolymers enhancing myoblast differentiation. *Biomaterials* 2015;71:158-167.
- 236 Kotwal A., and Schmidt C. E. Electrical stimulation alters protein adsorption and nerve cell interactions with electrically conducting biomaterials. *Biomaterials* 2001;22(10):1055-1064.
- 237 Meng S., Rouabhia M., and Zhang Z. Electrical stimulation modulates osteoblast proliferation and bone protein production through heparin-bioactivated conductive scaffolds. *Bioelectromagnetics* 2013;34(3):189-199.
- 238 Hardy J. G., Mouser D. J., Arroyo-Currás N., Geissler S., Chow J. K., Nguy L. *et al.* Biodegradable electroactive polymers for electrochemically-triggered drug delivery. *Journal of Materials Chemistry B* 2014;2(39):6809-6822.
- 239 Svirskis D., Travas-Sejdic J., Rodgers A., and Garg S. Electrochemically controlled drug delivery based on intrinsically conducting polymers. *Journal of Controlled Release* 2010;146(1):6-15.

- 240 Hardy J. G., Amend M. N., Geissler S., Lynch V. M., and Schmidt C. E. Peptide-directed assembly of functional supramolecular polymers for biomedical applications: electroactive molecular tongue-twisters (oligoalanine-oligoaniline-oligoalanine) for electrochemically enhanced drug delivery. *Journal of Materials Chemistry B* 2015;3(25):5005-5009.
- 241 Kaneto K., Kaneko M., Min Y., and MacDiarmid A. G. "Artificial muscle": Electromechanical actuators using polyaniline films. *Synthetic Metals* 1995;71(1-3):2211-2212.
- 242 Madden J. D., Cush R. A., Kanigan T. S., and Hunter I. W. Fast contracting polypyrrole actuators. *Synthetic Metals* 2000;113(1-2):185-192.
- 243 Li L., Wang Y., Pan L., Shi Y., Cheng W., Shi Y. *et al.* A nanostructured conductive hydrogels-based biosensor platform for human metabolite detection. *Nano letters* 2015;15(2):1146-1151.
- 244 Hong W. Y., Jeon S. H., Lee E. S., and Cho Y. An integrated multifunctional platform based on biotin-doped conducting polymer nanowires for cell capture, release, and electrochemical sensing. *Biomaterials* 2014;35(36):9573-9580.
- 245 Brahim S., and Guiseppi-Elie A. Electroconductive hydrogels: Electrical and electrochemical properties of polypyrrole-poly (HEMA) composites. *Electroanalysis* 2005;17(7):556-570.
- 246 Shi G., Rouabhia M., Wang Z., Dao L. H., and Zhang Z. A novel electrically conductive and biodegradable composite made of polypyrrole nanoparticles and polylactide. *Biomaterials* 2004;25(13):2477-2488.
- 247 Ghasemi-Mobarakeh L., Prabhakaran M. P., Morshed M., Nasr-Esfahani M. H., Baharvand H., Kiani S. *et al.* Application of conductive polymers, scaffolds and electrical stimulation for nerve tissue engineering. *Journal of tissue engineering and regenerative medicine* 2011;5(4):e17-e35.
- 248 Jiang X., Marois Y., Traoré A., Tessier D., Dao L. H., Guidoin R. *et al.* Tissue reaction to polypyrrole-coated polyester fabrics: an in vivo study in rats. *Tissue engineering* 2002;8(4):635-647.
- 249 Butler D. L., Goldstein S. A., Guldberg R. E., Guo X. E., Kamm R., Laurencin C. T. *et al.* The impact of biomechanics in tissue engineering and regenerative medicine. *Tissue Engineering Part B: Reviews* 2009;15(4):477-484.

- 250 Kolarcik C. L., Luebben S. D., Sapp S. A., Hanner J., Snyder N., Kozai T. D. *et al.* Elastomeric and soft conducting microwires for implantable neural interfaces. *Soft Matter* 2015;11(24):4847-4861.
- 251 Seyedin S., Razal J. M., Innis P. C., Jeiranikhameneh A., Beirne S., and Wallace G. G. Knitted strain sensor textiles of highly conductive all-polymeric fibers. *ACS applied materials & interfaces* 2015;7(38):21150-21158.
- 252 Hwang B. U., Lee J. H., Trung T. Q., Roh E., Kim D. I., Kim S. W. *et al.* Transparent stretchable self-powered patchable sensor platform with ultrasensitive recognition of human activities. *ACS nano* 2015;9(9):8801-8810.
- 253 Li M., Li H., Zhong W., Zhao Q., and Wang D. Stretchable conductive polypyrrole/polyurethane (PPy/PU) strain sensor with netlike microcracks for human breath detection. *ACS applied materials & interfaces* 2014;6(2):1313-1319.
- 254 Qazi T. H., Rai R., Dippold D., Roether J. E., Schubert D. W., Rosellini E. *et al.* Development and characterization of novel electrically conductive PANI-PGS composites for cardiac tissue engineering applications. *Acta biomaterialia* 2014;10(6):2434-2445.
- 255 Jun I., Jeong S., and Shin H. The stimulation of myoblast differentiation by electrically conductive sub-micron fibers. *Biomaterials* 2009;30(11):2038-2047.
- 256 Broda C. R., Lee J. Y., Sirivisoot S., Schmidt C. E., and Harrison B. S. A chemically polymerized electrically conducting composite of polypyrrole nanoparticles and polyurethane for tissue engineering. *Journal of Biomedical Materials Research Part A* 2011;98(4):509-516.
- 257 Madrigal M. M. P. r., Giannotti M. I., Oncins G., Franco L., Armelin E., Puiggali J. *et al.* Bioactive nanomembranes of semiconductor polythiophene and thermoplastic polyurethane: thermal, nanostructural and nanomechanical properties. *Polymer Chemistry* 2013;4(3):568-583.
- 258 Pérez-Madrigal M. M., Giannotti M. I., del Valle L. J., Franco L., Armelin E., Puiggali J. *et al.* Thermoplastic polyurethane: polythiophene nanomembranes for biomedical and biotechnological applications. *ACS applied materials & interfaces* 2014;6(12):9719-9732.
- 259 Huang L., Hu J., Lang L., Wang X., Zhang P., Jing X. *et al.* Synthesis and characterization of electroactive and biodegradable ABA block copolymer of polylactide and aniline pentamer. *Biomaterials* 2007;28(10):1741-1751.

- 260 Green T. R., Fisher J., Matthews J. B., Stone M. H., and Ingham E. Effect of size and dose on bone resorption activity of macrophages by in vitro clinically relevant ultra high molecular weight polyethylene particles. *Journal of Biomedical Materials Research Part A* 2000;53(5):490-497.
- 261 Guo Y., Li M., Mylonakis A., Han J., MacDiarmid A. G., Chen X. *et al.* Electroactive oligoaniline-containing self-assembled monolayers for tissue engineering applications. *Biomacromolecules* 2007;8(10):3025-3034.
- 262 Smits F. Measurement of sheet resistivities with the four-point probe. *Bell Labs Technical Journal* 1958;37(3):711-718.
- 263 Gharibi R., Yeganeh H., Gholami H., and Hassan Z. M. Aniline tetramer embedded polyurethane/siloxane membranes and their corresponding nanosilver composites as intelligent wound dressing materials. *RSC Advances* 2014;4(107):62046-62060.
- 264 Wang X., Kluge J. A., Leisk G. G., and Kaplan D. L. Sonication-induced gelation of silk fibroin for cell encapsulation. *Biomaterials* 2008;29(8):1054-1064.
- 265 Hunter P., McCulloch A., and Ter Keurs H. Modelling the mechanical properties of cardiac muscle. *Progress in biophysics and molecular biology* 1998;69(2-3):289-331.
- 266 Gloeckner D. C., Sacks M. S., Fraser M. O., Somogyi G. T., de GROAT W. C., and Chancellor M. B. Passive biaxial mechanical properties of the rat bladder wall after spinal cord injury. *The Journal of urology* 2002;167(5):2247-2252.
- 267 Raghavan M. L., Webster M. W., and Vorp D. A. Ex vivo biomechanical behavior of abdominal aortic aneurysm: assessment using a new mathematical model. *Annals of biomedical engineering* 1996;24(5):573-582.
- 268 Delpech M. C., and Miranda G. S. Waterborne polyurethanes: influence of chain extender in ftir spectra profiles. *Central European Journal of Engineering* 2012;2(2):231-238.
- 269 Tang J., Jing X., Wang B., and Wang F. Infrared spectra of soluble polyaniline. *Synthetic Metals* 1988;24(3):231-238.
- 270 Mendes L. C., Falco A. P. S., Pinho M. S., and Marques P. O. Sulfonated polyaniline: influence of sulfonation routes on its thermal and structural characteristics. *Materials Research* 2011;14(4):466-471.

- 271 Chiolerio A., Bocchini S., and Porro S. Inkjet Printed Negative Supercapacitors: Synthesis of polyaniline-based inks, doping agent effect, and advanced electronic devices applications. *Advanced Functional Materials* 2014;24(22):3375-3383.
- 272 Dutra R., Salomão G., Alves J., Pereira V., Miranda F., Vallim V. *et al.* Using transparent polyurethane film and hydrocolloid dressings to prevent pressure ulcers. *Journal of wound care* 2015;24(6):268-275.
- 273 Xu C., Huang Y., Wu J., Tang L., and Hong Y. Triggerable Degradation of Polyurethanes for Tissue Engineering Applications. *ACS applied materials & interfaces* 2015;7(36):20377-20388.
- 274 Yu L., Zhou L., Ding M., Li J., Tan H., Fu Q. *et al.* Synthesis and characterization of novel biodegradable folate conjugated polyurethanes. *Journal of colloid and interface science* 2011;358(2):376-383.
- 275 Chen Y., Wang R., Zhou J., Fan H., and Shi B. On-demand drug delivery from temperature-responsive polyurethane membrane. *Reactive and Functional Polymers* 2011;71(4):525-535.
- 276 Sivak W. N., Zhang J., Petoud S., and Beckman E. J. Incorporation of ionic ligands accelerates drug release from LDI-glycerol polyurethanes. *Acta biomaterialia* 2010;6(1):144-153.
- 277 Blinova N. V., Stejskal J., Trchová M., and Prokeš J. Control of polyaniline conductivity and contact angles by partial protonation. *Polymer International* 2008;57(1):66-69.
- 278 Kaynak A., Rintoul L., and George G. A. Change of mechanical and electrical properties of polypyrrole films with dopant concentration and oxidative aging. *Materials Research Bulletin* 2000;35(6):813-824.
- 279 Jiang X., Harima Y., Zhu L., Kunugi Y., Yamashita K., Sakamoto M.-a. *et al.* Mobilities of charge carriers hopping between π -conjugated polymer chains. *Journal of Materials Chemistry* 2001;11(12):3043-3048.
- 280 Sapurina I. Y., and Shishov M. Oxidative polymerization of aniline: molecular synthesis of polyaniline and the formation of supramolecular structures. *New Polymers for Special Applications*. InTech, 2012
- 281 Weia Y., Yub Y., Zhangb W., Wangb C., Jiacc X., and Jansend S. A. A new approach to electroactive polymers via well-defined oligomerrrs with futher

- polymerizable end-groups. Chinese Journal of Polymer Science 2002;20(2):105-118.
- 282 Guo B., Finne-Wistrand A., and Albertsson A. C. Degradable and electroactive hydrogels with tunable electrical conductivity and swelling behavior. Chemistry of Materials 2011;23(5):1254-1262.
- 283 Lee J. W., Serna F., Nickels J., and Schmidt C. E. Carboxylic acid-functionalized conductive polypyrrole as a bioactive platform for cell adhesion. Biomacromolecules 2006;7(6):1692-1695.
- 284 Rivers T. J., Hudson T. W., and Schmidt C. E. Synthesis of a novel, biodegradable electrically conducting polymer for biomedical applications. Advanced Functional Materials 2002;12(1):33-37.
- 285 Wingborg N. Increasing the tensile strength of HTPB with different isocyanates and chain extenders. Polymer testing 2002;21(3):283-287.
- 286 De Groot J., De Vrijer R., Pennings A., Klomp maker J., Veth R., and Jansen H. Use of porous polyurethanes for meniscal reconstruction and meniscal prostheses. Biomaterials 1996;17(2):163-173.
- 287 Chen Q. Z., Bismarck A., Hansen U., Junaid S., Tran M. Q., Harding S. n. E. *et al.* Characterisation of a soft elastomer poly (glycerol sebacate) designed to match the mechanical properties of myocardial tissue. Biomaterials 2008;29(1):47-57.
- 288 Prigodin V., Hsu F., Park J., Waldmann O., and Epstein A. Electron-ion interaction in doped conducting polymers. Physical Review B 2008;78(3):035203.
- 289 Malmonge L. F., Langiano S. d. C., Cordeiro J. o. M. M., Mattoso L. H. C., and Malmonge J. A. Thermal and mechanical properties of PVDF/PANI blends. Materials Research 2010;13(4):465-470.
- 290 Li W., and Wan M. Porous polyaniline films with high conductivity. Synthetic Metals 1998;92(2):121-126.
- 291 Baek S., Green R. A., and Poole-Warren L. A. Effects of dopants on the biomechanical properties of conducting polymer films on platinum electrodes. Journal of Biomedical Materials Research Part A 2014;102(8):2743-2754.

- 292 Wang Z., Roberge C., Wan Y., Dao L. H., Guidoin R., and Zhang Z. A biodegradable electrical bioconductor made of polypyrrole nanoparticle/poly (D, L-lactide) composite: A preliminary in vitro biostability study. *Journal of Biomedical Materials Research Part A* 2003;66(4):738-746.
- 293 Ravichandran R., Sundarrajan S., Venugopal J. R., Mukherjee S., and Ramakrishna S. Applications of conducting polymers and their issues in biomedical engineering. *Journal of The Royal Society Interface* 2010;7 Suppl 5:S559-S579.
- 294 Cherneva E., Pavlovic V., Smelcerovic A., and Yancheva D. The effect of camphor and borneol on rat thymocyte viability and oxidative stress. *Molecules* 2012;17(9):10258-10266.
- 295 Ge J., Neofytou E., Cahill III T. J., Beygui R. E., and Zare R. N. Drug release from electric-field-responsive nanoparticles. *ACS nano* 2012;6(1):227-233.
- 296 Cheong G. M., Lim K. S., Jakubowicz A., Martens P. J., Poole-Warren L. A., and Green R. A. Conductive hydrogels with tailored bioactivity for implantable electrode coatings. *Acta biomaterialia* 2014;10(3):1216-1226.
- 297 Tsai T. S., Pillay V., Choonara Y. E., Du Toit L. C., Modi G., Naidoo D. *et al.* A polyvinyl alcohol-polyaniline based electro-conductive hydrogel for controlled stimuli-actuable release of indomethacin. *Polymers* 2011;3(1):150-172.
- 298 Nguyen H. T., Sapp S., Wei C., Chow J. K., Nguyen A., Coursen J. *et al.* Electric field stimulation through a biodegradable polypyrrole-co-polycaprolactone substrate enhances neural cell growth. *Journal of Biomedical Materials Research Part A* 2014;102(8):2554-2564.
- 299 Guimard N. K., Gomez N., and Schmidt C. E. Conducting polymers in biomedical engineering. *Progress in Polymer Science* 2007;32(8):876-921.
- 300 Xu C., Yepez G., Wei Z., Liu F., Bugarin A., and Hong Y. Synthesis and characterization of conductive, biodegradable, elastomeric polyurethanes for biomedical applications. *Journal of Biomedical Materials Research Part A* 2016;104(9):2305-2314.
- 301 Green R. A., Hassarati R. T., Goding J. A., Baek S., Lovell N. H., Martens P. J. *et al.* Conductive hydrogels: mechanically robust hybrids for use as biomaterials. *Macromolecular bioscience* 2012;12(4):494-501.

- 302 Green R. A., Poole-warren L. A., Baek S., and Martens P. J., "Polymeric material," Google Patents.
- 303 Smits F. Measurement of sheet resistivities with the four-point probe. *Bell System Technical Journal* 1958;37(3):711-718.
- 304 Hsu Y. Y., Gresser J. D., Trantolo D. J., Lyons C. M., Gangadharam P. R., and Wise D. L. Effect of polymer foam morphology and density on kinetics of in vitro controlled release of isoniazid from compressed foam matrices. *Journal of biomedical materials research* 1997;35(1):107-116.
- 305 Wan M. Absorption spectra of thin film of polyaniline. *Journal of Polymer Science Part A: Polymer Chemistry* 1992;30(4):543-549.
- 306 Mawad D., Gilmore K., Molino P., Wagner K., Wagner P., Officer D. L. *et al.* An erodible polythiophene-based composite for biomedical applications. *Journal of Materials Chemistry*;21(15):5555-5560.
- 307 Kai D., Prabhakaran M. P., Jin G., and Ramakrishna S. Polypyrrole-contained electrospun conductive nanofibrous membranes for cardiac tissue engineering. *Journal of Biomedical Materials Research Part A*;99(3):376-385.
- 308 Zhou J., Chen J., Sun H., Qiu X., Mou Y., Liu Z. *et al.* Engineering the heart: evaluation of conductive nanomaterials for improving implant integration and cardiac function. *Scientific reports*;4:3733.
- 309 Qi F., Wang Y., Ma T., Zhu S., Zeng W., Hu X. *et al.* Electrical regulation of olfactory ensheathing cells using conductive polypyrrole/chitosan polymers. *Biomaterials*;34(7):1799-1809.
- 310 Xiao H. M., Zhang W. D., Lv C., Fu S. Y., Wan M. X., and Mai Y. W. Large enhancement in conductivity of polyaniline films by cold stretching. *Macromolecular Chemistry and Physics*;211(10):1109-1116.
- 311 Loh X. J., Tan K. K., Li X., and Li J. The in vitro hydrolysis of poly (ester urethane) s consisting of poly [(R)-3-hydroxybutyrate] and poly (ethylene glycol). *Biomaterials* 2006;27(9):1841-1850.
- 312 Lyu S., and Untereker D. Degradability of polymers for implantable biomedical devices. *International journal of molecular sciences* 2009;10(9):4033-4065.
- 313 Heijkants R. G. J. C., Polyurethane scaffolds as meniscus reconstruction materials. Dissertation. Groningen: University Library Groningen; 2004.

- 314 Kagawa Y., Takaoka T., Hamamoto T., and Ohta T. Cytosol type electrolyte medium suitable for long term growth of human cells with very low membrane potential. *Biochemical and biophysical research communications* 1990;169(3):1217-1221.
- 315 Byers B. A., Guldborg R. E., Hutmacher D. W., and García A. J. Effects of Runx2 genetic engineering and in vitro maturation of tissue-engineered constructs on the repair of critical size bone defects. *Journal of Biomedical Materials Research Part A* 2006;76(3):646-655.
- 316 Lam C. X., Hutmacher D. W., Schantz J. T., Woodruff M. A., and Teoh S. H. Evaluation of polycaprolactone scaffold degradation for 6 months in vitro and in vivo. *Journal of Biomedical Materials Research Part A* 2009;90(3):906-919.
- 317 Schantz J. T., Ng M. M. L., Netto P., Ming J. C. L., Wong K. M., Hutmacher D. W. *et al.* Application of an X-ray microscopy technique to evaluate tissue-engineered bone-scaffold constructs. *Materials Science and Engineering: C* 2002;20(1):9-17.
- 318 Seyednejad H., Gawlitta D., Kuiper R. V., de Bruin A., van Nostrum C. F., Vermonden T. *et al.* In vivo biocompatibility and biodegradation of 3D-printed porous scaffolds based on a hydroxyl-functionalized poly (ϵ -caprolactone). *Biomaterials*;33(17):4309-4318.
- 319 Butler D. L., Goldstein S. A., and Guilak F. Functional tissue engineering: the role of biomechanics. *Journal of biomechanical engineering* 2000;122(6):570-575.
- 320 Nguyen J. K., Park D. J., Skousen J. L., Hess-Dunning A. E., Tyler D. J., Rowan S. J. *et al.* Mechanically-compliant intracortical implants reduce the neuroinflammatory response. *Journal of neural engineering*;11(5):056014.
- 321 Stewart S. F., and Lyman D. J. Effects of a vascular graft/natural artery compliance mismatch on pulsatile flow. *Journal of biomechanics* 1992;25(3):297-310.
- 322 Holzapfel G. A. Biomechanics of soft tissue. *The handbook of materials behavior models* 2001;3:1049-1063.
- 323 Hasan A., Ragaert K., Swieszkowski W., Selimović A. e., Paul A., Camci-Unal G. *et al.* Biomechanical properties of native and tissue engineered heart valve constructs. *Journal of biomechanics* 2014;47(9):1949-1963.

- 324 Christie G. Anatomy of aortic heart valve leaflets: the influence of glutaraldehyde fixation on function. *European journal of cardio-thoracic surgery* 1992;6(Supplement 1):S25-S33.
- 325 Weis S. M., Emery J. L., Becker K. D., McBride D. J., Omens J. H., and McCulloch A. D. Myocardial mechanics and collagen structure in the osteogenesis imperfecta murine (oim). *Circulation Research* 2000;87(8):663-669.
- 326 Xu Y., Patnaik S., Guo X., Li Z., Lo W., Butler R. *et al.* Cardiac differentiation of cardiosphere-derived cells in scaffolds mimicking morphology of the cardiac extracellular matrix. *Acta biomaterialia* 2014;10(8):3449-3462.
- 327 Fang J., Ye S. H., Wang J., Zhao T., Mo X., and Wagner W. R. Thiol Click Modification of Cyclic Disulfide Containing Biodegradable Polyurethane Urea Elastomers. *Biomacromolecules* 2015;16(5):1622-1633.
- 328 Silvestri A., Sartori S., Boffito M., Mattu C., Rienzo A. M., Boccafoschi F. *et al.* Biomimetic myocardial patches fabricated with poly (ϵ -caprolactone) and polyethylene glycol-based polyurethanes. *Journal of Biomedical Materials Research Part B: Applied Biomaterials* 2018;102(5):1002-1013.
- 329 Wittmann K., Storck K., Muhr C., Mayer H., Regn S., Staudenmaier R. *et al.* Development of volume-stable adipose tissue constructs using polycaprolactone-based polyurethane scaffolds and fibrin hydrogels. *Journal of tissue engineering and regenerative medicine*. 2016;10(10):E409-E418.
- 330 Li B., Davidson J. M., and Guelcher S. A. The effect of the local delivery of platelet-derived growth factor from reactive two-component polyurethane scaffolds on the healing in rat skin excisional wounds. *Biomaterials* 2009;30(20):3486-3494.
- 331 Caracciolo P., Buffa F., and Abraham G. Effect of the hard segment chemistry and structure on the thermal and mechanical properties of novel biomedical segmented poly (esterurethanes). *Journal of Materials Science: Materials in Medicine* 2009;20(1):145-155.
- 332 Thijs H. M., Becer C. R., Guerrero-Sanchez C., Fournier D., Hoogenboom R., and Schubert U. S. Water uptake of hydrophilic polymers determined by a thermal gravimetric analyzer with a controlled humidity chamber. *Journal of Materials Chemistry* 2007;17(46):4864-4871.

- 333 Alomayri T., Assaedi H., Shaikh F., and Low I. M. Effect of water absorption on the mechanical properties of cotton fabric-reinforced geopolymer composites. *Journal of Asian Ceramic Societies*;2(3):223-230.
- 334 Musto P., Ragosta G., Scarinzi G., and Mascia L. Probing the molecular interactions in the diffusion of water through epoxy and epoxy-bismaleimide networks. *Journal of Polymer Science Part B: Polymer Physics* 2002;40(10):922-938.
- 335 Bogdanov B., Vidts A., Van Den Buicke A., Verbeeck R., and Schacht E. Synthesis and thermal properties of poly (ethylene glycol)-poly (μ -caprolactone) copolymers. *Polymer* 1998;39(8):1631-1636.
- 336 Xu C., Yopez G., Wei Z., Liu F., Bugarin A., and Hong Y. Synthesis and characterization of conductive, biodegradable, elastomeric polyurethanes for biomedical applications. *Journal of Biomedical Materials Research Part A*. 2016;104(9):2305-2314.
- 337 Zhang R., and Ma P. X. Poly (α -hydroxyl acids)/hydroxyapatite porous composites for bone-tissue engineering. I. Preparation and morphology. *J Biomed Mater Res*. 1999;44(4):446-455.
- 338 Spaans C., De Groot J., Dekens F., and Pennings A. High molecular weight polyurethanes and a polyurethane urea based on 1, 4-butanediisocyanate. *Polymer Bulletin* 1998;41(2):131-138.
- 339 Storey R. F., and Hickey T. P. Degradable polyurethane networks based on D, L-lactide, glycolide, μ -caprolactone, and trimethylene carbonate homopolyester and copolyester triols. *Polymer* 1994;35(4):830-838.
- 340 Saad B., Matter S., Ciardelli G., Neuenschwander P., Suter U., Uhlschmid G. *et al.* Interactions of osteoblasts and macrophages with biodegradable and highly porous polyesterurethane foam and its degradation products. *Journal of biomedical materials research* 1996;32(3):355-366.
- 341 Cohn D., Stern T., González M. F., and Epstein J. Biodegradable poly (ethylene oxide)/poly (ϵ -caprolactone) multiblock copolymers. *Journal of biomedical materials research* 2002;59(2):273-281.
- 342 Yang C., Lin W., and Liu F. Waterborne polyurethane single-ion electrolyte from aliphatic diisocyanate and various molecular length of polyethylene glycol. *Express Polym. Lett* 2007;1:142-149.

- 343 Yiu C., King N., Pashley D. H., Suh B., Carvalho R., Carrilho M. *et al.* Effect of resin hydrophilicity and water storage on resin strength. *Biomaterials* 2004;25(26):5789-5796.
- 344 Tokiwa Y., and Suzuki T. Hydrolysis of polyesters by lipases. *Nature* 1977;270(5632):76-78.
- 345 Gu J. D., Yang S., Welton R., Eberiel D., McCarthy S. P., and Gross R. A. Effect of environmental parameters on the degradability of polymer films in laboratory-scale composting reactors. *Journal of environmental polymer degradation* 1994;2(2):129-135.
- 346 Van Minnen B., Van Leeuwen M., Kors G., Zuidema J., Van Kooten T., and Bos R. In vivo resorption of a biodegradable polyurethane foam, based on 1, 4-butanediisocyanate: A three-year subcutaneous implantation study. *Journal of Biomedical Materials Research Part A* 2008;85(4):972-982.
- 347 Liao J., Yang L., Grashow J., and Sacks M. S. Molecular orientation of collagen in intact planar connective tissues under biaxial stretch. *Acta biomaterialia* 2005;1(1):45-54.
- 348 Freytes D. O., Badylak S. F., Webster T. J., Geddes L. A., and Rundell A. E. Biaxial strength of multilaminated extracellular matrix scaffolds. *Biomaterials* 2004;25(12):2353-2361.
- 349 Huang Y., Ren J., Chen C., Ren T., and Zhou X. Preparation and properties of poly (lactide-co-glycolide)(PLGA)/nano-hydroxyapatite (NHA) scaffolds by thermally induced phase separation and rabbit MSCs culture on scaffolds. *Journal of biomaterials applications* 2008;22(5):409-432.
- 350 Wei G., and Ma P. X. Structure and properties of nano-hydroxyapatite/polymer composite scaffolds for bone tissue engineering. *Biomaterials* 2004;25(19):4749-4757.
- 351 Mozaffarian D., Benjamin E. J., Go A. S., Arnett D. K., Blaha M. J., Cushman M. *et al.* Heart disease and stroke statistics-2015 update: a report from the American Heart Association. *Circulation* 2015;131(4):e29-322.
- 352 Bolooki H. M., and Askari A. Acute myocardial infarction. *Disease Manag Proj.*
- 353 Isomura T., Fukada Y., Miyazaki T., Yoshida M., Morisaki A., and Endo M. Posterior ventricular restoration treatment for heart failure: a review, past,

present and future aspects. *General thoracic and cardiovascular surgery* 2017;65(3):137-143.

- 354 Taylor D. O., Edwards L. B., Boucek M. M., Trulock E. P., Deng M. C., Keck B. M. *et al.* Registry of the International Society for Heart and Lung Transplantation: twenty-second official adult heart transplant reportâ€”2005. *The Journal of heart and lung transplantation* 2005;24(8):945-955.
- 355 Ota T., Gilbert T. W., Badylak S. F., Schwartzman D., and Zenati M. A. Electromechanical characterization of a tissue-engineered myocardial patch derived from extracellular matrix. *The Journal of thoracic and cardiovascular surgery* 2007;133(4):979-985.
- 356 Dor V., Sabatier M., Di Donato M., Montiglio F., Toso A., and Maioli M. Efficacy of endoventricular patch plasty in large postinfarction akinetic scar and severe left ventricular dysfunction: comparison with a series of large dyskinetic scars. *The Journal of thoracic and cardiovascular surgery* 1998;116(1):50-59.
- 357 Isomura T., Horii T., Suma H., and Buckberg G. D. Septal anterior ventricular exclusion operation (Pacopexy) for ischemic dilated cardiomyopathy: treat form not disease. *European journal of cardio-thoracic surgery* 2006;29(suppl_1):S245-S250.
- 358 Suma H., Isomura T., Horii T., and Buckberg G. Role of site selection for left ventriculoplasty to treat idiopathic dilated cardiomyopathy. *Heart failure reviews* 2005;9(4):329-336.
- 359 Ratner B. D. A pore way to heal and regenerate: 21st century thinking on biocompatibility. *Regenerative biomaterials* 2016;3(2):107-110.
- 360 Ozawa T., Mickle D. A., Weisel R. D., Koyama N., Ozawa S., and Li R. K. Optimal biomaterial for creation of autologous cardiac grafts. *Circulation* 2002;106(12 suppl 1):I-176-I-182.
- 361 Wendel J. S., Ye L., Zhang P., Tranquillo R. T., and Zhang J. J. Functional consequences of a tissue-engineered myocardial patch for cardiac repair in a rat infarct model. *Tissue Engineering Part A* 2014;20(7-8):1325-1335.
- 362 Wang H., Zhou J., Liu Z., and Wang C. Injectable cardiac tissue engineering for the treatment of myocardial infarction. *Journal of cellular and molecular medicine* 2010;14(5):1044-1055.

- 363 Pok S., and Jacot J. G. Biomaterials advances in patches for congenital heart defect repair. *Journal of cardiovascular translational research* 2011;4(5):646-654.
- 364 Feric N. T., and Radisic M. Strategies and challenges to myocardial replacement therapy. *Stem cells translational medicine* 2016;5(4):410-416.
- 365 Jawad H., Ali N., Lyon A., Chen Q., Harding S., and Boccaccini A. Myocardial tissue engineering: a review. *Journal of tissue engineering and regenerative medicine* 2007;1(5):327-342.
- 366 Rai R., Tallawi M., Barbani N., Frati C., Madeddu D., Cavalli S. *et al.* Biomimetic poly (glycerol sebacate)(PGS) membranes for cardiac patch application. *Materials Science and Engineering: C* 2013;33(7):3677-3687.
- 367 Park H., Radisic M., Lim J. O., Chang B. H., and Vunjak-Novakovic G. A novel composite scaffold for cardiac tissue engineering. *In Vitro Cellular & Developmental Biology-Animal* 2005;41(7):188-196.
- 368 Chen Y., Wang J., Shen B., Chan C. W., Wang C., Zhao Y. *et al.* Engineering a Freestanding Biomimetic Cardiac Patch Using Biodegradable Poly (lactic-co-glycolic acid)(PLGA) and Human Embryonic Stem Cell-derived Ventricular Cardiomyocytes (hESC-VCMs). *Macromolecular bioscience* 2015;15(3):426-436.
- 369 Piao H., Kwon J. S., Piao S., Sohn J. H., Lee Y. S., Bae J. W. *et al.* Effects of cardiac patches engineered with bone marrow-derived mononuclear cells and PGCL scaffolds in a rat myocardial infarction model. *Biomaterials* 2007;28(4):641-649.
- 370 Shin M., Ishii O., Sueda T., and Vacanti J. Contractile cardiac grafts using a novel nanofibrous mesh. *Biomaterials* 2004;25(17):3717-3723.
- 371 Ishii O., Shin M., Sueda T., and Vacanti J. P. In vitro tissue engineering of a cardiac graft using a degradable scaffold with an extracellular matrix-like topography. *The Journal of thoracic and cardiovascular surgery* 2005;130(5):1358-1363.
- 372 Srinivasan A., and Sehgal P. K. Characterization of biocompatible collagen fibers: a promising candidate for cardiac patch. *Tissue Engineering Part C: Methods* 2009;16(5):895-903.

- 373 Serpooshan V., Zhao M., Metzler S. A., Wei K., Shah P. B., Wang A. *et al.* The effect of bioengineered acellular collagen patch on cardiac remodeling and ventricular function post myocardial infarction. *Biomaterials* 2013;34(36):9048-9055.
- 374 Leor J., Aboulaflia-Etzion S., Dar A., Shapiro L., Barbash I., Battler A. *et al.* Bioengineered cardiac grafts: a new approach to repair the infarcted myocardium. *Circulation* 2000;102: III56-56.
- 375 Leor J., Gerecht-Nir S., Cohen S., Miller L., Zarin P., Holbova R. *et al.*, "Undifferentiated human embryonic stem cells are not guided to form new myocardium by transplantation into normal and infarcted heart." pp. 151A-151A.
- 376 Chrobak M. O. B., Hansen K. J., Gershlak J. R., Vratsanos M., Kanellias M., Gaudette G. R. *et al.* Design of a Fibrin Microthread-Based Composite Layer for Use in a Cardiac Patch. *ACS Biomaterials Science & Engineering*. 2017;3(7):1394-1403
- 377 Xiong Q., Ye L., Zhang P., Lepley M., Swingen C., Zhang L. *et al.* Bioenergetic and Functional Consequences of Cellular Therapy Novelty and Significance. *Circulation Research* 2012;111(4):455-468.
- 378 Kofidis T., De Bruin J. L., Hoyt G., Lebl D. R., Tanaka M., Yamane T. *et al.* Injectable bioartificial myocardial tissue for large-scale intramural cell transfer and functional recovery of injured heart muscle. *The Journal of thoracic and cardiovascular surgery* 2004;128(4):571-578.
- 379 Tan M. Y., Zhi W., Wei R. Q., Huang Y. C., Zhou K. P., Tan B. *et al.* Repair of infarcted myocardium using mesenchymal stem cell seeded small intestinal submucosa in rabbits. *Biomaterials* 2009;30(19):3234-3240.
- 380 Robinson K. A., Li J., Mathison M., Redkar A., Cui J., Chronos N. A. *et al.* Extracellular matrix scaffold for cardiac repair. *Circulation* 2005;112(9 suppl):I-135-I-143.
- 381 Lakshmanan R., Krishnan U. M., and Sethuraman S. Living cardiac patch: the elixir for cardiac regeneration. *Expert opinion on biological therapy* 2012;12(12):1623-1640.
- 382 Hashizume R., Hong Y., Takanari K., Fujimoto K. L., Tobita K., and Wagner W. R. The effect of polymer degradation time on functional outcomes of temporary elastic patch support in ischemic cardiomyopathy. *Biomaterials* 2013;34(30):7353-7363.

- 383 D'Amore A., Yoshizumi T., Luketich S. K., Wolf M. T., Gu X., Cammarata M. *et al.* Bi-layered polyurethane-Extracellular matrix cardiac patch improves ischemic ventricular wall remodeling in a rat model. *Biomaterials* 2016;107:1-14.
- 384 Baheiraei N., Gharibi R., Yeganeh H., Miragoli M., Salvarani N., Di Pasquale E. *et al.* Electroactive polyurethane/siloxane derived from castor oil as a versatile cardiac patch, part II: HL-1 cytocompatibility and electrical characterizations. *Journal of Biomedical Materials Research Part A* 2016;104(6):1398-1407.
- 385 Xu C., Huang Y., Tang L., and Hong Y. Low-Initial-Modulus Biodegradable Polyurethane Elastomers for Soft Tissue Regeneration. *ACS applied materials & interfaces* 2017;9(3):2169-2180.
- 386 Hsu Y. Y., Gresser J. D., Trantolo D. J., Lyons C. M., Gangadharam P. R., and Wise D. L. Effect of polymer foam morphology and density on kinetics of in vitro controlled release of isoniazid from compressed foam matrices. *Journal of Biomedical Materials Research Part A* 1997;35(1):107-116.
- 387 Feola A., Barone W., Moalli P., and Abramowitch S. Characterizing the ex vivo textile and structural properties of synthetic prolapse mesh products. *International urogynecology journal* 2013;24(4):559-564.
- 388 Grashow J. S., Yoganathan A. P., and Sacks M. S. Biaxial stress–stretch behavior of the mitral valve anterior leaflet at physiologic strain rates. *Annals of biomedical engineering* 2006;34(2):315-325.
- 389 Wang B., Wang G., To F., Butler J. R., Claude A., McLaughlin R. M. *et al.* Myocardial scaffold-based cardiac tissue engineering: application of coordinated mechanical and electrical stimulations. *Langmuir* 2013;29(35):11109-17.
- 390 Wang B., Tedder M. E., Perez C. E., Wang G., de Jongh Curry A. L., To F. *et al.* Structural and biomechanical characterizations of porcine myocardial extracellular matrix. *J Mater Sci Mater Med* 2012;23(8):1835-47.
- 391 Wang B., Borazjani A., Tahai M., Curry A. L., Simionescu D. T., Guan J. *et al.* Fabrication of cardiac patch with decellularized porcine myocardial scaffold and bone marrow mononuclear cells. *J Biomed Mater Res A* 2010;94(4):1100-10.
- 392 Singelyn J. M., DeQuach J. A., Seif-Naraghi S. B., Littlefield R. B., Schup-Magoffin P. J., and Christman K. L. Naturally derived myocardial matrix as an

- injectable scaffold for cardiac tissue engineering. *Biomaterials* 2009;30(29):5409-5416.
- 393 Jeffords M. E., Wu J., Shah M., Hong Y., and Zhang G. Tailoring material properties of cardiac matrix hydrogels to induce endothelial differentiation of human mesenchymal stem cells. *ACS applied materials & interfaces* 2015;7(20):11053-61.
- 394 Li Y., Ma T., Kniss D. A., Lasky L. C., and Yang S. T. Effects of filtration seeding on cell density, spatial distribution, and proliferation in nonwoven fibrous matrices. *Biotechnology progress* 2001;17(5):935-944.
- 395 Wang B., Borazjani A., Tahai M., de Jongh Curry A. L., Simionescu D. T., Guan J. *et al.* Fabrication of cardiac patch with decellularized porcine myocardial scaffold and bone marrow mononuclear cells. *Journal of Biomedical Materials Research Part A* 2010;94(4):1100-1110.
- 396 Lam M. T., and Wu J. C. Biomaterial applications in cardiovascular tissue repair and regeneration. *Expert review of cardiovascular therapy* 2012;10(8):1039-1049.
- 397 Yoon H., and Kim G. Micro/nanofibrous scaffolds electrospun from PCL and small intestinal submucosa. *Journal of Biomaterials Science, Polymer Edition* 2010;21(5):553-562.
- 398 Hong S., and Kim G. Electrospun micro/nanofibrous conduits composed of poly (ϵ -caprolactone) and small intestine submucosa powder for nerve tissue regeneration. *Journal of Biomedical Materials Research Part B: Applied Biomaterials* 2010;94(2):421-428.
- 399 Hong Y., Huber A., Takanari K., Amoroso N. J., Hashizume R., Badylak S. F. *et al.* Mechanical properties and in vivo behavior of a biodegradable synthetic polymer microfiber-extracellular matrix hydrogel biohybrid scaffold. *Biomaterials* 2011;32(13):3387-3394.
- 400 Janmey P. A., and Miller R. T. Mechanisms of mechanical signaling in development and disease. *J Cell Sci* 2011;124(1):9-18.
- 401 Connelly C. M., McLaughlin R. J., Vogel W. M., and Apstein C. S. Reversible and irreversible elongation of ischemic, infarcted, and healed myocardium in response to increases in preload and afterload. *Circulation* 1991;84(1):387-399.

- 402 Venugopal J. R., Prabhakaran M. P., Mukherjee S., Ravichandran R., Dan K., and Ramakrishna S. Biomaterial strategies for alleviation of myocardial infarction. *Journal of The Royal Society Interface* 2012;9(66):1-19.
- 403 Urech L., Bittermann A. G., Hubbell J. A., and Hall H. Mechanical properties, proteolytic degradability and biological modifications affect angiogenic process extension into native and modified fibrin matrices in vitro. *Biomaterials* 2005;26(12):1369-1379.
- 404 Soofi S. S., Last J. A., Liliensiek S. J., Nealey P. F., and Murphy C. J. The elastic modulus of Matrigel as determined by atomic force microscopy. *Journal of structural biology* 2009;167(3):216-219.
- 405 Banerjee A., Arha M., Choudhary S., Ashton R. S., Bhatia S. R., Schaffer D. V. *et al.* The influence of hydrogel modulus on the proliferation and differentiation of encapsulated neural stem cells. *Biomaterials* 2009;30(27):4695-4699.
- 406 Prabhakaran M. P., Kai D., Ghasemi-Mobarakeh L., and Ramakrishna S. Electrospun biocomposite nanofibrous patch for cardiac tissue engineering. *Biomedical Materials* 2011;6(5):055001.
- 407 Kai D., Prabhakaran M. P., Jin G., and Ramakrishna S. Guided orientation of cardiomyocytes on electrospun aligned nanofibers for cardiac tissue engineering. *Journal of Biomedical Materials Research Part B: Applied Biomaterials* 2011;98(2):379-386.
- 408 Kwon I. K., Kidoaki S., and Matsuda T. Electrospun nano-to microfiber fabrics made of biodegradable copolyesters: structural characteristics, mechanical properties and cell adhesion potential. *Biomaterials* 2005;26(18):3929-3939.
- 409 Roberts E. G., Lee E. L., Backman D., Buczek-Thomas J. A., Emani S., and Wong J. Y. Engineering myocardial tissue patches with hierarchical structure-function. *Annals of biomedical engineering* 2015;43(3):762.
- 410 Meng F., Hennink W. E., and Zhong Z. Reduction-sensitive polymers and bioconjugates for biomedical applications. *Biomaterials* 2009;30(12):2180-2198.
- 411 Zhu B., Luo S. C., Zhao H., Lin H. A., Sekine J., Nakao A. *et al.* Large enhancement in neurite outgrowth on a cell membrane-mimicking conducting polymer. *Nature communications* 2014;5:4523.

- 412 Lee S. Y., Kim S., Tyler J. Y., Park K., and Cheng J. X. Blood-stable, tumor-adaptable disulfide bonded mPEG-(Cys) 4-PDLLA micelles for chemotherapy. *Biomaterials* 2013;34(2):552-561.
- 413 Liu C., Yuan J., Luo X., Chen M., Chen Z., Zhao Y. *et al.* Folate-decorated and Reduction-sensitive micelles assembled from amphiphilic polymer–Camptothecin conjugates for intracellular drug delivery. *Molecular pharmaceutics* 2014;11(11):4258-4269.
- 414 Ge J., Neofytou E., Cahill III T. J., Beygui R. E., and Zare R. N. Drug release from electric-field-responsive nanoparticles. *ACS nano* 2011;6(1):227-233.

Biographical Information

Cancan Xu was born in Hubei, China. She received her Bachelor Degree in Biomedical Engineering from the Sichuan University, Sichuan, China, in June 2009. Given her good performance in study and research, she was exempted from the graduate record examination and got accepted by one of the prestigious institutes in China (National Engineering Research Center for Biomaterials, Sichuan University). She worked in Dr. Yujiang Fan's laboratory on the project of porous collagen scaffold development for cartilage tissue engineering. She then received her Master Degree in Biomedical Engineering from the National Engineering Research Center for Biomaterials, Sichuan University in June, 2012. Then she came to the U.S.A and started her Ph.D. study at the University of Texas at Arlington, Arlington, TX, under the supervision of Dr. Yi Hong to pursue her Ph.D. in Biomedical Engineering in January 2014. Her work mainly focused on the development of biodegradable functionalized polyurethanes for soft tissue repair and regeneration. As a Doctoral student, Cancan has published ten peer-reviewed research articles, and ten conference abstracts. She is still working with Dr. Hong in the preparation of several manuscripts for submission. Cancan has received two awards including the Graduate Research Assistant Fellowship, and the Alfred and Janet Potvin Award for Outstanding Bioengineering Student from the University of Texas at Arlington. After graduation, Cancan plans to continue her research career in biomaterials and tissue engineering.